Aalto University
School of Engineering
Department of Engineering Design and Production

Mikko Peltonen

Weldability of high-strength steels using conventional welding methods

Thesis submitted as a partial fulfillment of the requirements for the degree of Master of Science in Technology

Espoo, October 13, 2014

Supervisor: **Professor Hannu Hänninen**
Advisor: **Sami Nummela, M.Sc. (Tech.)**

Aalto University
School of Engineering

Aalto University, P.O. BOX 11000, 00076
AALTO
www.aalto.fi

Abstract of master's thesis

Author	Mikko Peltonen
Title of thesis	Weldability of high-strength steels using conventional welding methods
Department	Department of Engineering Design and Production
Professorship	Engineering materials
Code of professorship	Kon-67
Thesis supervisor	Professor Hannu Hänninen
Thesis advisor	Sami Nummela, M.Sc. (Tech.)

Date	**Number of pages**	**Language**
October 13, 2014	118 + 103	English

Abstract

The objective of this thesis was to compare conventional welding methods and their suitability for high-strength steels as alternative choice for laser or laser-hybrid welding. Test welds were evaluated by visual inspections, tensile tests, impact tests and hardness profiles. Test materials were ferritic-bainitic Optim 700 MC Plus and bainitic-martensitic Optim 900 QC. Parameter windows for each welding process were also determined.

In the literature part, the ultra-high-strength steels and how their properties are achieved are discussed. Weldability and transformations in the heat-affected zone, and the effects of cooling time are also discussed. The functionality of conventional welding methods such as metal-active gas welding, plasma arc welding and submerged arc welding are reviewed.

Experimental part of the work consists of sample preparation, consumable selection and test equipment introduction for single-pass butt welded specimens. Mechanical testing and metallography were carried out to determine the effect of heat input on the welded materials.

The studies showed that the conventional welding methods can produce high quality welds if the possibilities and limitations of each welding method are recognized. Mechanical properties of the welded structure are controlled by the heat input, cooling time from 800 °C to 500 °C and consumable. Increased heat input is shown to have a drastic effect on the yield and tensile strength, softening in the heat-affected zone and impact toughness. Modifying the joint preparations for single-pass welding, the dilution rate and heat input can be decreased to enhance the mechanical properties of the welded joint.

Keywords Advanced High-Strength Steels, Heat-Affected Zone, Metal-Active Gas Welding, Plasma Arc Welding, Submerged Arc Welding

Aalto University
School of Engineering

Aalto University, P.O. BOX 11000, 00076
AALTO
www.aalto.fi

Diplomityön tiivistelmä

Tekijä Mikko Peltonen		
Työn nimi Suurlujuusterästen liittäminen perinteisillä hitsausmenetelmillä		
Laitos Koneenrakennustekniikka		
Professuuri Koneenrakennuksen materiaalitekniikka		**Professuurikoodi** Kon-67
Työn valvoja Professori Hannu Hänninen		
Työn ohjaaja Diplomi-insinööri Sami Nummela		
Päivämäärä	**Sivumäärä**	**Kieli**
13.10.2014	118 + 103	Englanti

Tiivistelmä

Tämän diplomityön tavoitteena oli vertailla suurlujuusterästen hitsattavuutta käyttäen perinteisiä liittämismenetelmiä kuten MAG-hitsausta, plasmahitsausta ja jauhekaarihitsausta. Testihitsien soveltuvuutta arvioitiin silmämääräisellä tarkastuksella, vetokokein, iskukokein ja mikrokovuus -mittausten perusteella. Tutkittavat materiaalit olivat ferriittis-bainiittinen Optim 700 MC Plus ja bainiittis-martensiittinen Optim 900 QC.

Kirjallisuusosassa käsitellään suurlujuusteräksiä ja miten niiden ominaisuudet ovat saavutettu. Materiaalien hitsattavuutta, mikrorakennemuutoksia ja jäähtymisajan vaikutusta muutosvyöhykkeessä tarkastellaan yksityiskohtaisemmin. Perinteisten hitsausmenetelmien käytettävyyttä on lisäksi arvioitu.

Kokeellisessa osassa käsitellään hitsattavien koekappaleiden esivalmistelua, lisäainevalintoja sekä testilaitteiston esittely päittäisliitoksille. Lämmöntuonnin vaikutusta suurlujuusteräksille arvioidaan hitsattujen koekappaleiden osalta mekaanisella aineenkoetuksella ja metallografisella tutkimuksella.

Tutkitut hitsausmenetelmät soveltuvat suurlujuusterästen yksipalkohitsaukseen, kun niiden rajoitukset ovat tunnistettu. Hitsatun liitoksen mekaaniset ominaisuudet ovat erittäin riippuvaisia lämmöntuonnista, jäähtymisajasta 800 °C - 500 °C ja lisäainevalinnoista. Suurella lämmöntuonnilla on merkittävä vaikutus liitoksen myötö- ja murtolujuuteen, muutosvyöhykkeen pehmenemiseen ja iskusitkeyteen. Liitoksen mekaanisia ominaisuuksia voidaan parantaa oikealla lisäainevalinnalla, vähentämällä lämmöntuontia sekä muuttamalla railogeometriaa hitsauslisäaineen ja perusaineen sekoittumisen vähentämiseksi.

Avainsanat Suurlujuus teräkset, Muutosvyöhyke, MAG-hitsaus, Plasmahitsaus, Jauhekaarihitsaus

FOREWORD

This Master´s Thesis was a part of FIMECC (Finnish Metals and Engineering Competence Cluster) program. The project was titled LIGHT II - Novel Manufacturing Technologies for Innovative and Sustainable Solutions, which was made during 2012 to 2014.

I would like to thank Professor Hannu Hänninen for his support and the opportunity for this interesting work. I am grateful for Sami Nummela for his assistance and support. I am also thankful all the support that I have had during this thesis from Heikki Vestman, Jari Hellgren, Kim Widell, Professor Pedro Vilaça, Tapio Saukkonen, Harri Toivonen and Tommi Seppänen. In addition, I would like express my appreciation to Juha Lukkari who supplied all the consumables to the project.

Finally, I would like to express my gratitude to my wife Elina and my daughter Ella for their support and understanding through the years. Special thanks to my family and friends.

Espoo, October 13, 2014

Mikko Peltonen

TABLE OF CONTENTS

LIST OF SYMBOLS AND ABBREVIATIONS

SYMBOLS

A_0	Initial Cross-Sectional Area of the Specimen
A	Elongation to Fracture
d	Material Thickness
E	Welding Energy
F_2	Shape Factor for 2-Dimensional Heat Flow
F_3	Shape Factor for 3-Dimensional Heat Flow
F	Axial Load
I	Current
k	Thermal Efficiency Factor
n	Number of Specimens
Q	Heat Input
$R_{p0,2}$	Yield Strength
R_m	Tensile Strength
S_x	Standard Deviation
T_0	Working Temperature
U	Voltage
v	Welding Speed
$\bar{x}$	Average Value
x_i	Individual Value
α	Ferrite
α'	Martensite
γ	Austenite
ε_{eng}	Engineering Strain
σ_{eng}	Engineering Stress
$\Delta t_{8/5}$	Cooling Time from 800 to 500 ºC

ABBREVIATIONS

AHSS	Advanced High-Strength Steel
BCC	Body-Centered Cubic
BCT	Body-Centered Tetragonal
CCT	Continuous Cooling Transformation
CGHAZ	Coarse Grained Heat-Affected Zone
CP	Complex-Phase
DCEN	Direct-Current Electrode Negative
DCEP	Direct-Current Electrode Positive
DP	Dual-Phase
DBT	Ductile-to-Brittle Transition
EBSD	Electron Backscatter Diffraction
FCAW	Flux-Cored Arc Welding
FCC	Face-Centered Cubic
FGHAZ	Fine Grained Heat-Affected Zone
FL	Fusion Line
FZ	Fusion Zone
FSW	Friction Stir Welding
HAZ	Heat-Affected Zone
HSLA	High-Strength Low Alloy Steel
HSS	High-Strength Steel
ICHAZ	Inter Critical Heat-Affected Zone
IPF	Inverse Pole Figure
LBW	Laser Beam Welding
MAG	Metal-Active Gas Welding
PA	Flat Position
PAW	Plasma Arc Welding
PMZ	Partially Melted Zone
pWPS	Preliminary Welding Procedure Specification
SAW	Submerged Arc Welding
SCHAZ	Subcritical Heat-Affected Zone
TIG	Tungsten Inert Gas Welding
WM	Weld Metal

1 INTRODUCTION

The usage of low carbon high-strength steels has increased over the years. A new generation of steels is taking the mechanical properties to a new level and the marketplace has expanded globally. Light-weight structures have attracted the interest of many different industrial branches where the lighter structures can be utilized effectively. Applications can be found in the field of transportation such as material handling and containers, lifting such as mobile cranes, and construction engineering. These structures and components will provide better energy efficiency and durability in all applications and reduce the environmental impact.

Joining is one of the most important features of steel. Novel high-strength steels are extremely sensitive to welding, especially when dealing with high heat input processes. A special attention must be taken to the welding procedure to minimize the effects of heat input without losing the properties in the heat-affected zone (HAZ).

The objective of this work is to study the weldability of Optim 700 MC Plus and Optim 900 QC steels. Alternative welding methods for laser beam welding and laser-hybrid welding such as metal-active gas welding (MAG), plasma arc welding (PAW) and submerged arc welding (SAW) are used to study the limitations and possibilities for single-pass butt welds. Welding processes are compared in terms of mechanical properties and the microstructures are analyzed. Comparison offers new possibilities to design efficient and economical light-weight structures. For using the benefits of the mechanical properties, pros and cons of each welding method can be categorized and the most suitable welding process for each application can be chosen.

2 ULTRA-HIGH-STRENGTH STEELS AND THEIR PROPERTIES

The need of light-weight structures and components has increased over the years. This has been one of the cross-roads of development of light-weight and high-strength steels. New innovations in steel manufacturing processes have played an important role to accomplish the new generation high-strength low-alloy steels. Modern steels have more homogeneous microstructure than ever with low content of carbon and impurities which increases weldability. Microstructures are being manipulated to produce impressive mechanical properties. Material properties such as tensile strength and ductility are brought to a new level in the era of high-strength steels.

Structural steel is the most common and the most versatile material in the world. For the past 40 years development has been very innovative and new discoveries have been made. Mild steel was the first step to structural materials in the 20th century. Since then development has been significant. The first high-strength low-alloy steels (HSLA) came to market in the 1970's and first generation advanced high-strength steels (AHSS) came in the 1990's. Since then the second generation AHSS has been developed with extreme tensile strength and elongation. Know-how in the steel manufacturing has come to the phase where varying the quantities and combinations of the phases, desired properties can be achieved.

AHSSs are generally the referred term for a group that has a wide range on steel grades. The tensile strength can vary from 500 MPa and beyond. Different applications need different properties which are established by changing the alloying elements and their content, and also strengthening mechanisms. Automotive industry is using sheet metals in its applications and those steels have usually very high strength which can decrease structural weight and increase absorbed energy in collisions. These applications take advantage of the properties where the structure is maintained through the deformation process. Other structures like in mobile cranes are using plates the thickness of which has decreased through the development of high-strength steels.

Conventional high-strength steels (HSSs) are basically composed of ferritic microstructures which means that complicated microstructures of various phases are not present. This is one of the biggest differences between HS and AHS steels. Figure 1 combines these two groups and their properties.

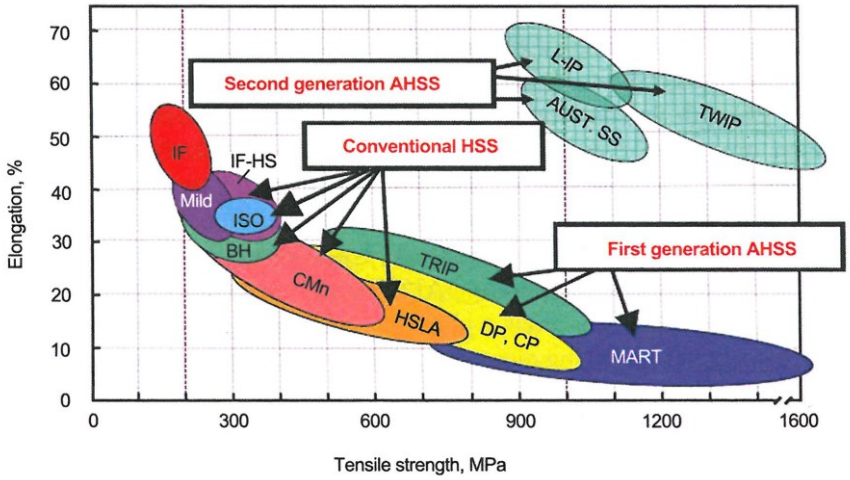

Figure 1. Categorizing high-strength steels against elongation and tensile strength. (Demeri 2013)

It can be seen that the tensile strength of HSSs is restricted approximately to 800 MPa, whereas Dual-phase (DP) and Complex-phase (CP) steels exceed 1000 MPa. The excellent properties of AHSSs are established by modifying their microstructure without adding high levels of alloying elements but by forming multiple phases in the ferritic matrix and by controlling the rolling through varying thermal routes. (Mallick 2010)

2.1 Advanced high-strength steels

One of the biggest differences between conventional HSSs and AHSSs is the microstructure. The microstructure in HSS is a single-phase ferritic structure, whereas the AHSS has a multiphase microstructure. AHSS contains hard islands of martensite, bainite and/or retained austenite which have been dispersed in a ductile ferritic matrix. Varying the quantities and combinations of the phases, desired properties can be achieved (Figure 2). (Demeri 2013 & Mallick 2010)

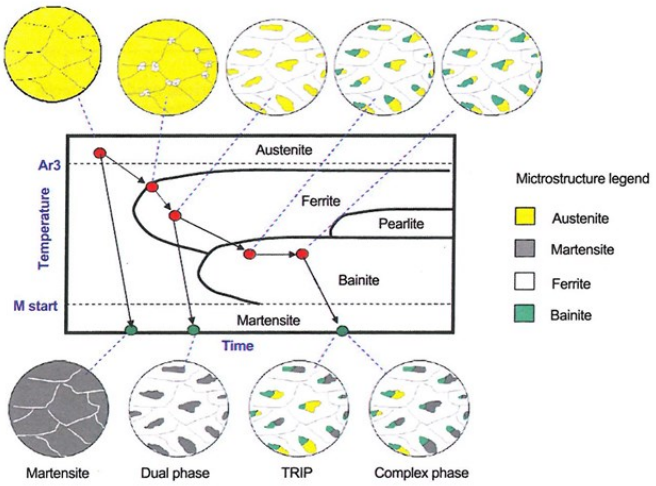

Figure 2. Thermal processing routes for AHSS and final microstructures. (Demeri 2013)

Martensite (α´) is considered to be very hard but brittle phase the properties of which can be used to increase the strength. Structure can be either fully martensitic or partially martensitic. Hard martensite islands are embedded to soft ferritic (α) matrix through controlled cooling. Material can be heated to fully austenized region where the body-centered cubic (bcc) structure is thus formed to face-centered cubic (fcc) structure. Carbon (C) solubility is higher in fcc than it is in bcc crystal structure. C atoms are placed in the interstitial positions in octahedral interstitial sites of fcc. The transformation from fcc to bcc is diffusionless, so the Z-positions in Figure 3 are the possible octahedral sites for C. Therefore in both structures C can occupy these sites. This means that the structure is expanded to a tetragonal shape. As the temperature is decreased C atoms are trapped to produce a dilational misfit in volume and cause a tetragonal distortion in which the fcc structure is transformed to body-centered tetragonal (bct) structure. (Bhadeshia 2006)

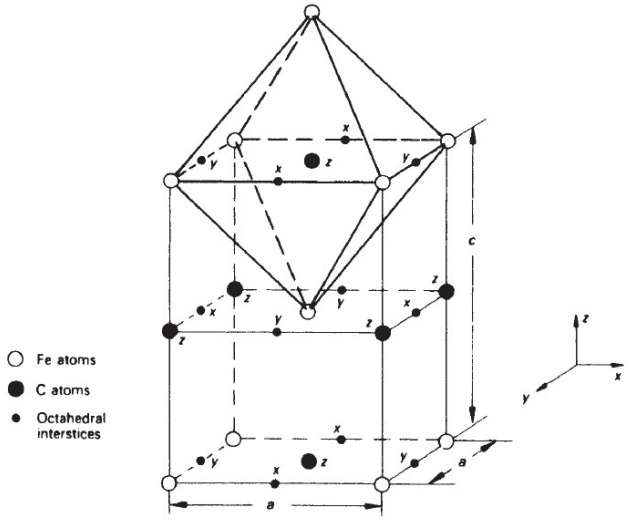

Figure 3. Carbon atoms trapped in body-centered tetragonal (bct) lattice. (Bhadeshia 2006)

The carbon supersaturated solid solution can be considered martensite. The distorted lattice resists the dislocation movement within the lattice by producing a barrier to dislocation glide. Martensite volume fraction can be controlled by the isothermal treatment from intercritical region. In the intercritical temperature both austenite and ferrite ($\gamma+\alpha$) are present. The remaining part of the γ can be transformed to martensite. (Bhadeshia 2006)

Bainite is a microstructure that is formed in isothermal transformation of austenite. Diffusion of carbon is time dependent and it has the same composition as pearlite but is formed in faster cooling. The cooling is, however, not as fast as in the martensite transformation. Two types of bainite can be present, the upper and lower bainite (Figure 4). Upper bainite is formed in the temperature range of 550 - 440 ºC, where the ferrite plates are nucleated from the austenite grain boundaries as temperature is decreased. The growth of the plates enriches the remaining austenite by carbon. As the time evolves cementite carbides precipitate from the remaining austenite layers. (Bhadeshia 2006)

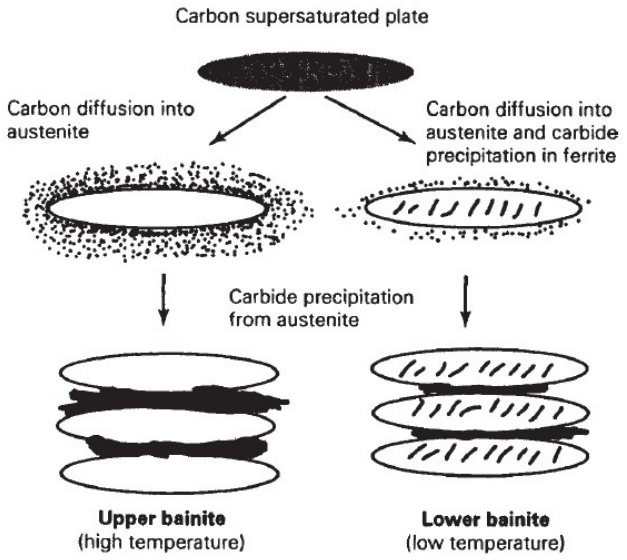

Figure 4. A schematic presentation of the two forms of bainite. (Bhadeshia 2006)

The other form of bainite is lower bainite which is formed in a temperature range of 400 - 250 ºC. Difference to upper bainite is that the carbon diffuses into phase boundary and the cementite particles precipitate both at the boundary and within the ferrite plates. Size of the precipitated particles in lower bainite is relatively fine. This is caused by the precipitations within ferrite where the carbon has distributed into the residual austenite and particles between the ferrite plates are formed. Combinations of lower bainite together with martensite can produce high-strength and ductile material properties. (Bhadeshia 2006)

2.1.1 Dual-phase steels

Dual-phase (DP) steels can be categorized into the first generation of AHSS. Mechanical properties of these steels are primarily related to the volume fraction of each phase. Mechanical properties such as tensile strength varies from 450 - 1000 MPa. Microstructure can be categorized basically into two phases, where the hard martensite islands are embedded to ferrite matrix. Figure 5 presents the typical microstructure of DP steel. From the microstructure, two different phases can be seen: darker martensite is dispersed in the ferrite. It should be pointed out that for some applications bainitic structure may also be desirable. Ferrite improves the toughness and elongation, whereas martensite improves the strength and hardness. Martensite volume fraction is set to between 20 - 70 %. The strength level can be adjusted by increasing the martensite content in the structure. Microalloying elements such as nio-

bium (Nb), vanadium (V) and titanium (Ti) are added individually or in combination to form fine-grained carbides and nitrades. (Demeri 2013 & Gladman 1997 & Kuziak et al. 2008)

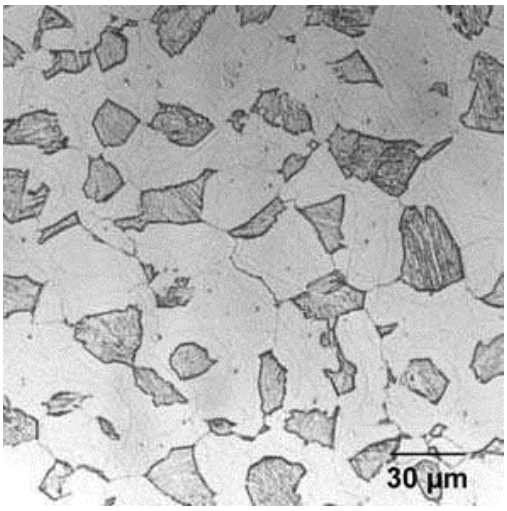

Figure 5. Microstructure of DP steel. (Bhadeshia 2006)

To produce DP steels, controlled cooling is needed. This can be done either via thermomechanical treatment or intercritical annealing. In thermomechanical treatment, DP microstructure is developed during cooling after hot rolling. Cooling is controlled from the austenite (γ) phase or from the region where there are both, ferrite and austenite phases present (Figure 2). To produce the final microstructure, rapid cooling is carried out to transform some of the austenite to ferrite and to transform the remaining austenite to martensite. (Demeri 2013, Kuziak et al. 2008)

Another way to achieve DP microstructure is to use intercritical annealing. In this process, hot or cold rolled steel strips are uncoiled and then annealed at specific temperature. The alloyed steel is heated into the two-phase (α + γ) region below 800 ºC. At this point, ferrite and pearlite microstructure transforms to austenite. The steel is then rapidly cooled to cause the austenite regions to transform to martensite. Other products, such as bainite may form in higher temperatures. (Bhadeshia 2006, Demeri 2013)

Like most of the AHSSs, DP steels have low carbon content to improve weldability. Carbon content is set typically between 0,06 - 0,15 wt% to achieve desired strength level but also to minimize carbon equivalent, and therefore decrease the hardenability. (Kuziak et al. 2008)

2.1.2 Complex-phase steels

Complex-phase (CP) steels can be categorized into the first generation of AHSS. Chemical composition is fairly similar with transformation-induced plasticity (TRIP) steels. The biggest differences are that the CP steels contain elements that can cause precipitation strengthening, slightly lower alloy content and less retained austenite is present. Small quantities of Nb, Ti and V are added individually or in combination to form fine carbides and nitrides which raise the tensile strength up to 800 MPa and beyond. (Kuziak et al. 2008 & Demeri 2013)

The microstructure is a combination of fine ferrite, hard phases of martensite and bainite, precipitates and typically retained austenite is not present in CP steels. The volume fraction of martensite and bainite islands is controlled through its cooling routes. To produce bainitic-ferrite matrix, intercritical heat treatment and isothermal hold are needed whether the strip is cold-rolled or hot-rolled. In cold-rolled products the structure is reheated to $\gamma+\alpha$ region, whereas the hot-rolled strip is first in γ region and then lowered to $\gamma+\alpha$ region. In $\gamma+\alpha$ region, partial transformation to austenite has happened. As the temperature is decreased to bainite transformation range, some of the austenite transforms to allotriomorphic ferrite from the austenite grain boundaries and cementite carbides precipitate from the remaining austenite layers to form bainitic-ferrite structure. Retained austenite transforms into martensite during the cooling cycle. CP steels have relatively low silicon and carbon content to minimize the portion of retained austenite in room temperature and improve weldability. Microstructure of hot-rolled CP steel is presented in Figure 6. (Krauss 2005 & Bhadeshia 2006)

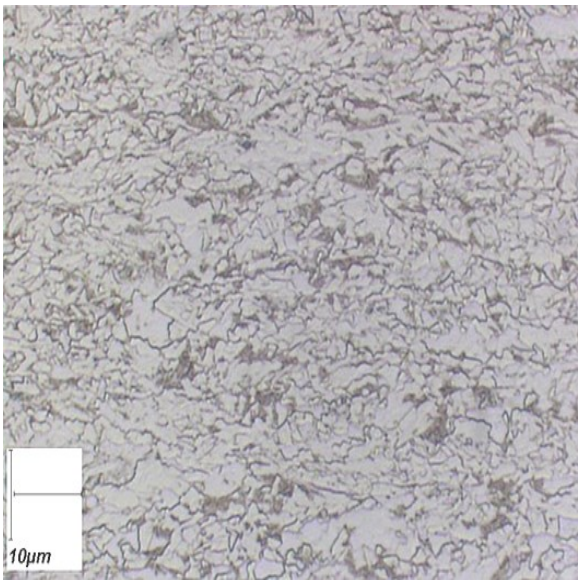

Figure 6. Microstructure of hot-rolled CP steel. (Arcelor Mittal 2013)

Alloying elements used for CP steels are quite similar to DP steels. Carbon content is set below 0,15 wt%, manganese 1,5 - 2,5 wt%, silicon 0,25 - 0,60 wt%, vanadium <0,06 wt%, niobium <0,04 wt% and titanium <0,02 wt%. (Demeri 2013)

Typically the structure contains more bainite than martensite which increases the formability. The distribution can be for instance 40 % of bainite and 13 % of martensite for a steel grade that has yield strength of 800 MPa. The bainitic-ferrite structure is strengthened by the high dislocation density and the interactions between precipitations and martensite. (Demeri 2013 & Kuziak et al. 2008)

2.2 Manufacturing of high-strength steels

High-strength steels can be produced in many ways. Manufacturing can be categorized mainly into three groups. The first method is thermo-mechanical control process (TMCP) where the fine-grained microstructure is achieved by accelerated cooling through different phases. The second method is closely related to TMCP. It is direct quenching (DQ) where the rolling part is similar with TMCP but the cooling is carried out more rapidly by quenching. The third method is direct quenching with tempering (DQ-T). All the methods are presented in Figure 7. (Nishioka et al. 2012)

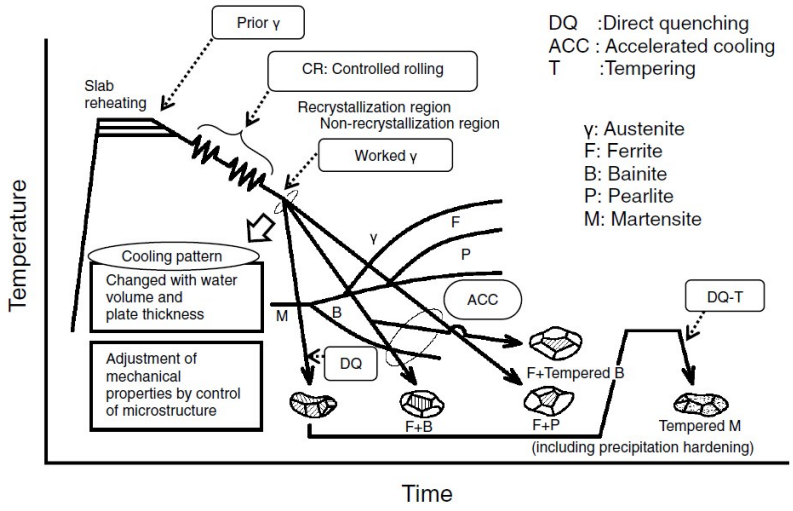

Figure 7. Microstructure control by TMCP. (Nishioka et al. 2012)

In TMCP steel manufacturing the rolling forces and the operating temperatures are carefully controlled through the whole process which has not been the case with conventional rolling facilities. The goal of TMCP treatment is to achieve a fine grain structure with good strength and ductility, and reduce the alloying. Although alloying is needed to increase the tensile strength. Process can be divided into two stages: slab reheating and cooling. In the slab reheating where the main goal is to straighten and deform the slab. In the cooling stage the start and the finish temperature, and cooling rate are determined based on the desired microstructure. (Bhadeshia 2006)

Reheating the slab takes place near to A_3 temperature where the structure is fully austenitic. In rolling and hot deformation the grain refinement is achieved by the recrystallization of austenite through dynamic recrystallization. Dynamic recrystallization is highly dependent on the temperature and degree of deformation in rolling. In the austenite region, precipitation of carbides and nitrides of Nb, V and Ti restrains the grain growth. The refinement is achieved as the rolling temperature is gradually decreased and fine particles are precipitated. Recrystallization of austenite may occur several times before it reaches the intercritical ($\gamma+\alpha$) temperature. If the rolling is continued, recrystallized austenite grains are elongated, and ledges and deformation bands are introduced. These will act as potential nucleation sites in the austenite to ferrite transformation. In the accelerated cooling (ACC), the growth of transformed structure is suppressed and the refinement is established via the nucleation sites mentioned before. (Bhadeshia 2006 & Nishioka et al. 2012)

Good strength and ductility and reduced cold cracking tendency are based on a sufficient balance between grain refinement and strengthening mechanisms. If the rolling is carried out significantly lower than A_3 temperature it can stretch the ferrite crystals and inclusions which causes misorientations in the microstructure. Thus, mechanical properties can become undesirable as they are anisotropic. Heavily deformed ferrite crystals have significant dislocation density and internal residual stresses which may cause sharp drop of strength after welding. (Bhadeshia 2006)

As said, DQ is fairly similar to the TMCP, especially the hot rolling stages. The material is reheated to $\alpha+\gamma$ region where the carbon content is higher in austenite as the intercritical temperature is decreased. In this two-phase region hardenability is higher and by direct quenching to ambient temperature high-strength martensitic steels can be produced. (Demeri 2013)

Conventional DQ-T steel involves rapid cooling followed by tempering. Martensitic structure is heat treated afterwards to increase ductility. Carbon atoms trapped by the bct structure combine with the atoms of iron to form Fe_3C precipitates. (Demeri 2013)

DP and CP structural steels are produced by controlled cooling. Several manufacturing routes can be used. In hot-rolled products the material is reheated to austenite or intercritical region and then some of the austenite is transformed to ferrite before the rapid cooling takes place to transform the remaining austenite to martensite. The final structure is a combination of ferrite and martensite. However, in the case of CP steels the structure is produced by slightly different procedure. It requires an isothermal hold at specific temperature to produce a certain amount of bainite. This means that the structure is a combination of ferrite, martensite, retained austenite and bainite. (Demeri 2013 & Bhadeshia 2006)

2.3 Strengthening mechanisms

There are many different ways to increase the strength of the steel by manipulating the microstructure. It is a mixture of perfection and imperfection where the desirable imperfections arrest the plastic deformation by impeding the movement of dislocations. Modern microalloyed AHSSs are strengthened at least with three strengthening mechanisms. In most cases with modern HSSs, there is additionally the fourth mech-

anism present. The contributions of each mechanism are determined by the chemical composition of the steel and the purpose it is being subjected. The strengthening mechanisms in AHSSs can be divided into the following types (Demeri 2013):

- Solid-solution strengthening
- Grain refinement
- Phase transformation
- Dispersion strengthening.

Manipulating the structure by the strengthening mechanisms, restriction to dislocation motion can be observed.

2.3.1 Solid-solution strengthening

Solid-solution strengthening is a type of alloying where the dislocation mobility in a solid is restricted by the misfitting interstitial or substitutional atoms in the metal lattice. The extent of the strengthening is dependent on the volume fractions of the alloying elements and the size of the alloying atoms. Solid-solution strengthening can be characterized into two forms. When the solute atoms are fairly close to the size of the solvent atoms they can substitute those in their normal position. This is called substitutional solid solution. If the solute and the solvent atoms are very different of their atomic size, the interstitial solid solution takes place in interstitial positions in the solvent lattice. Both scenarios are presented in Figure 8. (Meyers 2009 & Bhadeshia 2006)

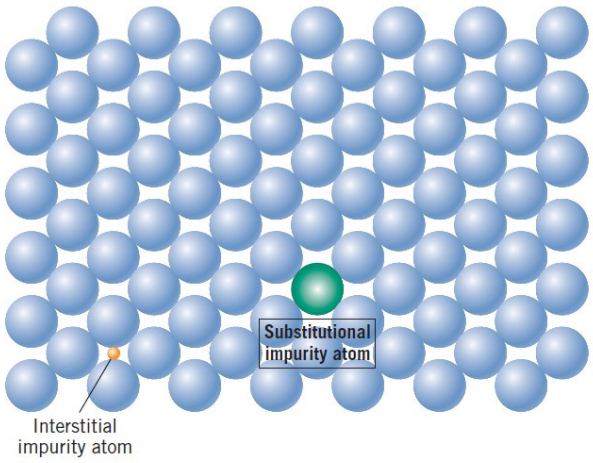

Figure 8. A schematic presentation of solid solution atoms. (Callister 2007)

In steels, like AHSSs, substitutional solid solutions are more common than interstitial solid solutions. The main reason for this is the atomic size. Alloying elements such as chromium (Cr), molybdenum (Mo), manganese (Mn), nickel (Ni), silicon (Si), titanium (Ti), niobium (Nb) and vanadium (V) are relatively the same size that can substitute the solvent atoms. Carbon and nitrogen atoms are small enough to occupy interstitial positions and produce a dilational misfit in volume and cause a tetragonal distortion in the body-centered cubic structure. In case of carbon, this supersaturated solution can be considered martensite at fast cooling rates, where the carbon atoms are trapped in octahedral interstices. Martensite transformation distorts the lattice to body-centered tetragonal (bct). The carbon and nitrogen atoms interact and form conditions at both edge and screw dislocations which will lead to a more effective impediment to the movement of dislocations than in the case of substitutional atoms. As the movement of dislocations becomes more difficult, the energy interaction between the dislocation and the barrier increases. This phenomenon leads to an increased strength of the steel. (Meyers 2009 & Bhadeshia 2006)

2.3.2 Grain refinement strengthening

Grain refinement strengthening is one of the most important mechanisms in AHSSs. During the manufacturing of TMCP, steel slab experiences various types of rolling and cooling stages to its final form. These processes along with microalloying elements reduce the average grain size, and hence the grain boundaries work as an effective barrier to the movement of dislocations. As the grain size is decreased, the total area of grain boundary per unit volume is larger than with larger grains. Structure refinement impedes the movement of dislocations, and hence the grain boundaries work as effective barriers to arrest dislocation movement so that they can pile-up against the grain boundaries. Together with small grain size and crystallographic misorientations, dislocation movement from grain to grain needs more energy to change its direction of motion. As the dislocation pile-up is introduced at the grain boundary, especially with high-angle grain boundaries, a stress concentration is brought ahead of their slip plane. So the new disclocations are generated to the neighbor grains. (Meyers 2009 & Callister 2007)

A well-known relationship between the grain size and the yield strength can be expressed by the Hall-Petch equation. Relationship deals with yield strength and its

dependence on the grain size of materials. It is known that as the grain size is reduced the yield strength of material is increased, respectively. So the evaluation of mechanical properties can be done through this equation. (Bhadeshia 2006)

2.3.3 Phase transformation strengthening

Phase transformation is part of the general view of TMCP steel manufacturing. This is controlled in cooling process and desired microstructure is achieved with continuous cooling and hold time through different phase regions. Hard phases like martensite can be established during rapid cooling from austenite region to the ambient temperature where the diffusion is not present. Softer structures can be achieved with lower cooling rates by controlling the rolling temperature and hold time. The ratio between each phase can also take place in the rolling process.

The importance of the heat treatment of the steel is based on solid-state diffusion where the solubility changes as the temperature increases. The transformation from ferrite to austenite increases the solubility of carbon as the microstructure changes from bcc to fcc. This is due the fact that fcc structure has more space in its interstices for interstitial atoms like carbon. Based on the cooling conditions and desired microstructure nonequilibrium phases can form. Phase transformations are presented in Figure 9. (Bhadeshia 2006)

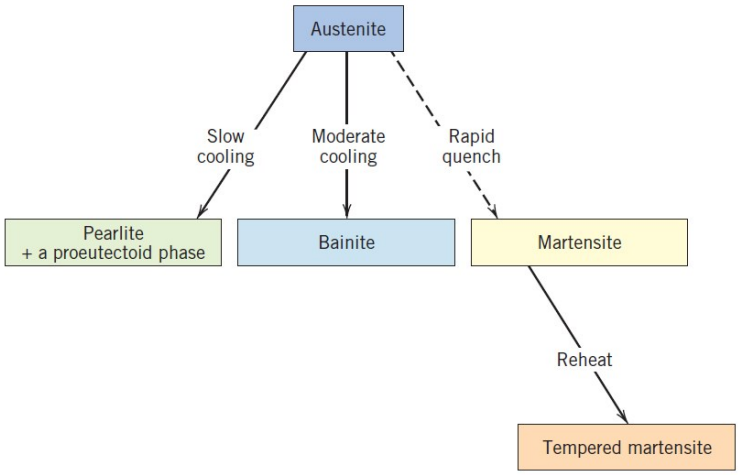

Figure 9. Phase transformations through various paths. (Callister 2007)

Various microstructures for alloyed steels can be achieved when different routes for cooling are carried out. By changing the cooling rate and chemical composition pearlite forms during slow cooling and as the cooling rate changes, harder phases

like bainite and martensite form. The structure can consist entirely of some of the phases or it can be a mixture of two or even more phases. This is the case, when material is continuously cooled through different phases to its final form. Most of the AHSSs have a microstructure of ferrite-bainite and bainite-martensite or entirely martensite. These can be categorized as DP, CP or MS steels. (Bhadeshia 2006)

The high strength level in AHSSs is achieved by the internal distortions through phase transformations. Internal distortion is created by the lattice strains by the trapped carbon atoms in interstitial positions in octahedral interstice. They produce a dilational misfit in volume and cause a tetragonal distortion where the fcc structure is transformed to bct structure. The carbon supersaturated solid-solution is considered martensite. The distorted lattice resists the dislocation movement by producing a barrier to dislocation glide. (Bhadeshia 2006)

2.3.4 Dispersion strengthening

Dispersion strengthening is commonly used strengthening mechanisms in AHSSs. The main concept behind it is how the microalloying elements precipitate as the rolling temperature is decreased. These precipitations affect incoherency in the ferrite lattice and distort it. They also restrict the grain growth through the pinning effect. Commonly used microalloying elements are Nb, V and Ti which form the precipitation of second-phase particles during the austenitization treatment. The effects of microalloying elements are presented in Figure 10. (Bhadeshia 2006)

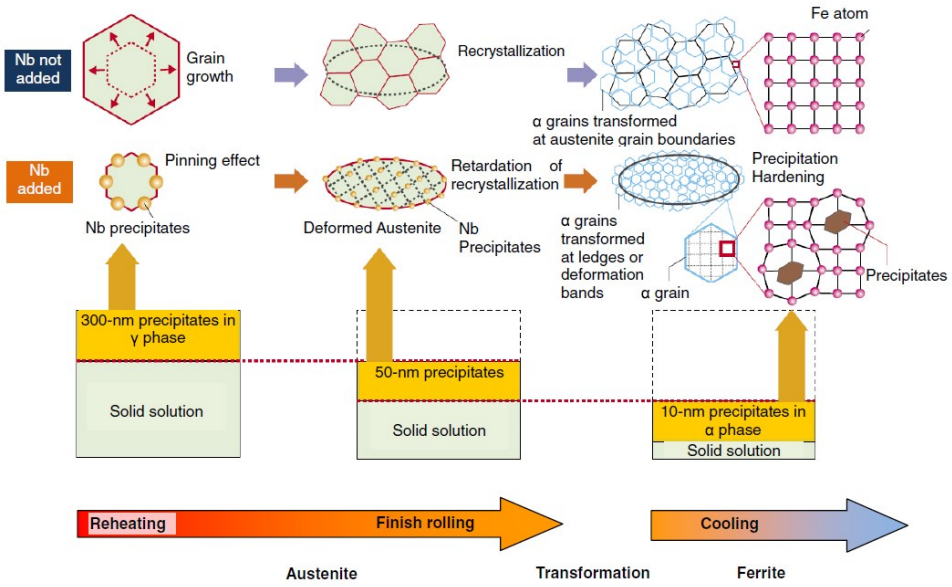

Figure 10. The effects of Nb precipitations. (Nishioka et al. 2012)

During the rolling stages of TMCP, Nb, V and Ti precipitate to the grain boundaries of austenite and as the rolling temperature is gradually reduced the size of the precipitations, carbonitrides or carbides, decreases by the strain energy of rolling. Precipitation particles are present through the whole process and do not dissolve completely in austenite. The particle size is decreased in every subsequent processes and the final size (e.g. 10 nm) of the precipitations is very fine and evenly distributed. Precipitations with small size will prevent austenite recrystallization, and hence the grain growth. Lattice mismatch occurs for Nb and V precipitates in austenite and after the austenite to ferrite transformation has happened there is incoherency between ferrite and precipitates. This mismatch between ferrite and NbVN, VCN, TiC and TiC increases resistance to dislocation motion by lattice strains in the vicinity of the small particles. As the movement of dislocations is more difficult the strength increases. Mechanical properties vary according to the size, amount and shape of the particles. (Nishioka et al. 2012 & Hertzberg 1996 & Bhadeshia 2006 & Gladman 1997)

2.4 Alloying elements

The main objective of manufacture of AHSSs is to produce materials with extreme high-strength and superb ductility at low temperatures. At the same time, alloying should be kept reasonably low to improve welding. The alloying content is depend-

ent on the application where the steel is designed for but in all cases elements are used to inhibit grain growth of austenite, reduce grain size and for precipitations.

Alloying elements such as Cr, Mo, Mn, Ni, Si, Ti, Nb and V are widely used elements in AHSSs. Due the development of AHSSs, the carbon content has decreased over the years. Figure 11 presents a relationship between yield strength and alloy content in low carbon steels. The figure does not show the real contents of the alloys in AHSSs but it does indicate the effect. Some of the elements like nitrogen (N) and phosphorus (P) are harmful and unwanted especially in AHSSs, even though their strengthening effect would be significant.

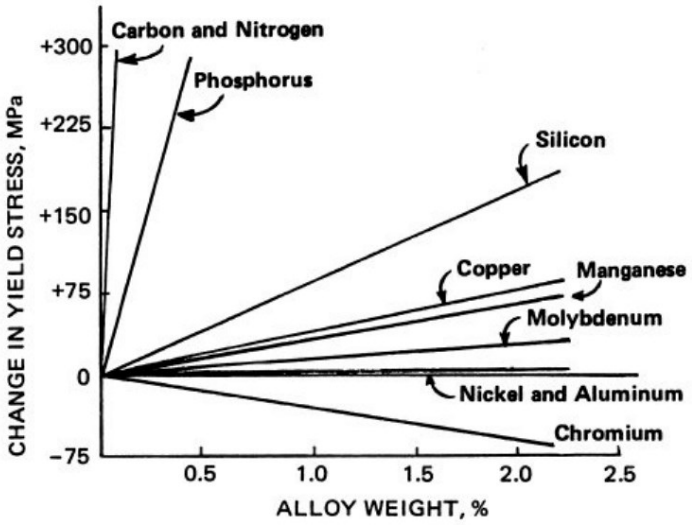

Figure 11. Effects on the alloying elements in low carbon steels. (Krauss 2005)

C content is normally set between 0,02 - 0,13 wt%, but even higher concentrations are used. The content of C is very important when optimizing the microstructure and mechanical properties. It has important effect on weldability through carbon equivalent, and hence the hardenability. Hard structures are brittle and very sensitive to hydrogen cracking as the strength increases. (Bhadeshia 2006)

Together Mn and C are used to improve the strength of the steel. Mn content is usually limited around 1,0 - 1,6 wt% to avoid excessive hardening. It increases the strength through solid-solution hardening and also promotes grain refinement by lowering the A_3 temperature and therefore impact toughness increases. Mn also promotes bainite transformation during cooling sequence. (Bhadeshia 2006)

Cr and Mo are used to increase hardness and strength. Hardening is provided by solid-solution strengthening and carbide formation. Ni does not have a significant effect on the strength but it will improve toughness and adds solid-solution strengthening. (Bhadeshia 2006)

Microalloying elements Ti, V and Nb are used to form precipitates to contribute the strength. They will also limit the grain growth during manufacturing and welding when fine-grained carbides and nitrides form to the austenite grain boundaries. In addition, they will elevate the recrystallization temperature. (Bhadeshia 2006)

2.5 Applications

Automotive industry along with steel manufacturers has led the way to a new advanced materials which are adopted in several applications. One of the biggest goals is to reduce the weight by using high-strength materials that can maintain high formability. At the same time, material costs are kept low, so that the new material can be easily implemented into regular cars. Long-term plan is to meet future needs by customizing the material properties individually for each application and develop even stronger, safer, lighter and low-cost materials (Demeri 2013).

In terms of weight, AHSSs are not lighter nor have better Young´s modulus than other steels but because of the extreme high-strength and good formability, thinner components can be used to reduce the structure weight. To achieve enough rigidity in the structure, the component is usually formed to have complex geometry in order to prevent buckling. Table 1 presents a trend, how the weight reduction of a vehicle depends on materials yield strength.

Table 1. Weight reduction against materials yield strength.(Demeri 2013)

Yield strength, MPa (ksi)	Weight reduction, %
400 (58)	15–25
700 (102)	35–45
900 (131)	45–50
1100 (160)	50–55

The weight reduction highly depends on the volume fraction of hard phases which means that as the weight is dropped, the fuel consumption is decreased and at the same time the fuel economy increases. This will provide better energy efficiency

through all its applications and reduce the environmental impact. Automotive industry is aiming not only for weight reduction but good energy absorption ability. Typical placement of AHSSs in auto body parts are bumper reinforcement, crash boxes, door beams and different pillars in body structure (Demeri 2013). AHSSs with austenite-based microstructure offer a good crash performance as the material is hardened under collision. The use of sheet metal products is usually restricted to auto body parts more than heavy duty vehicles where the weight reduction is more important than crash performance.

In the engineering industry high-strength steels have been used in shipbuilding, offshore, oil and gas, pressure vessel, mobile crane, cargo container and construction applications due to their mechanical properties such as yield and tensile strength, ductility at low temperatures, formability, fracture toughness and good weldability. Some of the everyday applications are presented in Figure 12.

Figure 12. An example of the use of AHSSs in mobile applications.

Crane beam is a typical component where high formability, good weld placement and buckling resistance are needed. Other components like truck chassis and sandwich panels of cargo containers can utilize the properties of DP and CP steels, due to weight factor and good weldability.

3 WELDABILITY OF HIGH-STRENGTH STEELS

The development of modern AHSS has been significant for the past 20 years. Materials have homogeneous microstructure with low content of impurities. Majority of these steels can be found in structural applications such as offshore structures, buildings, automotive industry and shipbuilding. The requirements for each application have its own standards to meet, for instance standard EN 13001-3-1+A1 gives guidelines for crane design. In most cases, steel is the most versatile material. Microstructures are being manipulated to produce impressive mechanical properties. Mechanical properties such as tensile strength and ductility can handle extreme environmental conditions, for instance high ductility at low temperature.

One of the most important thing is the low carbon content which differs AHSS from the conventional HSS. Low carbon content improves the weldability and decreases the risk of cold cracking. On the other hand as the strength of the steel increases, the requirements of the welding process will increase even more. This is a problem, not only to steel manufacturers but also to manufacturers of the welding machines and consumables. Steels with high strength cannot be applied to any major application as it is, joining and forming are practically always needed. In terms of joining, welding is the most common technique. Welding machine manufacturers have to keep up with the progress and offer reasonable priced equipment which will meet the requirements of the industrial use. Machines can also be implemented into welding shops. Consumable selection is normally wide with lower strength levels, but when the strength level exceeds, for instance, 900 MPa the selection can be quite narrow. Consumable selection is normally based on to meet the base material requirements.

Steel manufacturers are finding novel solutions to increase the material properties without losing weldability or formability. Improved weldability can be achieved by reducing the hardenability of the steel. Hardenability can be reduced by lowering the carbon content. AHSS have a low carbon content, and therefore can be welded without preheat in most cases. As the carbon content decreases, weldability increases but at the same time strength is dropping. To compensate the loss of carbon and to increase tensile strength, small additions of alloying elements have to be introduced. Microalloying elements such as Nb, Ti and V have been used. These elements form fine carbides and nitrides. Fine-grained microstructures can be achieved because the

elements also reduce the grain size. Grain size reduction is based on the elements ability to produce fine dispersions of stable precipitates which inhibit grain growth during hot rolling. They also elevate the recrystallization temperature and assist in nucleating fine-grained ferrite during cooling. At the same time, the microstructure becomes more sensitive to high temperatures, which makes the welding harder because the properties can be lost. (Kou 2002 & Bracke 2011)

Conventional fusion welding methods such as MAG, PAW and SAW are very flexible with high deposition rate, excluding PAW. It should be also pointed out that the equipments are very affordable compared to friction stir welding (FSW) or laser beam welding (LBW) equipment. It is not profitable for a company to invest in state of the art welding station if the volumes in production line are significantly low. On the other hand, if the company has a high-end component and a few competitors then it may be profitable to invest in expensive equipment.

The joining abilities of the conventional welding methods are suitable for various metals, but new steels with ultra-high tensile strength give a great challenge for joining. One of the things is relatively low energy density and high heat input. When welding AHSSs it is essential to keep heat input as low as possible to maintain homogeneous weld joint with the base metal. Usually this kind of situation cannot be achieved and the result is more or less heterogeneous, in terms of mechanical properties and metallurgical point of view. Low energy density usually means that more thermal energy has to be put into the material to achieve a proper weld joint. As a result, the total heat input is high and the weld joint can be relatively wide. The width of the joint depends also on how thick are the base metals and what kind of groove geometry is involved. AHSSs are sensitive to high heat input which can be seen from the recommended short cooling rates. Due the martensitic and bainitic microstructures cooling times have to be kept short to minimize softening in the HAZ. When dealing with conventional welding methods this can be hard to achieve.

In welding, the hardenability of the base material is often evaluated by carbon equivalent (CE). In Europe, the most common formula for CE is the International Institute of Welding (IIW) equation. IIW formula is presented in Equation 1 (SFS-EN 1011-2).

$$CE = C + \frac{Mn}{6} + \frac{Cr+Mo+V}{5} + \frac{Ni+Cu}{15}, \quad (1)$$

where

CE = carbon equivalent [wt%]

C = carbon content [wt%]

Mn = manganese content [wt%]

Cr = chromium content [wt%]

Mo = molybdenum content [wt%]

V = vanadium content [wt%]

Ni = nickel content [wt%]

Cu = copper content [wt%].

The CE can be also used to address susceptibility to hydrogen-induced cold cracking, hardness in HAZ, necessity for preheat and steel strength based on carbon content. If the CE is relatively high it will predict the tendency for hard phase transformation which is carried out by the fast cooling rates. Hard and brittle structures are usually undesirable when joining is done by welding, so restraining the cooling rate by pre-heating will produce a better result. (Lancaster 1999)

3.1 Welding energy and heat input

In terms of arc welding, welding energy is one of the most important attributes in the process. Welding energy determines how much of energy is needed to produce fusion state conditions. The input energy, in arc welding, created by the electric arc is controlled by current, arc voltage and welding speed. The main difference between arc welding and beam welding is in the energy density. Laser beam welding is commonly used in AHSS welding. It has a high energy density value of 1000 W/mm^2, whereas conventional arc welding methods have energy density between 5 - 500 W/mm^2. This means that the melting efficiency is greater in laser beam welding and input energy is more efficiently used to establish a molten weld pool. In MAG, PAW and SAW processes the heat is distributed to a wider area, which will make the HAZ wider, and therefore undesirable for AHSSs. (Messler 2004)

Welding energy or arc energy (E) is the overall energy input that is transferred from the heat source to the workpiece. Welding energy can be determined from Equation 2 (SFS-EN 1011-1).

$$E = \frac{60*U*I}{1000*v}, \quad (2)$$

where

E = welding energy [kJ/mm]

U = voltage [V]

I = current [A]

v = welding speed [mm/min].

Welding energy is the sum of three factors which are the current, the voltage and the speed. Each of the factors affects the end result.

Heat input (Q) is one of the key figures to assess the weldability and how much the material can be exposed to thermal energy. It is a relative measure of the energy transferred per unit length of the weld. Heat input can be determined from Equation 3 (SFS-EN 1011-1).

$$Q = \frac{k*60*U*I}{1000*v}, \quad (3)$$

where

Q = heat input [kJ/mm]

k = thermal efficiency factor of the welding process.

Characteristic of heat input has a great significance for the cooling rate which is the primary factor that determines the final metallurgical structure of the weld and HAZ. Thermal efficiency factor (k) describes the amount of energy that can be transferred to the workpiece. It is the ratio between the output and the input energy. Efficiency of the heat source depends on what welding process is being used but in general factor k is always under 1. Most of the energy is lost by radiation, through the conduction, convection and metal vapor. (Messler 2004)

The distribution of the heat input against the power density is presented in Figure 13. It includes conventional welding methods and novel high energy welding methods. Like many of the AHSSs, heat input and cooling time should be kept low to achieve similar properties in the weld and HAZ like in the base material. Conventional arc welding processes tend to have a low power density which will set boundaries to the usage. Excessive heat input can occur when conventional welding methods are used. This leads to a situation where the conditions do not meet the requirements and each zone of the HAZ gets wider and softener. Mechanical properties such as yield strength and impact toughness are highly dependent on the input energy, cooling time from 800 ºC to 500 ºC, alloying, the peak temperature and its duration. At high temperatures, strengthening mechanisms can be lost. For instance, phase transformations occur through the HAZ and precipitations like Nb carbonitrides (NbCN), V carbonitrides (VCN), Ti carbides (TiC) and Ti nitrides (TiN) can be dissolved. This leads to a situation where the pinning effect is lost and grain growth occurs. (Nishioka et al. 2012 & Kou 2002 & Gladman 1997)

Increasing power density improves penetration and decreases the heat input. Commonly used high power density processes for AHSSs are laser beam welding and laser-hybrid welding which are capable of single-pass butt welds for thick plates. In terms of AHSSs, the material is for a short period of time under high temperatures and it is possible that the most stable particles like TiN do not dissolve. With low heat input the extent of grain growth decreases and the desirable microstructure can be achieved with short cooling times. (Nishioka et al. 2012 & Mitchell et al. 1995)

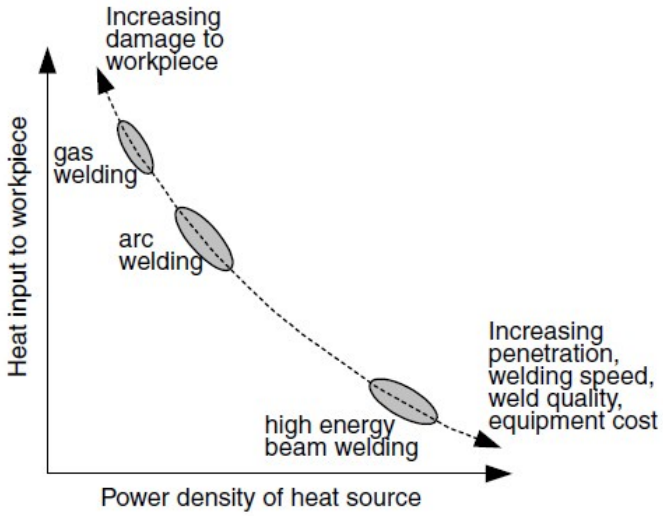

Figure 13. Relationship with heat input and power density. (Kou 2002)

Thermal efficiency factors for different fusion welding methods are (Messler 2004 & Kou 2002 & SFS-EN 1011-1):

- Plasma arc welding (PAW), k = 0,50 - 0,80
- Laser beam welding (LBW), k = 0,50 - 0,75
- Metal-inert/active gas welding (MIG/MAG), k = 0,60 - 0,85
- Submerged arc welding (SAW), k = 0,85 - 1,00.

It is not possible to give any constant thermal efficiency factor to each method because there are many variables in the process. In PAW, the efficiency varies approximately from 0,50 to 0,75 depending what plasma mode is used. In keyhole mode the efficiency is much higher than in melt-in mode because the reflectivity is not a problem. (Kou 2002)

In LBW, the efficiency can drop to a region from 0,005 to 0,50 because of the high reflectivity of metal surfaces. The keyhole mode increases the efficiency up to 0,75. (Kou 2002 & Messler 2004)

In MIG/MAG, the heat is transferred from the consumable electrode back to the workpiece, which increases the efficiency of the arc. Also, the metal transfer mode has an effect on the efficiency. (Kou 2002 & Messler 2004)

One of the efficient welding methods is SAW. Almost all losses of the energy can be eliminated. The reason for the high thermal efficiency factor is that the arc is submerged under the flux. The flux itself and the molten slag isolate the arc from its surroundings, so almost all of the losses are eliminated. (Kou 1999)

3.2 Transformation and microstructure in the heat-affected zone

The material properties are achieved after many different manufacturing stages. During the rolling and the cooling stages, a fine and homogeneous microstructure can be accomplished. Material joining is always needed when it comes to engineering components and structures. In many cases welding is the most efficient way to produce complicated structures and therefore a necessary evil.

In fusion welding, thermal energy is brought to the base material to establish a joint. The heat from the source is conducted to the surrounding material. The base material experiences locally very fast heating from ambient temperature to melting point. As the material cools down it experiences a thermal cycle. The thermal cycle influences the properties of the welded joint. Especially, the maximum temperature and the cooling rate do play an important role in the resulting microstructure. The thermal cycle is effected by the following factors: dimensions and thermal conductivity of the material, thermal factor of the welding method and the welding speed.

During the welding process, the external energy creates local zones, where the material has been in its melting point and effected by the thermal cycle. This thermal cycle is causing irregularity to the material in which case the joint is the weakest link of the structure. The width of the heterogeneous area is controlled mainly by the heat input. The heat input together with the alloying elements are controlling the mechanical properties of the HAZ. The higher the heat input, the wider is the HAZ. The effects on the microstructure depend on the heat input and the cooling time. The cooling time is controlled not only by the heat input but also the plate thickness. The heat flow in the plate can be categorized into two conditions. When the plate is relatively thin, the heat flow is two-dimensional and the heat is conducted through the whole material thickness in 2D-space. As the plate thickness increases, the heat flow is three-dimensional and the heat can be conducted in 3D-space. The three-dimensional heat flow is for partially penetrated welds in thick plates. The peak temperature de-

creases more rapidly in a three-dimensional heat flow and the HAZ will be narrower. (Messler 2004)

As the heat source interacts with the material, the influence of thermal variation experienced by the material varies from region to region. This leads to a heterogeneous microstructure in the welded joint. Mechanical properties vary from zone to zone, which is not only affected by the heat input but also the filler metal. A welded joint can be categorized roughly into three different zones: the fusion zone (FZ), the partially melted zone (PMZ) and the heat-affected zone (HAZ). (Kou 2002)

For a better understanding of the microstructure, the three main zones can be divided into regions (Figure 14) which are (Bhadeshia 2006):

- Weld metal
- Fusion line
- Coarse grained
- Fine grained
- Partially austenized and tempered
- Tempered and unaffected base material.

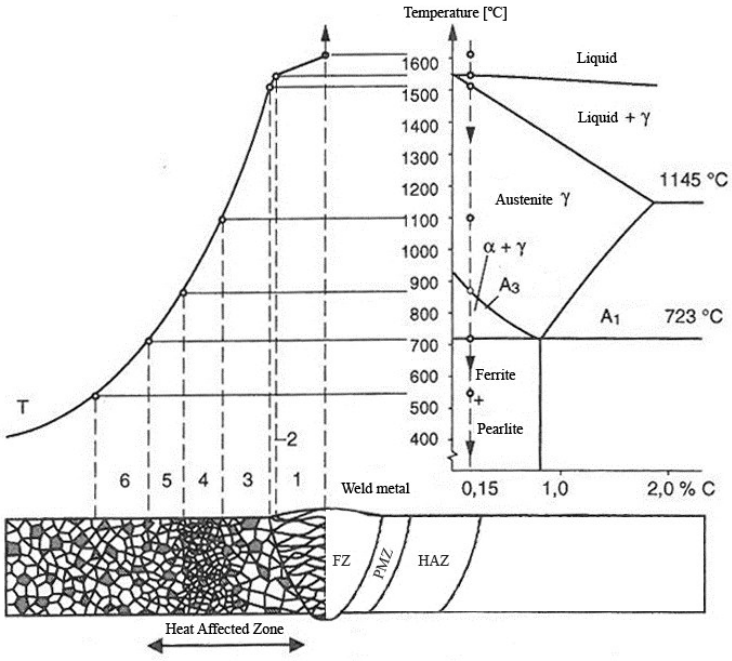

Figure 14. A schematic presentation of different regions in the welded joint. (Modified from Hitsaajan opas 2003)

The weld metal (WM) or the FZ is the weld deposit and consists of a mixture of base and filler material. The dilution of base and filler metal depends on the joint type, the joint edge preparations and the welding process. The FZ will undergo two different states, melting and solidification. In the first state, melting takes place above the liquidus temperature. The width of the FZ is controlled by the heat input. The FZ expands and the cooling rate decreases when the heat input is higher. The properties of the FZ can be affected with right consumable selection and the control of the heat input. It should be pointed out that the heat input not only affects the FZ but also the whole HAZ. (Messler 2004)

The partially melted zone is a narrow region which is located between the FZ and the HAZ. In the partially melted zone, thermal energy affected by the arc cause the temperature of the base material to rise between the liquidus and the solidus. The fusion line (FL) is located in the partially melted zone. At high temperatures microalloying elements like Nb and V are almost certainly dissolved and their ability to restrain the grain growth is lost (Mitchell et al. 1995). As a result a coarse austenite grain size can be developed. AHSSs with Ti, especially TiN particles close to the fusion boundary can constrain the growth of the grain boundaries and refine the austenite grain size even at high temperatures. Alloying elements which are even more stable at high temperatures can be used to exhibit the pinning effect against excessive austenite grain growth. Rare-earth metals (REM) can used to control the grain size at high temperatures. For instance, fine particles of oxides or sulfides containing magnesium (Mg) or calcium (Ca) are observed to establish a fine austenite grain structure (Nishioka et al. 2012). (Mitchell et al. 1995 & Messler 2004)

The HAZ can be divided into several zones depending on how the temperature has changed the microstructure. The properties will vary from region to region as a function of heat input, cooling rate and the properties of base material. The first region in the HAZ is the coarse grained heat-affected zone (CGHAZ). Coarse grained zone is placed next to the FZ and is exposed to high temperatures around 1200 - 1500 ºC. During the thermal cycle, temperature has risen over the A_3 at which point the re-transformation of austenite is completed. At high temperatures the grain size of austenite has grown and the coarsening depends on many factors. Grain size coarsening is highly dependent on the peak temperature, the time above the A_3 temperature

where the coarsening is happening and the chemical composition of the material. The presence of precipitations which are accomplished using microalloying elements such as V, Nb and Ti can be lost. At high temperatures precipitations that have a pinning effect and hence constrain the growth of the grains the effect is reduced. The most of the particles are dissolved, excluding TiN which still can be present even in extreme temperatures. TiN elevates the grain coarsening temperature. The importance of carbon content in the material is reflected to the mechanical properties of the zone. During the cooling stage, the coarse grained austenite transforms to non-equilibrium products which are highly dependent on the cooling rate. With relatively high cooling rate, hard phases can form during cooling. Hard phases like upper bainite or even martensite can form to the structure which reduces the toughness. (Messler 2004 & Bhadeshia 2006 & Kou 2002 & Easterling 1992 & Mitchell et al. 1995 & Gladman 1997)

The region adjacent to the CGHAZ is the fine grained heat-affected zone (FGHAZ). At this zone austenite grain size has decreased when compared to the CGHAZ. Fine grained zone is exposed to high temperatures around A_3 - 1200 ºC which has become fully austenitic due to the thermal cycle. Although the temperature has been high and the structure has been in austenite region, the transformation from ferrite to austenite has not had the time to develop properly. Therefore, the grain size of austenite remains small and the large grain boundary area favors nucleation of fine ferrite grains. In the cooling sequence the transformation from austenite to ferrite leads to more desirable ferritic phases than in the CGHAZ. This leads to a better toughness but hardness is decreased. Because of the thermal cycle, the homogenization of austenite is not carried out perfectly, which can lead to a higher fraction of hardening ferritic structures. Transformation to martensite may occur because of the retained austenite has been enriched by carbon. (Bhadeshia 2006)

The region adjacent to the FGHAZ is the intercritical heat-affected zone (ICHAZ). It can be also referred to partially austenized heat-affected zone. ICHAZ is exposed to temperature range around A_1 - A_3, where the structure cannot transform entirely to austenite. The part that does transform to austenite has a higher carbon concentration. Due to the carbon enriched austenite, hard ferritic structures (e.g. martensite) may occur if the cooling rate is relatively high. This can lead to a situation where the

structure has local zones which are harder than its surroundings. If the cooling rate is low, the martensitic structure will not occur and the austenite region transforms to various structures. These structures can be decomposed to a mixture of coarse cementite and ferrite. (Bhadeshia 2006)

The outer part of HAZ is the subcritical heat-affected zone (SCHAZ) which is exposed to temperatures below A_1. In this region the temperature has not reached the austenite region and the part that has not been transformed to austenite becomes tempered. In AHSSs, this region is tempered martensite or bainite. In addition to tempered structure, the nucleation and spheroidization of carbides occurs. This is because spheroidization of the pearlite carbide plates occurs as a result of tempering. The longer the base material is exposed to temperatures just below the A_1, the greater the spheroidization. In some steels this can cause hardening, especially if there are higher concentrations of Mo, V, W, Ti and Cr available to produce fine alloy carbide dispersions. (Bhadeshia 2006 & Kou 2002)

As a result of welding, the structure has discontinuity which weakens the properties. The width of each zone and their properties are controlled through the heat input and cooling rate. The limitations of heat input for each individual material should be known to minimize the grain growth, and hence the material properties. If the limitations cannot be followed, the design of the welded structure does play even more important role.

3.3 Cooling time $\Delta t_{8/5}$

Cooling time together with heat input is one of the factors which can be used to determine the resulting microstructure. It is required for AHSSs to minimize the use of heat input and keep the cooling time short to establish mechanical properties that are similar with those of the base material.

Cooling time represents the time that it will take to a welded joint to cool down from 800 to 500 ºC ($\Delta t_{8/5}$). It will define what kind of microstructure the welded joint is going to have. This is because the phase transformation on a cooling stage in AHSS starts at around 800 ºC and finishes at 500 ºC. Austenite regions will decompose to various ferrite morphologies. As the $\Delta t_{8/5}$ decreases the cooling rate increases and the hardness in HAZ increases. The decomposition of austenite can be evaluated from

the continuous cooling transformation diagram (CCT). The microstructure in the HAZ can have many different phases which highly depend on the $\Delta t_{8/5}$ and the composition. At higher cooling rates structure can form into martensite and as the cooling rate decreases bainite and other ferritic products can form.

Cooling time is affected by following factors such as heat input, thermal conductivity, preheat temperature, plate thickness and joint configuration. Heat input is commonly used factor to evaluate how much energy is put into the material being welded. It is controlled by the welding current, the voltage and the welding speed. Increased heat input increases the area of the weld and width of the HAZ, therefore the cooling time is elevated. (Kou 2002)

Thermal conductivity is a physical property of a material which has an important influence on the heat input and cooling time. As the thermal conductivity factor increases the ability to conduct heat improves but higher heat input is needed to bring the material to fusion state. This has an effect also on the HAZ and its width, and through that the cooling time. (ASM Handbook 2004)

Preheat temperature is the temperature where the base material is heated before welding. Preheating is used to control the cooling time and to avoid excessive hardening, and hence undesired microstructures. It is often required when welding high carbon steels with thicker plates. The most of the commercially available AHSSs do not need preheating because of the low carbon content. If preheating is needed in AHSSs it is used to prevent hydrogen cracking and maintain hydrogen in low levels. (Kou 2002)

Together the plate thickness and the joint configuration define what are the conditions for the heat flow. Two different conditions for the heat flow can be established. If the plate is relatively thin, the heat flow is two-dimensional and the heat is conducted through the whole material thickness in 2D-space. This is a common situation for single-pass welds, where the heat can be conducted only in two directions. As the plate thickness is increased, the heat flow is three-dimensional and the heat can be conducted in 3D-space. The three-dimensional heat flow occurs in thicker plates when the weld is partially penetrated. The peak temperature decreases more rapidly

in a three-dimensional heat flow and the HAZ will be narrower. Cooling time can be calculated for the two-dimensional heat flow from Equation 4 (SFS-EN 1011-2):

$$\Delta t_{8/5} = (4300 - 4{,}3 * T_0) * 10^5 * \frac{k^2 * E^2}{d^2} * \left[\left(\frac{1}{500 - T_0}\right)^2 - \left(\frac{1}{800 - T_0}\right)^2\right] * F_2, \quad (4)$$

where

$\Delta t_{8/5}$ = cooling time from 800 to 500 ºC [s]

T_0 = working temperature [ºC]

d = material thickness [mm]

F_2 = shape factor for 2D heat flow.

Cooling time can be calculated for the three-dimensional heat flow from Equation 5 (SFS-EN 1011-2):

$$\Delta t_{8/5} = (6700 - 5 * T_0) * k * E * \left(\frac{1}{500 - T_0} - \frac{1}{800 - T_0}\right) * F_3, \quad (5)$$

where

F_3 = shape factor for 3D heat flow.

Both factors F_2 and F_3 vary as the joint type and number of runs changes. Situation where the plates are welded in single-pass to butt joint, both F_2 and F_3 have the value of 1. (SFS-EN 1011-2)

To separate two-dimensional heat flow and three-dimensional heat flow, Equation 6 can be used to determine the critical plate thickness (d_{cr}). (den Ouden 2009)

$$d_{cr} = \sqrt{\frac{\alpha Q}{2\lambda}} \left\{\frac{1}{500 - T_0} + \frac{1}{800 - T_0}\right\}, \quad (6)$$

where

d_{cr} = critical plate thickness from 2D to 3D heat flow [mm]

α = thermal diffusivity [m^2/s]

λ = coefficient of thermal conductivity [W/m*K].

4 WELDING METHODS AND MECHANICAL TESTING

4.1 Plasma arc welding

Plasma arc welding (PAW) is a fusion welding process where a nonconsumable tungsten electrode produces an arc to a workpiece. Welding can take place with or without a filler metal. It can be divided in two methods: plasma melt-in and plasma keyhole welding, depending is the arc power density high enough. PAW process is quite similar to Tungsten Inert Gas (TIG) welding process. The differences between these two methods are in the arc. The arc in the PAW process is constricted because of the converging action of the orifice plasma nozzle (Figure 15). Because of this PAW has a great energy density, high heat content, stable arc, deep penetration, high welding speed and clean welds. (Messler 2004)

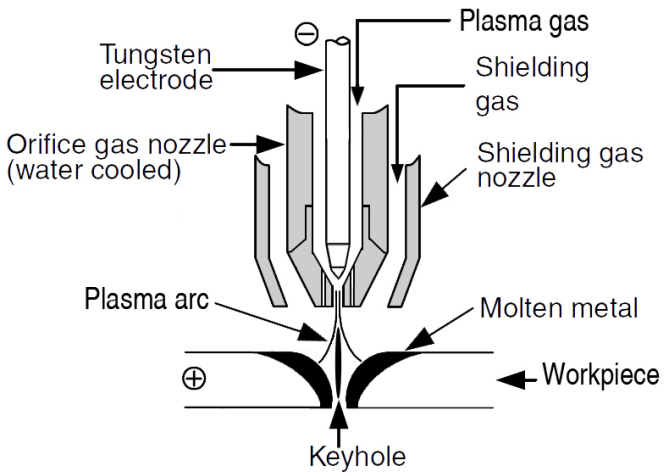

Figure 15. Plasma arc welding process. (Modified from Kou 2002)

In PAW process the plasma itself is generated by constricting the electric arc passing through the orifice of the nozzle and the hot ionized gases that are forced through this opening. Constricting keeps the plasma quite columnar which gives the high energy density and great amount of kinetic energy to the plasma jet. (Messler 2004)

The plasma arc works as a high intensity heat source that is the outcome of multiple phases. Plasma is the ionized state of a gas that consists of a balance of negative electrons and positive ions. Balance between electrons and ions maintains charge neutrality. Both of the electrons and ions are created by thermionic emission. Without the ionized path welding current cannot be transferred to the workpiece. Thermionic

emission is created in an inert gas environment to have a greater current intensity. As said, electrons and ions are created in emission where the heat-induced gas flow is in touch with the electrode and colliding electrons and atoms. As the ionized path is formed between a cathode (-) and an anode (+) current can be conducted to the workpiece. Conduction of the current is mostly handled by the electrons, because of their smaller mass and higher mobility. To have a neutral plasma state equilibrium temperature is required for accomplishment. (Messler 2004)

4.1.1 Keyhole plasma arc welding

PAW can be classified either with conventional gas shielded arc welding methods like TIG or high density welding methods like laser beam welding. PAW is a combination of plasma arc fusion welding and plasma arc cutting. Keyhole welding is possible only when arc power concentration is high enough. (Martikainen 1989)

As said, when the density of the energy is high enough keyhole is formed through the material thickness. The energy density in keyhole mode is typically around 10^9 W/m^2. This means that the concentrated thermal energy is much greater than the rate at which the heat is being conducted away from a workpiece, and hence temperature raises and causes melting. As the plasma jet is focused on to a solid material the surface heats up quickly and the temperature exceeds the boiling point. The high energy is concentrated in a spot and it will start to form of vapor to the center of liquid metal. Pressure from escaping vapor pushes down the molten metal and absorbs even more the energy of plasma. Material is in a state in which its sections are molten and boiling at the same time. As a result, a vapor cavity through the material thickness forms and is known as the keyhole (Figure 16). After the keyhole forms the vapor cavity moves along through the material and the keyhole mode is on as long as the welding continues. Behind the keyhole metallic continuity is established and weld solidification takes place once the molten metal flows backwards to close the gap under surface tension forces. To maintain the keyhole mode, welding parameters must be balanced with each other. Deeply penetrating keyhole plasma is capable of single-pass welding with relatively wide range of material thicknesses. Keyhole mode is suitable for material thickness within the range of 3 - 8 mm in carbon steels. (Messler 2004)

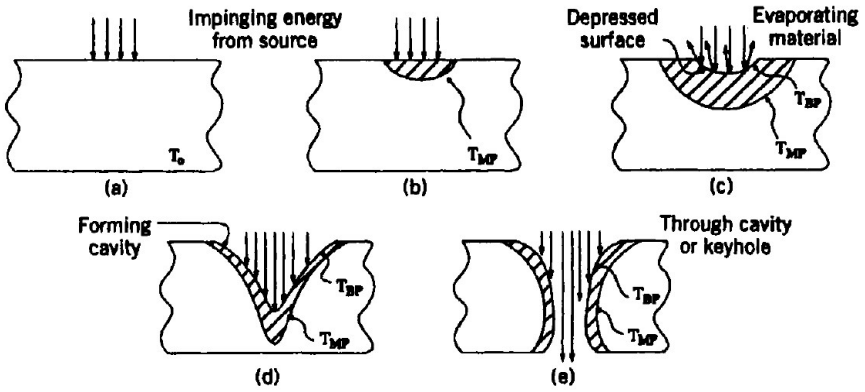

Figure 16. A schematic presentation of a keyhole mode. (Messler 2004)

The narrow parameter window associated with the keyhole conditions limits its wide application, especially for welding thicker plates. The keyhole mode of welding is the primary attribute of high-power-density welding processes that can penetrate thicker workpieces with a single-pass and produce welds with a high aspect ratio. Keyhole PAW is more cost effective and more tolerant of joint preparation. (Messler 2004)

In keyhole PAW the quality of the weld depends on the keyhole stability which itself depends on a large number of factors, especially the physical characteristics of the material to be welded and the welding parameters to be used. In normal keyhole PAW the keyhole is maintained open and stable to ensure weld quality. To this end, the welding parameter, especially the welding current has to be within a narrow range. If the welding current is a little lower, the keyhole may be closed, but if the welding current is a little higher, the keyhole expands too large and there is a tendency for the molten metal to be blown away from the weld pool. This will cause melt-through or cutting instead of joining. (Messler 2004)

4.1.2 Welding parameters

In order to have a stable welding process all the parameters must be on balance. The welding parameters must be carefully balanced to maintain the stability of the keyhole and weld pool. When the keyhole becomes unstable it can easily generate weld defects, for instance penetration can be excessive or insufficient. In addition undercutting can also take place from a faulty plasma gas flow or welding speed.

Conventional plasma torches where the plasma is mechanically constricted by the nozzle, welding currents tend to be under 250 A. As the current increases 250 A and higher, the keyhole becomes unstable and double arcs are involved. This is due to the fact that the outer layers of cold gas that normally isolate the plasma from the nozzle are destroyed. (Martikainen 1989)

The electrode tip and its angles have a significant effect on weld pool shape and penetration. In TIG welding the electrode has only one angle but when it comes to high power density processes like PAW, the electrode is usually double angled (Figure 17). As said, in PAW with direct-current electrode negative (DCEN), the power density distribution of heat source is highly affected by the shape of an electrode. The blunter the tip angle, the diameter of the arc decreases and the power density distribution increases. As a result, penetration increases and the weld gets narrower. Vice versa, if the conical tip angle of the electrode increases the arc becomes more constricted. Very sharp tips are usually operated with low currents and are more common in TIG welding. Double-angled electrode tip is a combination of good penetration ability and high power density distribution. (Kou 2002)

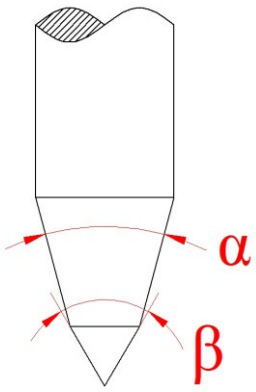

Figure 17. Double-angled tungsten electrode tip.

It should be pointed out that other parameters such as current, speed, gas and distance between the electrode and workpiece affect the angles and therefore the final power density distribution.

If filler metal is needed it can be fed in two different ways. Filler metal can be fed directly into the arc from the front of the plasma torch. Wire feed direction is then against the welding direction. Using small diameter filler metals the arc energy is not

lost. In the other method filler wire is fed directly to the molten weld pool and the wire feed direction is parallel to the welding direction. One of the disadvantages when feeding the filler metal into the weld pool is the possibility that the wire gets jammed as the weld pool solidifies.

In keyhole PAW welding current is normally placed between range of 200 - 300 A. The current affects the arc pressure and the arc temperature through ionized gas. Lack of penetration occurs if the current level is too low, which can also lead to lack of fusion. With high currents the size of the molten weld pool increases as well as heat input and cooling time.

4.1.3 Plasma and shielding gas

There are many different gases that can be used in PAW. Selections between gases are made on the basis which is the thickness of the material and what kind of material is being welded. The shielding gas and the plasma gas are often the same.

Argon (Ar) is very versatile gas which can be used in PAW. It has low ionization potential, and therefore the arc starting is easy. The plasma jet is highly dependent on the used gas and the flow rate. Used gas defines the arc temperature, and hence its penetration. With thin plates argon is quite sufficient. Keyhole is stable and heat input can be kept low because keyhole can be maintained even with high welding speed. As the plate thickness increases keyhole becomes unstable and the penetration can be lost. This can cause porosity to a weld and lack of penetration, whereas excessive plasma gas flow can cause undercutting. Too low shielding gas flow can cause damage to electrode and also oxidize the molten weld pool. (Messler 2004)

Other plasma gases can also be used. Mixtures of argon and hydrogen, and argon and helium are used. Both of the mixtures increase the arc temperature and therefore a better energy density can be established. In AHSSs, the effect of hydrogen content to the material should be known first to avoid hydrogen cracking. (Messler 2004)

4.2 Submerged arc welding

Submerged arc welding (SAW) is a common fusion welding process with consumable electrode. It is a process where the electric arc is established between the electrode and the base material, with the arc being beneath a bed of granulated flux (Figure 18). Granulated flux protects the molten weld pool and the arc from atmospheric oxidization, therefore shielding gas is not needed. As the flux covers the molten weld pool it will also increase the thermal efficiency factor, because the arc energy is not lost by radiation or convection. The generated arc produces enough heat to melt the consumable and the base material. (Messler 2004 & Kou 2002)

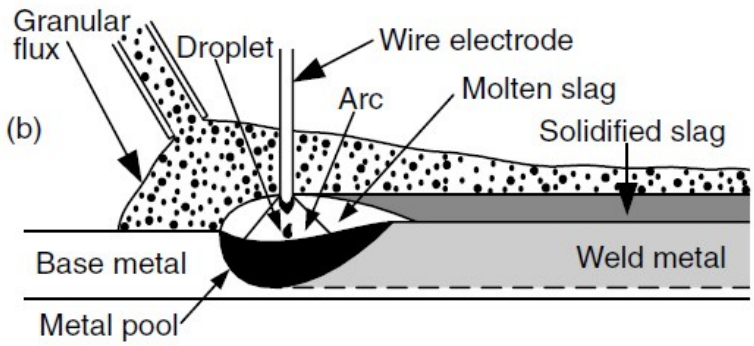

Figure 18. Submerged arc welding process. (Kou 2002)

Consumable is fed continuously from the wire feeder which is connected to the constant voltage power source. The polarity of the consumable is most often set to direct-current electrode positive (DCEP), but alternating current (AC) power source is also possible. AC power source is preferred to use when welding currents are over 1000 A to minimize arc blow. The electric arc is ignited with short-circuiting beneath the flux. Penetration is directly proportional to the welding current (e.g., 1 mm / 100 A). Both the flux and the consumable are fed continuously and the solidified slag protects the molten and hot weld metal. (Kou 2002 & Lukkari 2002)

Welding currents are relatively high, usually between 300 to 2000 A, therefore the process is always mechanized. High deposition rates (27 - 45 kg/h) can be achieved with high welding currents which makes the SAW very productive. The process can be operated with single wire or multiple wires, also strip welding is possible. Filler metal diameter can vary from 2,0 to 6,0 mm. Thin wires can be used when welding

with multiple wires, but also thicker wires can be used to increase the deposition rate. Strip welding is used for cladding. (Messler 2004 & Lukkari 2002)

The process is normally restricted to the flat and horizontal welding positions, because of the effects of gravity. With high deposition rates, the volumes of molten weld pool and slag restrict the possibilities to weld in any other positions. When dealing with high deposition rates, the heat input can be relatively high. In terms of weld quality, cooling time increases and the HAZ gets wider. In addition, backing is needed to avoid excessive penetration.

4.2.1 Welding parameters

In order to achieve a high quality weld and a stable process, welding parameters must be carefully chosen. With a proper parameter window, penetration can be controlled, weld defects can be minimized and good mechanical properties are established. The main welding parameters are welding current, arc voltage and welding speed. Other parameters such as groove geometry, filler wire and stick out have also a major influence for the final weld.

Welding current is one of the most important factor that has an effect on penetration, bead geometry and dilution. Productivity and deposition rate will increase as the current gets higher. Welding current selection is based on what kind of penetration is desired (e.g., single-pass or multi-pass weld), thickness of the base material, type of joint preparation, but also filler metal size has an effect on current range that can be used. Penetration is usually great in SAW process and therefore sensitivity for hot cracking is present. The width and depth ratio has to be controlled through the whole welding procedure to avoid and minimize hot cracking. The possibility of hot cracking is more probable when the weld is narrow and deep. The ratio should be between 1 and 2 in such a way that the width is larger than the depth. This may be an issue when welding with small diameter filler metals, because the current density is higher and the penetration may be greater than is desirable. Weld bead shape is highly depending on the current. As said, when the current increases, penetration will also increase when the current density and arc pressure rise. At the same time, the height of the weld bead grows which is undesirable in terms of fatigue life. The effect on the weld bead width is much less. (Lukkari 2002)

Arc voltage is one of the three main factors that has an effect on the welding process. The size and shape of the arc are highly depending on the voltage. Arc voltage has an influence to the width and height of the weld. As the arc voltage increases, the arc is wider and longer than with lower arc voltage. The molten consumable is spread around a larger area, because of the conical shape of the arc. The arc shape is narrow with lower voltage which concentrates the energy to a smaller area and increases the penetration. At the same time, the risk of hot cracking is increasing. (Lukkari 2002)

Welding speed is one of the factors that have a tremendous effect on the size and the shape of weld bead, and heat input. As the welding speed increases, the width of the bead and penetration are reduced. The easiest way to control heat input is via welding speed which can be reduced by enhancing the travelling speed. If the welding speed is decreased too much the penetration is not efficient anymore. This is because the contact between the arc and the base material is prevented by the molten weld pool. (Lukkari 2002)

4.2.2 Flux and consumable

Welding consumables for SAW are selected according to the requirements of the joint design. Both the filler metal and the flux are selected together to meet the requirements. The wire and the flux have an effect on the weld metal composition, and hence on the mechanical properties of the joint.

The main function of granular flux is to protect the welding process. The electric arc melts the flux and the molten slag creates a gas shield to protect the molten weld pool. Solidified slag protects the hot weld as it cools down and shapes the bead. From metallurgical point of view, the flux will deoxidize the weld pool to provide clean, high quality joints. In some situations, the flux is used to provide additional alloying elements to the weld. (Lukkari 2002)

The filler wire has generally a composition that matches with the base material. The selection is made to undermatch, match or overmatch the properties of the base material. Alloying elements are added to increase the mechanical properties and consider the issues with dilution rate. Like MAG welding, both solid and cored wires can be used in SAW process. One of the biggest advantages of cored wire against the solid

wire is the high deposition rate. Cored wire has a bigger current density than solid wire, so the electric arc melts filler metal more efficiently.

4.3 Metal-active gas welding

Gas-metal arc welding (GMAW), also known as metal-inert gas (MIG) or metal-active gas (MAG) welding is one of the most used welding methods. It combines good weld productivity, flexibility, affordable equipment price and process stability under demanding conditions. MAG welding is a fusion welding process with consumable electrode.

Welding process employs a continuous consumable filler wire as an electrode and externally supplied shielding gas. Shielding gas can be either inert or active depending on what material is being welded. Inert gases are basically used for non-ferrous materials and active gases for ferrous materials. Welding can be done either by hand-held, mechanized or robotic. Mechanization or robotization are common when welding currents are high or precision is needed. (Kou 2002)

Welding process includes filler wire which works as an electrode and is fed to the arc by the wire feeder (Figure 19). The electrode (DCEP) and workpiece (DCEN) create the electric circuit which produces the arc itself. The arc works as the heat source and creates the molten weld pool by melting base material and filler wire. Shielding gas is brought through a gas nozzle which protects the arc, the molten weld pool and the hot metal from atmospheric gases such as oxygen (O_2) and nitrogen (N_2). It also plays an important role what kind of arc is created by the ionization potential of the gas mixture being used. (Kou 2002)

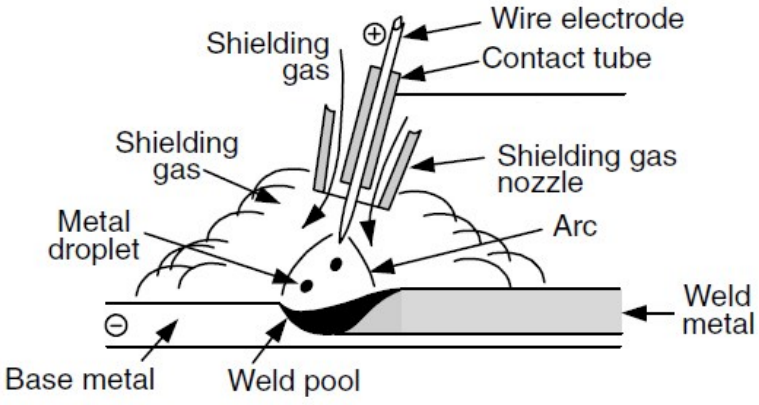

Figure 19. Schematic principle of the MAG welding process. (Kou 2002)

4.3.1 Welding parameters

The primary welding parameters in MAG welding are current, arc voltage and speed which can be used to estimate the heat input. Other factors like shielding gas, diameter of the filler metal, welding position and free wire extension have significant effects to the end result.

Welding current is one of the key factors in the process which defines how much thermal energy is put into the weld. Because of the constant voltage power source, current is proportional to the filler wire feed rate. Therefore, the higher the filler feed rate, the higher is the welding current. The level of current is set according to desired penetration and mode of metal transfer. Used current range should also follow the requirements which are set to the filler wire. Since the penetration is highly depended on current, it has significant effect on weld deposition rate and weld bead size. (ASM Handbook 1993)

Constant voltage power source is used in MAG welding which makes the arc voltage adjustable. Arc voltage is depended on current, shielding gas and wire extension. It can be adjusted during welding, so that in low voltage the arc is shorter and thermal energy of the arc is concentrated, and hence the width of the weld is decreased. An increase of voltage makes the arc longer and the arc energy is distributed more widely. This is affected to penetration in a way that molten weld pool is shallower. (ASM Handbook 1993)

Welding speed has a significant effect to heat input and penetration. Among the other parameters, speed is set to a desired level to maximize the penetration if that is the

case. Below this intermediate speed heat input and deposition per unit length has been increased. If the speed is relatively high, less thermal energy of the arc is introduced to base material, and hence heat input is decreased. On the other hand, penetration is decreased and undercutting may occur along the edge of weld bead. (ASM Handbook 1993)

Other parameters such as shielding gas and its composition have an effect on mode of metal transfer and therefore the molten metal droplet size and rate. Diameter of the filler wire is affecting current density and through that energy concentration and penetration. Welding position means in this context how the torch is placed and what is the direction of the arc pressure. The torch can be placed in pushing, vertical or pulling position. Penetration is highest in pulling where the arc pressure is pushing the molten metal backwards. Free wire extension is the distance between contact tube and the arc. Due to increased resistance in the wire, arc voltage is also increased. Excessive free wire extension affects penetration by decreasing it and desired mode for metal transfer may not work properly. (ASM Handbook 1993)

4.3.2 Modes of metal transfer

There are basically four different metal transfer modes in MAG process. Each of those can be categorized based on the used amperage and voltage. The electrical interaction with metal transfer in the arc will define the mode of metal transfer. Modes of metal transfer behave differently as the conditions change. Different transfer modes are discussed briefly. Welding consumable can transfer according to following modes (Messler 2004):

- Short-circuit transfer
- Globular transfer
- Spray transfer
- Pulsed-current transfer.

The molten metal is transferred to workpiece as the electrode tip has touched the molten weld pool and short circuiting has occurred. Molten drops are relatively large which are detached by the surface tension of the molten pool and electromagnetic forces. In short-circuit transfer mode operating amperage and voltage are low. (Kou 2002)

As the welding parameters are increased the mode of transfer changes from short-circuit to globular transfer. In this mode, molten drops are travelling in the arc without touching the wire and the pool same time. The molten drop is larger than the electrode. (Kou 2002)

Spray transfer mode can be achieved when a critical current level has been exceeded. The critical level can be estimated to be around 300 A but it can vary as the filler wire dimensions and the composition of the shielding gas are changed. Either way, the transfer mode of molten metal is no longer happening via globular transfer but through a metal spray stream across the arc gap. The increased electromagnetic force has decreased the droplet size and therefore no big individual drops are formed. Penetration is better and also the weld bead is narrow. (Kou 2002)

The final mode of metal transfer is called pulsed-current transfer. It is based on the control of the current through welding where metal transfer happens periodically. The mode has two current levels which are the pulse peak current and the background current. The background current does melt the filler wire and the peak current detaches the molten metal drop to the pool and does the penetration. At the peak current, transfer happens in spray transfer. Using pulse-transfer mode the current is not constant, and thereby the heat input can be much lower than using only spray transfer mode. (Messler 2004)

4.3.3 Shielding gas

There are many gases that can be used for protection in the MAG welding process. Selection between the gases depends on the reactivity of the metal being welded, the joint design and what kind of arc is desired. The most used shielding gases for low-alloy steels in MAG welding are argon-based mixtures with carbon dioxide (CO_2) content. The amount of CO_2 usually varies from 8 to 20 % and the selection is based on accordance to the filler wire being used. The primary use of CO_2 is to increase penetration, stabilize the arc, decrease the spray transition current and affect the weld bead shape. As the content of CO_2 exceeds over 20 %, spray transfer mode cannot be obtained and the filler metal droplet size and rate are disturbed. In addition, the arc becomes unstable and spatter level is increased. When the conditions for spray transfer mode cannot be established, the benefit of pulsed-current transfer mode is lost. The presence of active CO_2 in inert Ar is also affecting to oxidation potential in weld

metal which is reflected to mechanical properties. The amount of oxygen in weld metal is in relation to the loss of alloying elements such as silicon and manganese. Those elements are decreased in weld metal composition as the active component in shielding gas is increased. As a result, the drop of yield strength, tensile strength and toughness properties can be seen. (Kou 2002 & ASM Handbook 1993)

4.3.4 Flux-cored arc welding

Flux-cored arc welding (FCAW) is fairly similar to MAG welding. The only difference is the filler wire which is cored. The cored wires can be categorized into two groups that are self-shielding flux-cored wires and metal-cored wires. The flux-cored wire can be self-shielding, and hence separate shielding gas is not needed to protect the molten weld pool. The flux is embedded to tubular wire and the needed protection is generated of the gases that are formed from the core like in shielded-metal arc welding (SMAW). In metal-cored wires external shielding gas is usually needed and the structure of the wire is also tubular. The polarity used for FCAW can be set either DCEP or DCEN depending on the filler wire type. The concept of FCAW is presented in Figure 20. (Kou 2002)

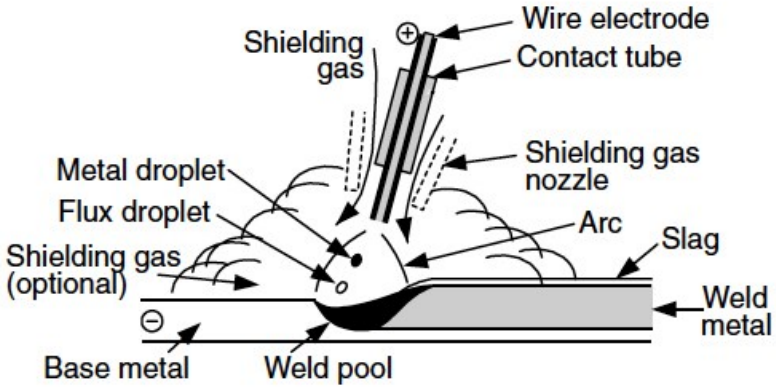

Figure 20. A schematic presentation of FCAW process.

The biggest advantage of FCAW is high deposition rate which is caused by the relatively high current density in the electrode tube. The high current density in the tubular means that less energy is needed to melt the wire than in the case of solid wire, therefore higher wire feed rates can be used. The arc energy in FCAW is distributed to wider area than in MAG which constrains the penetration, especially in single-pass

butt joints. In MAG, arc energy is more concentrated because the whole cross-section of the wire can conduct the current. (Messler 2004)

4.4 Cooling time determination with thermocouples

When two conductors of different materials are joined at the one end, a voltage is produced that increases in magnitude as the temperature difference between the joined end (T_1) and the open end (T_0) increases (Figure 21). The open end is connected to a meter that automatically measures the voltage and corrects for effects caused by the temperature at the open end. The current temperature is then displayed to a measuring instrument. (Kerlin 1999)

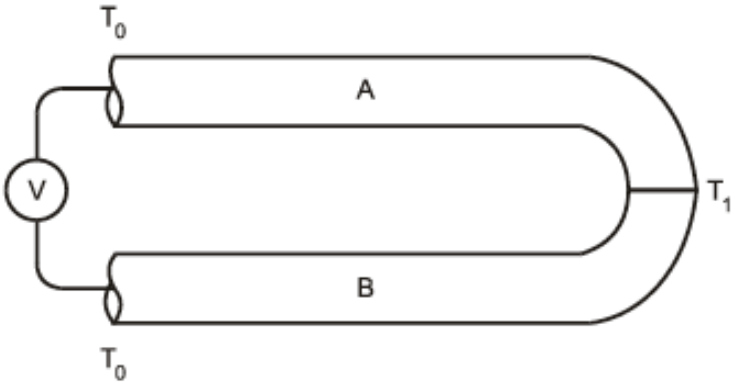

Figure 21. A schematic presentation of thermocouple element. (Kerlin, 1999)

What happens inside of the conductor, is that the density of free electrons varies and the conductor experiences an electrical potential. In high-temperature region (T_1) electrons have a higher kinetic energy than those in region T_0 where the temperature is lower. This local electron fluctuation causes production of a potential difference along a wire that experiences a temperature gradient. The magnitude of the effect depends on what kind of composition the conductor has and its metallurgical state. The wires (A and B) are made of different materials so they have different tendencies to generate variations in free electron densities and therefore they produce different electrical potentials. Results in potential differences are shown at the open end and it is called open-circuit voltage. In open-circuit voltage the voltage is produced in the absence of electrical current. A current would reduce the differences in free electron densities if it was present. (Kerlin 1999)

Thermocouple elements, in other words two wires can be fused together or spot welded directly to an object to be measured. These are basically the same thing, but sometimes the application may affect the way how the wires can be placed. Only thing that matters is to know thermocouple´s temperature measuring capability and follow those.

There are many different thermocouple wires. Each of them has a specific purpose, depending on what temperature range and accuracy are wanted to measure. Specimen size is also important. American National Standard Institute (ANSI) gives eight standard types of thermocouples. Each of these has their own letter designation such as J, T, K, E, N, S, R and B. The differences between the thermocouple types are in composition, temperature range and tolerance. For instance, the thermocouple type K has a typical temperature range of -200 to 1250 °C with composition of nickel - chromium alloy vs. chromium or nickel - chromium alloy vs. nickel - manganese - silicon - aluminium alloy. It should be pointed out that there are some variations in the main compositions because of different manufacturers.

In welding, thermal cycles are fast and therefore hard to measure. Because of this the sampling interval of the thermocouple element and the recording device has to be high enough. Typically the sampling interval is higher with small diameter wires, but also the type of the thermocouple has an effect on this. Different types of thermocouples have a different Seebeck coefficient (μV/°C) which is a physical property of a material and does vary with temperature. The lower the Seebeck coefficient is, approximately 10 μV/°C, the lower sensitivity it has. Lower sensitivity means that those are usually used only for stable high temperature measurements and are not capable to register quick changes in temperature. (Kerlin 1999)

4.5 Destructive testing

4.5.1 Hardness testing

In engineering, hardness represents materials ability to resist local deformation. Indentation is carried out by using a round ball or a diamond point which is pressed against the sample. Indentation results from plastic deformation under controlled conditions of load. The size or the depth of the indentation is measured and turned into hardness number. There are many different hardness testing methods but the

most commonly used are Brinell (HB), Vickers (HV) and Rockwell (HR). The principle of Vickers hardness testing is presented in Figure 22. (Callister 2007)

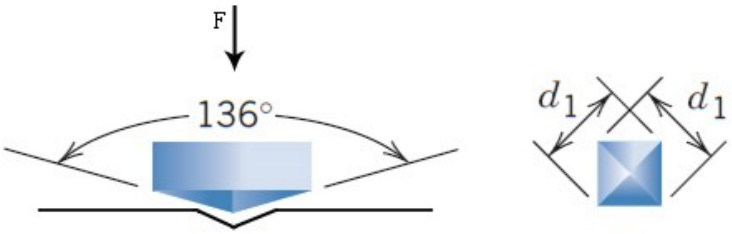

Figure 22. Vickers hardness testing. (Modified from Callister 2007)

Correlation between hardness value and tensile strength can be done because both of these factors are indicators of metals resistance against the plastic deformation. This approximation can be used to define tensile strength based on hardness values. (Callister 2007)

4.5.2 Tensile testing

Strength represents materials ability to resist deformation which can be measured with tensile test. In tensile testing, sample is gradually pulled with an axial force until it reaches its ultimate tensile strength and breaks. The principle of tensile test is presented in Figure 23.

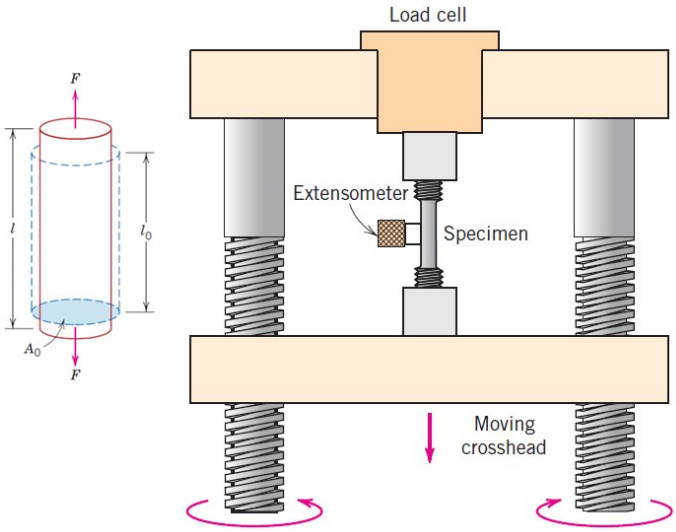

Figure 23. Tensile testing. (Modified from Callister 2007)

The specimen cross-section can be either circular or rectangular which is placed between the jaws from both ends. An extensometer is then placed to the middle section of the specimen to measure displacement during tension. During the slow load rate, material is deformed to its breaking point. Several properties of the material can be found out from the results such as yield strength, tensile strength and elongation. (Callister 2007)

4.5.3 Charpy-V impact testing

The standardized Charpy impact test is designed to measure the toughness of materials and the impact loading in multi-axial stress state. The specimen absorbs part of the pendulums energy which indicates how much energy is required to fracture the specimen. In the Charpy-V impact test, the notched specimen is placed from the both ends to the anvil. The pendulum hammer is released from the starting position and struck from the opposite side to the notch. The principle of impact test is presented in Figure 24. Rising of the hammer continues to a maximum height which is lower than the starting point. The difference between start and end point determines the energy absorption, and hence is the measure of impact energy at specified temperature. This will represent material behavior and the changes in ductility when the conditions vary. (Callister 2007)

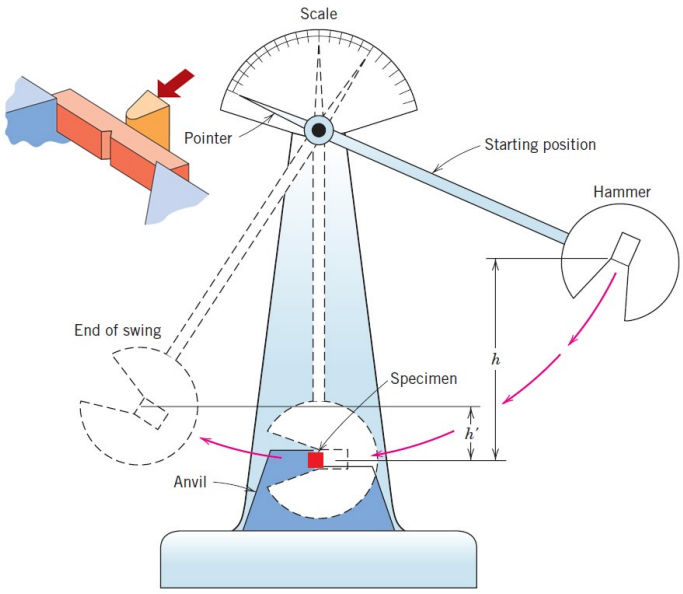

Figure 24. Charpy impact test equipment. (Modified from Callister 2007)

The standard full-size Charpy-V impact test specimen is 10 * 10 * 55 mm by its height, width and length. When the standard specimens cannot be used, the specimens are called sub-sized, due to reduced thickness. Typical size for sub-sized specimens are 7,5 * 10 * 55 mm, 5 * 10 * 55 mm and 2,5 *10 * 55 mm. (SFS-EN ISO 148-1)

Materials with body-centered cubic crystal structure show a characteristic S-shape curve of the impact energy versus temperature. In the upper shelf region the material absorbs a lot of energy and behaves in a tough manner. At low temperature, in the lower shelf, only a small amount of impact energy is absorbed and brittle fracture occurs. This kind of behavior is called ductile-to-brittle transition (DBT). (Callister 2007)

Correlation between a sub-sized specimen and a full-size specimen can be carried out basically by using two different methodologies. The first way is to correct sub-sized specimens to correspond full-size specimens by constant multiplier. This is done directly to impact energy of sub-sized specimen using a factor of 3/2 for 5 * 10 * 55 mm and 6/5 to 7,5 * 10 * 55 mm. Due to simplicity, it is very straightforward procedure to estimate the impact energies of full-size specimen. The biggest problem of this method which should be considered is the fact that as the specimen thickness is reduced, the thickness yields different effects in different regions in the transition curve. This can be seen from the lower shelf region where the sub-sized specimen can produce higher impact energies as compared to full-size specimen. Behaviour on the upper shelf region is opposite where the sub-sized specimen yields equal or lower impact energies than the full-size specimen. Due to different fracture micromechanisms, it does provide different specimen thickness effects, and thus the results should be handled with caution. (Wallin 2011)

The second way to correct the sub-sized specimens to correspond the standard full-sized specimens is based on transition temperature criterion. A lot of samples are required to produce a transition curve from which the transition temperature of a given material is determined by the 28 J impact energy level criterion. Transition temperature is then corrected to correspond standard full-size specimen by using a certain formula. Corrected transition temperature is a little higher than the sub-sized transition temperature. (Wallin 2011)

5 TEST MATERIAL INTRODUCTION

5.1 Optim 700 MC Plus

Ruukki´s Optim 700 MC Plus is a hot-rolled structural steel which is categorized as high-strength steel and meets the requirements of EN 10149-2. The material is manufactured using thermomechanical rolling. The designation "700" means a minimum yield strength level. The letter "M" stands for thermomechanical rolling and the letter "C" refers to suitability of cold forming. Mechanical properties are presented in Table 2. In the scope of this thesis, material thickness 6 and 8 mm was used.

Table 2. Mechanical properties of Optim 700 MC Plus. (Ruukki 2013a)

MATERIAL	Yield Strength $R_{p0,2}$ [MPa]	Tensile Strength R_m [MPa]	Elongation A [%]	Impact Energy KV [J]
Optim 700 MC Plus	≥ 700	750 - 950	≥ 13	≥ 40 at -60 ℃

According to the manufacturer, yield and tensile strength are tested longitudinally to the rolling direction. Properties are guaranteed in the longitudinal and transverse directions. Impact energy is tested both in longitudinal and transverse direction. Ruukki has characterized the microstructure of Optim 700 MC Plus to quasi-polygonal ferrite and granular bainite. (Ruukki 2013a)

Chemical composition is presented in Table 3 and was provided by Ruukki. Carbon equivalent is based on Equation 1. Under normal conditions preheating in welding is not necessary.

Table 3. Chemical composition (wt%) is based on Ruukki´s cast analysis for Optim 700 MC Plus.

MATERIAL	C	Si	Mn	P	S	Al	Nb	V	Ti	CEV
Optim 700 MC Plus	0,059	0,205	1,790	0,007	0,002	0,026	0,083	0,013	0,113	0,38

As said, material is thermomechanically rolled and microalloying elements such as Ti, V and Nb have been used. These elements form fine carbides and nitrides. In addition, fine-grained microstructure can be achieved because the elements also reduce the grain size. Grain size reduction is based on the elements ability to restrict the

grain growth and they also elevate the recrystallization temperature. (Kou 2002 & Bracke 2011)

Critical zone of the welded joint is located in the FL and HAZ where the impact toughness values are dropped relatively low whether the cooling time is 5 s or 20 s. The biggest effect of the cooling time can be seen from the WM and ICHAZ (Figure 25).

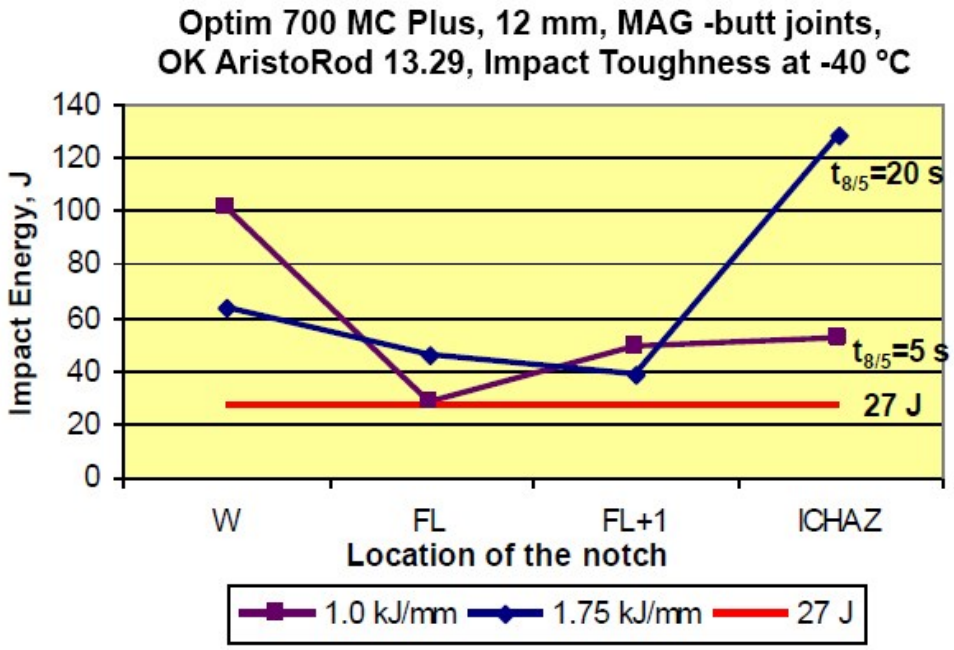

Figure 25. Effect of the heat input on impact toughness in multipass MAG welded butt joint. (Hemmilä 2011)

Undesired microstructure occurs in the WM at 20 s cooling time, whereas cooling time of 5 s provides base material-like properties. In ICHAZ, the effect of cooling time is opposite where the higher heat input provides a better impact toughness at -40 ºC. According to research of Hemmilä et al. (2011), good toughness and strength can be achieved to the welded joint when the cooling time is restricted to 5 - 20 s. The used heat input will vary depending on the plate thickness. (Hemmilä et al. 2011)

5.2 Optim 900 QC

Ruukki´s Optim 900 QC is a structural steel which is categorized as ultra-high-strength steel and meets the requirements of EN 10149-2. The material is thermomechanically rolled and quenched. The designation “900” means the minimum yield strength level. The letter “Q” stands for quenching which is carried out after hot roll-

ing. The letter “C” refers to suitability of cold forming. Mechanical properties are presented in Table 4. In the scope of this thesis, material thickness 4, 6 and 8 mm was used.

Table 4. Mechanical properties of Optim 900 QC. (Ruukki 2013b)

MATERIAL	Yield Strength $R_{p0,2}$ [MPa]	Tensile Strength R_m [MPa]	Elongation A [%]	Impact Energy KV [J]
Optim 900 QC	≥ 900	930 - 1200	≥ 8	≥ 27 at -40 °C

According to the manufacturer, yield and tensile strength are tested longitudinally to the rolling direction. Properties are guaranteed in the longitudinal and transverse directions. Impact energy is tested in the longitudinal direction. (Ruukki 2013b)

Chemical composition is presented in Table 5 and was provided by Ruukki. Carbon equivalent is based on Equation 1. Under normal conditions preheating is not necessary when welding thin plates. The hydrogen content must be kept at low level to avoid cracking. In order to maintain low hydrogen level in the weld, special attention must be paid to the right selection of the consumable.

Table 5. Chemical composition (wt%) is based on Ruukki's cast analysis for Optim 900 QC.

MATERIAL	C	Si	Mn	P	S	Al	Nb	V	Ti	CEV
Optim 900 QC	0,083	0,183	1,070	0,008	0,004	0,027	0,002	0,011	0,034	0,48

Ruukki has characterized the microstructure of Optim 900 QC to martensitic-bainitic structure. The classification can be either DP or CP because bainite can consist of several metallographic phases. Welding methods with low heat input and high energy density are recommended to use. The most suitable novel welding methods are laser and laser-MAG welding. Conventional welding method such as MAG and especially pulse-MAG can be used to achieve high quality welds. (Ruukki 2013b)

To evaluate the microstructure under different cooling rate conditions, a continuous cooling transformation (CCT) phase diagram can be used. A CCT phase diagram for Optim 900 QC is presented in Figure 26 and was provided by Ruukki.

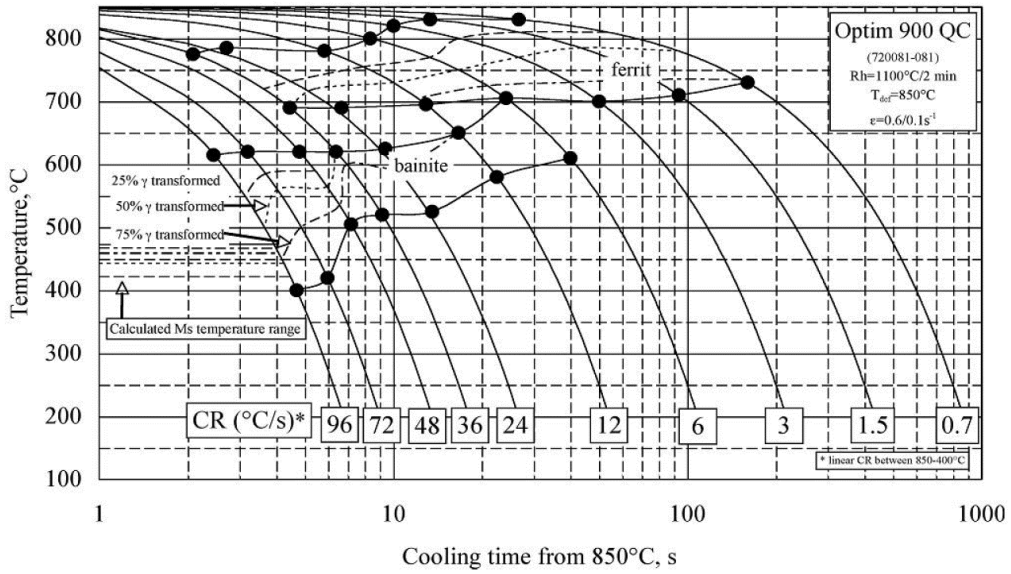

Figure 26. CCT diagram for Optim 900 QC.

MAG welding is highly used process in AHSSs welding, especially pulsed-current transfer. Compared to novel welding methods such as laser beam welding or laser hybrid welding, MAG does not have similar high power density properties. Restrictions are mainly in the field of penetration, heat input and cooling time. Requirements for groove geometry and air gap are usually needed in MAG welding, and hence single-pass weld can be harder to accomplish. Due to high power density of laser, lower heat input and cooling times are easier to achieve, which can be seen from the microhardness properties. Figure 27 presents microhardness profiles of LBW and MAG welded butt joints of Optim 960 QC which is fairly similar to 900 QC.

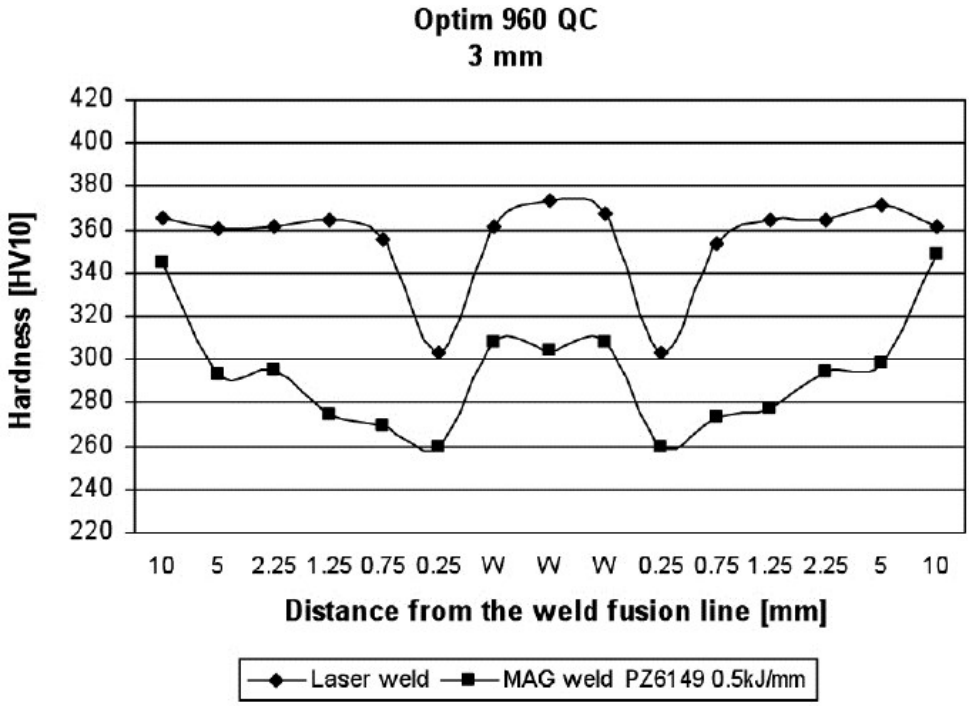

Figure 27. Hardness profile of LBW and MAG welded butt joints. (Hemmilä et al. 2010a)

The softened region in HAZ is much narrower in LBW than in MAG which can be explained by the faster cooling time. Even at 0,5 kJ/mm the hardness is dropped through the HAZ below the base material hardness in MAG process. Hardness of the weld is undermatching, whereas in LBW the hardness matches with base material properties. According to Hemmilä et al. (2010a) the narrow softened zone in LBW does not lower tensile strength properties. Heat input in MAG should be kept low to match the base material properties without exceeding 0,8 kJ/mm. Figure 28 presents how the increased heat input affects impact toughness properties of Optim 900 QC. (Hemmilä et al. 2010a)

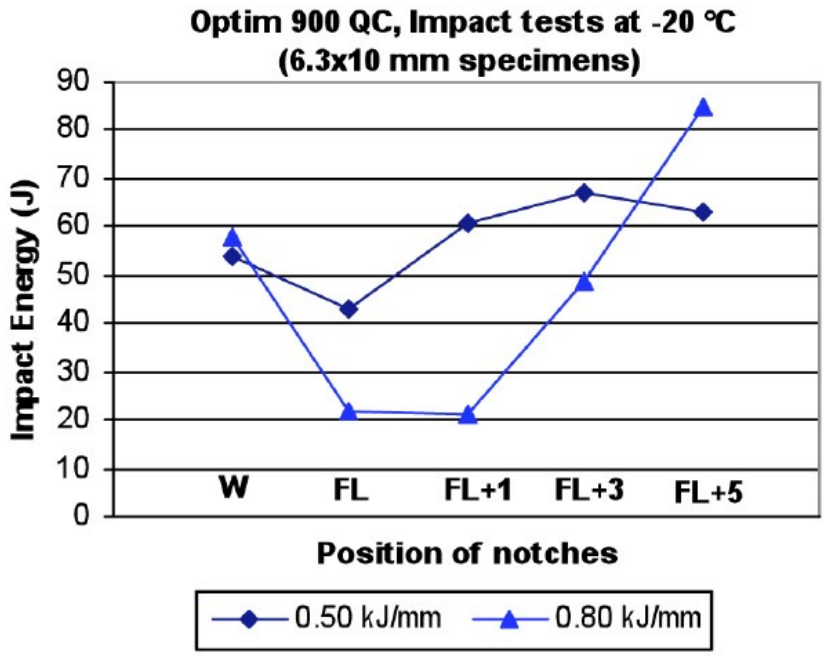

Figure 28. Effect of the heat input on impact toughness in MAG welded butt joint. (Hemmilä et al. 2010b)

Due to grain growth, impact toughness in HAZ, especially in FL and CGHAZ is dropped substantially as the heat input is increased, which should be taken into consideration in structural design. To minimize the width of the soft zones and achieve base material-like properties in weld, cooling time should not exceed 4 s (Hemmilä et al. 2010b). Figure 29 presents relationship between yield and tensile strength properties as a function of cooling time for MAG welds of Optim 960 QC.

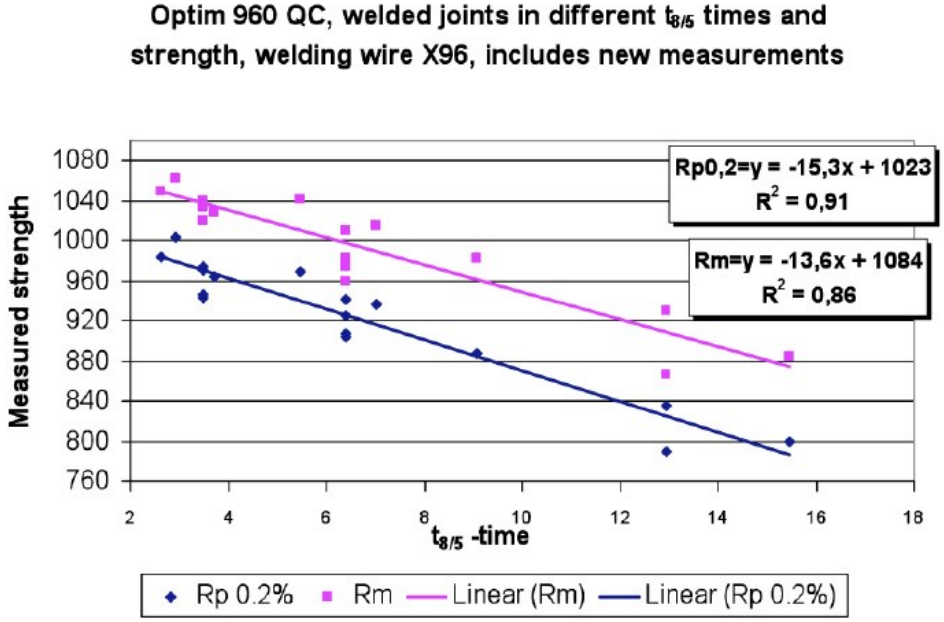

Figure 29. $R_{p0.2}$ and R_m against cooling time for MAG welds. (Hemmilä et al. 2010b)

Effect of increased cooling time on the decrease of measured strength is significant as the time increases. Short cooling times can be achieved by using LBW and laser-hybrid welding, which offer the best strength and toughness combinations for the martensitic-bainitic high-strength steel. Local softened zones near the weld can be found whatever fusion welding process is used. It is a matter of how much softening is allowable in a structure and can conventional welding process fulfill the requirement. In general, acceptable heat input for MAG or other welding process can be placed to a range of 0,5 - 0,8 kJ/mm and cooling time to 5 - 15 s for Optim 900 QC and Optim 960 QC steels. However, heat input should not exceed 0,4 kJ/mm with material thickness of 4 mm. Due to low carbon content, preheating is not necessary under normal conditions. (Hemmilä et al 2010a).

6 EXPERIMENTAL PROCEDURES

6.1 Test matrix

All the welding tests were done in the Engineering Materials welding laboratory in the Department of Engineering Design and Production at Aalto University School of Engineering.

The objective was to determine the parameter window for each welding method and material thickness. In addition, the scope was to define whether or not air gap and backing are needed. Parameter window defines limits where the welding can take place and the weld quality is acceptable. The goal was to weld a single-pass butt joint without an air gap and backing. Test procedure is presented in Figure 30.

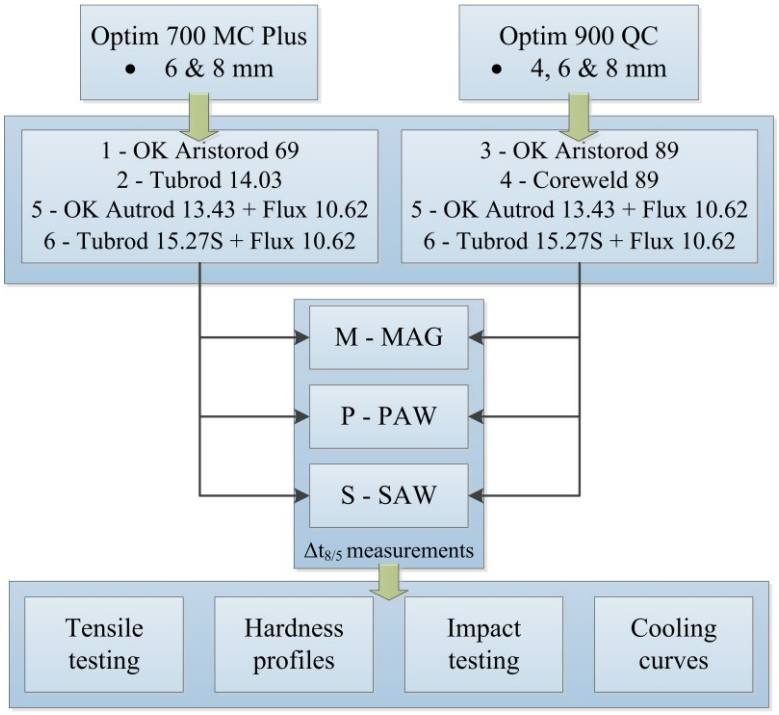

Figure 30. Test procedure for the welding tests.

The entire test matrix was based on two different grades of high-strength steels. Each of the base material has the consumables of its own. Exception was made in SAW, where both steel grades had the same consumable. Cooling time was measured in each welding test. After final welding tests; tensile testing, hardness measurements, impact testing and cooling curves were measured to evaluate the weldability.

Table 6 presents identifications for each welded sample. Sample marking includes all the designations about the base material, material thickness, consumable and the welding method.

Table 6. Sample identification.

Sample	Material	Thickness [mm]	Consumable	Welding Method
7006-1M	Optim 700 MC Plus	6	ESAB OK Aristorod 69	MAG
7006-2M	Optim 700 MC Plus	6	ESAB Tubrod 14.03	MAG
7008-1M	Optim 700 MC Plus	8	ESAB OK Aristorod 69	MAG
7008-2M	Optim 700 MC Plus	8	ESAB Tubrod 14.03	MAG
9004-3M	Optim 900 QC	4	ESAB OK Aristorod 89	MAG
9004-4M	Optim 900 QC	4	ESAB Coreweld 89	MAG
9006-3M	Optim 900 QC	6	ESAB OK Aristorod 89	MAG
9006-4M	Optim 900 QC	6	ESAB Coreweld 89	MAG
9008-3M	Optim 900 QC	8	ESAB OK Aristorod 89	MAG
9008-4M	Optim 900 QC	8	ESAB Coreweld 89	MAG
7006-1P	Optim 700 MC Plus	6	ESAB OK Aristorod 69	PAW
7006-2P	Optim 700 MC Plus	6	ESAB Tubrod 14.03	PAW
7008-1P	Optim 700 MC Plus	8	ESAB OK Aristorod 69	PAW
7008-2P	Optim 700 MC Plus	8	ESAB Tubrod 14.03	PAW
9004-3P	Optim 900 QC	4	ESAB OK Aristorod 89	PAW
9004-4P	Optim 900 QC	4	ESAB Coreweld 89	PAW
9006-3P	Optim 900 QC	6	ESAB OK Aristorod 89	PAW
9006-4P	Optim 900 QC	6	ESAB Coreweld 89	PAW
9008-3P	Optim 900 QC	8	ESAB OK Aristorod 89	PAW
9008-4P	Optim 900 QC	8	ESAB Coreweld 89	PAW
7006-5S	Optim 700 MC Plus	6	ESAB OK Autrod 13.43 + OK Flux 10.62	SAW
7006-6S	Optim 700 MC Plus	6	ESAB OK Tubrod 15.27S + OK Flux 10.62	SAW
7008-5S	Optim 700 MC Plus	8	ESAB OK Autrod 13.43 + OK Flux 10.62	SAW
7008-6S	Optim 700 MC Plus	8	ESAB OK Tubrod 15.27S + OK Flux 10.62	SAW
9004-5S	Optim 900 QC	4	ESAB OK Autrod 13.43 + OK Flux 10.62	SAW
9004-6S	Optim 900 QC	4	ESAB OK Tubrod 15.27S + OK Flux 10.62	SAW
9006-5S	Optim 900 QC	6	ESAB OK Autrod 13.43 + OK Flux 10.62	SAW
9006-6S	Optim 900 QC	6	ESAB OK Tubrod 15.27S + OK Flux 10.62	SAW
9008-5S	Optim 900 QC	8	ESAB OK Autrod 13.43 + OK Flux 10.62	SAW
9008-6S	Optim 900 QC	8	ESAB OK Tubrod 15.27S + OK Flux 10.62	SAW

* WM = Weld Metal
* FL = Fusion Line
* FL+1 = Fusion Line + 1 mm

6.2 Preliminary welding tests

The objective of the preliminary welding tests was to determine a parameter window for each welding method and material thickness before the full-scale welding tests took place. In all cases, the goal was to weld a single-pass butt joint without an air gap and backing.

The welding parameters were not selected according to any standard. All the parameters were selected based on visual inspection and macroscopic examination. Visual inspection gives a good evaluation of the geometrical dimensions and surface defects of the weld. The weld penetration, lack of fusion and other internal weld defects can be seen from the macroscopic examination of the weld cross-section.

The most important welding parameters such as the wire feed rate, the welding speed and the current were adjusted in order to maintain acceptable weld quality. The target was to keep the heat input as low as possible but still to achieve a single-pass butt weld. The need for the air gap was evaluated according to the penetration. In the preliminary welding tests plates were 100 * 300 mm. Both, preliminary and the final welding tests were made at room temperature of 20 ºC.

The selection of the consumables was based on Ruukki´s and Esab´s recommendations. Shielding gas and flux was selected according to the consumable. The diameters of the different consumables were selected based on experience.

6.3 Sample preparation

All the test plates were welded with single-pass butt welds in flat position (PA). In flat position two plates are flat and parallel to each other. Dimensions for the test plates were 200 * 600 mm with 4 mm, 6 mm and 8 mm thickness. Plates were laser cut with squared edges. Joint preparation for the butt joint is presented in Figure 31.

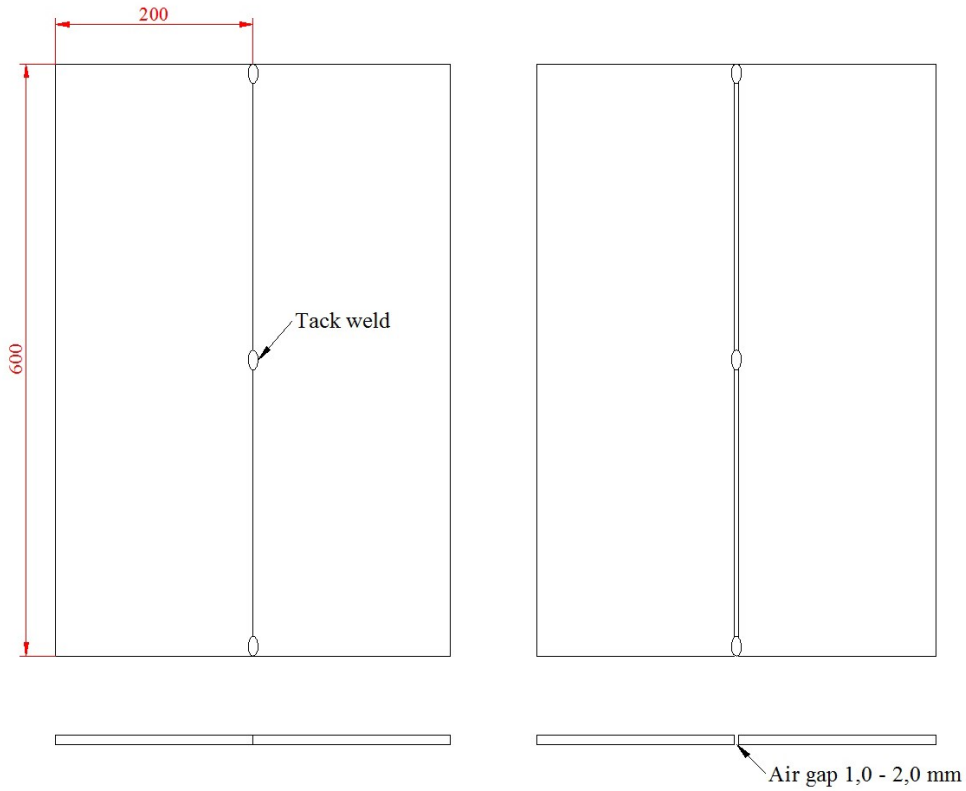

Figure 31. Test plate dimensions and joint preparation.

Plates were tack welded together from both sides. Tack welds were placed at both ends and the middle section using TIG welding. After tack welds the oxide layer was removed by grinding using nylon sanding fleece disk to keep the surface smooth and avoid electrode contamination in PAW. All the dirt and grease was removed using ethanol (C_2H_5OH). The need for an air gap was based on the preliminary welding tests. Air gap was used only in MAG welding and it varied from 1,0 mm to 2,0 mm.

All the plates were heavily clamped to the welding jig to avoid any misalignment, movements or thermal distortions during welding.

6.4 Consumables for welding

The selection of the consumables was based on Ruukki´s and Esab´s recommendations. The higher the strength of the steel is, the more difficult it is to find commercially available consumables that match with the base material. Steels with high-strength are usually welded with a matching consumable to achieve the maximum benefit of mechanical properties of the base materials. Undermatching consumables can also be used if the structural design allows it. In this thesis, there were two dif-

ferent types of wires involved, solid and cored wires. All the consumables were supplied by Esab.

The following Esab consumables were used for the Optim 700 MC Plus:

- OK AristoRod 69
- OK Autrod 14.03
- OK Autrod 13.43 + OK Flux 10.62
- OK Tubrod 15.27S + OK Flux 10.62.

For the Optim 900 QC the consumables were:

- OK AristoRod 89
- Coreweld 89
- OK Autrod 13.43 + OK Flux 10.62
- OK Tubrod 15.27S + OK Flux 10.62.

The diameter of the filler metal was 1,2 mm for MAG and PAW, excluding SAW where the wire diameter was 3,0 mm. Figure 32 presents the yield strength values for each filler metal. Consumables are more alloyed than the base material, due to dilution. Higher alloying content is used to prevent the effects of dilution, when the weld metal can be markedly undermatching.

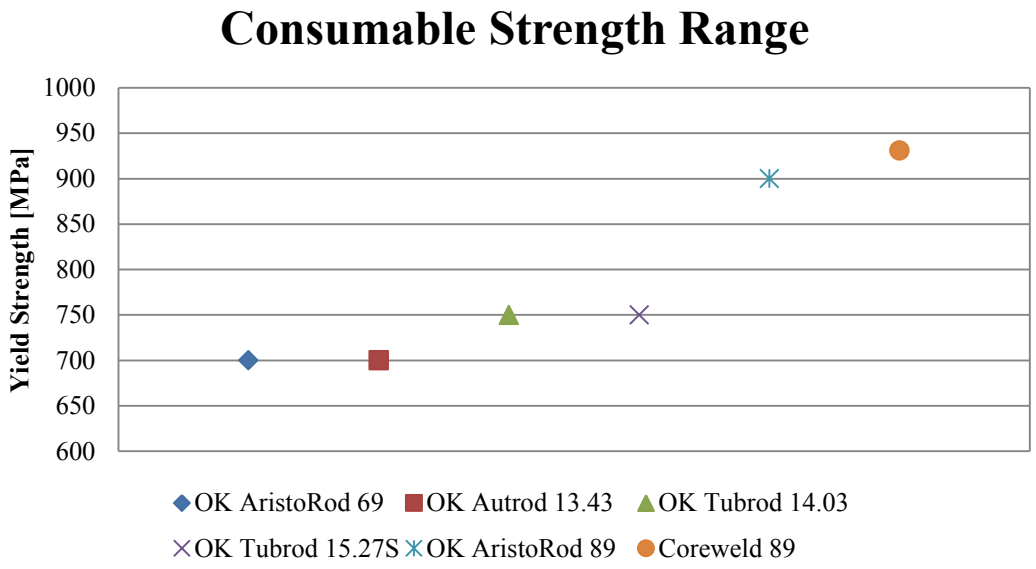

Figure 32. Yield strength range of the consumables.(Information from Esab Welding Handbook 2007 & Esab 2014a & Esab 2014b)

OK AristoRod 69 is a Cr-Ni-Mo alloyed solid wire. It is used for high-strength steels such as Optim 700 MC Plus and has yield strength of 700 MPa. Ni content is increased to improve impact toughness at low temperatures. Recommended shielding gas for the wire is 20 - 21 % CO_2 with argon base (Esab Welding Handbook 2007).

OK Autrod 14.03 is a Ni-Mo alloyed metal-cored wire which has a good ductility at low temperatures, due to high Ni content. The wire has yield strength over 700 MPa and is suitable for Optim 700 MC Plus. Recommended shielding gas for the wire is 20 % CO_2 with argon base. (Esab Welding Handbook 2007)

OK Autrod 13.43 is a Cr-Ni-Mo alloyed solid wire for SAW with yield strength over 690 MPa. The wire combines two features, high strength and good low temperature impact toughness. Recommended flux for the wire is OK Flux 10.62. (Esab Welding Handbook 2007)

OK Tubrod 15.27S is a Ni-alloyed basic-cored wire for SAW with a minimum yield strength of 750 MPa. Recommended flux for the wire is OK Flux 10.62. (Esab Welding Handbook 2007)

OK Flux 10.62 is a high-basic flux with no alloying elements and it is suitable for low-alloyed high-strength steels. It is used for SAW together with OK Autrod 13.43 and OK Tubrod 15.27S. (Esab Welding Handbook 2007)

OK AristoRod 89 is designed for steels with yield strength over 900 MPa. It is a Cr-Ni-Mo alloyed solid wire with good low temperature ductility. Recommended shielding gas for the wire is 18 % CO_2 with argon base. (Esab 2014a)

Coreweld 89 is a low-alloyed metal-cored wire with minimum yield strength of 900 MPa. The wire combines two features, high strength and low hydrogen content. High Ni content improves impact toughness at low temperatures. Recommended shielding gas for the Coreweld 89 is 5 - 25 % CO_2 with argon base. (Esab 2014b)

6.5 Test equipment

6.5.1 MAG welding

MAG welding equipment is presented in Figure 33. Welding was carried out by using Kemppi FastMig Pulse 450 DC power source with maximum current of 450 A. Power source was connected to FastMig MXF 65 wire feeder unit. Welding was done in flat position on one side using mechanized welding. Mechanization was carried out by using KemecWeld KCU 101 welding station. All the MAG welded butt joints were done using synergic pulse mode.

Figure 33. Kemppi FastMig Pulse 450 power source and FastMig MXF 65 wire feeder.

Heat input is traditionally calculated from the average amperage and voltage using Equation 3. Kemppi´s FastMig Pulse 450 power source has an algorithm which measures amperage and voltage constantly during pulsed-current welding. As a result it will give the average amperage and voltage which is then turned into welding power (P). In the traditional U*I-method, the current and voltage are placed separate-

ly to Equation 3. According to Kumpulainen et al. (2011), the power-based heat input calculation is thus more accurate in pulsed-current welding, and therefore was used in the calculations.

Test plates were clamped to welding jig and thermocouples were prepared for cooling time measurements (Figure 34). Thermocouples were spot welded to the plate surface and plunged to the molten weld pool.

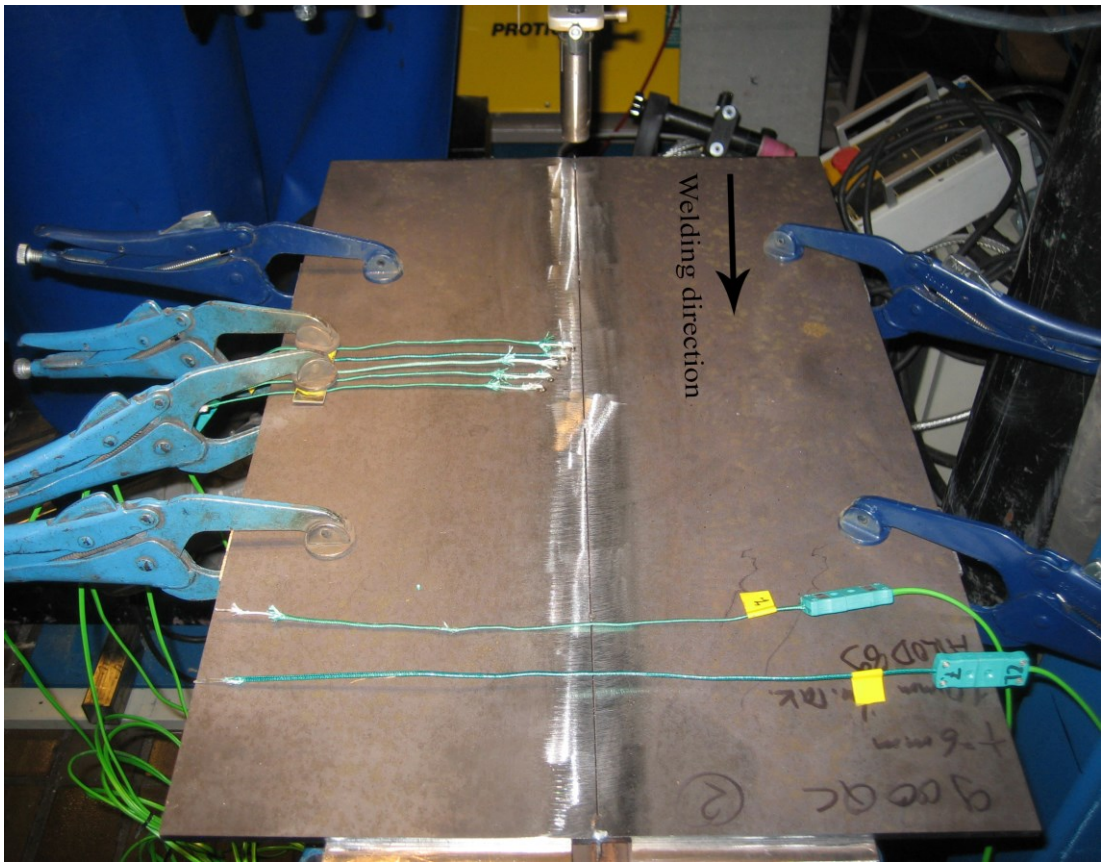

Figure 34. Test plates clamped and prepared for MAG welding. Thermocouples were used for cooling time measurements.

All the welding parameters are presented in Table 7. Heat input varied from 0,48 to 0,81 kJ/mm. The nozzle distance to workpiece was set to 12 mm. As a result, preliminary welding procedure specifications (pWPS) were made, and are presented in Appendix 1 - 10.

Table 7. Welding parameters for MAG welded butt joints.

Test case	Backing	Air gap [mm]	Welding speed [mm/min]	Current [A]	Welding voltage [V]	Shielding gas	Filler wire feed rate [m/min]
7006-1M	-	1,0	900	338	29,1	82% Ar + 18% CO_2	10,6
7006-2M	-	1,0	900	336	31	82% Ar + 18% CO_2	13,1
7008-1M	Fiberglass	2,0	700	355	25,3	82% Ar + 18% CO_2	13,2
7008-2M	Fiberglass	2,0	700	348	31,8	82% Ar + 18% CO_2	14,5
9004-3M	-	0,0	950	328	27,2	82% Ar + 18% CO_2	10,6
9004-4M	-	0,0	950	333	27,2	92% Ar + 8% CO_2	12,8
9006-3M	-	1,0	900	319	26,3	82% Ar + 18% CO_2	10,3
9006-4M	-	1,0	900	347	28,3	92% Ar + 8% CO_2	13,4
9008-3M	Fiberglass	2,0	700	360	24,9	82% Ar + 18% CO_2	13,4
9008-4M	Fiberglass	2,0	700	358	28	92% Ar + 8% CO_2	14,3

6.5.2 PAW welding

Plasma welding equipment is presented in Figure 35. Welding was carried out by using Esab LTG 400 DC power source with maximum current of 400 A. The plasma torch PTW 300 was limited to 300 A. Parameters such as current and different gas flows were adjusted using PW3000 control unit. Welding was done in flat position with single-pass weld using mechanized welding.

Figure 35. Esab LTG 400 power source, PW3000 control unit, PTW 300 torch and CW3000 wire feeder.

Selection of the nozzle was based on preliminary welding tests and Esab´s recommendation. Maximum welding current determines what size of the nozzle is recommended to use. The higher the nozzle number is the bigger the hole diameter the nozzle has.

The same tungsten electrode was used for all cases. Diameter of the electrode was 4 mm and the angles of the electrode tip were ground to the range of α = 15 - 21 degrees and β = 60 - 63 degrees. A schematic presentation of the electrode tip was presented in Figure 17.

The cold filler wire was fed directly into the arc. Wire was placed in front of the plasma torch. Wire feed direction was against to the welding direction because air gap was not involved. Based on the preliminary welding tests this worked better than feeding the wire into the weld pool. One of the disadvantages when feeding the filler

wire into the weld pool is the possibility that the wire gets jammed when the pool solidifies, and hence may cause damage to filler wire feeder mechanism.

The feed angle of the filler metal is relatively low, under 20 degrees. The wire was fed against the plate surface so that it slightly bends. Bending is needed because the distance from the plasma torch to the plate is relatively low and the wire nozzle can be damaged due to the high arc temperature. Wire feeding direction and thermocouple installation is presented in Figure 36. Camera was used for monitoring the wire and the arc.

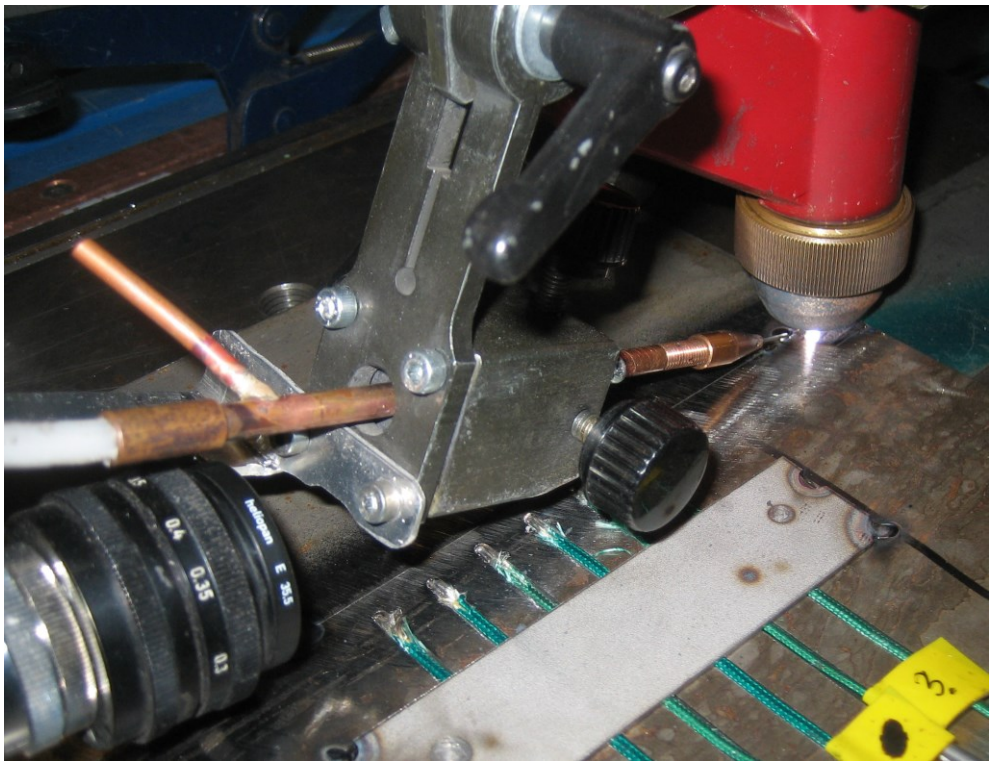

Figure 36. Test plates clamped to welding jig and prepared for PAW. Root protection was handled by backing gas. Thermocouples were spot welded to the end of the machined grooves.

Backing gas was used in all cases against oxidation. The gas for the shielding, plasma and backing was argon. The backing gas flow direction was against the welding direction and the gas flow was kept even through the entire length. The plasma torch was perpendicular to the workpiece in all cases. The plasma torch was set to distance of 5 mm from the workpiece. All the test plates were welded without the air gap.

All the welding parameters are presented in Table 8. Heat input varied from 0,54 to 1,48 kJ/mm. As a result, preliminary welding procedure specifications (pWPS) were made, and are presented in Appendix 11 - 20.

Table 8. Welding parameters for PAW welded butt joints.

Test case	Welding speed [mm/min]	Current [A]	Welding voltage [V]	Backing gas flow [l/min]	Plasma gas flow [l/min]	Shielding gas flow [l/min]	Filler wire feed rate [m/min]
7006-1P	230	231,5	27,5	17	4	17	0,35
7006-2P	220	232	27,8	17	4	16	0,30
7008-1P	180	231	28,6	17	4,5	17	0,30
7008-2P	170	230	28,8	18	4,3	18	0,26
9004-3P	350	210	24,8	20	3,5	17,5	0,42
9004-4P	320	214	26,4	17	3,5	17	0,33
9006-3P	230	231	27,5	19	4	17,5	0,30
9006-4P	230	230	27,5	17	4	17,5	0,27
9008-3P	180	240,1	27,9	18	4,5	17,5	0,25
9008-4P	170	243	28,7	18	3,7	17,5	0,33

6.5.3 SAW welding

SAW welding equipment is presented in Figure 37. Welding was carried out by using Esab LAE 1250 DC power source with maximum current of 1250 A. Welding was controlled via PEG 1 control unit. For the single wire welding, A6 SFD 1 welding head was used. Welding was done in flat position on one side using mechanized welding.

Figure 37. Esab LAE 1250 power source, A6 SFD 1 welding head and PEG 1 control unit.

Test plates were clamped to welding jig and thermocouples were prepared for cooling time measurements (Figure 38). Thermocouples were spot welded to the plate surface. Due to high welding current and arc pressure, fiberglass backing tape was used to eliminate excessive penetration. As the arc energy density is decreased, the ability to penetrate efficiently is decreased, and therefore run-on and -off plates were placed to the start and the end positions to enable the full penetrated section of the weld. In addition, the aim was to prevent the weld defects in both ends. All the test plates were welded without the air gap. The flux was in all test cases the same, OK Flux 10.62. The stick out of the wire was set to 25 mm.

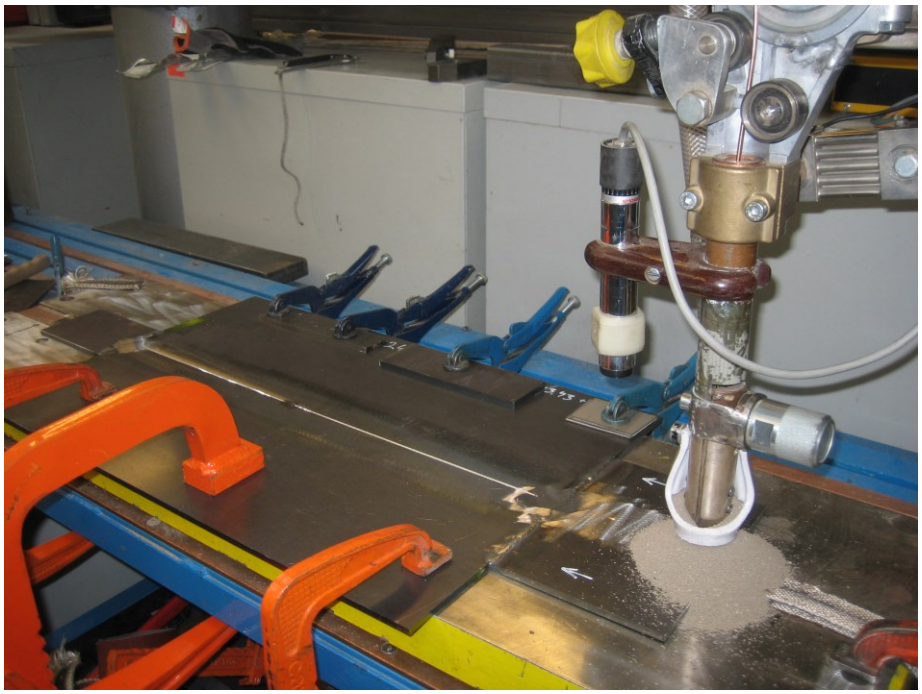

Figure 38.Test plates clamped and prepared for SAW. Fiberglass backing tape, run-on and run-off plates were used.

All the welding parameters are presented in Table 9. Heat input varied from 0,79 to 2,29 kJ/mm. As a result, preliminary welding procedure specifications (pWPS) were made, and are presented in Appendix 21 - 30.

Table 9. Welding parameters for SAW welded butt joints.

Test case	Backing	Welding speed [mm/min]	Current [A]	Welding voltage [V]
7006-5S	Fiberglass	1100	701	27,7
7006-6S	Fiberglass	850	701	28,5
7008-5S	Fiberglass	600	640	29,8
7008-6S	Fiberglass	500	641	29,8
9004-5S	Fiberglass	1090	512	28
9004-6S	Fiberglass	1000	501	28,5
9006-5S	Fiberglass	1050	703	27,7
9006-6S	Fiberglass	900	701	28,5
9008-5S	Fiberglass	600	641	29,8
9008-6S	Fiberglass	500	640	29,8

6.6 Measuring of the cooling time $\Delta t_{8/5}$

One of the most important things to determine the microstructures and properties of the weld is to know the cooling rate. Cooling time between 800 - 500 ºC can be measured with many different methods, for instance with thermocouples and infrared camera. Mathematical models can also be used in prediction of the cooling rates. The most straightforward method is to use thermocouple wires with a data logger.

Locating the thermocouple wire into measured object is crucial. The closer to the weld it is located, the ability to measure accurate cooling curves becomes uncertain. Main reason for this is that the thermocouple can touch the electric arc in PAW, SAW and MAG welding, where the temperatures are much higher than the thermocouple can endure.

In addition to measure cooling times for Optim 700 MC Plus and 900 QC, thermal distributions in test pieces were also measured. In this procedure thermocouples were put at different distances from the weld centreline on both sides of the plates. These results were used for evaluation of weld residual stresses in Master´s thesis of Akseli Kukkonen titled "Residual stresses and distortions in welded ultra-high-strength steels" (2014), but are not included in this thesis.

Measurements were performed by using K-type (Nickel / Chromium - Nickel) thermocouple wire with temperature range between 0 to 1250 ºC. Diameter for the each wire was 0,81 mm, which is the thickest that can be used satisfactorily. Using thicker than Ø 0,81 mm the response time increases and the sampling interval cannot be set fast enough. Also the wire length was kept as short as possible to avoid too long response times. (Moore 2003)

Two measuring arrangements were used to determine cooling rates. First one is plunging, where the wires are melt together using TIG welding and embedded to the molten weld pool. In the second one, wires are spot welded to the surface of the plate. Both set-ups for temperature measurements are presented in Figure 39.

Figure 39. K-type thermocouple used for cooling time determination. A) Thermocouple that is plunged to the molten weld pool and B) spot welded to plate surface.

In PAW, thermocouples could not be plunged to the molten weld pool because of the small gap between the plasma torch and the plate surface. Thermocouples were spot welded to the end of milled grooves. The depth of the groove varied on the basis of how thick plates were welded. Grooves were placed as close to the weld edge as possible. Many welding tests were made to determine what is the optimal distance to place the groove.

In SAW thermocouples were spot welded to the plate surface as close to the weld as possible and no grooves were needed. This was due to the fact that the flux protected the wires. MAG welding was the only process where the plunging can be used. The space between MAG torch and the plate is sufficient enough to embed the thermocouple wire to the molten pool.

Data logger was set to record the temperature information with sampling intervals of 200 ms. When the temperature in the weld has dropped under 500 ºC recording was stopped. After that data was transferred to USB-memory and then to the computer. Process of the temperature measurements is presented in Figure 40.

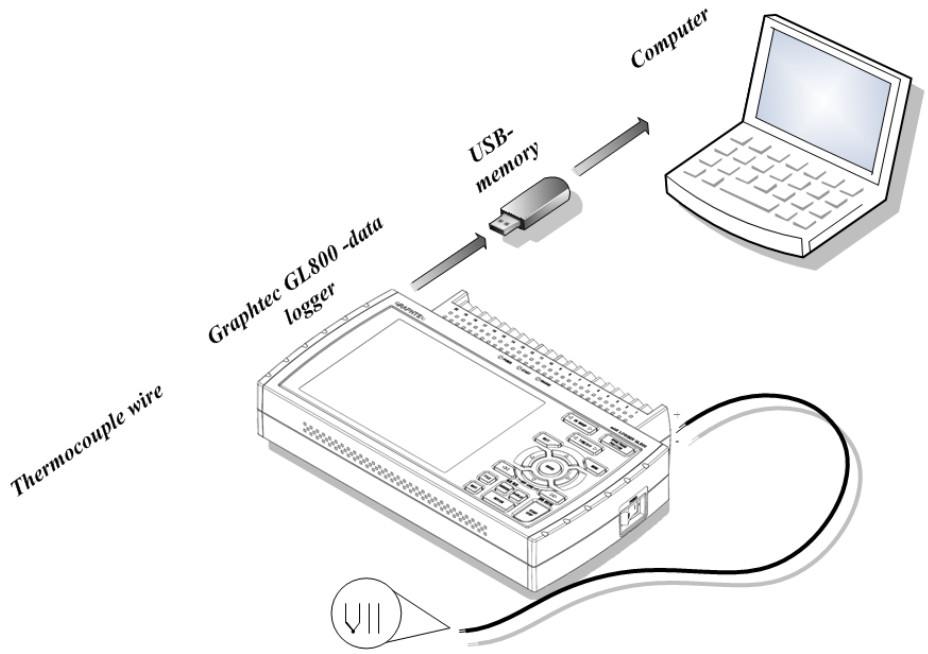

Figure 40. Set-up for temperature measurements and data handling.

Data analysis and cooling curve determination with the large amount of information is the easiest way to handle by a computer. Cooling time was determined for each individual process as an average of three test points. In addition to the measurement of the cooling times via thermocouples, calculations were done using the Equation 4. The usage of Equation 4 is based on the information from Equation 6.

6.7 Hardness testing

Hardness testing was carried out to estimate the base material properties before and after welding as well as the properties of the welded joints.

The test force in microhardness testing was 0,5 kgf because of the sampling interval was only 0,2 mm. The hardness profile was measured from mid-thickness of the plate. Buehler NMT-7 digital microhardness tester with Omnimet controller was used in microhardness measurements (Figure 41).

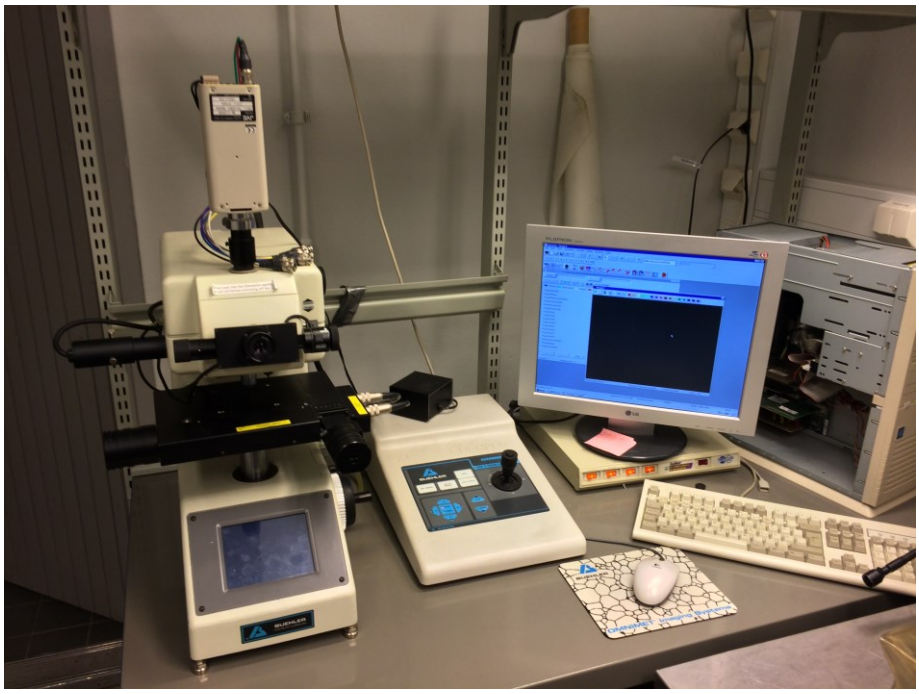

Figure 41. Buehler NMT-7 microhardness tester with Omnimet Stage & Focus controller.

Hardness of the base material was tested with test force of 10 kgf. Hardness tester Gnehm Brickers 220 was used to base material hardness measurements (Figure 42).

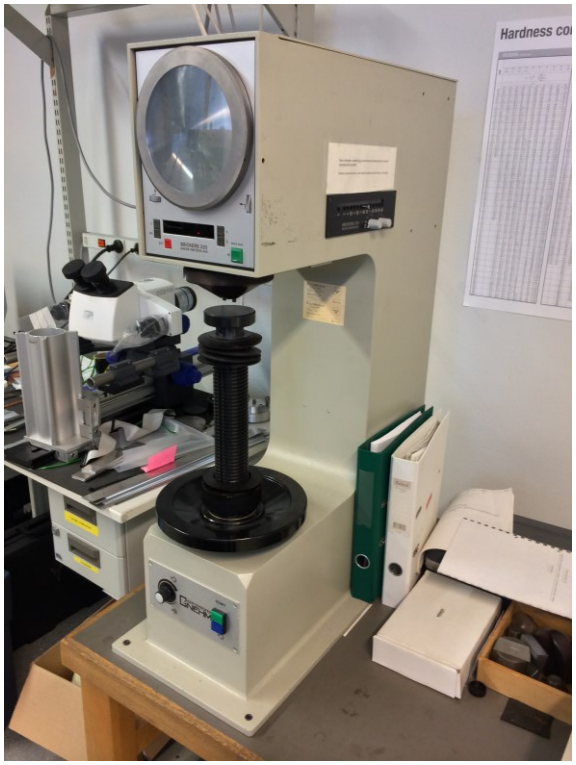

Figure 42. Gnehm Brickers 220 hardness tester.

6.8 Mechanical testing

Test specimens were removed from welded plates according to standard SFS-EN ISO 15614-1 + A1 + A2. Locations of tensile test and impact test specimens are presented in Figure 43.

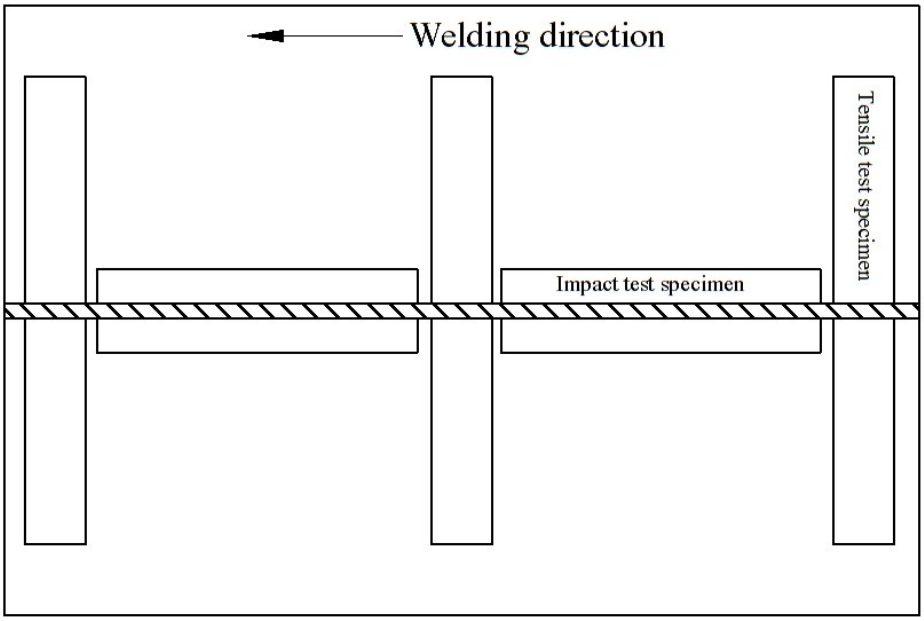

Figure 43. Location of test specimens.

Small sections were removed from both ends to avoid any weld defects in specimens. All the test specimens were removed by sawing.

All the mechanical testing was done in the Engineering Materials Laboratory in the Department of Engineering Design and Production at Aalto University School of Engineering.

6.8.1 Tensile testing

Tensile testing was carried out according to SFS-EN ISO 4136 and SFS-EN ISO 15614-1. Tensile tests were made transverse to the rolling direction. MTS 810 was used for the base material tensile testing (Figure 44). The values for yield strength ($R_{p0.2}$), tensile strength (R_m) and elongation (A) were determined as the average of the three samples. Ambient test temperature was 23 ºC.

Figure 44. MTS 810 material test system used for base material tensile testing.

For the welded plates, MTS Landmark (Figure 45) was used to determine the engineering stress-strain curves.

Equation 7 was used to determine engineering stress (σ_{eng}). (Hertzberg 1996)

$$\sigma_{eng} = \frac{F}{A_0}, \tag{7}$$

where

F = axial load

A_0 = initial cross-sectional area of the specimen.

Axial extensometer was used to define the engineering strain (ε_{eng}). Extensometer was attached in the middle of the each test piece.

Equation 8 was used to determine the percentage elongation after fracture (SFS-EN ISO 6892-1).

$$A = \frac{L_u - L_o}{L_o} * 10, \quad (8)$$

where

A = elongation to fracture

L_o = the original gauge length

L_u = the final gauge length.

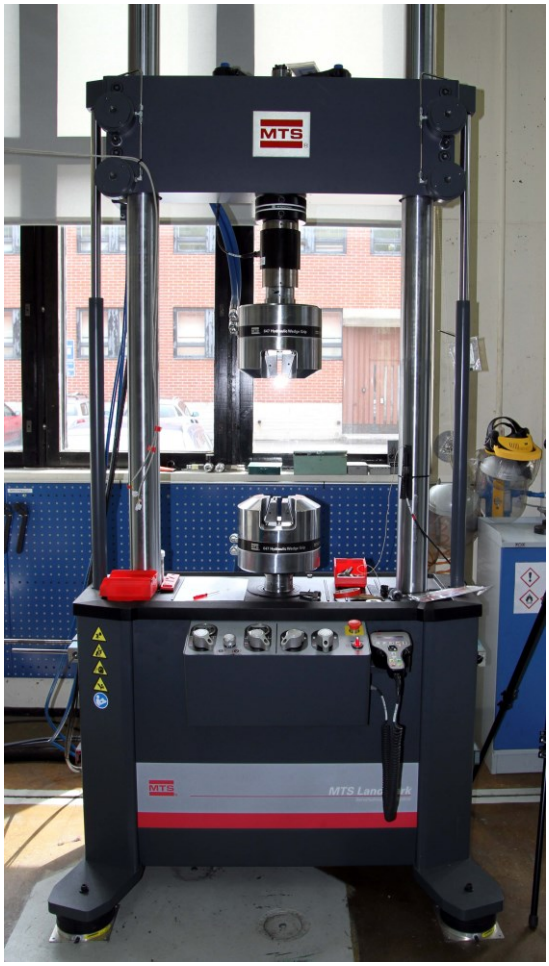

Figure 45. MTS Landmark test machine was used for the welded samples.

Tensile test specimen dimensions are presented in Figure 46. The thickness for all the test specimens was equal to the thickness of the base material. Excess weld metal was machined to the plate surface level from both sides.

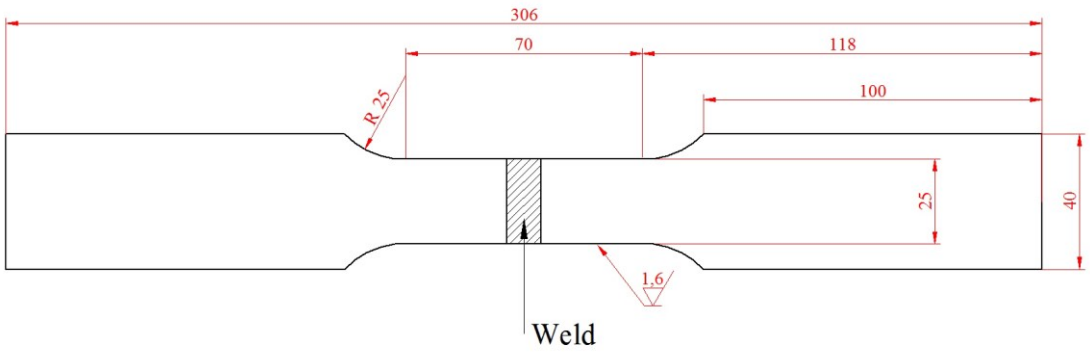

Figure 46. Dimensions of the welded samples for tensile testing.

6.8.2 Charpy-V notch impact test

Impact testing was carried out according to standard SFS-EN ISO 148-1 and SFS-EN ISO 9016. Tests were made transverse to the rolling direction. The potential energy of the pendulum hammer was 300 J, whereas the striker radius was 2 mm. Test temperatures varied from -60 to 60 ºC. Based on the test material thicknesses, standardized 10 * 10 * 55 mm impact test specimens could not be used. In order to determine the amount of absorbed energy (KV_2), sub-sized specimens were used. The mixture of liquid nitrogen and ethanol was used to achieve the test temperature. Equipment for the impact testing is presented in Figure 47.

Figure 47. Losenhausenwerk impact test equipment for Charpy-V notched specimens.

Samples were etched to locate the desired region of the weld and HAZ. All the samples were notched face perpendicular to the surface of the test piece (T-position) by milling. Dimensions are shown in Figure 48.

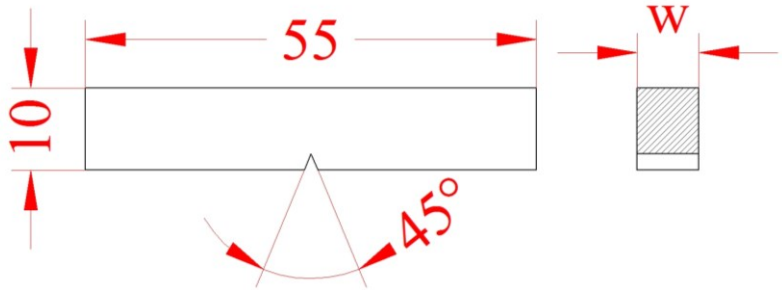

Figure 48. Dimensions for the Charpy pendulum impact test piece.

Nominal dimension w is variable and under 10 mm, therefore all the specimens are categorized as sub-sized. For the 8 mm material thickness, dimension w was machined to 7,5 mm. Dimension w for the 6 mm material thickness was 5,0 mm. Impact tests were not carried out for the 4 mm material thickness, due to the size effect. The

notch locations are presented in Figure 49. The notches were placed to centre of the weld (WM), fusion line (FL) and fusion line +1 mm (FL+1).

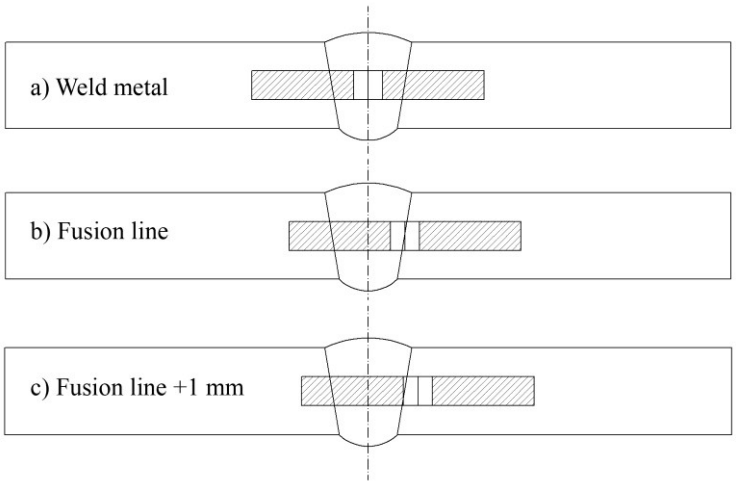

Figure 49. A schematic presentation of sample positions.

The values of KV_2 are determined as the average of the three samples. Equation 9 was used to determine the standard deviation.

$$s_x = \sqrt{\frac{\sum(x_i - \bar{x})^2}{n-1}}, \qquad (9)$$

where

x_i = individual value

$\bar{x}$ = average value

n = number of test specimens.

Impact energies are corrected to correspond standard 10 * 10 * 55 mm specimen size (according to DNV Rules for Ships, Pt. 2 Ch. 3). All the samples with 7,5 mm material thickness are corrected using conversion factor of 6/5 and samples with 5,0 mm are corrected with a factor of 3/2. Sample identification is presented in Table 6.

6.9 Metallography

Sample preparation was made after the welding tests were finished. Samples were removed by sawing from the test plates. For the microscopic examination, samples were ground, polished and etched.

Grinding was made using silicon carbide (SiC) sandpapers from 320 to 4000 grit. Polishing was done with water-based diamond suspension. Diamond grain size was ranging from 3 to 1 µm.

Nital 2% etchant was used to reveal grain boundaries and constituents. Nital 2% contains 2 ml nitric acid (HNO_3) and 98 ml ethanol (C_2H_5OH).

Nikon Epiphot 200 microscope with Nikon Digital Sight DS-U1 was used for microscopic examination (Figure 50).

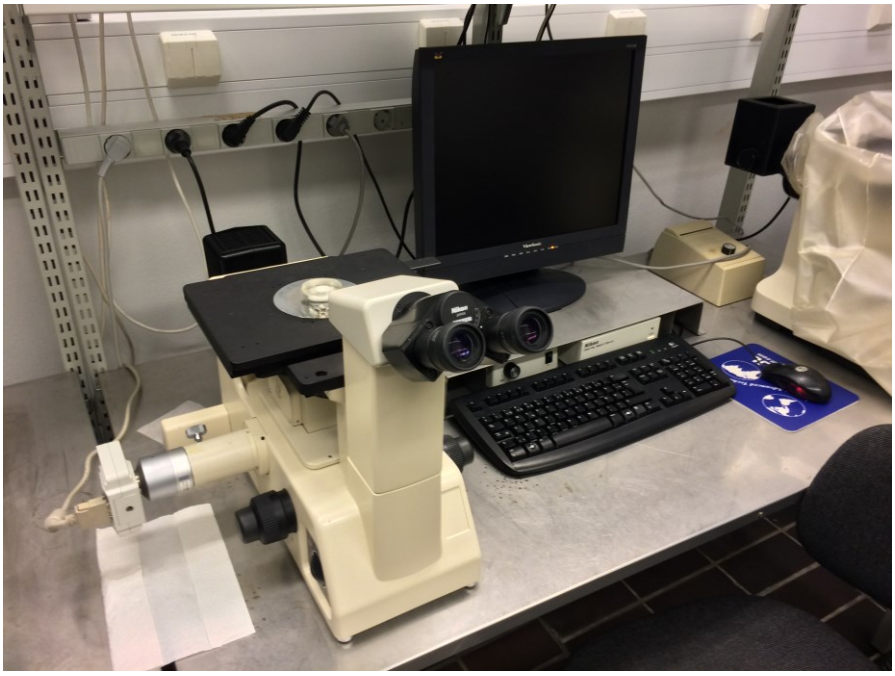

Figure 50. Nikon Epiphot 200 microscope for microscopic examination.

All the samples were macro photographed using Canon 7D with fixed focal length macro lens. Microstructures were analyzed and photographed using microscopic examination with different magnifications.

In addition to optical microscopy, sample preparation to future electron backscatter diffraction (EBSD) analysis was carried out by the same procedure as for the optical microscopy examination. In addition to the procedure, samples were polished with 0,25 µm diamond wax and 0,05 µm alumina oxide. Surface finishing was done using 0,02 µm colloidal silica suspension.

7 RESULTS

7.1 Results of hardness testing

7.1.1 Hardness of base material OPTIM 700 MC Plus and 900 QC

The hardness values of the base materials were measured to evaluate the impact of thermal cycle after welding. Base material hardness values for each steel grade and material thickness are presented in Figure 51. Standard deviation is marked on the results.

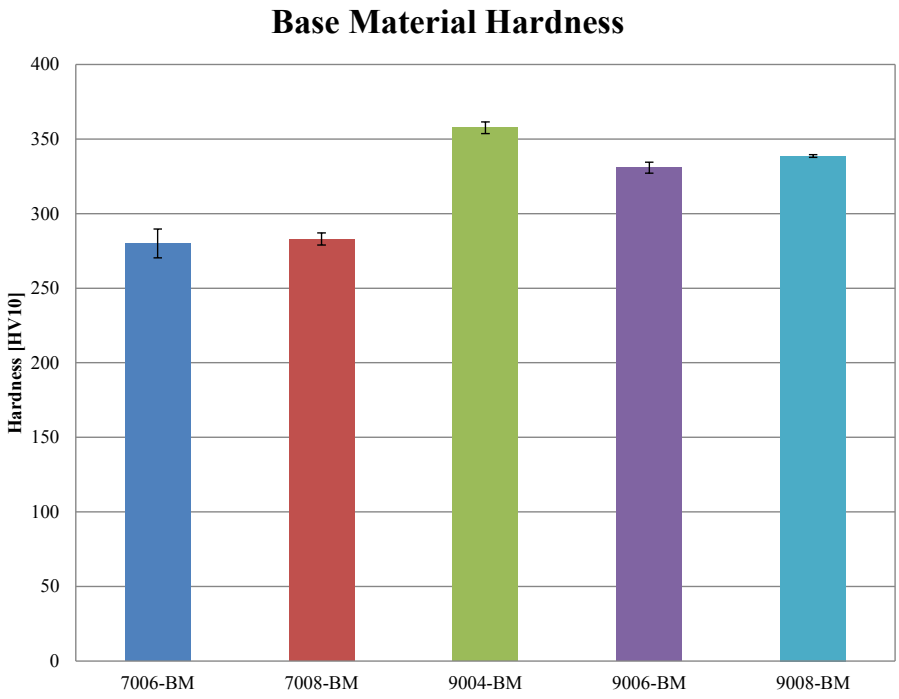

Figure 51. Base material hardness for Optim 700 MC Plus and Optim 900 QC.

7.1.2 Microhardness of welded joints

The hardness profile was measured from the mid-thickness of each sample. Sampling interval for each measuring point was set to 0,2 mm. Due to large number of samples, microhardness profiles are presented in Appendix 31 - 45. Weld metal, heat-affected zone and base material regions are marked to the charts.

Hardness values for the weld metal and the heat-affected zone are presented in Table 10. Table presents heat input and cooling time against minimum and maximum hardness values.

Table 10. Hardness values of the butt welded samples for the weld and the heat-affected zone.

Sample	Heat Input Q [kJ/mm]	Cooling Time $\Delta t_{8/5}$ [s]	Consumable	Hardness [HV0,5]			
				Weld Metal		HAZ	
				Min.	Max.	Min.	Max.
7006-1M	0,56	9,2	ESAB OK Aristorod 69	250	269	226	305
7006-2M	0,59	13,5	ESAB Tubrod 14.03	258	294	242	312
7008-1M	0,65	11,5	ESAB OK Aristorod 69	324	355	243	322
7008-2M	0,81	13,1	ESAB Tubrod 14.03	262	296	225	296
9004-3M	0,48	15,6	ESAB OK Aristorod 89	339	402	258	299
9004-4M	0,49	15,9	ESAB Coreweld 89	308	358	242	277
9006-3M	0,48	9,0	ESAB OK Aristorod 89	393	433	259	316
9006-4M	0,56	9,6	ESAB Coreweld 89	274	342	264	356
9008-3M	0,65	9,1	ESAB OK Aristorod 89	347	422	272	314
9008-4M	0,73	11,3	ESAB Coreweld 89	328	420	236	298
7006-1P	1,00	23,6	ESAB OK Aristorod 69	233	264	211	298
7006-2P	1,06	24,8	ESAB Tubrod 14.03	233	277	183	313
7008-1P	1,32	30,6	ESAB OK Aristorod 69	216	264	218	280
7008-2P	1,40	33,2	ESAB Tubrod 14.03	233	265	214	295
9004-3P	0,54	17,5	ESAB OK Aristorod 89	252	315	247	313
9004-4P	0,64	18,0	ESAB Coreweld 89	221	296	249	338
9006-3P	0,99	24,8	ESAB OK Aristorod 89	248	282	228	315
9006-4P	0,99	24,0	ESAB Coreweld 89	225	283	252	329
9008-3P	1,34	31,8	ESAB OK Aristorod 89	240	289	237	347
9008-4P	1,48	33,2	ESAB Coreweld 89	256	305	277	348
7006-5S	1,06	38,8	ESAB OK Autrod 13.43 + OK Flux 10.62	269	287	225	309
7006-6S	1,41	43,6	ESAB OK Tubrod 15.27S + OK Flux 10.62	248	280	221	298
7008-5S	1,91	49,7	ESAB OK Autrod 13.43 + OK Flux 10.62	254	289	210	298
7008-6S	2,29	62,0	ESAB OK Tubrod 15.27S + OK Flux 10.62	207	255	178	295
9004-5S	0,79	25,7	ESAB OK Autrod 13.43 + OK Flux 10.62	276	305	240	314
9004-6S	0,86	29,4	ESAB OK Tubrod 15.27S + OK Flux 10.62	266	287	234	285
9006-5S	1,11	39,0	ESAB OK Autrod 13.43 + OK Flux 10.62	257	291	257	307
9006-6S	1,33	42,2	ESAB OK Tubrod 15.27S + OK Flux 10.62	219	267	221	287
9008-5S	1,91	49,4	ESAB OK Autrod 13.43 + OK Flux 10.62	248	290	244	303
9008-6S	2,29	62,9	ESAB OK Tubrod 15.27S + OK Flux 10.62	240	268	251	316

7.2 Cooling time of the welds

Thermal efficiency factors for each welding method are based on the standard SFS-EN 1011-1. Following factors were used:

- k = 0,60 on PAW
- k = 0,80 on MAG
- k = 1,00 on SAW.

The same factors are used for heat input and cooling time calculations. Measured cooling times for each sample are presented in Table 11. Calculated cooling time is based on two-dimensional heat flow from Equation 4.

In each welding case, the heat input was determined according to Equation 3. In MAG welding, the welding energy was determined according to the average power, which was carried out from the power source. Based on the tests and calculations, the power based output in pulsed-current mode gives 6 to 7 % bigger value for the heat

input than the traditional U*I-method. The heat input calculation comparison of MAG welded samples are presented in Appendix 46.

Table 11. Measured cooling times for each welded sample against heat input and calculated cooling time.

Sample	Heat Input Q [kJ/mm]	Measured Cooling Time $\Delta t_{8/5}$ [s]	Calculated Cooling Time $\Delta t_{8/5}$ [s]
7006-1M	0,56	9,2	9,9
7006-2M	0,59	13,5	11,2
7008-1M	0,65	11,5	7,6
7008-2M	0,81	13,1	11,6
9004-3M	0,48	15,6	16,3
9004-4M	0,49	15,9	17,0
9006-3M	0,48	9,0	7,2
9006-4M	0,56	9,6	9,8
9008-3M	0,65	9,1	7,5
9008-4M	0,73	11,3	9,4
7006-1P	1,00	23,6	31,3
7006-2P	1,06	24,8	35,2
7008-1P	1,32	30,6	31,0
7008-2P	1,40	33,2	34,9
9004-3P	0,54	17,5	20,4
9004-4P	0,64	18,0	28,7
9006-3P	0,99	24,8	31,2
9006-4P	0,99	24,0	30,9
9008-3P	1,34	31,8	31,9
9008-4P	1,48	33,2	38,7
7006-5S	1,06	38,8	35,4
7006-6S	1,41	43,6	62,8
7008-5S	1,91	49,7	64,6
7008-6S	2,29	62,0	93,3
9004-5S	0,79	25,7	44,2
9004-6S	0,86	29,4	52,1
9006-5S	1,11	39,0	39,1
9006-6S	1,33	42,2	56,0
9008-5S	1,91	49,4	64,8
9008-6S	2,29	62,9	93,0

According to measured data, cooling curves are plotted and presented in Appendix 47 - 61.

7.3 Results of tensile tests

Tensile tests were carried out according to standards SFS-EN ISO 4136 and SFS-EN ISO 15614-1. The following material properties were determined from the tensile tests:

- Yield strength [$R_{p0,2}$]
- Tensile strength [R_m]
- Elongation [A].

7.3.1 Tensile tests for base materials OPTIM 700 MC Plus and 900 QC

Tensile test results for the base material and each thickness are presented in Table 12.

Table 12. Tensile test results for the base materials.

Sample	Yield Strength $R_{p0,2}$ [MPa]	Tensile Strength R_m [MPa]	Elongation A [%]
7006-BM	761	845	17,5
7008-BM	741	836	18,0
9004-BM	995	1125	8,6
9006-BM	1018	1118	9,0
9008-BM	974	1094	13,0

Stress-strain curves are presented in Appendix 62 - 64.

7.3.2 Tensile tests for welded joints

Tensile test results for each welded sample are presented in Table 13. Heat input, cooling time and location of fracture is also included in the table.

Table 13. Tensile test results for the welded joints.

Sample	Consumable	Heat Input Q [kJ/mm]	Cooling Time $\Delta t_{8/5}$ [s]	Yield Strength $R_{p0,2}$ [MPa]	Tensile Strength R_m [MPa]	Elongation A [%]	Location of Fracture
7006-1M	ESAB OK Aristorod 69	0,56	9,2	683	788	8,8	FL/WELD
7006-2M	ESAB Tubrod 14.03	0,59	13,5	666	749	4,5	WELD/HAZ
7008-1M	ESAB OK Aristorod 69	0,65	11,5	751	831	16,6	HAZ
7008-2M	ESAB Tubrod 14.03	0,81	13,1	686	791	9,4	HAZ
9004-3M	ESAB OK Aristorod 89	0,48	15,6	729	873	6,0	HAZ
9004-4M	ESAB Coreweld 89	0,49	15,9	707	863	6,1	HAZ
9006-3M	ESAB OK Aristorod 89	0,48	9,0	868	992	8,3	HAZ
9006-4M	ESAB Coreweld 89	0,56	9,6	770	922	7,0	FL/HAZ
9008-3M	ESAB OK Aristorod 89	0,65	9,1	904	1014	7,8	HAZ
9008-4M	ESAB Coreweld 89	0,73	11,3	867	1011	9,6	HAZ
7006-1P	ESAB OK Aristorod 69	1,00	23,6	607	726	14,1	WELD
7006-2P	ESAB Tubrod 14.03	1,06	24,8	601	724	14,7	WELD
7008-1P	ESAB OK Aristorod 69	1,32	30,6	570	681	6,1	WELD
7008-2P	ESAB Tubrod 14.03	1,40	33,2	576	694	9,5	WELD
9004-3P	ESAB OK Aristorod 89	0,54	17,5	647	807	8,8	HAZ
9004-4P	ESAB Coreweld 89	0,64	18,0	674	831	7,8	HAZ
9006-3P	ESAB OK Aristorod 89	0,99	24,8	613	785	11,2	FL/HAZ
9006-4P	ESAB Coreweld 89	0,99	24,0	632	805	9,2	FL
9008-3P	ESAB OK Aristorod 89	1,34	31,8	635	816	9,0	FL/WELD
9008-4P	ESAB Coreweld 89	1,48	33,2	598	807	12,3	FL/WELD
7006-5S	ESAB OK Autrod 13.43 + OK Flux 10.62	1,06	38,8	655	788	9,4	FL
7006-6S	ESAB OK Tubrod 15.27S + OK Flux 10.62	1,41	43,6	606	745	11,5	FL
7008-5S	ESAB OK Autrod 13.43 + OK Flux 10.62	1,91	49,7	596	748	12,7	FL/HAZ
7008-6S	ESAB OK Tubrod 15.27S + OK Flux 10.62	2,29	62,0	568	711	16,1	HAZ
9004-5S	ESAB OK Autrod 13.43 + OK Flux 10.62	0,79	25,7	613	810	8,1	HAZ
9004-6S	ESAB OK Tubrod 15.27S + OK Flux 10.62	0,86	29,4	622	821	8,5	HAZ
9006-5S	ESAB OK Autrod 13.43 + OK Flux 10.62	1,11	39,0	631	820	9,0	FL/WELD
9006-6S	ESAB OK Tubrod 15.27S + OK Flux 10.62	1,33	42,2	598	794	10,8	WELD
9008-5S	ESAB OK Autrod 13.43 + OK Flux 10.62	1,91	49,4	594	816	12,4	WELD
9008-6S	ESAB OK Tubrod 15.27S + OK Flux 10.62	2,29	62,9	561	794	14,3	WELD

Stress-strain curves are presented in Appendix 65 - 79. Stress-strain curves for MAG welded specimens are presented in Appendix 65 - 69, PAW welded specimens in 70 - 74 and SAW welded specimens 75 - 79, respectively.

7.4 Results of the Charpy-V notch impact tests

Impact tests were done according to standards SFS-EN ISO 148-1 and SFS-EN ISO 9016. The test results are corrected to correspond the impact test results of standard full-size specimen. Samples with thickness of 4 mm were not included on the procedure.

7.4.1 Impact tests of base materials OPTIM 700 MC Plus and 900 QC

Base materials were tested at temperatures of -20, -40 and -60 ºC. Standard deviation is marked on the results. The average values of the impact energies for 6 mm Optim 700 MC Plus are presented in Figure 52.

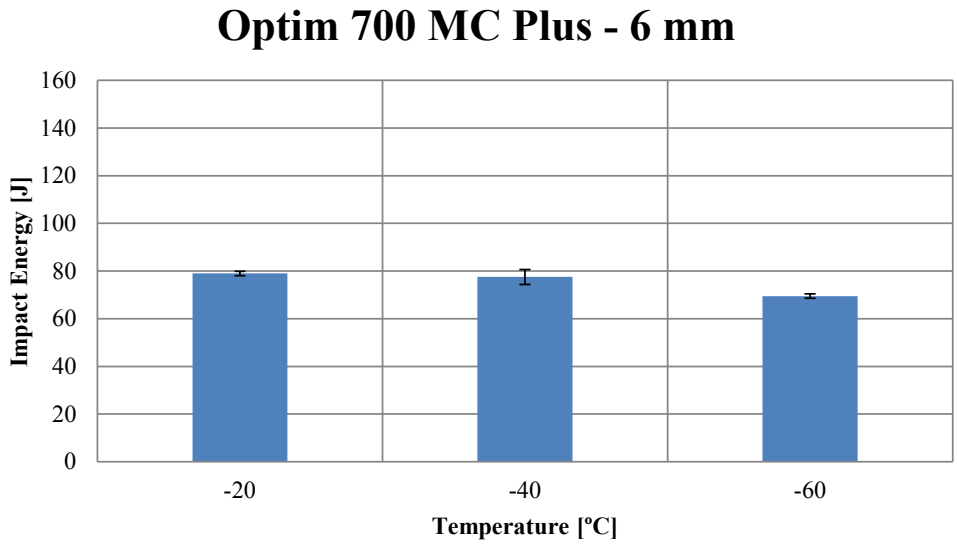

Figure 52. Impact energy of 6 mm Optim 700 MC Plus.

The average values for the 8 mm Optim 700 MC Plus are presented in Figure 53.

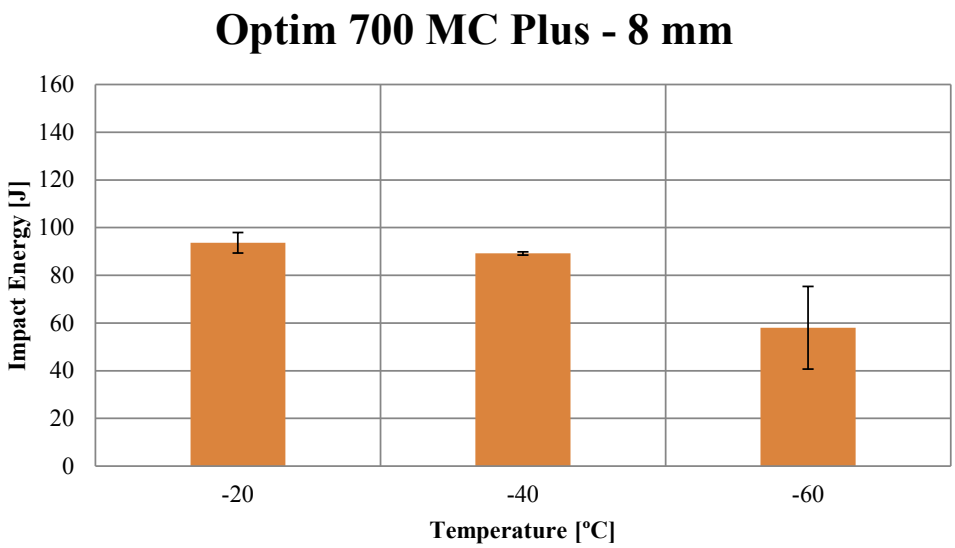

Figure 53. Impact energy of 8 mm Optim 700 MC Plus.

The average values for the 6 mm Optim 900 QC are presented in Figure 54.

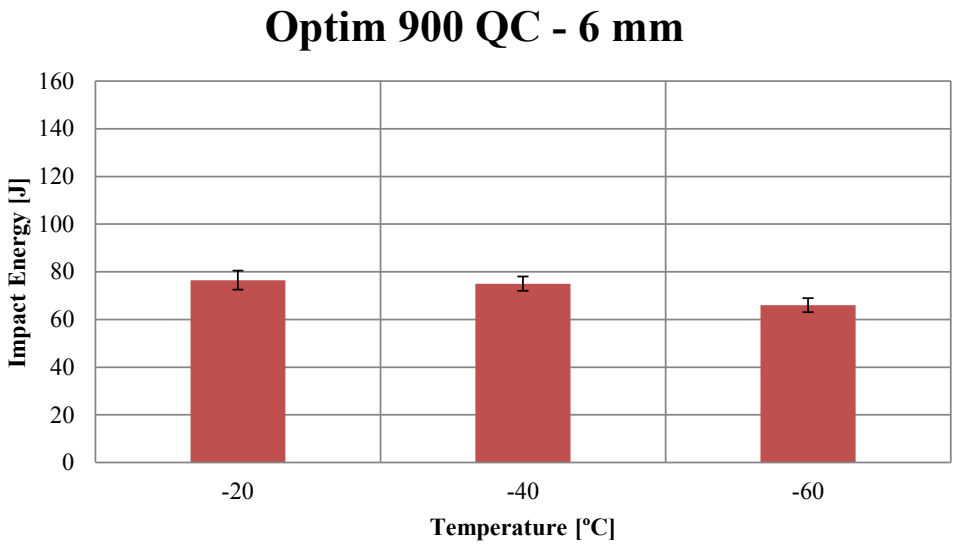

Figure 54. Impact energy of 6 mm Optim 900 QC.

The average values for the 8 mm Optim 900 QC are presented in Figure 55.

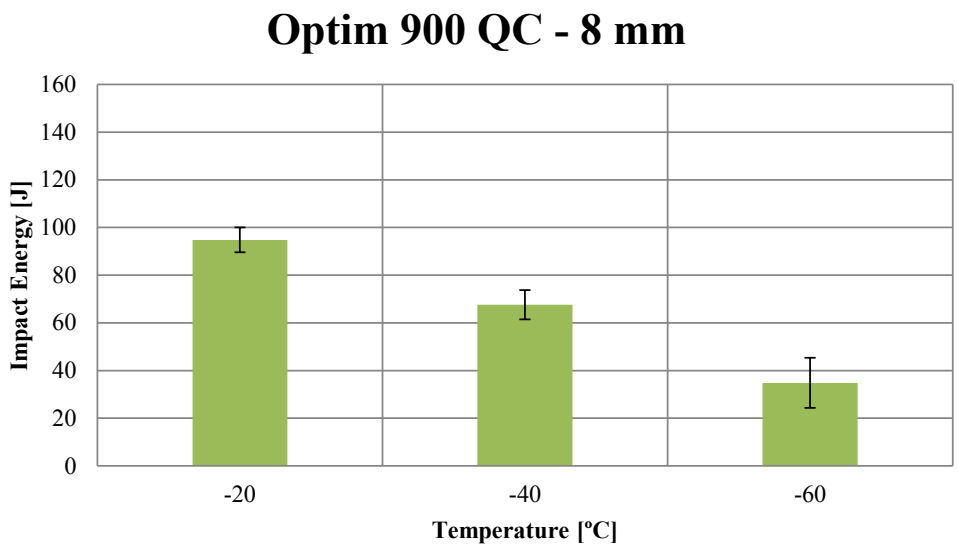

Figure 55. Impact energy of 8 mm Optim 900 QC.

7.4.2 Impact tests of welded joints

Welded samples were tested within temperature range from -60 to 60 ºC. Due to large number of samples, impact energies of MAG welded samples are presented in Appendix 80 - 82, PAW welded samples in Appendix 83 - 85 and SAW welded samples in Appendix 86 - 88. Standard deviation is marked on the results.

Due to size factor, Charpy-V impact testing was not carried out for the 4 mm plates. Thinner plates have a tendency to behave naturally ductile, and hence the correlation from sub-sized specimen to full-size specimen should be handeled with caution.

7.5 Microstructural characterization

7.5.1 Characterization of base materials Optim 700 MC Plus and Optim 900 QC

Optical microscopy was used to study the microstructures of the base materials. Figure 56 presents typical microstructure of Optim 700 MC Plus. The microstructure consists of bainite and ferrite. The volume fraction of bainite is higher than that of ferrite. Based on microstructure analysis of the samples, the volume fraction of bainite is evaluated to be approximately 70 % and ferrite is roughly 30 %.

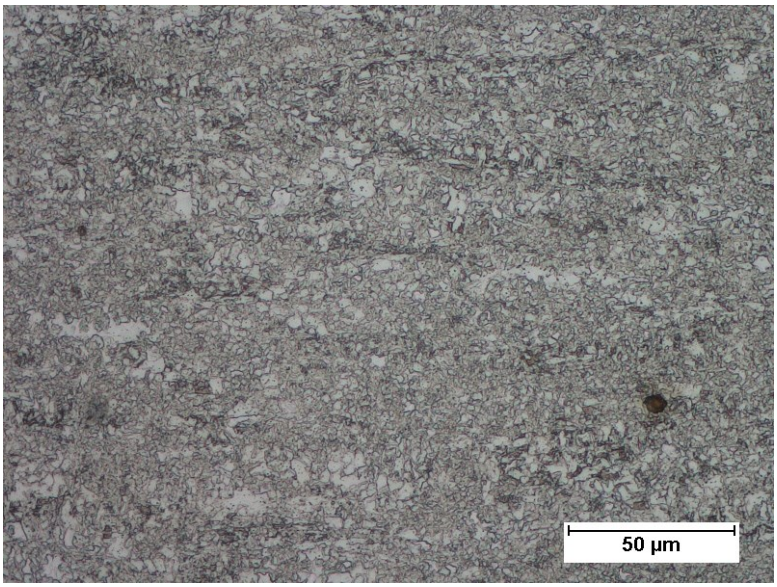

Figure 56. Microstructure of Optim 700 MC Plus.

Figure 57 presents the microstructure of Optim 900 QC. Material is hot-rolled and quenched, and consists of martensite and bainite. Based on microstructure analysis, the volume fraction of bainite is approximately 70 % and martensite is about 25 %. Ferrite and retained austenite has also been observed.

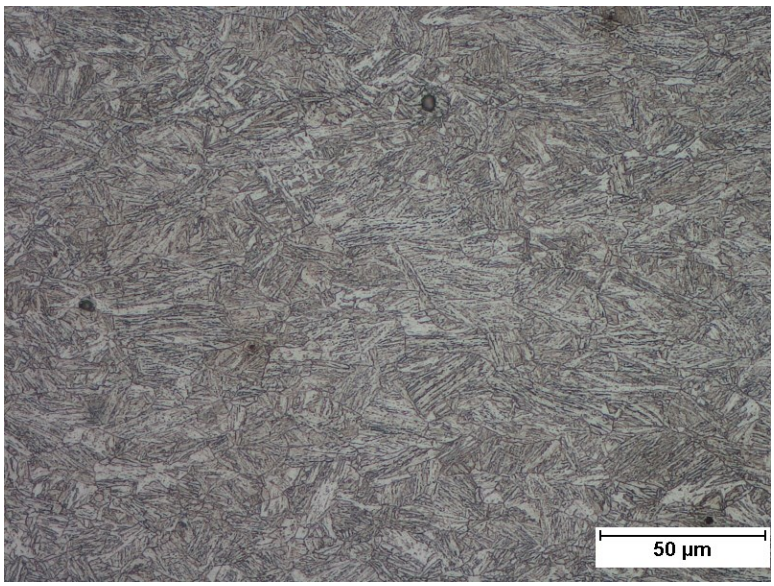

Figure 57. Microstructure of Optim 900 QC.

EBSD inverse pole figure (IPF) maps of Optim 700 MC Plus are presented in Figure 58, which are taken in all directions to determine the average grain size. In the map, Z-plane presents the rolling direction, X-plane the cross-section and the Y-plane presents the side, which is parallel with the rolling direction.

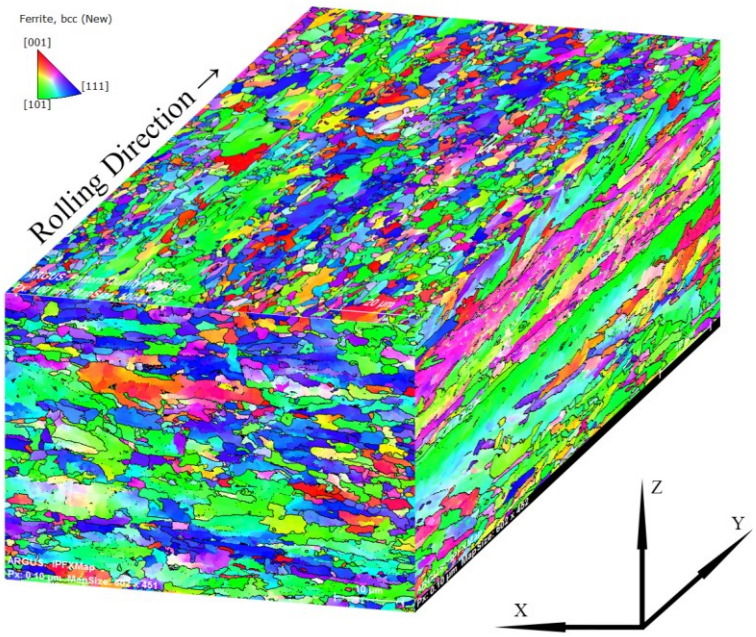

Figure 58. EBSD inverse pole figure maps taken from 6 mm Optim 700 MC Plus. The maps are combined from three different samples of different orientations.

IPF maps of Optim 900 QC are presented in Figure 59.

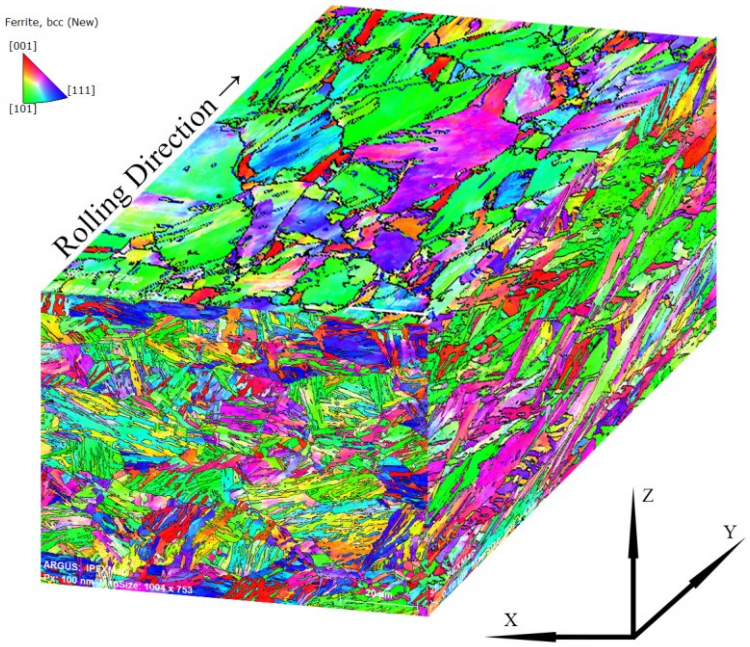

Figure 59. EBSD inverse pole figure maps taken from 6 mm Optim 900 QC. The maps are combined from three different samples of different orientations.

The average grain size is defined using mean linear intercept method. The EBSD detector was set to 10 degree angle to recognize grain boundaries. Using lower an-

gles than 10º, it is possible that the detector does not recognize the grains properly, and hence gives a smaller average grain size than it actually is.

Table 14 presents average grain size for both of the materials. EBSD mapping was used to determine the average grain size in three different methods. Horizontal line, vertical line and area-based methods were used.

Table 14. Average grain size of Optim 700 MC Plus and Optim 900 QC.

	Optim 700 MC Plus			Optim 900 QC		
	X	Y	Z	X	Y	Z
Grain Size, Horizontal [µm]	2,97	2,90	2,50	2,59	2,78	3,33
Grain Size, Vertical [µm]	1,90	1,72	1,65	1,35	1,52	1,72
Area method [µm]	6,35	4,80	5,10	4,23	5,33	8,00

7.5.2 Characterization of welded joints

All the welds were photographed to evaluate the penetration and locate possible internal defects. Photos were also taken from the microstructures of the welds and different zones of the HAZ, which are CGHAZ, FGHAZ and base material.

Due to large number of samples, microstructures and weld cross-sections of MAG welded samples are presented in Appendix 89 - 93, PAW welded samples in Appendix 94 - 98 and SAW welded samples in Appendix 99 - 103.

Based on microscopic examinations of the microstructures, the main composition is ferrite and bainite in most of MAG samples. It can be observed that acicular ferrite is present in samples where the heat input is the low, particularly in WM. In addition, martensite can be observed in WM where the cooling rate has been the highest. In CGHAZ, ferrite is the main structure and bainite can also be seen. Widmannstätten ferrite, polygonal ferrite and granular bainite can be observed in FGHAZ in both of the material.

Main composition in PAW samples are ferrite and bainite. But grain boundary ferrite, Widmannstätten ferrite, carbides and polygonal ferrite can be seen in all tested zones, which can explain decreased impact toughness.

The microstructure of SAW samples similar with PAW samples, but the used consumables favor acicular ferrite composition in WM, which improves the impact toughness. The effect of heat input can be seen in CGHAZ, where the austenite grains have grown during the thermal cycle. The difference in size is evident when MAG and SAW samples are compared to each other. Grain boundary ferrite, Widmannstätten ferrite and carbides are present in CGHAZ and FCHAZ.

Base material is mainly bainitic ferrite in Optim 700 MC Plus and tempered martensite and bainite in Optim 900 QC, but also fine cementite can be observed.

8 DISCUSSION

MAG welding was carried out by using filler wire of 1,2 mm in all cases. Based on the cross-section photos of the welded samples, it is clear that the size of the weld bead is too excessive in 4 mm steel plates. Using Ø 1,0 mm filler wire may have been much more suitable to avoid high weld toe angle and to decrease both heat input and cooling time. Cross-section views of the samples 9004-3M and 9004-4M are presented in Figure 60. High weld toe angle produces high stress concentration which will decrease the fatigue life of the joint.

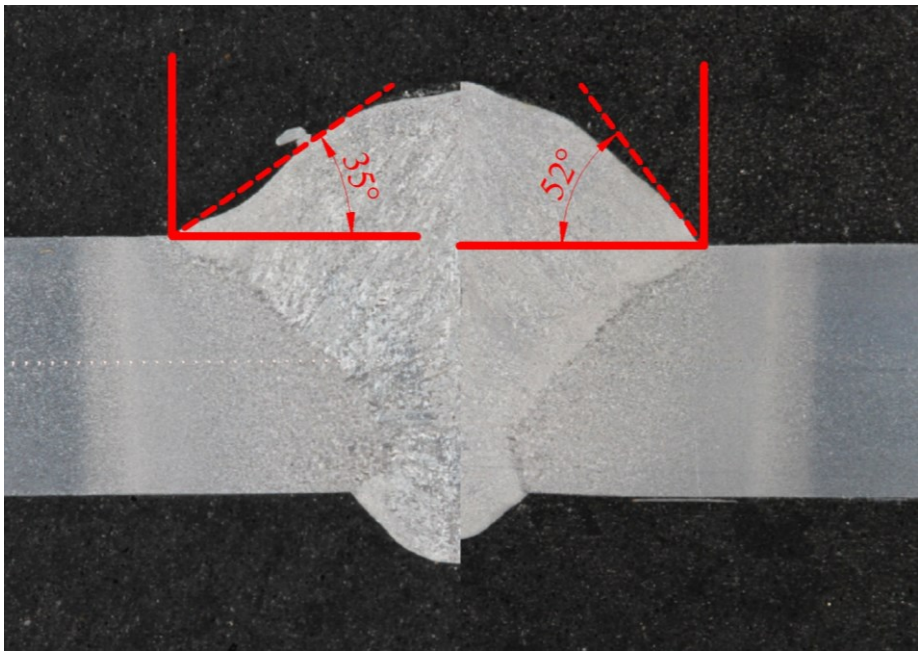

Figure 60. Comparison of the weld toe angles of MAG welded samples 9004-3M (left) and 9004-4M (right).

All the 4 mm plates were single-pass welded without backing or air gap which was the objective. The control of the penetration without backing or air gap was easy, but the sufficient parameter windows were extremely narrow. The use of air gap would have decreased heat input and the weld toe angle.

In preliminary welding tests air gap was used to determine the effects on thermal distortions, heat input and bead geometry (Figure 61). Sample 9004-3M was welded without air gap which increased the longitudinal shrinkage, and hence bending can be observed. Bending is much less in the case where air gap was set at 1 mm. In both cases transverse shrinkage was not significant. The use of 1,2 mm filler wire is justified when air gap is present, and hence the bead geometry is more acceptable.

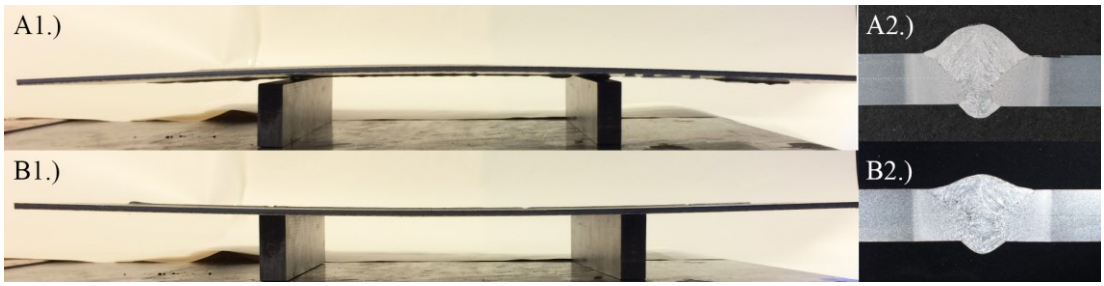

Figure 61. The effect of air gap and weld bead geometry in 4 mm Optim 900 QC plates. Pictures A1 and A2 are taken from sample 9004-3M without air gap and pictures B1 and B2 are from sample pre-9004-3M that has air gap of 1 mm.

Microhardness was measured from sample pre-9004-3M, and no major difference can be observed compared to 9004-3M. The only difference is that when the heat input is decreased the softened HAZ is a little narrower. Comparison of hardness profiles of the samples is presented in Figure 62. No further studies were done for the sample pre-9004-3M.

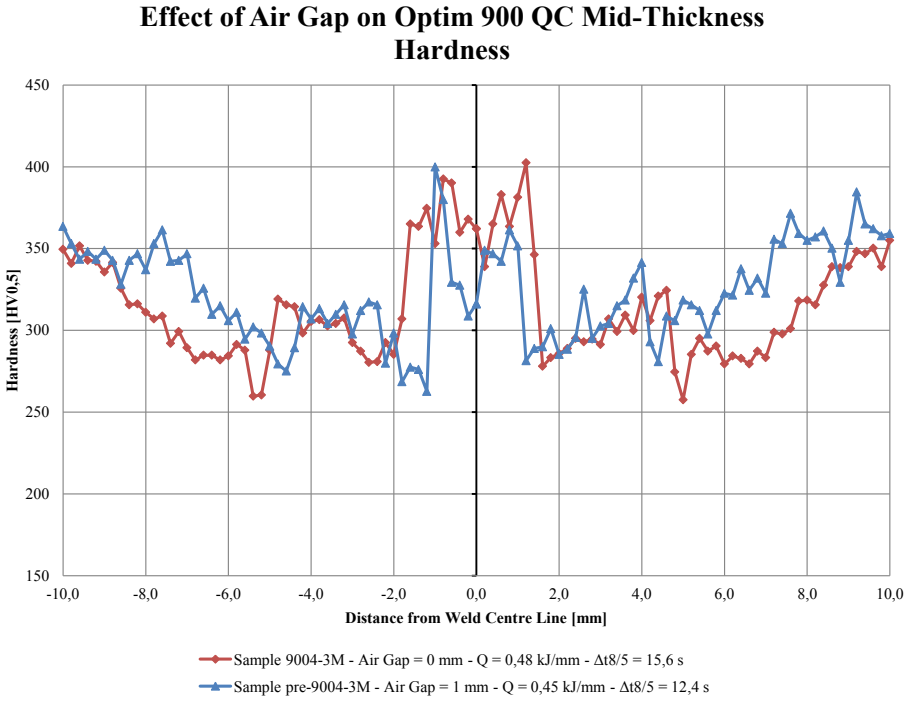

Figure 62. Effect of air gap in 4 mm MAG welded Optim 900 QC plate.

All the 6 mm plates were welded with single-pass. Groove geometry was selected according to preliminary welding tests as squared groove. To establish the conditions for single-pass weld it was essential to use an air gap. Air gap was set to 1 mm which was enough to control the penetration properly without the need for backing. In all cases where the backing was not used, the parameter window was extremely narrow.

Changes in the parameters, especially in the arc voltage, and in the width of air gap led to excessive penetration. In laboratory conditions, penetration can be controlled when the plate size is small, but in production line it has to be monitored all the time. Excessive penetration can be seen in the samples 7006-1M and 9006-3M which was noticeable for solid wires.

Plates with 8 mm thickness were welded with single-pass and squared groove with air gap of 2 mm. Due to air gap, backing was needed to produce a good quality weld and less heat input was introduced to the base material. In addition, the parameter window is much wider when backing is used, and hence the process is not as sensitive as in case where there are no backing involved.

PAW welding was carried out by using filler wire of 1,2 mm in all cases. Groove geometry was selected according to the preliminary welding tests to squared groove. All the plates, 4 mm, 6 mm, and 8 mm, were welded with single-pass and air gap was not needed. Due to the excellent control of penetration, backing was not used; only backing gas was used. Filler wire was fed against the welding direction, which turned out to be the most suitable way in all cases.

All the 4 mm plates were welded using Ø 1,2 mm filler wire. Filler wires with a diameter of 0,8 mm or 1,0 mm may have been more suitable. Due to the size of the wire, the filler wire feed rate was kept low, and hence the alloying effect to the weld itself was minor. The bead shape and size was excellent in all cases and only in sample 9004-3P minor undercutting can be observed. The keyhole was stable in all cases.

The importance of the filler wire size stands out even more in thicker plates. The droplet size of the molten filler wire increased significantly in 6 mm and 8 mm steel plates. Due to the fact that more thermal energy is needed to establish a stable keyhole, less energy is available to melt the wire, and hence significant porosity can be observed. Figure 63 presents porosity as a consequence of too thick filler wire and too high filler feed rate in 8 mm plates. On the final welds, porosity was not observed.

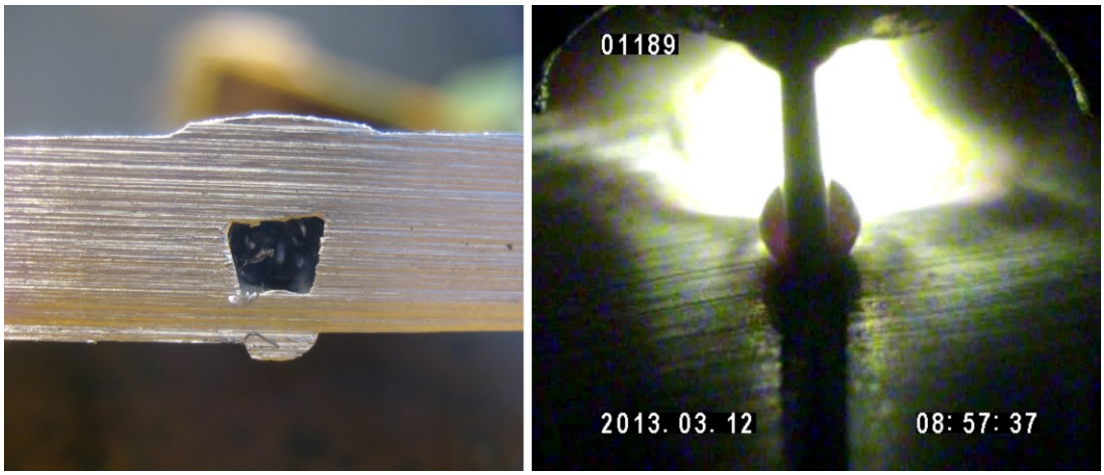

Figure 63. Porosity in 8 mm plate thickness was observed in preliminary PAW welding tests.

In 6 mm plates, minor undercutting was observed only in sample 9006-4P. Undercutting and excessive penetration can be observed in sample 9008-4P. As a result of increased heat input in 8 mm plates, PAW is suitable only for 4 mm and 6 mm plates when using filler wire of 1,2 mm. In preliminary welding tests, it was observed that small changes in welding parameters can affect the end result significantly. Biggest problem was to find the balance between the welding speed and the current, especially for 8 mm plates, where the parameter window is narrow. Figure 64 presents typical weld defects in 8 mm plates which were eliminated in the final welds. The removal of the oxide layer was essential to avoid damage of the electrode.

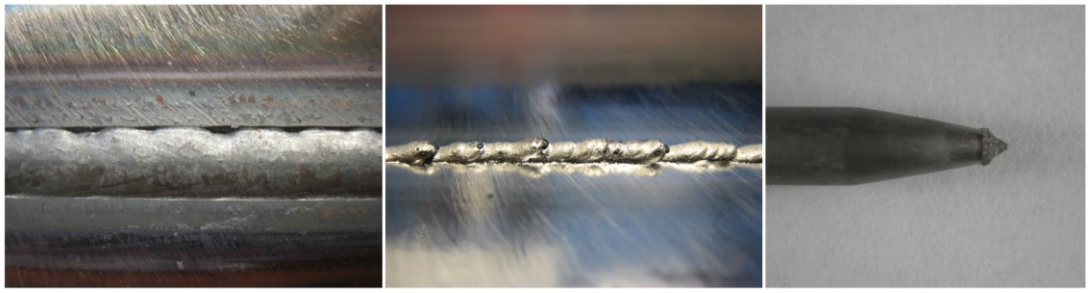

Figure 64. Typical weld defects in preliminary weld tests in 8 mm plates: undercuts (left), excessive penetration (middle) and damaged electrode (right).

In addition to argon plasma gas, helium-argon and hydrogen-argon mixtures were used in the preliminary tests to evaluate the suitability. Due to the high ionization potential of helium, the arc ignition was hard to establish when the helium content was 30 %. The arc temperature is increased and at the same time the arc column gets wider when helium is introduced. In theory, this should lead to a situation where the

welding speed can be increased, and hence lower the heat input, but in practice the 30 % helium content was too much. Any major difference to pure argon could not be visually observed in 6 mm plates. In 4 mm test plates, the bead surface was much smoother. In 8 mm plates, the penetration was not sufficient and the weld pool was much wider than with argon. The 30 % helium content was too much, and hence should be restricted to less than 30 %. In the hydrogen-argon mixture, the hydrogen content was 5 %. Hydrogen-argon mixture was tested only for 6 mm and 8 mm plates. The biggest difference was in weld pool size compared to argon, but any major advantage was not observed. In both cases, no further research was done.

SAW welding was carried out by using filler wire of 3,0 mm in all cases. Groove geometry was selected according to the preliminary welding tests to squared groove. All the plates, 4 mm, 6 mm, and 8 mm, were welded with single-pass and air gap was not used. Due to high deposition rate and arc pressure backing was used to control the penetration.

In 4 mm plates, excessive penetration can be observed in sample 9004-5S because of the backing tape was fitted too loosely. To accomplish a narrow weld and introduce less heat input to material, a smaller filler wire may have been a better choice. For instance, a single 2 mm wire or even twin wire of 2 * 1,2 mm would have made a drastic change to outcome.

In sample 9006-5S, the backing tape was fitted too tight against the back of the plate, and hence undercutting can be observed in the longitudinal edge of root face. Due to higher current density, the solid filler wire (OK Autrod 13.43) lead to a better penetration than the cored wire (OK Tubrod 15.27S), which can be seen from the weld cross-sections. Due to lack of an air gap, the weld bead is excessive in samples 7006-6S and 9006-6S.

Excessive penetration can be observed in the 8 mm plates in samples 7008-5S and 9008-5S. Backing tape was not properly attached in 9008-5S, and therefore the root penetration is not sufficient and local stress concentrations may occur.

All the samples were visually inspected according to standard SFS-EN ISO 5817. Ultrasonic or radiographic inspections were not performed to evaluate internal flaws. Following defect types were observed:

- 5011 Continuous undercut
- 5013 Shrinkage groove
- 502 Excess weld metal
- 504 Excess penetration
- 505 Incorrect weld toe
- 506 Overlap
- 515 Root concavity.

The most common defects were undercuts, excessive weld metal and excessive penetration. Undercuts were the most common in PAW, but also excessive penetration was observed in some samples. Excess weld metal and excess penetration was observed in MAG and SAW, respectively. According to visual inspections the majority of the samples fulfilled the requirements at least of quality level C, which is minimum requirement for the statically loaded steel structures.

Base material hardness was measured to evaluate the impact of heat input. The hardness in Optim 700 MC Plus is the same whether the plate thickness is 6 mm or 8 mm. Optim 900 QC has also relatively the same hardness values between 4 mm, 6 mm and 8 mm plates. The 4 mm plate has slightly higher hardness than the others.

In this study, it can be shown that both of the steel grades show a behavior of softening in HAZ. Due to grain growth, higher heat input and slower cooling times leads to lower hardness values in HAZ. It can be observed that in Optim 700 MC Plus the heat input affects directly the width of the HAZ, as the heat input is increased the width increases with it. However, the maximum hardness drop in HAZ is not dependent directly on the heat input. It can be observed from the sample 7006-1M, which was welded using 0,56 kJ/mm, that the minimum hardness in HAZ is dropped to a region of 226 HV0,5, whereas the sample 7008-2P with 1,40 kJ/mm has the hardness of 220 HV0,5 in HAZ. Based on this, the hardness in HAZ does not show any direct gradual decrease as the heat input is increased, until it reaches 1,91 kJ/mm or higher. The base material softening starts at the FL in all cases except in PAW. In some PAW samples the hardness was even greater than the weld hardness. Softened HAZ extends from FL through CGHAZ and FGHAZ, which can be a result from recrystallization of the microstructure and transformation to austenite during the thermal cycle. This kind of behavior is typical for TMCP steels. The low hardenabil-

ity in CGHAZ and FGHAZ can be explained by the low carbon and alloying content. In the ICHAZ and SCHAZ the hardness starts to increase. The Optim 700 MC Plus shows a characteristic for increased hardening, which is located in SCHAZ. In this region the temperature is increased to temperatures below A_1. Due to the thermal cycle, the increase in hardness may be a result from precipitation of metastable carbides of Ti, which is used in the steel. Increased hardness can be seen from the microhardness profiles taken from mid-thickness of each sample despite what has been the heat input.

According to microhardness results the dilution rate plays an important role in Optim 700 MC Plus. Smaller air gap size leads to a bigger dilution rate which may be one of the reasons why the weld hardness is decreased in 7006-1M. In 8 mm material thickness when the air gap was 2 mm the weld hardness is higher, especially at 7008-1M. This may be caused by the lower dilution rate and higher content of deposited weld metal which hardened during the solidification, although the cooling was longer and the same filler wire was used. The same hardness drop cannot be seen when cored filler wire was used in samples 7006-2M and 7008-2M, though the air gap is different.

The microhardness results of PAW samples in Optim 700 MC Plus show that the drop in hardness is small between the WM and ICHAZ, which is the result from long cooling times and dilution rate. Due to low wire feed rate, the alloying effect of filler wire to the weld was minimal.

In SAW microhardness results, the softened HAZ is located next to the weld, to the boundary of the CGHAZ where the temperature has risen to the austenite region and grain size has grown. This can be seen from all of the samples.

It can be pointed out from the hardness profiles that Optim 900 QC has a strong tendency for softening. Two noticeable zones can be observed where the hardness is dropped in HAZ. Hardness is dropped in FL below the weld and the base material hardness. Due to high temperature, it is uncertain are the Nb and V particles dissolved, but most likely only the TiN particles are undissolved and can constrain the growth of the grain boundaries. Hardenability can be observed in CGHAZ, which can be caused by the carbon content of the base material and intense grain growth

during the heating and cooling stages, and hence hard phases can be observed. The second drop in hardness in located at FGHAZ. During the cooling stage, the transformation from austenite to ferrite leads to more desirable ferritic phases than in CGHAZ, therefore it is probable that polygonal ferrite is formed. Beyond this region the base material has been tempered and the hardness increases gradually. This kind of behavior in base material is common with MAG, PAW and SAW, however it is more noticeable in MAG because of the lower heat input.

WM hardness is below the base material hardness in all PAW samples, which may be caused by the dilution rate and high heat input. Same thing can be observed in SAW welded samples with the difference that in those hardness is are distributed more evenly but no major variation can be seen compared to MAG or PAW microhardness profiles.

Cooling times were measured from all the samples using thermocouples, and calculation was also carried out. It can be seen that increased heat input will lead to slower cooling times and also plate thickness and air gap affect the results. Based on Figure 65, the calculations have quite similar values than the measured ones when the heat input was low. Due to low heat input, especially with MAG samples, the values are relatively close to each other. Measured and calculated values start to differ when high welding heat input was used. As the heat input increased, the difference begins to increase that can be seen from SAW samples. Prediction of the cooling time using Equation 4, particularly with SAW, gave 23 - 44 % higher values than the ones that were measured. One of the reasons may be in the fact that the thermocouples were not plunged into the molten weld pool, and hence the difference is significant and not very reliable.

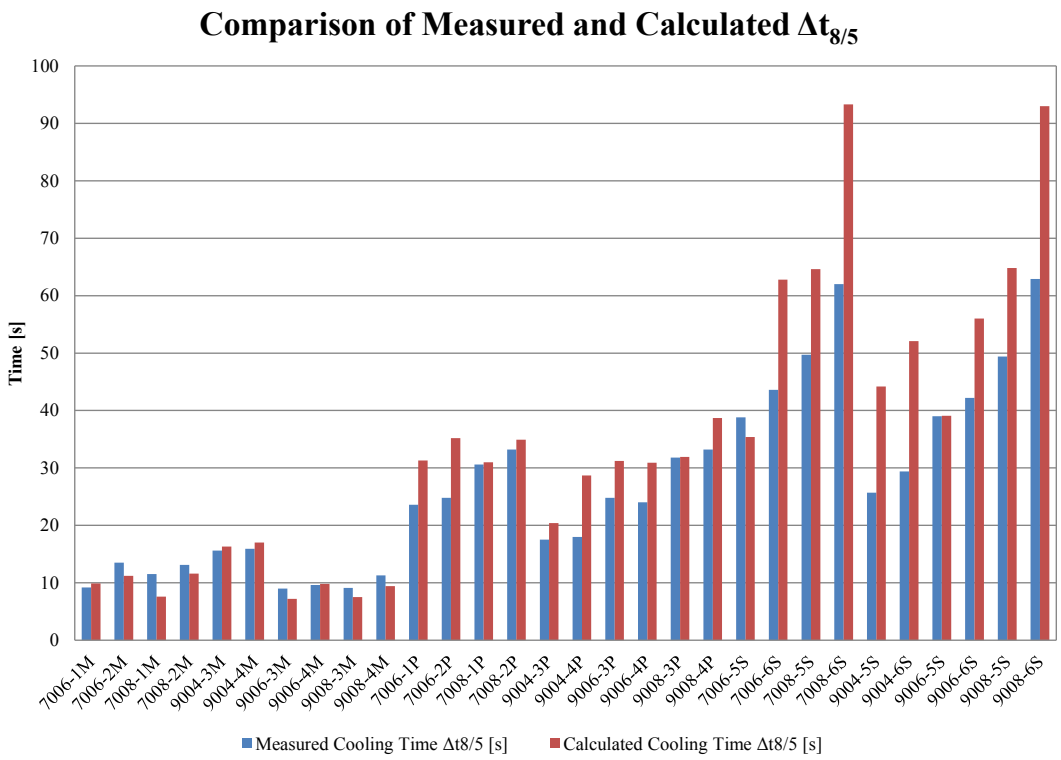

Figure 65. Cooling time comparison between measurements and calculations.

For the Optim 900 QC, acceptable heat input was 0,5 - 0,8 kJ/mm and the cooling time 5 - 15 s. All the MAG samples were in the range of 0,48 - 0,81 kJ/mm which fulfilled the requirements, excluding the 4 mm plates which should have been limited to 0,4 kJ/mm at the most. In addition, almost all of the samples meet the expected cooling time values, and remained under 15 s. PAW and SAW samples did not meet the requirements in any case, especially in terms of cooling time. This can be seen from the microhardness and tensile test results. Optim 700 MC Plus has the cooling time range of 5 - 20 s which was fulfilled in every MAG sample. PAW and SAW samples did not meet the requirements in any case.

Tensile testing was carried out for the welded samples according to SFS-EN ISO 4136. Figure 66 presents tensile test comparison of different welding methods for Optim 700 MC Plus. The best relationship with yield and tensile strength is achieved by using MAG welding. Due to lower heat input and slightly undermatching consumable, the tensile properties of welded samples are equal or higher than the base material yield strength. Using matching consumable with MAG the properties are expected to be enhanced. In PAW samples, the heat input and dilution affected the results and the welded samples do not meet the properties of the base material. Ten-

sile properties of the SAW samples are good compared to MAG and PAW even though the heat input was as much as 44 to 65 % higher than that of MAG welded samples. This is because the filler wires for SAW were more alloyed. Based on the studies, the Optim 700 MC Plus can keep its properties when using high heat input welding methods and the tensile properties are not reduced significantly. Tensile test results are dependent on the properties of HAZ and the consumable selection. HAZ properties are controlled by the heat input and the cooling time. Tensile test results show that as the heat input is increased and HAZ gets wider, the yield and tensile properties of the structure are decreased.

According to the tensile test results of Optim 700 MC Plus, the solid filler wires performed better than the cored filler wires. One of the reasons for the better performance is the fact that the required arc energy for a single-pass weld was lower.

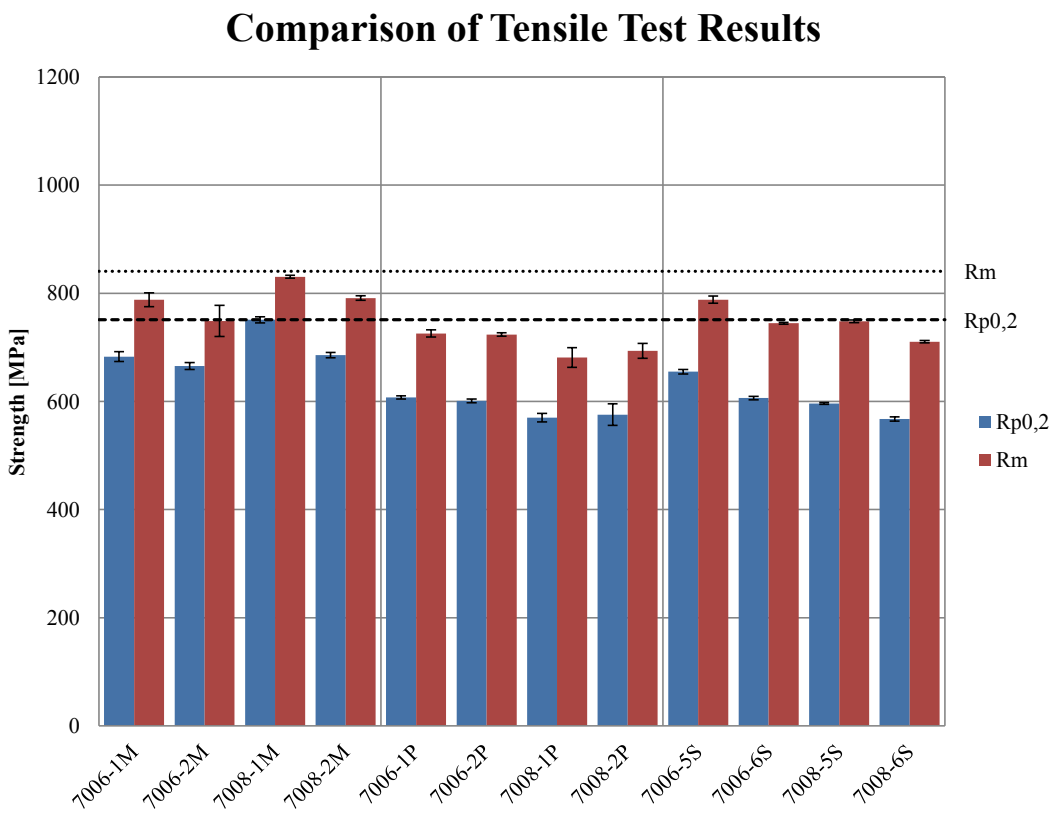

Figure 66. Comparison of the tensile test results between each welding method. Base material is Optim 700 MC Plus and base material yield and tensile strength are marked on the chart.

Figure 67 presents tensile test comparison of different welding methods for Optim 900 QC. Comparison chart shows the same behavior as for Optim 700 MC Plus, but

the drop in the strength level is more notable. The yield and tensile strength are decreased drastically when the heat input of 0,73 kJ/mm is exceeded in MAG. One of the reasons for the sharp drop is that the bainitic-martensitic microstructure is tempered and HAZ dimensions have increased. The behavior of softening becomes more dominant as the certain level of heat input is introduced to the base material.

Air gap, especially with 8 mm plates, does provide a better strength to the joint, because the heat flow is more efficient and dilution is decreased. Increasing the heat input in PAW and SAW samples between 0,54 - 2,29 kJ/mm, the difference in the results is not notable. Even at 0,54 kJ/mm in PAW the strength level should be much better compared to MAG results. This may be caused by the dilution, because air gap was not involved in any PAW or SAW procedures.

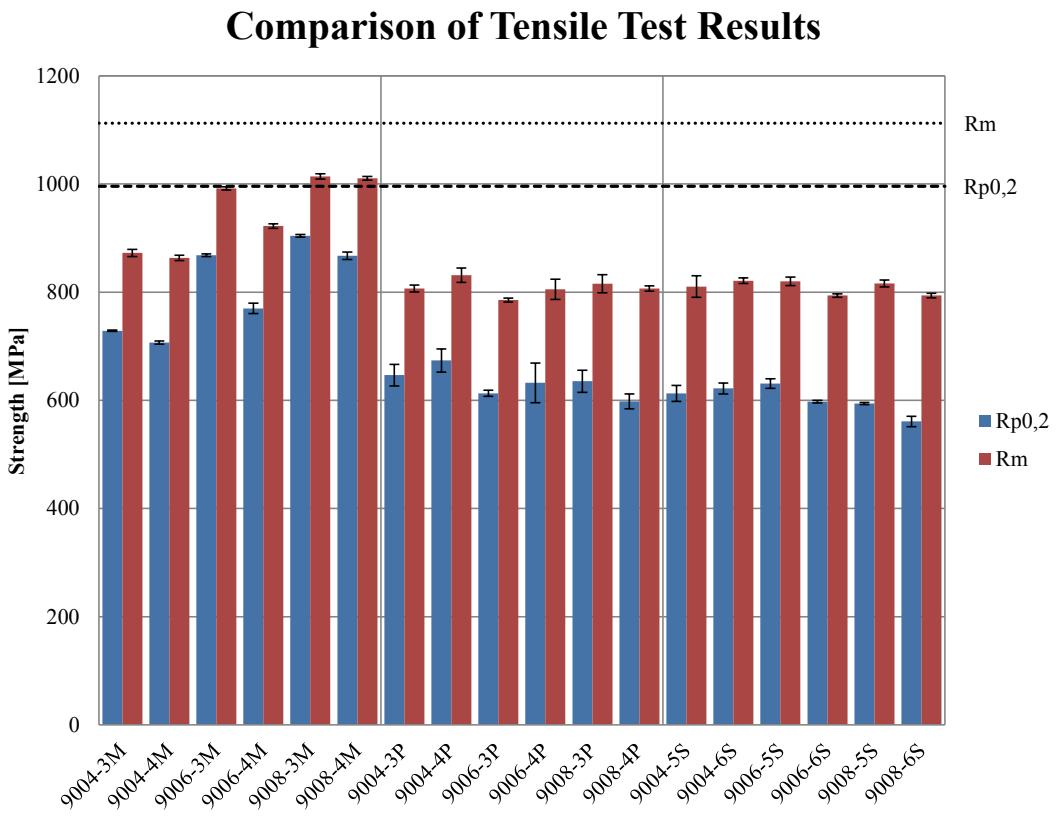

Figure 67. Comparison of tensile test results between each welding method. Base material is Optim 900 QC and base material yield and tensile strength are marked on the chart.

In addition to tensile and hardness testing, Charpy-V impact testing was carried out for better understanding of the behavior of different consumables in different conditions. To compare the impact test results between each welding method, temperature

of -20 ºC was selected as common factor. Impact testing was made according to SFS-EN ISO 148-1 and 9016.

The correlation between a sub-sized specimen and the full-size specimen was carried out by using the factors of 3/2 for the 6 mm plates and 6/5 for the 8 mm plates. In the test procedure only three different temperatures were involved, and therefore the transition temperature could not be calculated, and use of another method for size correlation was not possible. Based on this fact the results can only be compared to each other.

Impact energies of Optim 700 MC Plus and 900 QC are compared in Figure 68. Based on the test temperatures, both of the 6 mm plates do not show characteristic ductile-to-brittle behavior and the manufactures minimum requirements are met. The proportion of ductility in fracture surface at -60 ºC is approximately 80 % in Optim 700 MC Plus. In Optim 900 QC the ductility is estimated to be around 70 % in the same conditions. In 8 mm steel plates the proportion of ductility in fracture surface at -60 ºC is estimated to be about 90 % in Optim 700 MC Plus. Ductility in 8 mm Optim 900 QC plate is dropped drastically to a level of 20 %.

As the material thickness of test plates is changed to 8 mm, the impact energies are in the ductile-to-brittle transition, and start to be near to the lower shelf region, especially for sample 9008-BM.

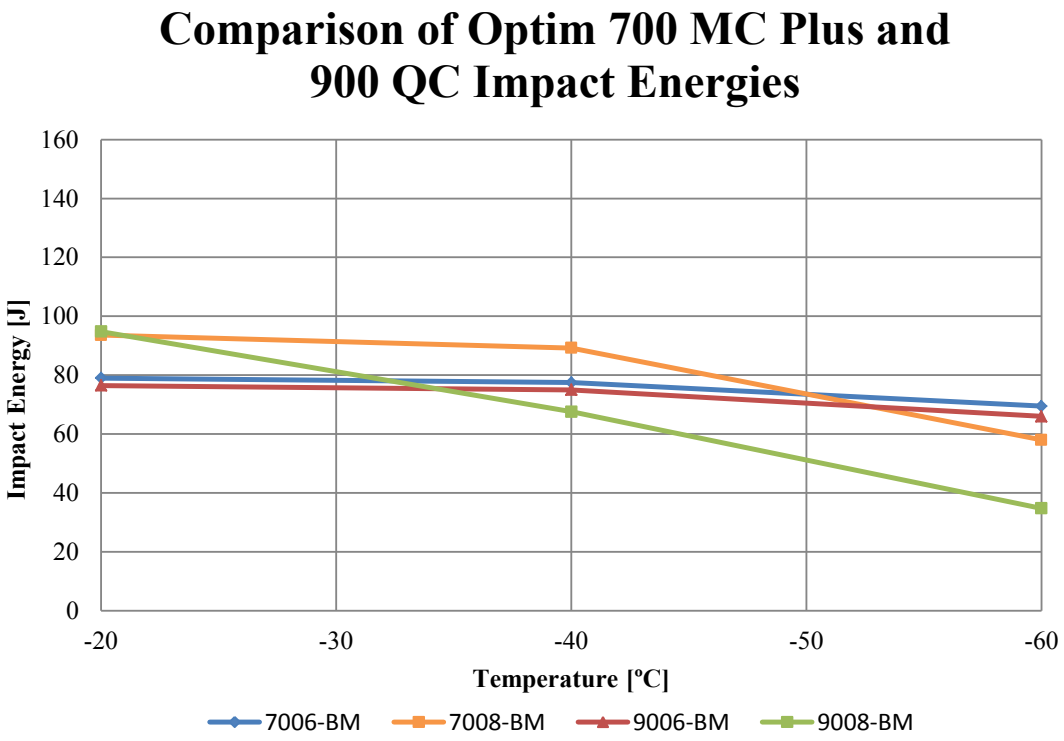

Figure 68. Comparison of base material impact energy properties.

Figure 69 presents impact energies for 6 mm Optim 700 MC Plus for each welding method. At the test temperature of -20 ºC MAG and SAW welded samples behaved in the most favorable way in all zones. Based on the studies, the microstructure in the samples favors acicular ferrite. It can be justified that increased heat input has a direct influence in the impact toughness, which can be seen from MAG and PAW samples where the same filler wires were used. When TMCP steels are alloyed with microalloying elements such as Nb, Ti and V, higher and longer cooling times provide undesired microstructures and properties in the HAZ. Nitrides and carbides that are used to restrict the grain growth can be dissolved if too much thermal energy is introduced to the base material. Even the most stable Ti precipitates can dissolve if the temperatures and holding times are too excessive, and hence the heat input should be kept as low as possible, especially when using conventional welding methods.

The PAW samples have low impact energies through the whole test procedure, especially in the HAZ. Impact energies are good only in WM, but in the HAZ the toughness is significantly decreased. Weakest region is located in the HAZ, more precisely in the FL and FL+1. According to studies, any straightforward conclusions cannot be

made which zone is better or worse. The main reason is in the fact that the notch cannot be placed precisely on the right narrow zone, and therefore results show variation. In addition, dependent on what is the heat input, groove geometry and whether the air gap is used or not, the shape of the weld curves horizontally which leads to conditions where the Charpy-V notch test area may include some weld metal. This should be also taken into consideration, because it will cause statistical scatter when comparing different welding methods.

In SAW, the cored wire was more alloyed than the solid wire which compensated the high heat input and caused the good results in WM. Higher content of Ni produced desirable microstructure. Even at FL and FL+1 the impact energies are very good, even though the heat input and cooling times were increased. It is mentioned earlier that high heat input, deposition rate and the lack of air gap will provide a wider weld dimensions especially in SAW which leads to a situation where weld metal is included in the test area. This particular reason may be the case since the SAW samples behaved excellently in FL and FL+1.

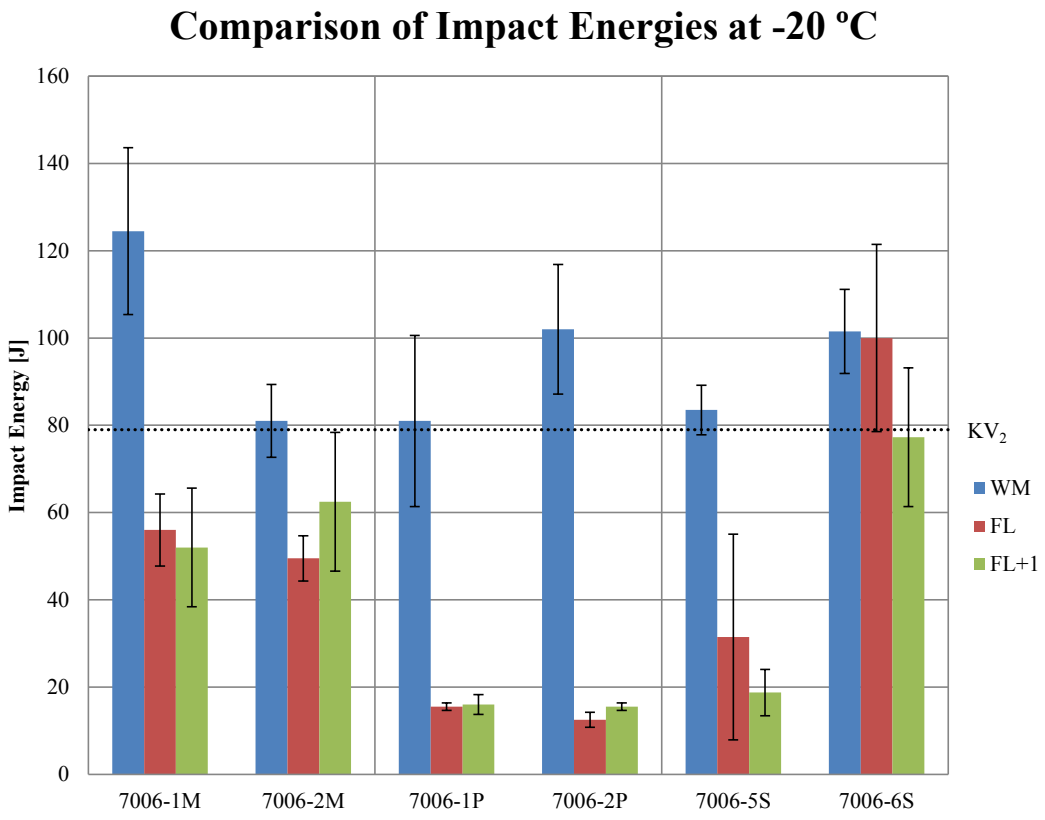

Figure 69. Comparison of impact energies between each welding method for 6 mm Optim 700 MC Plus. Base material energy level is marked on the chart.

The 8 mm Optim 700 MC Plus shows the decrease in impact toughness (Figure 70) when the heat input is increased compared to 6 mm plates. In WM the results are satisfying, but in FL and FL+1 the values are decreased. The sharp hardness drop in HAZ properties is the characteristic feature of Optim 700 MC Plus, which is more notable in the single-pass welded 8 mm plates. Due to lower dilution rate, higher deposition rate and alloying content, cored wires in MAG and SAW have a better impact toughness in WM than solid wires, which can be observed as the air gap in increased to 2 mm. The same feature cannot be observed in PAW samples. Due to dilution and unevenly distributed alloying in undermatching weld can cause local mismatches, and therefore the impact energies are near the lower shelf region.

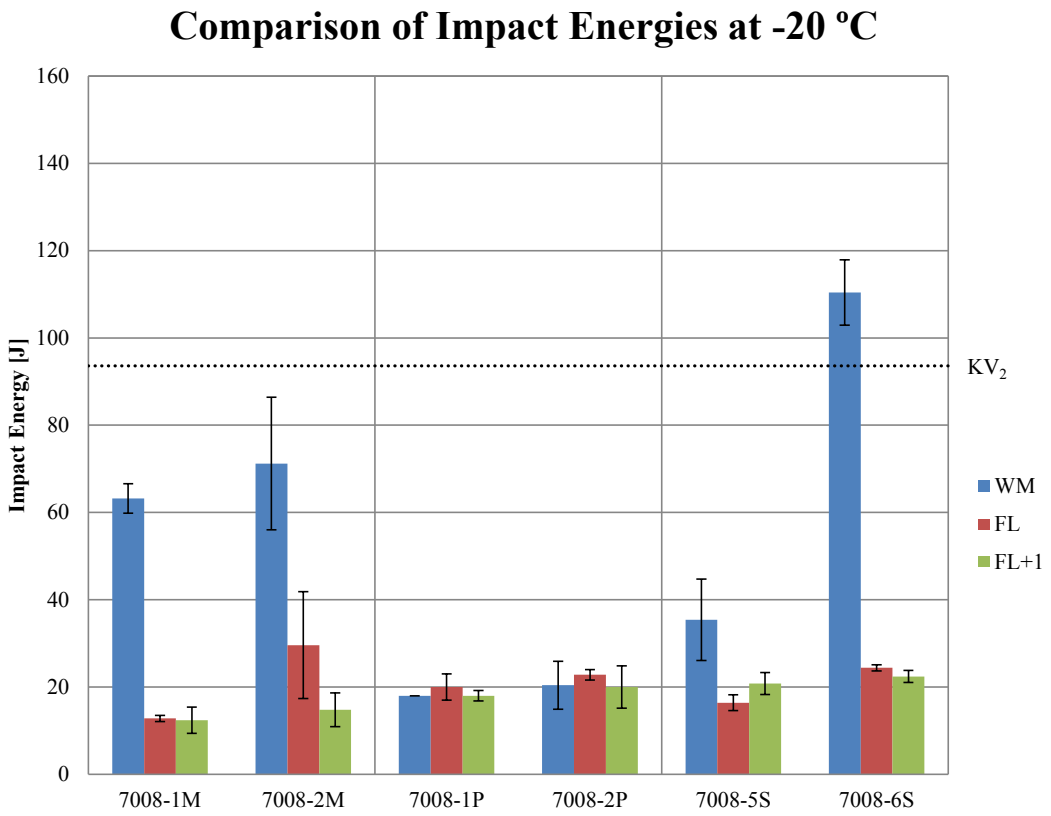

Figure 70. Comparison of impact energies between each welding method for 8 mm Optim 700 MC Plus. Base material energy level is marked on the chart.

Test results of the 6 mm Optim 900 QC show that the cored wires can produce higher impact energies than solid wires, although more welding energy is needed to make a single-pass weld. This can be seen from MAG and SAW results in Figure 71. The lack of air gap decreases impact toughness values in PAW which can be caused

mainly by the dilution rate and high heat input combined with increased cooling time.

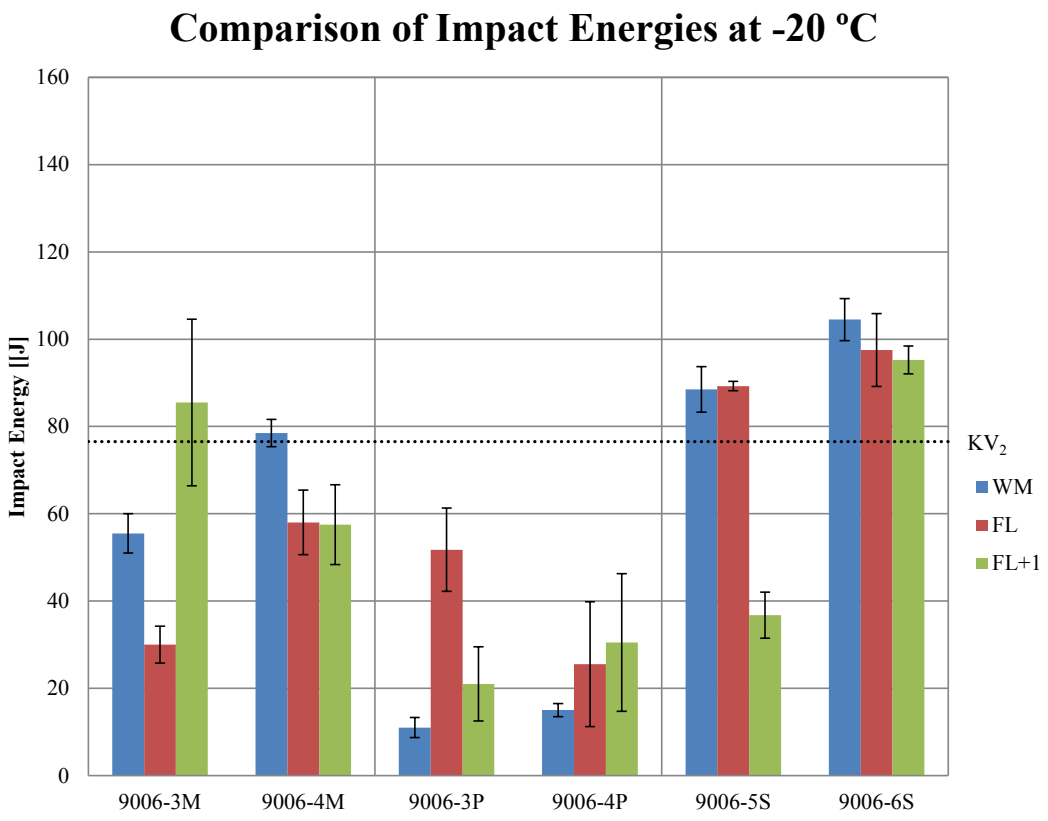

Figure 71. Comparison of impact energies between each welding method for 6 mm Optim 900 QC. Base material energy level is marked on the chart.

According to studies in 8 mm Optim 900 QC plates MAG and SAW produce the highest impact toughness values (Figure 72). The difference between cored and solid wires is relatively low in each zone for MAG. For SAW, the cored wire produces higher energy than solid wire in WM, but in the FL and FL+1 the values are similar. The PAW samples are able to produce no good toughness even at -20 ºC.

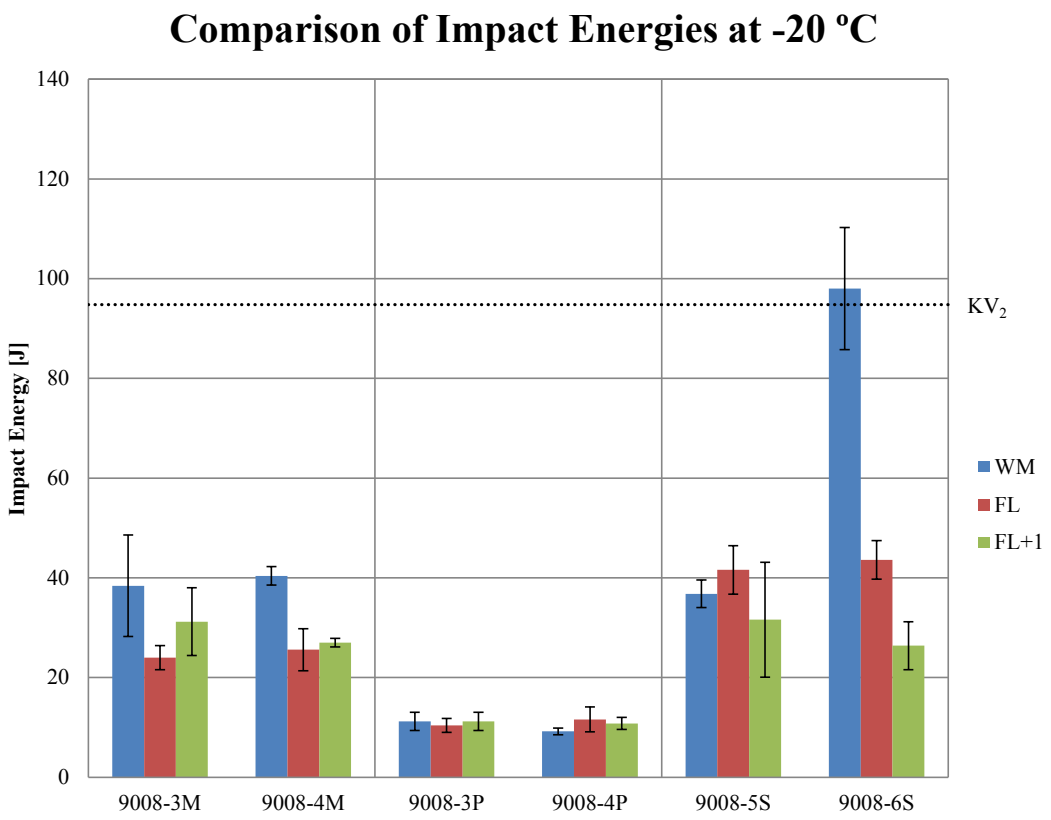

Figure 72. Comparison of impact energies between each welding method for 8 mm Optim 900 QC. Base material energy level is marked on the chart.

Inverse pole figure maps (Figure 58 and 59) taken by EBSD show in both cases that the material is anisotropic, and texture can be observed especially in the Y-plane, where the grains are elongated in the rolling direction. The average grain size from Table 14 using the EBSD area-based method shows that in every plane the grain size is significantly bigger than what is present in the manufacturers product information. According to literature review, the average grain size of Optim 900 QC was 1 µm. Any comparison data for the grain size of Optim 700 MC Plus was not found.

The estimate of expenses for each welding process depends on many factors such as size and shape of the component, production volume, weld design, base material and number of passes. This will determine the overall equipment costs for instance what kind of welding process is needed, level of automation, welding conveyors, joint tracking units and the costs from consumables, shielding gases and fluxes. Conventional welding methods are relatively inexpensive, but when the process is integrated to production, equipment and accessories are usually custom-made to each individual

application. The costs of MAG welding equipment with state of the art synergic power source and wire feeder for industrial use can be approximately 10 000 €. The equipment for PAW is around 30 000 €. The price range for SAW is case-specific among the others, and can be between 80 000 - 100 000 € or more. The price range of novel welding methods such as LBW and FSW is 200 000 - 600 000 €. Together with welding conveyor and jig, the price can be multiplied.

9 CONCLUSIONS

Manufacturing of lightweight structures using conventional and widely used welding methods, such as MAG, PAW and SAW, has been studied. Limitations and possibilities for each welding method are learned to known. This knowledge offers possibilities to design efficient and economical lightweight structures by using inexpensive equipment. By using the benefits of the mechanical properties, pros and cons of each welding methods are categorized. This can be used to choose the most suitable welding process for each application.

In order to select the most suitable welding method for each different application the requirements of the structure have to be known. Conventional welding methods have their own limitations when dealing with AHSSs. It is a matter of minimizing the costs and controlling the properties without losing material properties in the critical parts.

Thermal cycle during welding causes softening in HAZ on both steel grades. The softened HAZ is the characteristic phenomenon of quenched and thermomechanically rolled high-strength steels. The softened HAZ can be observed from all the welded samples. The amount of softening is highly dependent on the heat input and cooling time, and therefore higher heat input and longer cooling times provide wider CGHAZ which will lead to growth of austenite grain size and dissolution of unstable nitrides and carbides. In both steels, hardness of the HAZ must be taken into consideration, especially in the case where matching filler wires are used. Using undermatching consumables the hardening is not so much of an issue.

The studies showed that the conventional welding methods can produce high quality welds, if the possibilities and limitations of each welding method are recognized. Each of the methods has their own benefits and limitations. By far, MAG welding is the most suitable for all the test material thicknesses. It combines good penetration, low heat input and affordable equipment. The downside of the process is the fact that only 4 mm plates can be welded without air gap and backing, which restricts the usage. The 6 mm plates do not need necessarily backing, but air gap is needed. The main problem with air gap is that the parameter window is narrow and high precision is needed to avoid excessive or lack of penetration, and therefore joint tracking is

needed especially in larger scale applications for instance in crane booms. The biggest limitation of the process is the need of backing in 8 mm plates. The accessibility is restricted for instance in crane booms, and therefore the installation of backing can be difficult or impossible. PAW welding is suitable if air gap and backing are not accepted, but the effects of dilution rate and high heat input should be taken into consideration. In addition, the material thickness should be restricted to 6 mm. In fact, the best conditions for welding are achieved in the 4 mm plates. As the plate thickness increases, the weld defects become more dominant in terms of undercuts and porosity, and therefore the PAW should not be used to weld the 8 mm plates without air gap. The downside of the process is high equipment price and shielding gas consumption. Due to high deposition rate, backing is needed in SAW welding. To reduce the heat input, different groove geometries should be evaluated. According to manufacturers recommendations for the heat input and cooling time, MAG welding can follow the guidelines in every case. PAW and SAW are exceeding the recommendations, which can be observed from the results, especially with wide softened HAZ.

Mechanical properties of the welded structures are controlled by the heat input, cooling time from 800 ºC to 500 ºC and the selection of consumable. Increased heat input is shown to have a drastic effect on the yield and tensile strength, softening in the heat-affected zone and reduced impact toughness. Reducing the heat input and dilution rate by modifying the joint preparations for single-pass welding and the right selection of consumables can enhance the mechanical properties of the welded joint.

Recommendations for future study

In addition to tensile, hardness and impact tests, the test welds should be investigated with fatigue tests.

More detailed microstructure analysis using SEM and EBSD.

Dissolution of precipitations in HAZ should be studied, and also thermodynamics of the grain growth and stability of the microstructure.

The effects of alloying in the cooling time should be studied.

Weldability of 6 mm and 8 mm plates should be studied using tandem-MAG, and filler wire size should be optimized individually to each welding method and plate thickness.

REFERENCES

[1] Arcelor Mittal´s Webpage, 2013, Complex Phase Steels, referred 24.05.2014, availability: http://automotive.arcelormittal.com/automotive/saturnus/sheets/catalogue.pl?id_sheet=C&language=EN.

[2] ASM Handbook, 2004, Metallography and Microstructures, Vol. 9, ASM International, pp. 66 - 67

[3] ASM Handbook, 1993, Welding, Brazing and Soldering, Vol. 6, ASM International, pp. 64 - 69, 181 - 185.

[4] Bhadeshia H., K., D., H., Honeycombe R., W., K., 2006, Steels - Microstructure and Properties, 3rd ed., Elsevier Ltd., 344 p.

[5] Bracke, L., De Wispelaere, N., Ahmed, H. ja Güngör, Ö. E., 2011, S700MC/Grade 100 in Heavy Gauges: industralisation at ArcelorMittal Europe, Revue de Métallurgie, Vol. 108:6, pp. 323 - 330.

[6] Callister W., D., Jr., 2007, Materials Science and Engineering an Introduction, 7th ed., John Wiley & Sons, Inc., pp. 84, 135, 155 - 160, 188 - 190, 224, 347.

[7] Demeri M., Y., 2013, Advanced High-Strength Steels: Science, Technology, and Applications, ASM International, 300 p.

[8] Det Norske Veritas, 2013, Rules for Classification of Ships / High Speed, Light Craft and Naval Surface Craft, Newbuilding Materials and Welding - Fabrication and Testing of Ships, Part 2, Chapter 3, pp. 24 - 25.

[9] Easterling K., 1992, Introduction to the Physical Metallurgy of Welding, 2nd ed., Butterworth-Heinemann Ltd, pp. 126 - 190.

[10] Esab Welding Handbook, 2007, Consumables for Manual and Automatic Welding, 8th ed., Esab AB, pp. 77, 122, 134, 153,171.

[11] Esab´s Webpage, 2014a, Welding Consumables, OK AristoRod 89, referred 18.03.2014, availability: http://products.esab.com/Templates/T041.asp?id=181466.

[12] Esab´s Webpage, 2014b, Welding Consumables, Coreweld 89, referred 18.03.2014, availability: http://products.esab.com/Templates/T041.asp?id=194964.

[13] Gladman T., 1997, The Physical Metallurgy of Microalloyed Steels, The Institute of Materials, pp. 81 - 106, 325 - 336.

[14] Hemmilä M., Laitinen R., Liimatainen T., Porter D., 2010a, Mechanical and Technological Properties of Ultra-High-Strength Optim Steels, Rauraruukki Oyj, referred 03.04.2013, availability: http://www.ruukki.fi/~/media/Files/Steel-products/Technical-articles/Ruukki-Technical-article-Mechanical-and-technological-properties-of-ultra-high-strength-Optim-steels.ashx, 8 p.

[15] Hemmilä M., Hirvi A., Kömi J., Laitinen R., Lehtinen M., Mikkonen P., Porter D., Savola J., Tihinen S., 2010b, Technological Properties of Direct-Quenched Structural Steels with Yield Strengths 900 - 960 MPa as Cut Lengths and Hollow Sections, Rautaruukki Oyj, referred 25.10.2012, availability: http://www.ruukki.es/~/media/Files/Steel-products/Technical-articles/Ruukki-Technical-article-Technological-properties-of-direct-quenched-structural-steels.ashx, 8 p.

[16] Hemmilä M., Liimatainen T., Porter D., Kömi J., Laitinen R., Mikkonen P., 2011, Mechanical Properties and Weldability of 700 MPa Structural Steels with Excellent Formability, "The 3rd International Conference on Steels in Cars and Trucks, SCT 2011, June 5 - 9, 2011, Salzburg, Austria, Verlang Stahleisen GmbH, referred 06.06.2014, availability: http://www.ruukki.hr/~/media/Files/Steel-products/Technical-articles/Ruukki-Technical-article-Mechanical-properties-and-weldability-of-700-MPa-structural-steels-with-excellent-formability.ashx, 7 p.

[17] Hertzberg R. W., 1996, Deformation and Fracture Mechanics of Engineering Materials, 4th ed., John Wiley & Sons, Inc., pp. 3, 143 - 144.

[18] Kerlin, T.W., 1999, Practical Thermocouple Thermometry, 1st ed., Instrument Society of America, 112 p.

[19] Krauss G., 2005, Steels - Processing, Structure, and Performance, ASM International, pp. 214, 240 - 244.

[20] Kumpulainen J., Tihinen S., Laitinen R., 2011, Ultralujien terästen hitsaus uusilla MAG-menetelmillä, 02/2011 Hitsaustekniikka, Suomen Hitsausteknillinen Yhdistys ry, pp. 6 - 12.

[21] Kou S., 2002, Welding Metallurgy, 2nd ed., Wiley-Interscience, 461 p.

[22] Kuziak R., Kawalla R., Waengler S., 2008, Advanced High Strength Steels for Automotive Industry, Archives of Civil and Mechanical Engineering, Vol. VIII, No. 2, pp. 103 - 117.

[23] Lancaster J. F., 1999, Metallurgy of Welding, 6th ed., Abington Publishing, pp. 244 - 245.

[24] Lukkari J., 2002, Jauhekaarihitsaus, Esab, pp. 86, 116 - 129.

[25] Mallick P. K., 2010, Materials, Design and Manufacturing for Lightweight Vehicles, Woodhead Publishing, pp. 41 - 54.

[26] Martikainen J., 1989, On the Effects of Welding Parameters on Weld Quality of Plasma Arc Keyhole Welding of Structural Steels, Lappeenranta University of Technology, Research Papers 16, 132 p.

[27] Messler R. W. Jr., 2004, Principles of Welding, Processes, Physics, Chemistry, and Metallurgy, Wiley - VCH, 662 p.

[28] Meyers M, Chawla K., 2009, Mechanical Behavior of Materials, 2nd ed., Cambridge University Press, pp. 345 - 348, 558 - 564.

[29] Mitchell P.S., Hart P.H.M., Morrison W.B., 1995, The Effect of Micro-alloying on HAZ Toughness, MICROALLOING 95, Eds. M.Korchynsky et. al., I&SS, 24 p.

[30] Moore P. L., 2003, Novel Method of Recording Cooling Curves During Laser & Laser/arc Hybrid Welding, JOM 11, 25-28 May 2003, referred 20.10.2012, availability: http://www.twi-global.com/technical-knowledge/published-papers/novel-method-of-recording-cooling-curves-during-laser-laser-arc-hybrid-welding-may-2003/.

[31] Nishioka K., Ichikawa K., 2012, Progress in Thermomechanical Control of Steel Plates and Their Commercialization, IOP Publishing, Science and Technology of Advanced Materials, Volume 13, Number 2, 20 p.

[32] den Ouden G., Hermans M. J. M., 2009, Welding Technology, 1st ed., VSSD Publishing, pp. 81 - 88.

[33] Ruukki´s Webpage, 2013a, Optim 700 MC Plus, referred 13.02.2013, availability: http://www.ruukki.fi/Tuotteet-ja-ratkaisut/Terastuotteet/Kuumavalssatut-terakset/Rakenneterakset/Optim-MC.

[34] Ruukki´s Webpage, 2013b, Optim 900 QC, referred 13.02.2013, availability: http://www.ruukki.fi/Tuotteet-ja-ratkaisut/Terastuotteet/Kuumavalssatut-terakset/Rakenneterakset/Optim-QC.

[35] SFS-EN ISO 148-1, 2010, Metallic Materials. Charpy Pendulum Impact Test, Part 1: Test Method, Suomen Standardisoimisliitto SFS, 50 p.

[36] SFS-EN 1011-1, 2009, Welding. Recommendations for Welding of Metallic Materials. Part 1: General Guidance for Arc Welding, Suomen Standardisoimisliitto SFS, 25 p.

[37] SFS-EN 1011-2, 2001, Welding. Recommendations for Welding of Metallic Materials. Part 2: Arc Welding of Ferritic Steels, Suomen Standardisoimisliitto SFS, 113 p.

[38] SFS-EN ISO 4136, 2012, Destructive Tests on Welds in Metallic Materials. Transverse Tensile Tests, Suomen Standardisoimisliitto SFS, 21 p.

[39] SFS-EN ISO 5817, 2014, Welding. Fusion-welded Joints in Steel, Nickel, Titanium, and Their Alloys (Beam Welding Excluded). Quality Levels for Imperfections, Suomen Standardisoimisliitto SFS, 61 p.

[40] SFS-EN ISO 6892-1, 2009, Metallic Materials. Tensile Testing. Part 1: Method of Test at Room Temperature, Suomen Standardisoimisliitto SFS, 123 p.

[41] SFS-EN ISO 9016, 2012, Destructive Tests on Welds in Metallic Materials. Impact Tests. Test Specimen Location, Notch Orientation and Examination, Suomen Standardisoimisliitto SFS, 20 p.

[42] SFS-EN ISO 15614 + A1 + A2, 2012, Specification and Qualification of Welding Procedures for Metallic Materials. Welding Procedure Test. Part 1: Arc and Gas Welding of Steels and Arc Welding of Nickel and Nickel Alloys, Suomen Standardisoimisliitto SFS, 61 p.

[43] Vähäkainu O., 2003, Hitsaajan Opas, Otavan Kirjapaino Oy, 112 p.

[44] Wallin K., 2011, Fracture Toughness of Engineering Materials - Estimation and Application, Emas Publishing, pp. 279 - 290.

Preliminary Welding Procedure Specification (pWPS)

According to SFS-EN ISO 15609-1

Made by: Mikko Peltonen Date: 25.02.2013

Welder: Mikko Peltonen
WPQR No.: 7006-1M

Base Material:	Optim 700 MC Plus	Joint Preparation:	Laser Cutted
Material Thickness [mm]:	6	Backing:	-
Outside Diameter [mm]:	-	Welding Position:	PA
Working Temperature [°C]	20	Mode of Metal Transfer:	Pulse
Preheat Temperature [°C]:	-	Air Gap [mm]:	1
Interpass Temperature [°C]	-		

Joint Design and Welding Sequences

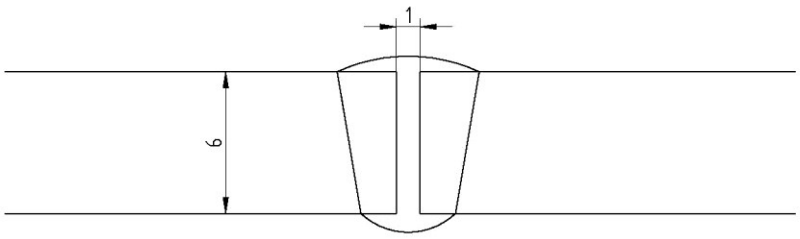

Run	Welding Process	Consumables	Diam. [mm]	Filler Feed Speed [m/min]	Classification	Gas / Flux
1	135	Esab OK Aristorod 69	1,2	10,3 - 10,6	-	82% Ar + 18% CO_2

Run	Polarity	Stick Out [mm]	Current [A]	Voltage [V]	Speed [mm/min]	Heat Input [kJ/mm]	Gas Flow Rate [l/min] Shielding	Backing
1	DC(+)	12	319 - 338	26,3 - 29,1	900	0,45 - 0,52	20	-

Address: Puumiehenkuja 3
PL 14200
FI-00076 Aalto
FINLAND

Figure 73. pWPS for MAG welded sample 7006-1M.

Preliminary Welding Procedure Specification (pWPS)

According to SFS-EN ISO 15609-1

Made by: Mikko Peltonen Date: 25.02.2013

Welder: Mikko Peltonen
WPQR No.: 7006-2M

Base Material:	Optim 700 MC Plus	Joint Preparation:	Laser Cutted
Material Thickness [mm]:	6	Backing:	-
Outside Diameter [mm]:	-	Welding Position:	PA
Working Temperature [°C]	20	Mode of Metal Transfer:	Pulse
Preheat Temperature [°C]:	-	Air Gap [mm]:	1
Interpass Temperature [°C]	-		

Joint Design and Welding Sequences

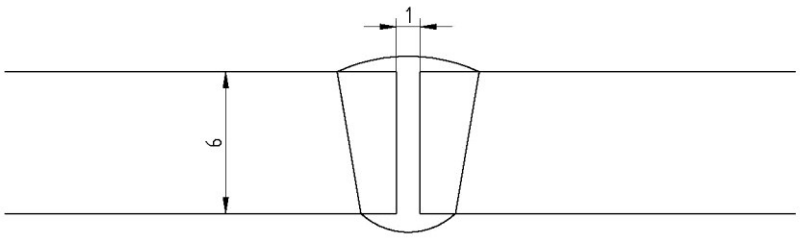

Run	Welding Process	Consumables	Diam. [mm]	Filler Feed Speed [m/min]	Classification	Gas / Flux
1	136	Esab Tubrod 14.03	1,2	12,8 - 13,1	-	82% Ar + 18% CO_2

Run	Polarity	Stick Out [mm]	Current [A]	Voltage [V]	Speed [mm/min]	Heat Input [kJ/mm]	Gas Flow Rate [l/min] Shielding	Backing
1	DC(+)	12	330 - 336	31,0 - 31,8	850 - 900	0,56 - 0,59	20	-

Address: Puumiehenkuja 3
PL 14200
FI-00076 Aalto
FINLAND

Figure 74. pWPS for MAG welded sample 7006-2M.

Welding Procedure Specification (WPS)

According to SFS-EN ISO 15609-1

Made by: Mikko Peltonen Date: 05.02.2013

Welder: Mikko Peltonen
WPQR No.: 7008-1M

Base Material:	Optim 700 MC Plus	Joint Preparation:	Laser Cutted
Material Thickness [mm]:	8	Backing:	Fiberglass Backing
Outside Diameter [mm]:	-	Welding Position:	PA
Working Temperature [°C]	20	Mode of Metal Transfer:	Pulse
Preheat Temperature [°C]:	-	Air gap [mm]:	2
Interpass Temperature [°C]	-		

Joint Design and Welding Sequences

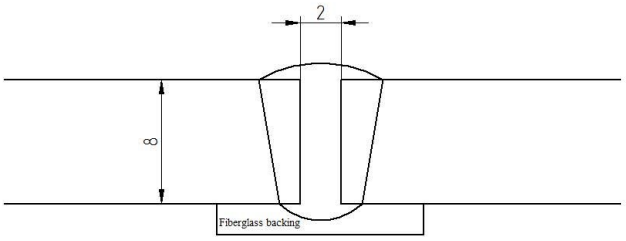

Run	Welding Process	Consumables	Diam. [mm]	Filler Feed Speed [m/min]	Classification	Gas / Flux
1	135	ESAB OK Aristorod 69	1,2	13,2 - 13,5	-	82% Ar + 18% CO_2

Run	Polarity	Stick Out [mm]	Current [A]	Voltage [V]	Speed [mm/min]	Heat Input [kJ/mm]	Gas Flow Rate [l/min] Shielding	Backing
1	DC(+)	12	348 - 360	24,9 - 25,3	700	0,45 - 0,47	20	-

Address: Puumiehenkuja 3
PL 14200
FI-00076 Aalto
FINLAND

Figure 75. pWPS for MAG welded sample 7008-1M.

Welding Procedure Specification (WPS)

According to SFS-EN ISO 15609-1

Made by: Mikko Peltonen Date: 05.02.2013

Welder: Mikko Peltonen
WPQR No.: 7008-2M

Base Material:	Optim 700 MC Plus	Joint Preparation:	Laser Cutted
Material Thickness [mm]:	8	Backing:	Fiberglass Backing
Outside Diameter [mm]:	-	Welding Position:	PA
Working Temperature [°C]	20	Mode of Metal Transfer:	Pulse
Preheat Temperature [°C]:	-	Air gap [mm]:	2
Interpass Temperature [°C]	-		

Joint Design and Welding Sequences

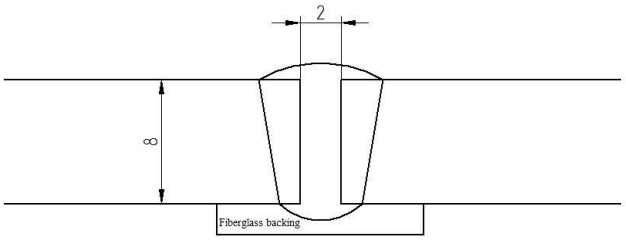

Run	Welding Process	Consumables	Diam. [mm]	Filler Feed Speed [m/min]	Classification	Gas / Flux
1	136	ESAB Tubrod 14.03	1,2	14,3 - 14,5	-	82% Ar + 18% CO_2

Run	Polarity	Stick Out [mm]	Current [A]	Voltage [V]	Speed [mm/min]	Heat Input [kJ/mm]	Gas Flow Rate [l/min] Shielding	Backing
1	DC(+)	12	348 - 360	31,0 - 31,8	700	0,76 - 0,77	20	-

Additional Information:

Address: Puumiehenkuja 3
PL 14200
FI-00076 Aalto
FINLAND

Figure 76. pWPS for MAG welded sample 7008-2M.

Preliminary Welding Procedure Specification (pWPS)

According to SFS-EN ISO 15609-1

Made by: Mikko Peltonen Date: 05.02.2013

Welder: Mikko Peltonen
WPQR No.: 9004-3M

Base Material:	Optim 900QC	Joint Preparation:	Laser Cutted
Material Thickness [mm]:	4	Backing:	-
Outside Diameter [mm]:	-	Welding Position:	PA
Working Temperature [°C]	20	Mode of Metal Transfer:	Pulse
Preheat Temperature [°C]:	-	Air Gap [mm]:	-
Interpass Temperature [°C]	-		

Joint Design and Welding Sequences

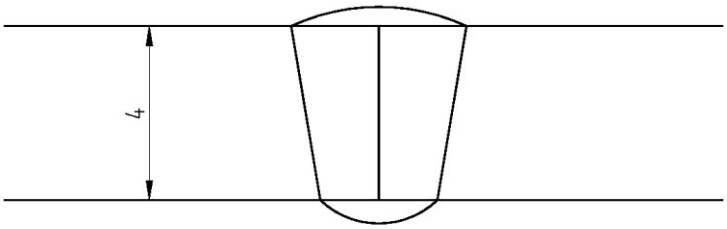

Run	Welding Process	Consumables	Diam. [mm]	Wire Speed Feed [m/min]	Classification	Gas / Flux
1	135	ESAB OK Aristorod 89	1,2	10,1 - 10,6	-	82% Ar + 18% CO_2

Run	Polarity	Stick Out [mm]	Current [A]	Voltage [V]	Speed [mm/min]	Heat Input [kJ/mm]	Gas Flow Rate [l/min] Shielding	Backing
1	DC(+)	12	328 - 333	27,2 - 31,7	900 - 1050	0,43 - 0,56	20	-

Address: Puumiehenkuja 3
PL 14200
FI-00076 Aalto
FINLAND

Figure 77. pWPS for MAG welded sample 9004-3M.

Preliminary Welding Procedure Specification (pWPS)

According to SFS-EN ISO 15609-1

Made by: Mikko Peltonen Date: 08.02.2013

Welder: Mikko Peltonen
WPQR No.: 9004-4M

Base Material:	Optim 900QC	Joint Preparation:	Laser Cutted
Material Thickness [mm]:	4	Backing:	-
Outside Diameter [mm]:	-	Welding Position:	PA
Working Temperature [°C]	20	Mode of Metal Transfer:	Pulse
Preheat Temperature [°C]:	-	Air Gap [mm]:	-
Interpass Temperature [°C]	-		

Joint Design and Welding Sequences

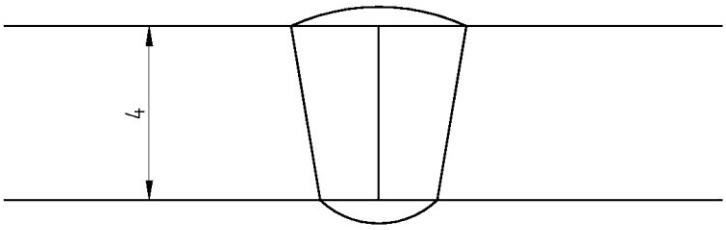

Run	Welding Process	Consumables	Diam. [mm]	Wire Feed Speed [m/min]	Classification	Gas / Flux
1	136	Esab Coreweld 89	1,2	12,5 - 12,8	-	92% Ar + 8% CO_2

Run	Polarity	Stick Out [mm]	Current [A]	Voltage [V]	Speed [mm/min]	Heat Input [kJ/mm]	Gas Flow Rate [l/min] Shielding	Backing
1	DC(+)	12	329 - 333	27,2 - 28,5	900 - 950	0,49 - 0,51	20	-

Address: Puumiehenkuja 3
PL 14200
FI-00076 Aalto
FINLAND

Figure 78. pWPS for MAG welded sample 9004-4M.

Preliminary Welding Procedure Specification (pWPS)

According to SFS-EN ISO 15609-1

Made by: Mikko Peltonen Date: 25.02.2013

Welder: Mikko Peltonen
WPQR No.: 9006-3M

Base Material:	Optim 900QC	Joint Preparation:	Laser Cutted
Material Thickness [mm]:	6	Backing:	-
Outside Diameter [mm]:	-	Welding Position:	PA
Working Temperature [°C]	20	Mode of Metal Transfer:	Pulse
Preheat Temperature [°C]:	-	Air Gap [mm]:	1
Interpass Temperature [°C]	-		

Joint Design and Welding Sequences

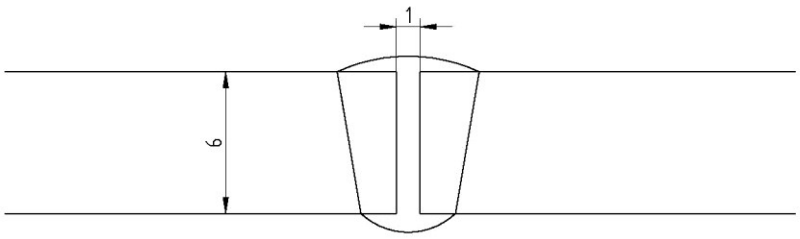

Run	Welding Process	Consumables	Diam. [mm]	Filler Feed Speed [m/min]	Classification	Gas / Flux
1	135	Esab OK Aristorod 89	1,2	10,3 - 10,6	-	82% Ar + 18% CO_2

Run	Polarity	Stick Out [mm]	Current [A]	Voltage [V]	Speed [mm/min]	Heat Input [kJ/mm]	Gas Flow Rate [l/min] Shielding	Backing
1	DC(+)	12	319 - 335	26,3 - 29,5	900	0,48 - 0,53	20	-

Address: Puumiehenkuja 3
PL 14200
FI-00076 Aalto
FINLAND

Figure 79. pWPS for MAG welded sample 9006-3M.

Preliminary Welding Procedure Specification (pWPS)

According to SFS-EN ISO 15609-1

Made by: Mikko Peltonen Date: 13.02.2013

Welder: Mikko Peltonen
WPQR No.: 9006-4M

Base Material:	Optim 900QC	Joint Preparation:	Laser Cutted
Material Thickness [mm]:	6	Backing:	-
Outside Diameter [mm]:	-	Welding Position:	PA
Working Temperature [°C]	20	Mode of Metal Transfer:	Pulse
Preheat Temperature [°C]:	-	Air Gap [mm]:	1
Interpass Temperature [°C]	-		

Joint Design and Welding Sequences

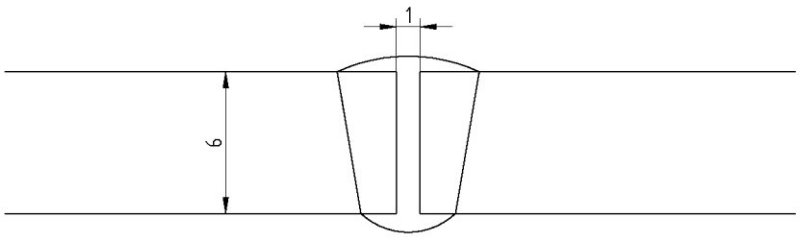

Run	Welding Process	Consumables	Diam. [mm]	Filler Feed Speed [m/min]	Classification	Gas / Flux
1	136	Esab Coreweld 89	1,2	13,4 - 13,7	-	92% Ar + 8% CO_2

Run	Polarity	Stick Out [mm]	Current [A]	Voltage [V]	Speed [mm/min]	Heat Input [kJ/mm]	Gas Flow Rate [l/min] Shielding	Backing
1	DC(+)	12	347 - 360	28,3 - 29,0	850 - 900	0,56 - 0,59	20	-

Address: Puumiehenkuja 3
PL 14200
FI-00076 Aalto
FINLAND

Figure 80. pWPS for MAG welded sample 9006-4M.

Welding Procedure Specification (WPS)

According to SFS-EN ISO 15609-1

Made by: Mikko Peltonen Date: 05.02.2013

Welder: Mikko Peltonen
WPQR No.: 9008-3M

Base Material:	Optim 900 QC	Joint Preparation:	Laser Cutted
Material Thickness [mm]:	8	Backing:	Fiberglass Backing
Outside Diameter [mm]:	-	Welding Position:	PA
Working Temperature [°C]	20	Mode of Metal Transfer:	Pulse
Preheat Temperature [°C]:	-	Air gap [mm]:	2
Interpass Temperature [°C]	-		

Joint Design and Welding Sequences

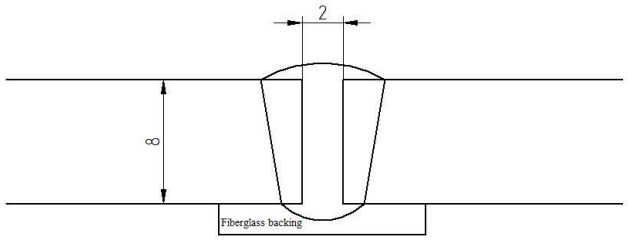

Run	Welding Process	Consumables	Diam. [mm]	Filler Feed Speed [m/min]	Classification	Gas / Flux
1	135	ESAB OK Aristorod 89	1,2	13,2 - 13,4	-	82% Ar + 18% CO_2

Run	Polarity	Stick Out [mm]	Current [A]	Voltage [V]	Speed [mm/min]	Heat Input [kJ/mm]	Gas Flow Rate [l/min] Shielding	Backing
1	DC(+)	12	360 - 370	24,9 - 25,3	700	0,61 - 0,64	20	-

Address: Puumiehenkuja 3
PL 14200
FI-00076 Aalto
FINLAND

Figure 81. pWPS for MAG welded sample 9008-3M.

Welding Procedure Specification (WPS)

According to SFS-EN ISO 15609-1

Made by: Mikko Peltonen Date: 05.02.2013

Welder: Mikko Peltonen
WPQR No.: 9008-4M

Base Material:	Optim 900 QC	Joint Preparation:	Laser Cutted
Material Thickness [mm]:	8	Backing:	Fiberglass Backing
Outside Diameter [mm]:	-	Welding Position:	PA
Working Temperature [°C]	20	Mode of Metal Transfer:	Pulse
Preheat Temperature [°C]:	-	Air gap [mm]:	2
Interpass Temperature [°C]	-		

Joint Design and Welding Sequences

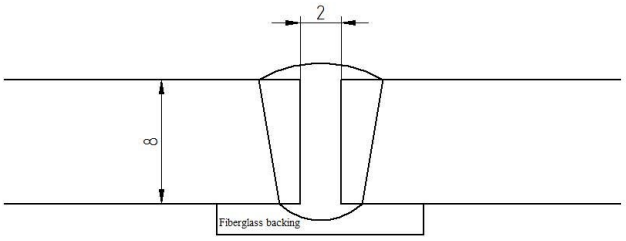

Run	Welding Process	Consumables	Diam. [mm]	Filler Feed Speed [mm]	Classification	Gas / Flux
1	136	ESAB Coreweld 89	1,2	13,1 - 14,3	-	92% Ar + 8% CO_2

Run	Polarity	Stick Out [mm]	Current [A]	Voltage [V]	Speed [mm/min]	Heat Input [kJ/mm]	Gas Flow Rate [l/min] Shielding	Backing
1	DC(+)	12	337 - 358	28,0 - 29,0	600 - 700	0,73 - 0,78	20	-

Additional Information:

Address: Puumiehenkuja 3
PL 14200
FI-00076 Aalto
FINLAND

Figure 82. pWPS for MAG welded sample 9008-4M.

Preliminary Welding Procedure Specification (pWPS)

According to SFS-EN ISO 15609-1

Made by: Mikko Peltonen Date: 25.02.2013

Welder: Mikko Peltonen
WPQR No.: 7006-1P

Base Material:	Optim 700 MC Plus	Joint Preparation:	Laser Cutted
Material Thickness [mm]:	6	Backing:	Shielding Gas
Outside Diameter [mm]:	-	Welding Position:	PA
Working Temperature [°C]	20	Mode of Metal Transfer:	-
Preheat Temperature [°C]:	-	Air Gap [mm]:	-
Interpass Temperature [°C]	-		

Joint Design and Welding Sequences

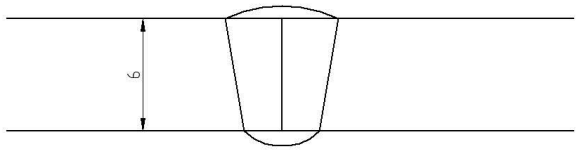

Run	Welding Process	Consumables	Diam. [mm]	Filler Feed Speed [m/min]	Classification	Gas / Flux
1	15	Esab OK Aristorod 69	1,2	0,27 - 0,35	-	99,99% Ar

Run	Polarity	Stick Out [mm]	Current [A]	Voltage [V]	Speed [mm/min]	Heat Input [kJ/mm]	Gas Flow Rate [l/min] Shielding	Backing
1	DC(-)	-	230 - 235	27,5 - 27,9	220 - 230	1,04 - 1,06	17	17

Additional Information:
- Plasma Gas Flow 4,0 l/min
- Nozzle Distance 5 mm

Address: Puumiehenkuja 3
PL 14200
FI-00076 Aalto
FINLAND

Figure 83. pWPS for PAW welded sample 7006-1P.

Preliminary Welding Procedure Specification (pWPS)

According to SFS-EN ISO 15609-1

Made by: Mikko Peltonen Date: 25.02.2013

Welder: Mikko Peltonen
WPQR No.: 7006-2P

Base Material:	Optim 700 MC Plus	Joint Preparation:	Laser Cutted
Material Thickness [mm]:	6	Backing:	Shielding Gas
Outside Diameter [mm]:	-	Welding Position:	PA
Working Temperature [°C]	20	Mode of Metal Transfer:	-
Preheat Temperature [°C]:	-	Air Gap [mm]:	-
Interpass Temperature [°C]	-		

Joint Design and Welding Sequences

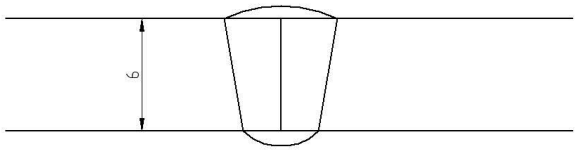

Run	Welding Process	Consumables	Diam. [mm]	Filler Feed Speed [m/min]	Classification	Gas / Flux
1	15	Esab Tubrod 14.03	1,2	0,27 - 0,35	-	99,99% Ar

Run	Polarity	Stick Out [mm]	Current [A]	Voltage [V]	Speed [mm/min]	Heat Input [kJ/mm]	Gas Flow Rate [l/min] Shielding	Backing
1	DC(-)	-	230 - 235	27,5 - 27,9	220 - 230	1,04 - 1,06	17	17

Additional Information:
- Plasma Gas Flow 4,0 l/min
- Nozzle Distance 5 mm

Address: Puumiehenkuja 3
PL 14200
FI-00076 Aalto
FINLAND

Figure 84. pWPS for PAW welded sample 7006-2P.

Preliminary Welding Procedure Specification (pWPS)

According to SFS-EN ISO 15609-1

Made by: Mikko Peltonen Date: 25.02.2013

Welder: Mikko Peltonen
WPQR No.: 7008-1P

Base Material:	Optim 700 MC Plus	Joint Preparation:	Laser Cutted
Material Thickness [mm]:	8	Backing:	Shielding Gas
Outside Diameter [mm]:	-	Welding Position:	PA
Working Temperature [°C]	20	Mode of Metal Transfer:	-
Preheat Temperature [°C]:	-	Air Gap [mm]:	-
Interpass Temperature [°C]	-		

Joint Design and Welding Sequences

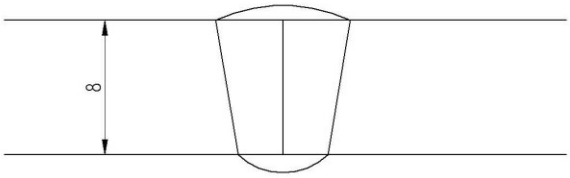

Run	Welding Process	Consumables	Diam. [mm]	Filler Feed Speed [m/min]	Classification	Gas / Flux
1	15	Esab OK Aristorod 69	1,2	0,25 - 0,33	-	99,99% Ar

Run	Polarity	Stick Out [mm]	Current [A]	Voltage [V]	Speed [mm/min]	Heat Input [kJ/mm]	Gas Flow Rate [l/min] Shielding	Backing
1	DC(-)	-	231 - 241	27,9 - 28,6	170 - 180	1,3 - 1,4	17	17

Additional Information:
- Plasma Gas Flow 4,5 l/min
- Nozzle Distance 5 mm

Address: Puumiehenkuja 3
PL 14200
FI-00076 Aalto
FINLAND

Figure 85. pWPS for PAW welded sample 7008-1P.

Preliminary Welding Procedure Specification (pWPS)

According to SFS-EN ISO 15609-1

Made by: Mikko Peltonen Date: 25.02.2013

Welder: Mikko Peltonen
WPQR No.: 7008-2P

Base Material:	Optim 700 MC Plus	Joint Preparation:	Laser Cutted
Material Thickness [mm]:	8	Backing:	Shielding Gas
Outside Diameter [mm]:	-	Welding Position:	PA
Working Temperature [°C]	20	Mode of Metal Transfer:	-
Preheat Temperature [°C]:	-	Air Gap [mm]:	-
Interpass Temperature [°C]	-		

Joint Design and Welding Sequences

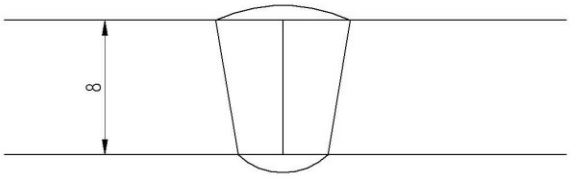

Run	Welding Process	Consumables	Diam. [mm]	Filler Feed Speed [m/min]	Classification	Gas / Flux
1	15	Esab Tubrod 14.03	1,2	0,25 - 0,33	-	99,99% Ar

Run	Polarity	Stick Out [mm]	Current [A]	Voltage [V]	Speed [mm/min]	Heat Input [kJ/mm]	Gas Flow Rate [l/min] Shielding	Backing
1	DC(-)	-	230 - 241	27,9 - 28,6	170 - 180	1,3 - 1,4	17	17

Additional Information:
- Plasma Gas Flow 4,5 l/min
- Nozzle Distance 5 mm

Address: Puumiehenkuja 3
PL 14200
FI-00076 Aalto
FINLAND

Figure 86. pWPS for PAW welded sample 7008-2P.

Preliminary Welding Procedure Specification (pWPS)

According to SFS-EN ISO 15609-1

Made by: Mikko Peltonen Date: 25.02.2013

Welder: Mikko Peltonen
WPQR No.: 9004-3P

Base Material:	Optim 900 QC	Joint Preparation:	Laser Cutted
Material Thickness [mm]:	4	Backing:	Shielding Gas
Outside Diameter [mm]:	-	Welding Position:	PA
Working Temperature [°C]	20	Mode of Metal Transfer:	-
Preheat Temperature [°C]:	-	Air Gap [mm]:	-
Interpass Temperature [°C]	-		

Joint Design and Welding Sequences

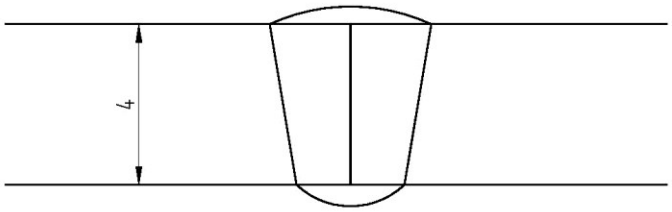

Run	Welding Process	Consumables	Diam. [mm]	Filler Feed Speed [m/min]	Classification	Gas / Flux
1	15	Esab OK Aristorod 89	1,2	0,33 - 0,42	-	99,99% Ar

Run	Polarity	Stick Out [mm]	Current [A]	Voltage [V]	Speed [mm/min]	Heat Input [kJ/mm]	Gas Flow Rate [l/min] Shielding	Backing
1	DC(-)	-	210 - 215	24,8 - 26,4	320 - 350	0,54 - 0,64	17	17

Additional Information:
- Plasma Gas Flow 3,5 l/min
- Nozzle Distance 5 mm

Address: Puumiehenkuja 3
PL 14200
FI-00076 Aalto
FINLAND

Figure 87. pWPS for PAW welded sample 9004-3P.

Preliminary Welding Procedure Specification (pWPS)

According to SFS-EN ISO 15609-1

Made by: Mikko Peltonen Date: 25.02.2013

Welder: Mikko Peltonen
WPQR No.: 9004-4P

Base Material:	Optim 900 QC	Joint Preparation:	Laser Cutted
Material Thickness [mm]:	4	Backing:	Shielding Gas
Outside Diameter [mm]:	-	Welding Position:	PA
Working Temperature [°C]	20	Mode of Metal Transfer:	-
Preheat Temperature [°C]:	-	Air Gap [mm]:	-
Interpass Temperature [°C]	-		

Joint Design and Welding Sequences

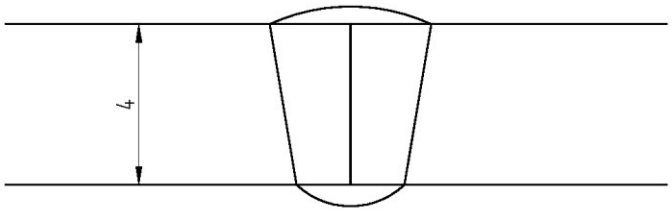

Run	Welding Process	Consumables	Diam. [mm]	Filler Feed Speed [m/min]	Classification	Gas / Flux
1	15	Esab Coreweld 89	1,2	0,33 - 0,42	-	99,99% Ar

Run	Polarity	Stick Out [mm]	Current [A]	Voltage [V]	Speed [mm/min]	Heat Input [kJ/mm]	Gas Flow Rate [l/min] Shielding	Backing
1	DC(-)	-	210 - 215	24,8 - 26,4	320 - 350	0,54 - 0,64	17	17

Additional Information:
- Plasma Gas Flow 3,5 l/min
- Nozzle Distance 5 mm

Address: Puumiehenkuja 3
PL 14200
FI-00076 Aalto
FINLAND

Figure 88. pWPS for PAW welded sample 9004-4P.

Preliminary Welding Procedure Specification (pWPS)

According to SFS-EN ISO 15609-1

Made by: Mikko Peltonen Date: 25.02.2013

Welder: Mikko Peltonen
WPQR No.: 9006-3P

Base Material:	Optim 900 QC	Joint Preparation:	Laser Cutted
Material Thickness [mm]:	6	Backing:	Shielding Gas
Outside Diameter [mm]:	-	Welding Position:	PA
Working Temperature [°C]	20	Mode of Metal Transfer:	-
Preheat Temperature [°C]:	-	Air Gap [mm]:	-
Interpass Temperature [°C]	-		

Joint Design and Welding Sequences

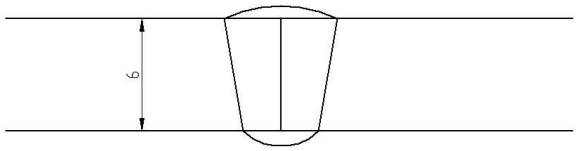

Run	Welding Process	Consumables	Diam. [mm]	Filler Feed Speed [m/min]	Classification	Gas / Flux
1	15	Esab OK Aristorod 89	1,2	0,27 - 0,35	-	99,99% Ar

Run	Polarity	Stick Out [mm]	Current [A]	Voltage [V]	Speed [mm/min]	Heat Input [kJ/mm]	Gas Flow Rate [l/min] Shielding	Backing
1	DC(-)	-	230 - 235	27,5 - 27,9	220 - 230	1,04 - 1,06	17	17

Additional Information:
- Plasma Gas Flow 4,0 l/min
- Nozzle Distance 5 mm

Address: Puumiehenkuja 3
PL 14200
FI-00076 Aalto
FINLAND

Figure 89. pWPS for PAW welded sample 9006-3P.

Preliminary Welding Procedure Specification (pWPS)

According to SFS-EN ISO 15609-1

Made by: Mikko Peltonen Date: 25.02.2013

Welder: Mikko Peltonen
WPQR No.: 9006-4P

Base Material:	Optim 900 QC	Joint Preparation:	Laser Cutted
Material Thickness [mm]:	6	Backing:	Shielding Gas
Outside Diameter [mm]:	-	Welding Position:	PA
Working Temperature [°C]	20	Mode of Metal Transfer:	-
Preheat Temperature [°C]:	-	Air Gap [mm]:	-
Interpass Temperature [°C]	-		

Joint Design and Welding Sequences

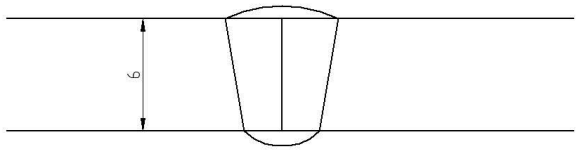

Run	Welding Process	Consumables	Diam. [mm]	Filler Feed Speed [m/min]	Classification	Gas / Flux
1	15	Esab Coreweld 89	1,2	0,27 - 0,35	-	99,99% Ar

Run	Polarity	Stick Out [mm]	Current [A]	Voltage [V]	Speed [mm/min]	Heat Input [kJ/mm]	Gas Flow Rate [l/min] Shielding	Backing
1	DC(-)	-	230 - 235	27,5 - 27,9	220 - 230	1,04 - 1,06	17	17

Additional Information:
- Plasma Gas Flow 4,0 l/min
- Nozzle Distance 5 mm

Address: Puumiehenkuja 3
PL 14200
FI-00076 Aalto
FINLAND

Figure 90. pWPS for PAW welded sample 9006-4P.

Preliminary Welding Procedure Specification (pWPS)

According to SFS-EN ISO 15609-1

Made by: Mikko Peltonen Date: 25.02.2013

Welder: Mikko Peltonen
WPQR No.: 9008-3P

Base Material:	Optim 900 QC	Joint Preparation:	Laser Cutted
Material Thickness [mm]:	8	Backing:	Shielding Gas
Outside Diameter [mm]:	-	Welding Position:	PA
Working Temperature [°C]	20	Mode of Metal Transfer:	-
Preheat Temperature [°C]:	-	Air Gap [mm]:	-
Interpass Temperature [°C]	-		

Joint Design and Welding Sequences

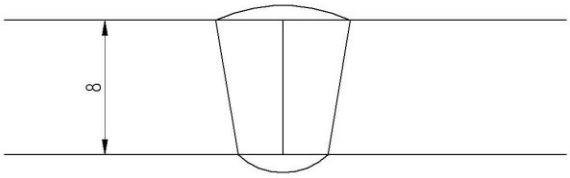

Run	Welding Process	Consumables	Diam. [mm]	Filler Feed Speed [m/min]	Classification	Gas / Flux
1	15	Esab OK Aristorod 89	1,2	0,25 - 0,33	-	99,99% Ar

Run	Polarity	Stick Out [mm]	Current [A]	Voltage [V]	Speed [mm/min]	Heat Input [kJ/mm]	Gas Flow Rate [l/min] Shielding	Backing
1	DC(-)	-	240 - 245	27,9 - 28,7	170 - 180	1,3 - 1,5	17	17

Additional Information:
- Plasma Gas Flow 4,0 - 4,5 l/min
- Nozzle Distance 5 mm

Address: Puumiehenkuja 3
PL 14200
FI-00076 Aalto
FINLAND

Figure 91. pWPS for PAW welded sample 9008-3P.

Preliminary Welding Procedure Specification (pWPS)

According to SFS-EN ISO 15609-1

Made by: Mikko Peltonen Date: 25.02.2013

Welder: Mikko Peltonen
WPQR No.: 9008-4P

Base Material:	Optim 900 QC	Joint Preparation:	Laser Cutted
Material Thickness [mm]:	8	Backing:	Shielding Gas
Outside Diameter [mm]:	-	Welding Position:	PA
Working Temperature [°C]	20	Mode of Metal Transfer:	-
Preheat Temperature [°C]:	-	Air Gap [mm]:	-
Interpass Temperature [°C]	-		

Joint Design and Welding Sequences

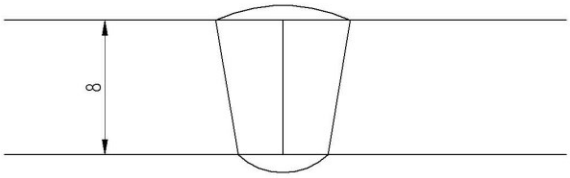

Run	Welding Process	Consumables	Diam. [mm]	Filler Feed Speed [m/min]	Classification	Gas / Flux
1	15	Esab Coreweld 89	1,2	0,25 - 0,33	-	99,99% Ar

Run	Polarity	Stick Out [mm]	Current [A]	Voltage [V]	Speed [mm/min]	Heat Input [kJ/mm]	Gas Flow Rate [l/min] Shielding	Backing
1	DC(-)	-	240 - 245	27,9 - 28,7	170 - 180	1,3 - 1,5	17	17

Additional Information:
- Plasma Gas Flow 4,0 - 4,5 l/min
- Nozzle Distance 5 mm

Address: Puumiehenkuja 3
PL 14200
FI-00076 Aalto
FINLAND

Figure 92. pWPS for PAW welded sample 9008-4P.

Preliminary Welding Procedure Specification (pWPS)

According to SFS-EN ISO 15609-1

Made by: Mikko Peltonen Date: 25.02.2013

Welder: Mikko Peltonen
WPQR No.: 7006-5S

Base Material:	Optim 700 MC Plus	Joint Preparation:	Laser Cutted
Material Thickness [mm]:	6	Backing:	Fiberglass Backing
Outside Diameter [mm]:	-	Welding Position:	PA
Working Temperature [°C]	20	Mode of Metal Transfer:	-
Preheat Temperature [°C]:	-	Air Gap [mm]:	-
Interpass Temperature [°C]	-		

Joint Design and Welding Sequences

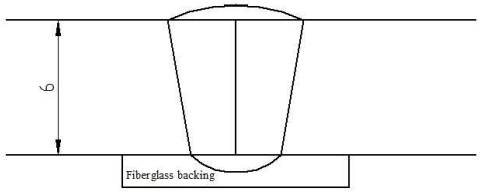

Run	Welding Process	Consumables	Diam. [mm]	Filler Feed Speed [m/min]	Classification	Gas / Flux
1	121	Esab OK Autrod 13.43	3,0	-	-	ESAB OK Flux 10.62

Run	Polarity	Stick Out [mm]	Current [A]	Voltage [V]	Speed [mm/min]	Heat Input [kJ/mm]	Gas Flow Rate [l/min] Shielding	Backing
1	DC(+)	25	700 - 710	27,7 - 28,0	1050 - 1100	1,06 - 1,11	-	-

Address: Puumiehenkuja 3
PL 14200
FI-00076 Aalto
FINLAND

Figure 93. pWPS for SAW welded sample 7006-5S.

Preliminary Welding Procedure Specification (pWPS)

According to SFS-EN ISO 15609-1

Made by: Mikko Peltonen Date: 25.02.2013

Welder: Mikko Peltonen
WPQR No.: 7006-6S

Base Material:	Optim 700 MC Plus	Joint Preparation:	Laser Cutted
Material Thickness [mm]:	6	Backing:	Fiberglass Backing
Outside Diameter [mm]:	-	Welding Position:	PA
Working Temperature [°C]	20	Mode of Metal Transfer:	-
Preheat Temperature [°C]:	-	Air Gap [mm]:	-
Interpass Temperature [°C]	-		

Joint Design and Welding Sequences

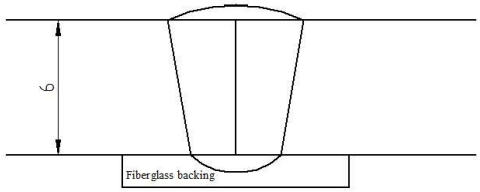

Run	Welding Process	Consumables	Diam. [mm]	Filler Feed Speed [m/min]	Classification	Gas / Flux
1	125	Esab OK Tubrod 15.27S	3,0	-	-	ESAB OK Flux 10.62

Run	Polarity	Stick Out [mm]	Current [A]	Voltage [V]	Speed [mm/min]	Heat Input [kJ/mm]	Gas Flow Rate [l/min] Shielding	Backing
1	DC(+)	25	700 - 710	28,0 - 28,5	850 - 900	1,33 - 1,41	-	-

Address: Puumiehenkuja 3
PL 14200
FI-00076 Aalto
FINLAND

Figure 94. pWPS for SAW welded sample 7006-6S.

Preliminary Welding Procedure Specification (pWPS)

According to SFS-EN ISO 15609-1

Made by: Mikko Peltonen Date: 25.02.2013

Welder: Mikko Peltonen
WPQR No.: 7008-5S

Base Material:	Optim 700 MC Plus	Joint Preparation:	Laser Cutted
Material Thickness [mm]:	8	Backing:	Fiberglass Backing
Outside Diameter [mm]:	-	Welding Position:	PA
Working Temperature [°C]	20	Mode of Metal Transfer:	-
Preheat Temperature [°C]:	-	Air Gap [mm]:	-
Interpass Temperature [°C]	-		

Joint Design and Welding Sequences

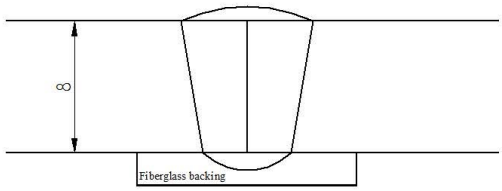

Run	Welding Process	Consumables	Diam. [mm]	Filler Feed Speed [m/min]	Classification	Gas / Flux
1	121	Esab OK Autrod 13.43	3,0	-	-	ESAB OK Flux 10.62

Run	Polarity	Stick Out [mm]	Current [A]	Voltage [V]	Speed [mm/min]	Heat Input [kJ/mm]	Gas Flow Rate [l/min] Shielding	Backing
1	DC(+)	25	640 - 650	29,8 - 30,5	600	1,9 - 2,0	-	-

Address: Puumiehenkuja 3
PL 14200
FI-00076 Aalto
FINLAND

Figure 95. pWPS for SAW welded sample 7008-5S.

Preliminary Welding Procedure Specification (pWPS)

According to SFS-EN ISO 15609-1

Made by: Mikko Peltonen Date: 25.02.2013

Welder: Mikko Peltonen
WPQR No.: 7008-6S

Base Material:	Optim 700 MC Plus	Joint Preparation:	Laser Cutted
Material Thickness [mm]:	8	Backing:	Fiberglass Backing
Outside Diameter [mm]:	-	Welding Position:	PA
Working Temperature [°C]	20	Mode of Metal Transfer:	-
Preheat Temperature [°C]:	-	Air Gap [mm]:	-
Interpass Temperature [°C]	-		

Joint Design and Welding Sequences

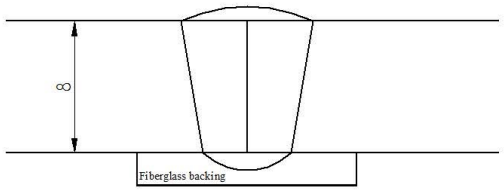

Run	Welding Process	Consumables	Diam. [mm]	Filler Feed Speed [m/min]	Classification	Gas / Flux
1	125	Esab OK Tubrod 15.27S	3,0	-	-	ESAB OK Flux 10.62

Run	Polarity	Stick Out [mm]	Current [A]	Voltage [V]	Speed [mm/min]	Heat Input [kJ/mm]	Gas Flow Rate [l/min] Shielding	Backing
1	DC(+)	25	640 - 650	29,8 - 30,5	500	2,3 - 2,4	-	-

Address: Puumiehenkuja 3
PL 14200
FI-00076 Aalto
FINLAND

Figure 96. pWPS for SAW welded sample 7008-6S.

Preliminary Welding Procedure Specification (pWPS)

According to SFS-EN ISO 15609-1

Made by: Mikko Peltonen Date: 25.02.2013

Welder: Mikko Peltonen
WPQR No.: 9004-5S

Base Material:	Optim 900 QC	Joint Preparation:	Laser Cutted
Material Thickness [mm]:	4	Backing:	Fiberglass Backing
Outside Diameter [mm]:	-	Welding Position:	PA
Working Temperature [°C]	20	Mode of Metal Transfer:	-
Preheat Temperature [°C]:	-	Air Gap [mm]:	-
Interpass Temperature [°C]	-		

Joint Design and Welding Sequences

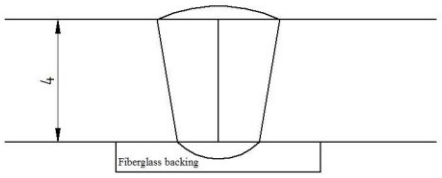

Run	Welding Process	Consumables	Diam. [mm]	Filler Feed Speed [m/min]	Classification	Gas / Flux
1	121	Esab OK Autrod 13.43	3,0	-	-	ESAB OK Flux 10.62

Run	Polarity	Stick Out [mm]	Current [A]	Voltage [V]	Speed [mm/min]	Heat Input [kJ/mm]	Gas Flow Rate [l/min] Shielding	Backing
1	DC(+)	25	500 - 520	28,0 - 28,5	1000 - 1100	0,8 - 0,9	-	-

Address: Puumiehenkuja 3
PL 14200
FI-00076 Aalto
FINLAND

Figure 97. pWPS for SAW welded sample 9004-5S.

Preliminary Welding Procedure Specification (pWPS)

According to SFS-EN ISO 15609-1

Made by: Mikko Peltonen Date: 25.02.2013

Welder: Mikko Peltonen
WPQR No.: 9004-6S

Base Material:	Optim 900 QC	Joint Preparation:	Laser Cutted
Material Thickness [mm]:	4	Backing:	Fiberglass Backing
Outside Diameter [mm]:	-	Welding Position:	PA
Working Temperature [°C]	20	Mode of Metal Transfer:	-
Preheat Temperature [°C]:	-	Air Gap [mm]:	-
Interpass Temperature [°C]	-		

Joint Design and Welding Sequences

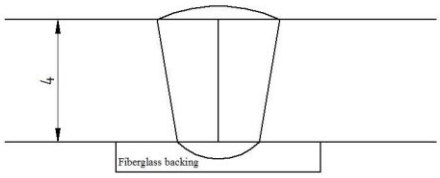

Run	Welding Process	Consumables	Diam. [mm]	Filler Feed Speed [m/min]	Classification	Gas / Flux
1	125	Esab OK Tubrod 15.27S	3,0	-	-	ESAB OK Flux 10.62

Run	Polarity	Stick Out [mm]	Current [A]	Voltage [V]	Speed [mm/min]	Heat Input [kJ/mm]	Gas Flow Rate [l/min] Shielding	Backing
1	DC(+)	25	500 - 520	28,0 - 28,5	1000 - 1100	0,8 - 0,9	-	-

Address: Puumiehenkuja 3
PL 14200
FI-00076 Aalto
FINLAND

Figure 98. pWPS for SAW welded sample 9004-6S.

Preliminary Welding Procedure Specification (pWPS)

According to SFS-EN ISO 15609-1

Made by: Mikko Peltonen Date: 25.02.2013

Welder: Mikko Peltonen
WPQR No.: 9006-5S

Base Material:	Optim 900 QC	Joint Preparation:	Laser Cutted
Material Thickness [mm]:	6	Backing:	Fiberglass Backing
Outside Diameter [mm]:	-	Welding Position:	PA
Working Temperature [°C]	20	Mode of Metal Transfer:	-
Preheat Temperature [°C]:	-	Air Gap [mm]:	-
Interpass Temperature [°C]	-		

Joint Design and Welding Sequences

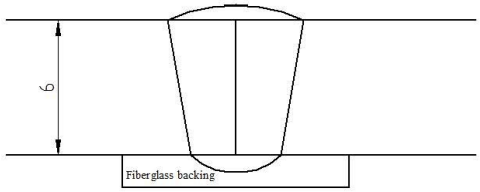

Run	Welding Process	Consumables	Diam. [mm]	Filler Feed Speed [m/min]	Classification	Gas / Flux
1	121	Esab OK Autrod 13.43	3,0	-	-	ESAB OK Flux 10.62

Run	Polarity	Stick Out [mm]	Current [A]	Voltage [V]	Speed [mm/min]	Heat Input [kJ/mm]	Gas Flow Rate [l/min] Shielding	Backing
1	DC(+)	25	700 - 710	27,7 - 28,0	1050 - 1100	1,06 - 1,11	-	-

Address: Puumiehenkuja 3
PL 14200
FI-00076 Aalto
FINLAND

Figure 99. pWPS for SAW welded sample 9006-5S.

Preliminary Welding Procedure Specification (pWPS)

According to SFS-EN ISO 15609-1

Made by: Mikko Peltonen Date: 25.02.2013

Welder: Mikko Peltonen
WPQR No.: 9006-6S

Base Material:	Optim 900 QC	Joint Preparation:	Laser Cutted
Material Thickness [mm]:	6	Backing:	Fiberglass Backing
Outside Diameter [mm]:	-	Welding Position:	PA
Working Temperature [°C]	20	Mode of Metal Transfer:	-
Preheat Temperature [°C]:	-	Air Gap [mm]:	-
Interpass Temperature [°C]	-		

Joint Design and Welding Sequences

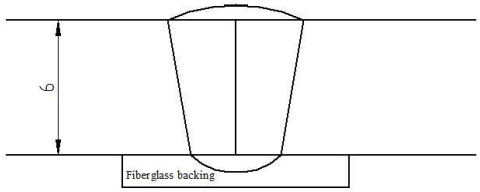

Run	Welding Process	Consumables	Diam. [mm]	Filler Feed Speed [m/min]	Classification	Gas / Flux
1	125	Esab OK Tubrod 15.27S	3,0	-	-	ESAB OK Flux 10.62

Run	Polarity	Stick Out [mm]	Current [A]	Voltage [V]	Speed [mm/min]	Heat Input [kJ/mm]	Gas Flow Rate [l/min] Shielding	Backing
1	DC(+)	25	700 - 710	28,0 - 28,5	850 - 900	1,30 - 1,40	-	-

Address: Puumiehenkuja 3
PL 14200
FI-00076 Aalto
FINLAND

Figure 100. pWPS for SAW welded sample 9006-6S.

Preliminary Welding Procedure Specification (pWPS)

According to SFS-EN ISO 15609-1

Made by: Mikko Peltonen Date: 25.02.2013

Welder: Mikko Peltonen
WPQR No.: 9008-5S

Base Material:	Optim 900 QC	Joint Preparation:	Laser Cutted
Material Thickness [mm]:	8	Backing:	Fiberglass Backing
Outside Diameter [mm]:	-	Welding Position:	PA
Working Temperature [°C]	20	Mode of Metal Transfer:	-
Preheat Temperature [°C]:	-	Air Gap [mm]:	-
Interpass Temperature [°C]	-		

Joint Design and Welding Sequences

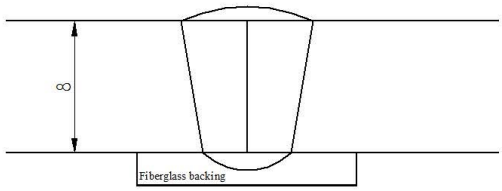

Run	Welding Process	Consumables	Diam. [mm]	Filler Feed Speed [m/min]	Classification	Gas / Flux
1	121	Esab OK Autrod 13.43	3,0	-	-	ESAB OK Flux 10.62

Run	Polarity	Stick Out [mm]	Current [A]	Voltage [V]	Speed [mm/min]	Heat Input [kJ/mm]	Gas Flow Rate [l/min] Shielding	Backing
1	DC(+)	25	640 - 650	29,8 - 30,5	600	1,9 - 2,0	-	-

Address: Puumiehenkuja 3
PL 14200
FI-00076 Aalto
FINLAND

Figure 101. pWPS for SAW welded sample 9008-5S.

Preliminary Welding Procedure Specification (pWPS)

According to SFS-EN ISO 15609-1

Made by: Mikko Peltonen Date: 25.02.2013

Welder: Mikko Peltonen
WPQR No.: 9008-6S

Base Material:	Optim 900 QC	Joint Preparation:	Laser Cutted
Material Thickness [mm]:	8	Backing:	Fiberglass Backing
Outside Diameter [mm]:	-	Welding Position:	PA
Working Temperature [°C]	20	Mode of Metal Transfer:	-
Preheat Temperature [°C]:	-	Air Gap [mm]:	-
Interpass Temperature [°C]	-		

Joint Design and Welding Sequences

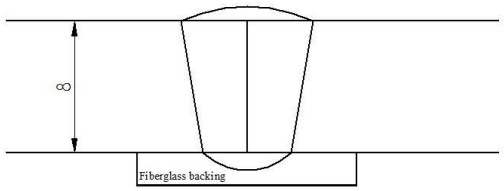

Run	Welding Process	Consumables	Diam. [mm]	Filler Feed Speed [m/min]	Classification	Gas / Flux
1	125	Esab OK Tubrod 15.27S	3,0	-	-	ESAB OK Flux 10.62

Run	Polarity	Stick Out [mm]	Current [A]	Voltage [V]	Speed [mm/min]	Heat Input [kJ/mm]	Gas Flow Rate [l/min] Shielding	Backing
1	DC(+)	25	640 - 650	29,8 - 30,5	500	2,3 - 2,4	-	-

Address: Puumiehenkuja 3
PL 14200
FI-00076 Aalto
FINLAND

Figure 102. pWPS for SAW welded sample 9008-6S.

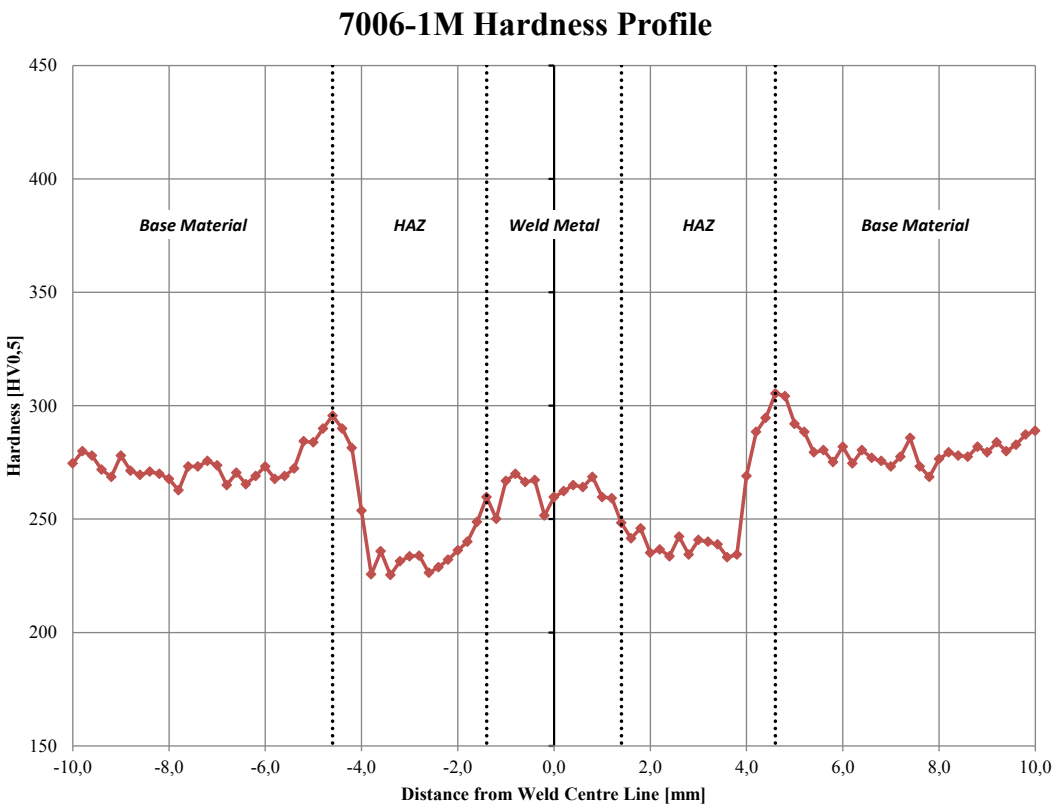

Figure 103. Microhardness profile of MAG welded sample 7006-1M.

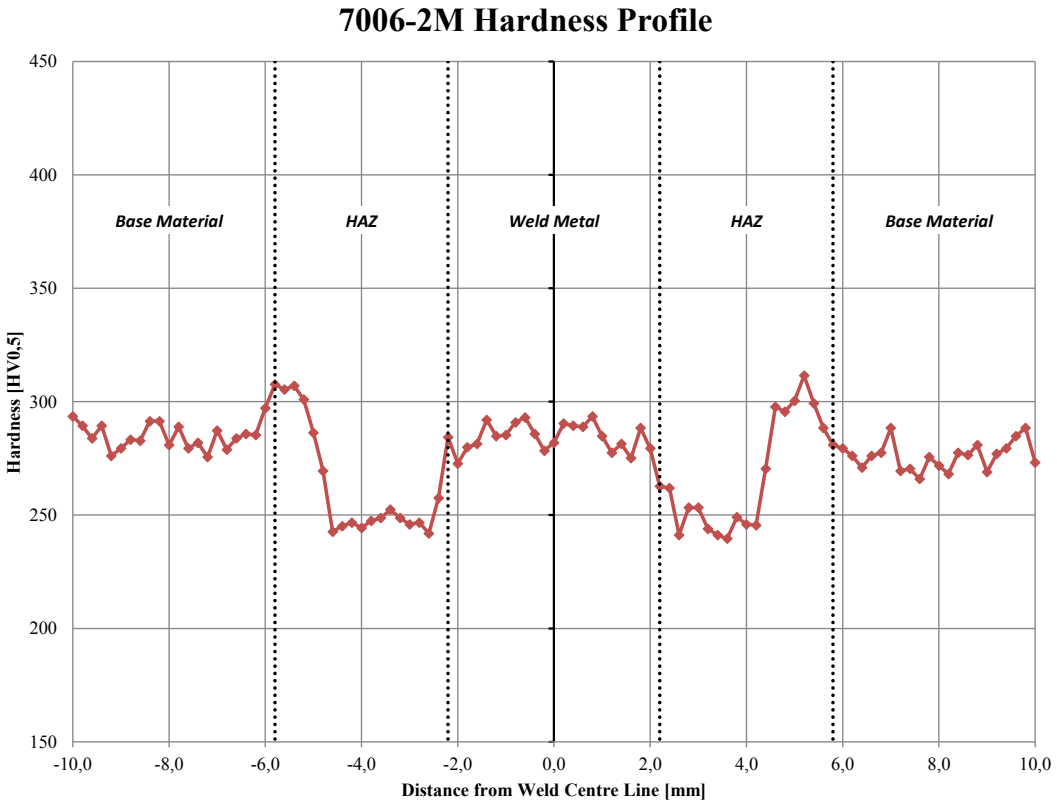

Figure 104. Microhardness profile of MAG welded sample 7006-2M.

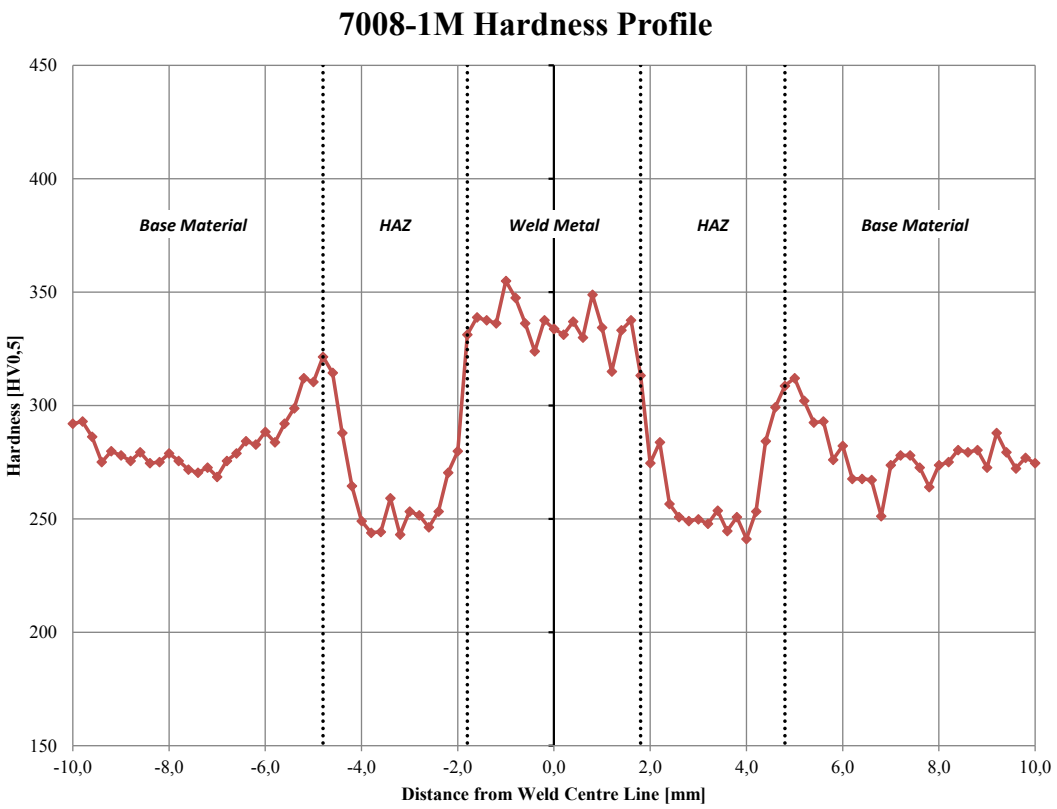

Figure 105. Microhardness profile of MAG welded sample 7008-1M.

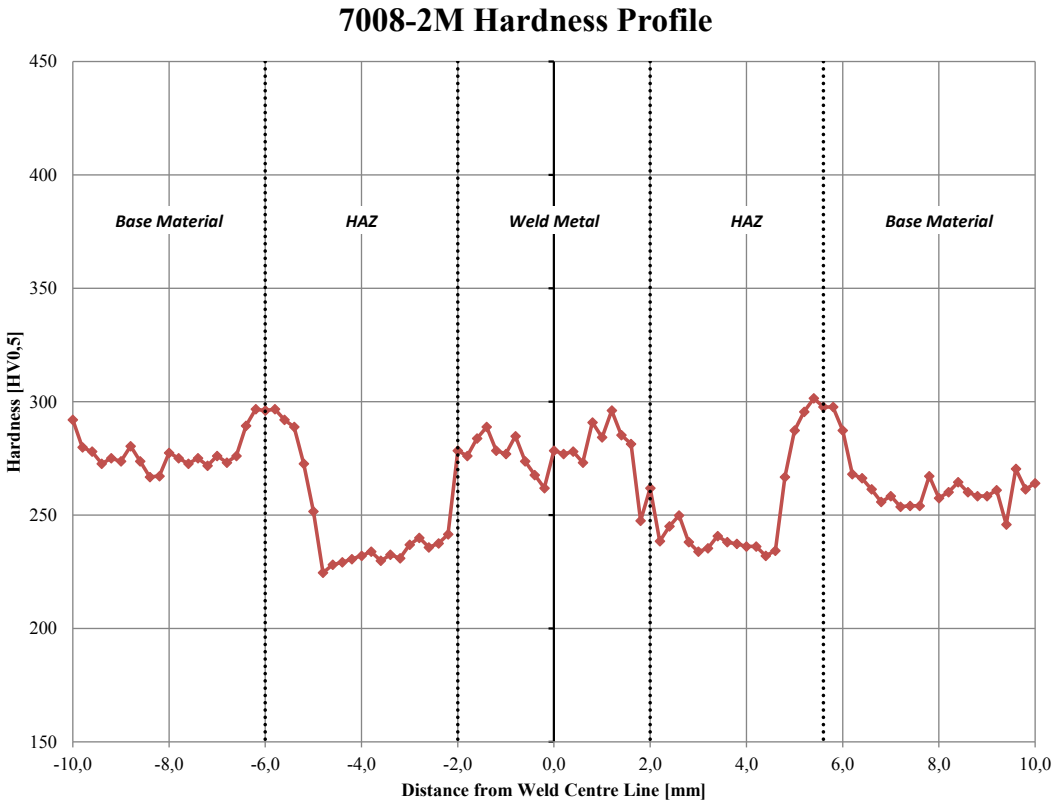

Figure 106. Microhardness profile of MAG welded sample 7008-2M.

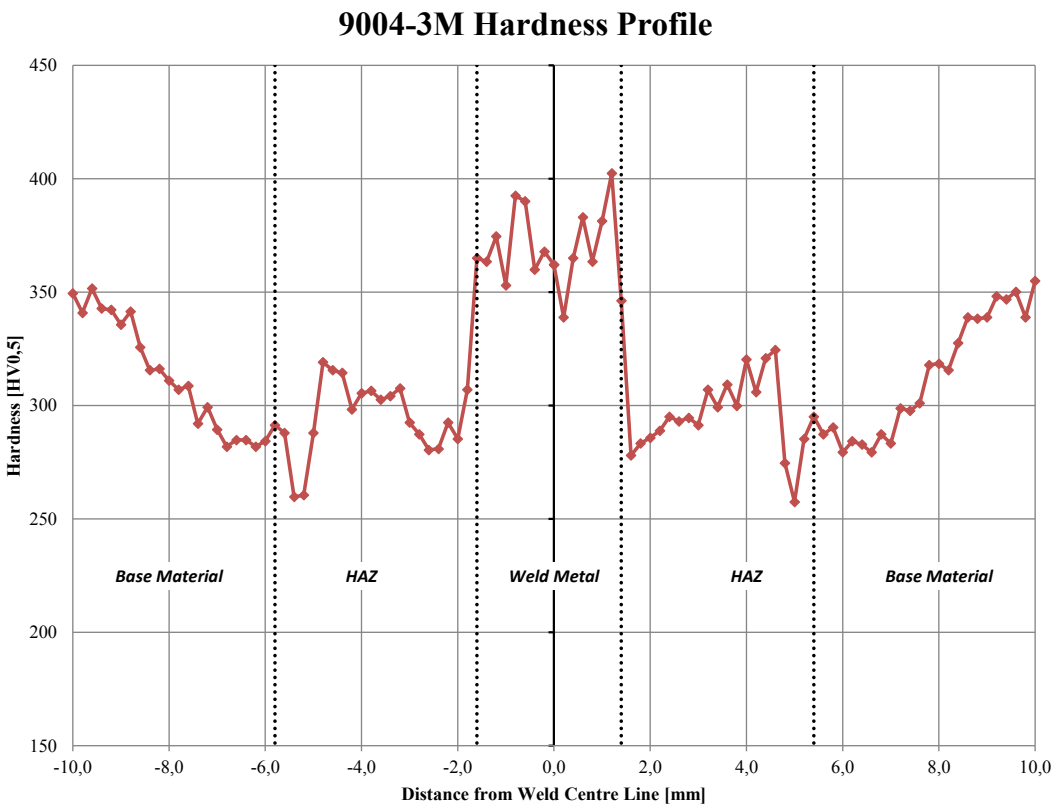

Figure 107. Microhardness profile of MAG welded sample 9004-3M.

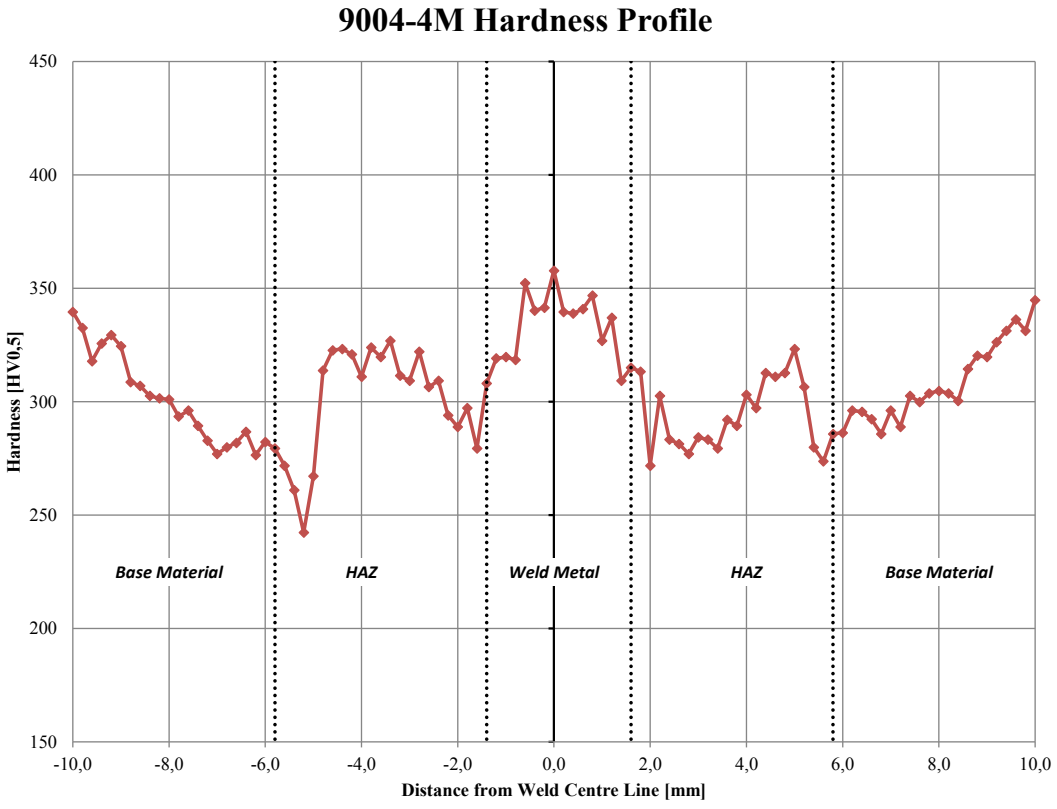

Figure 108. Microhardness profile of MAG welded sample 9004-4M.

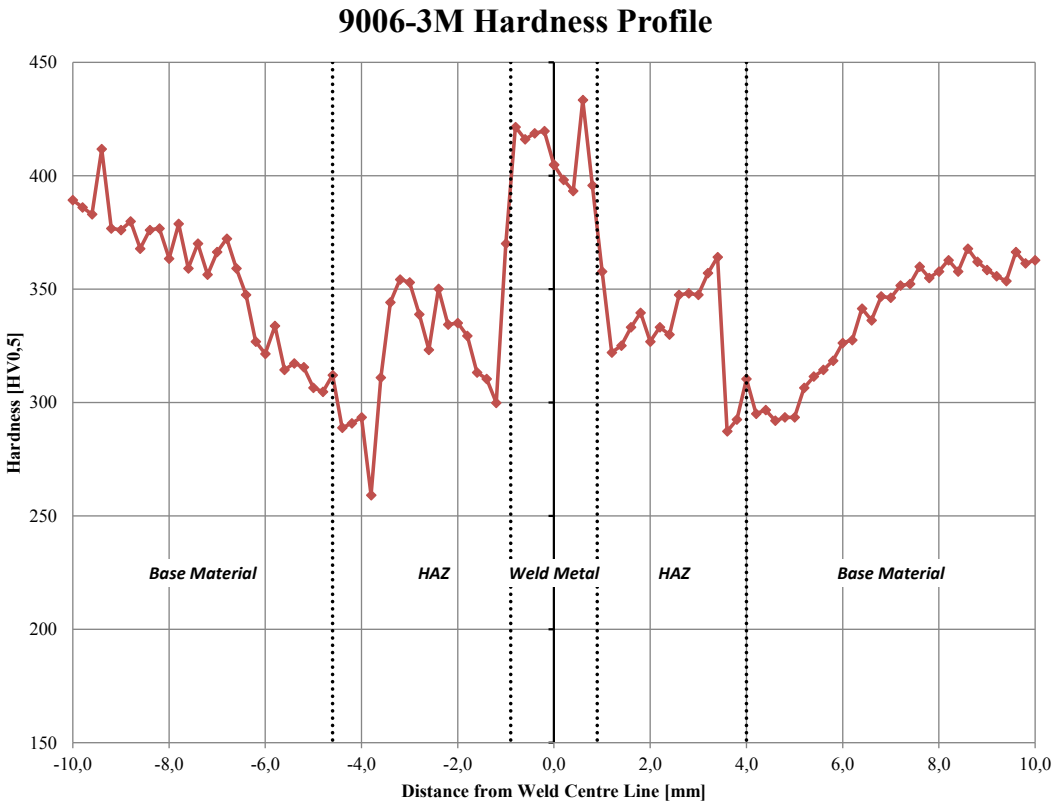

Figure 109. Microhardness profile of MAG welded sample 9006-3M.

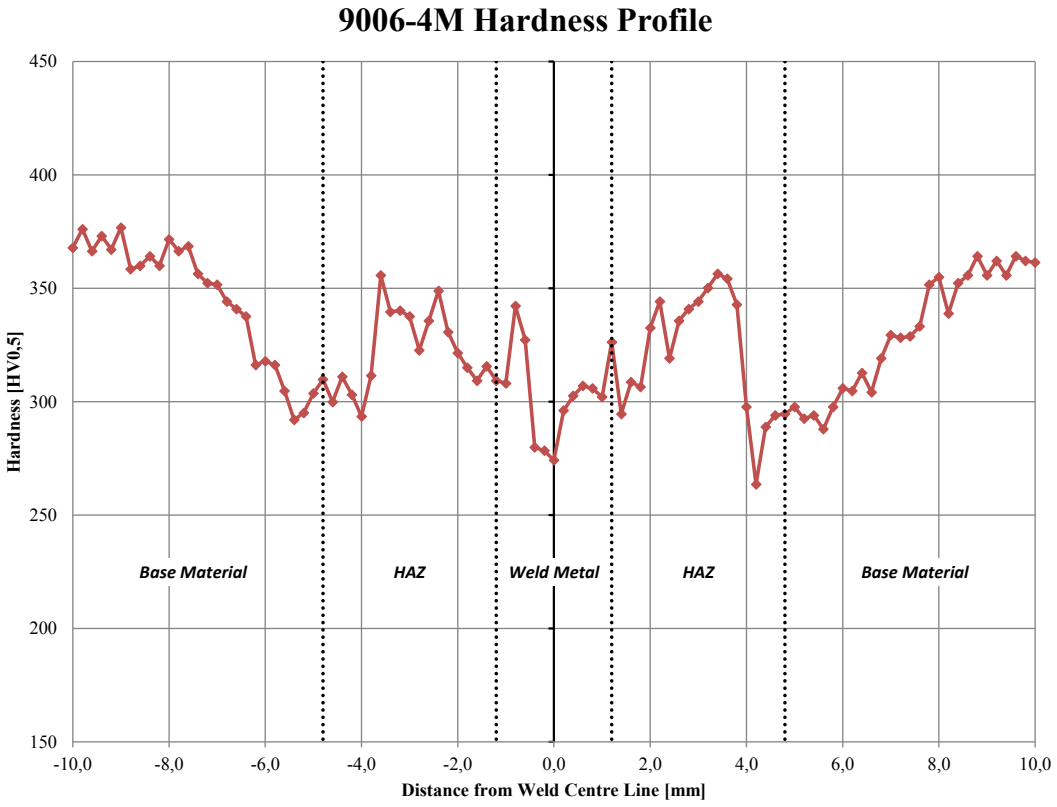

Figure 110. Microhardness profile of MAG welded sample 9006-4M.

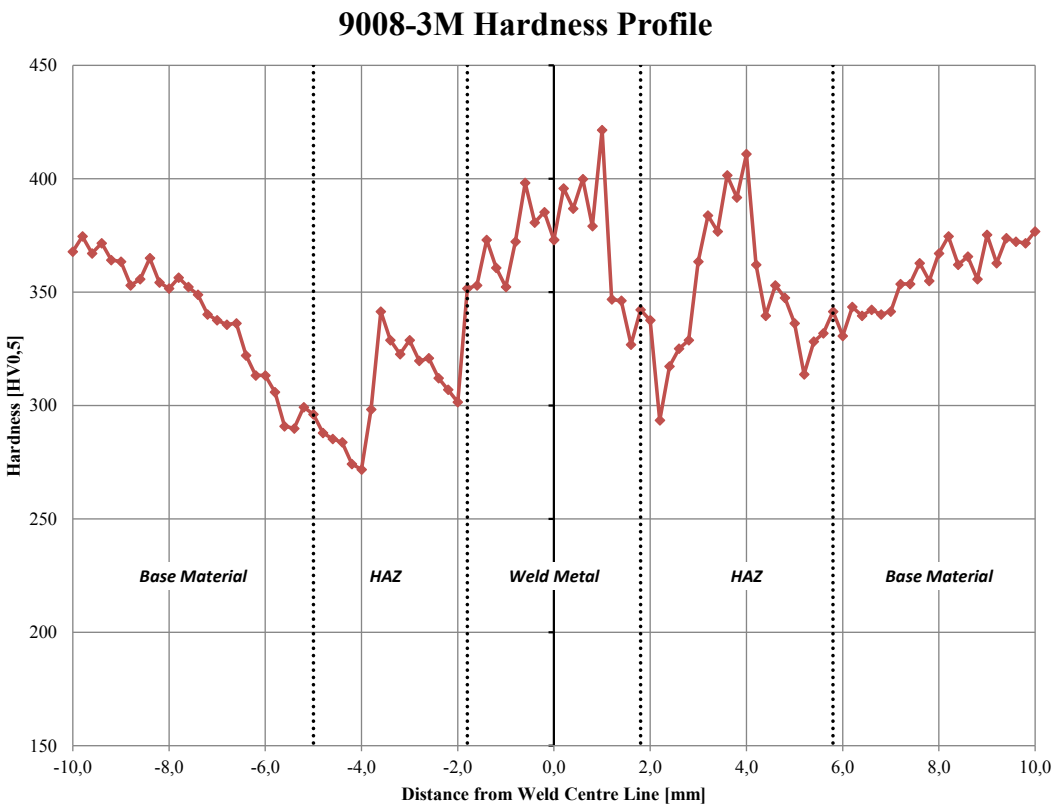

Figure 111. Microhardness profile of MAG welded sample 9008-3M.

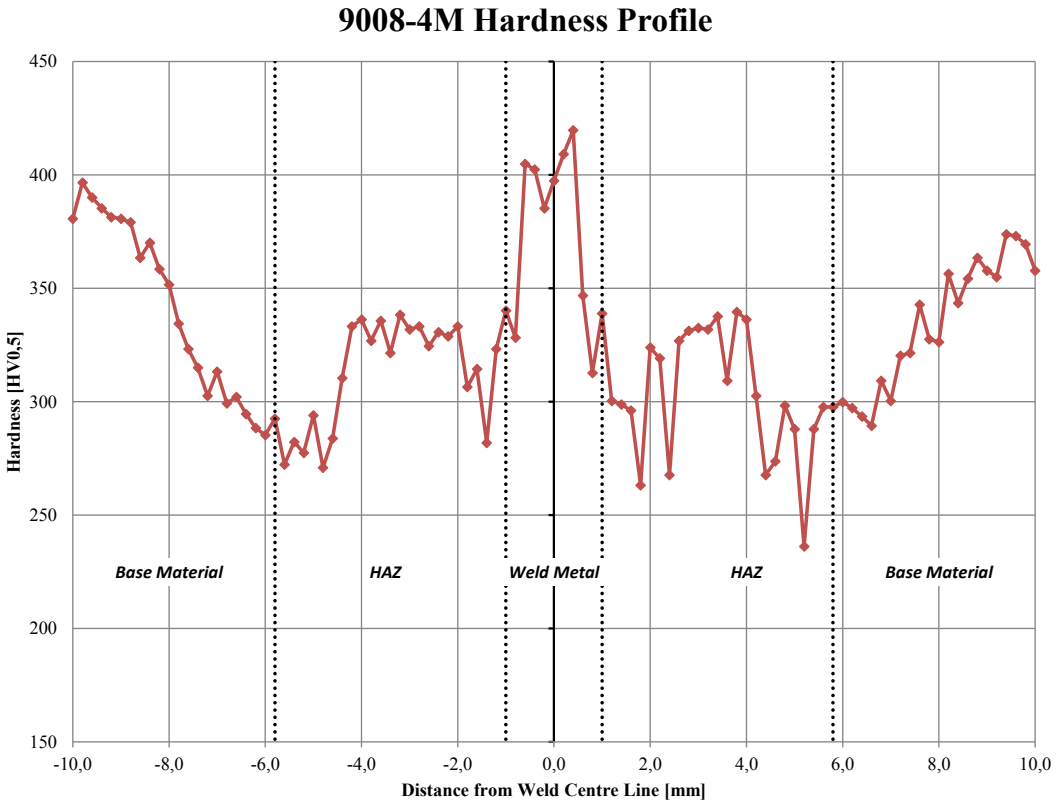

Figure 112. Microhardness profile of MAG welded sample 9008-4M.

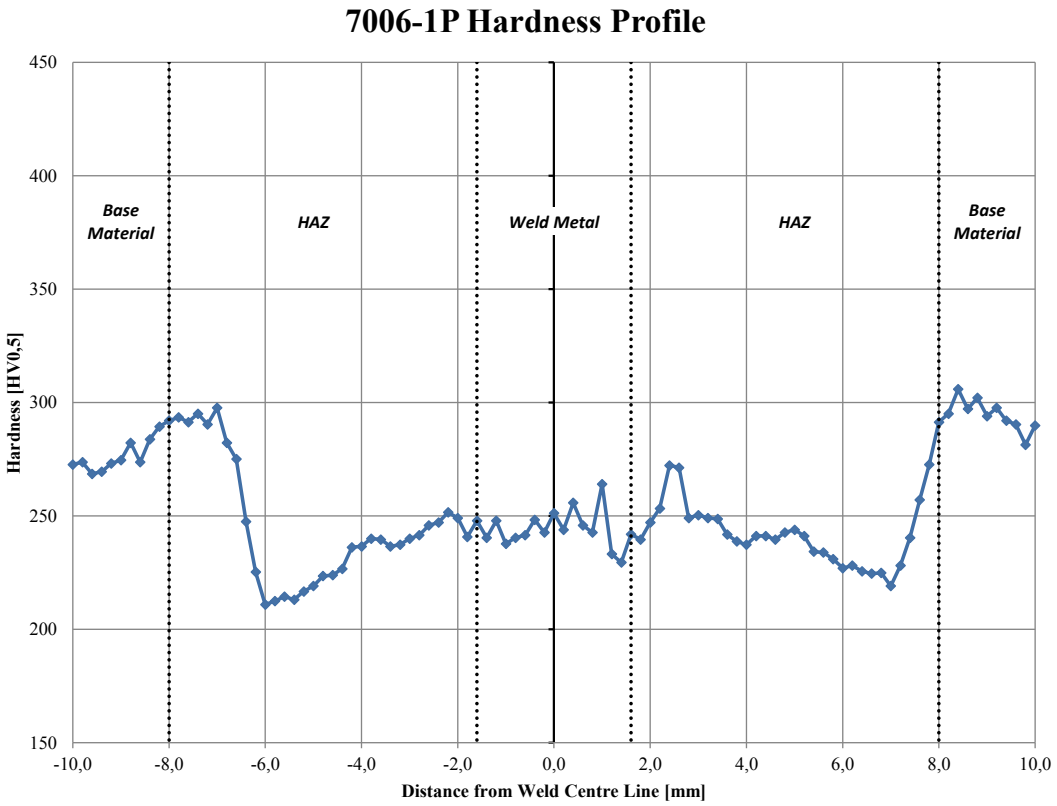

Figure 113. Microhardness profile of PAW welded sample 7006-1P.

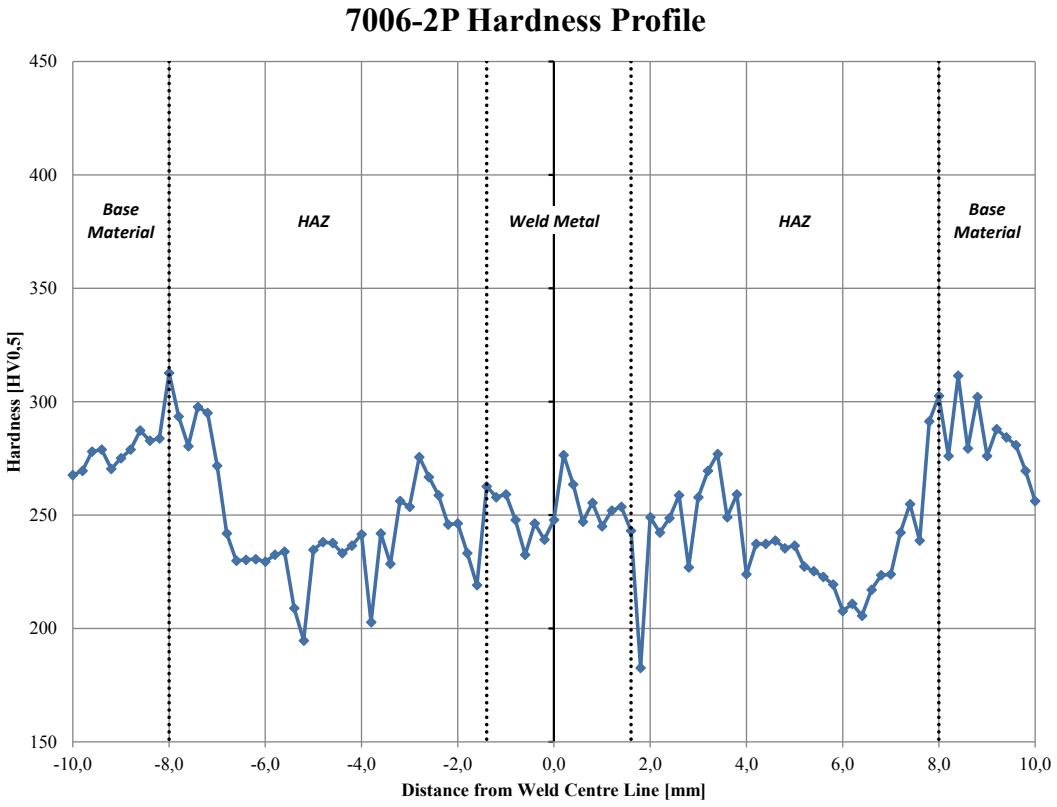

Figure 114. Microhardness profile of PAW welded sample 7006-2P.

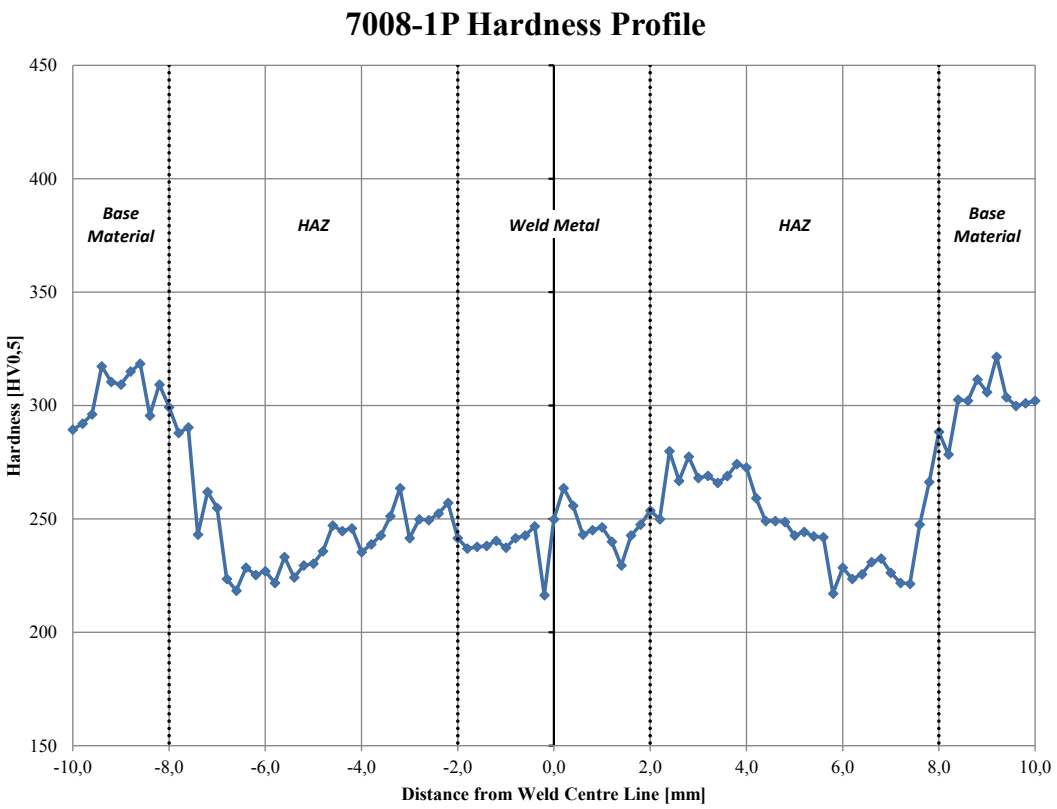

Figure 115. Microhardness profile of PAW welded sample 7008-1P.

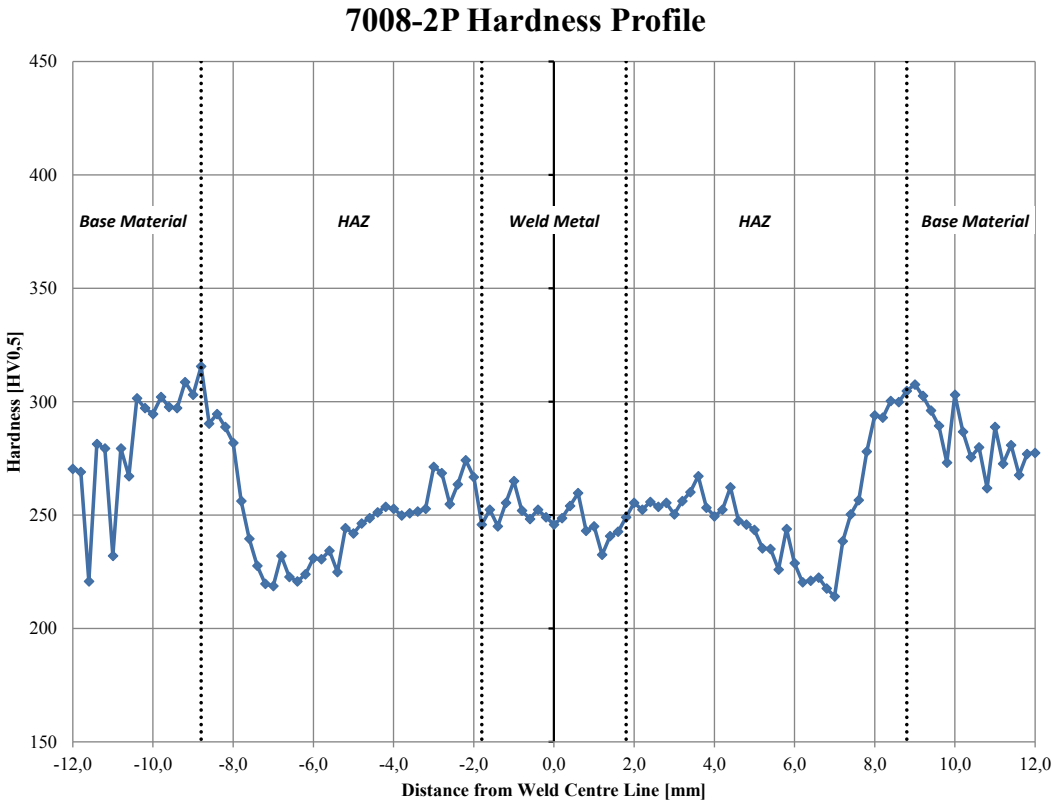

Figure 116. Microhardness profile of PAW welded sample 7008-2P.

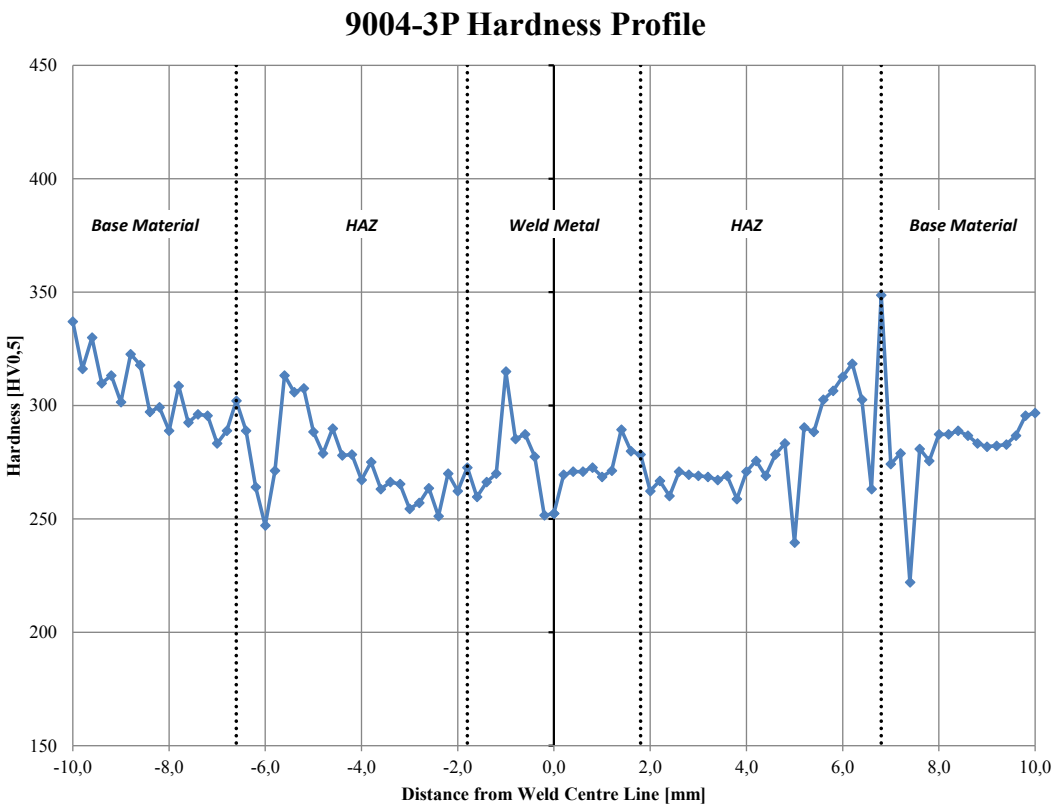

Figure 117. Microhardness profile of PAW welded sample 9004-3P.

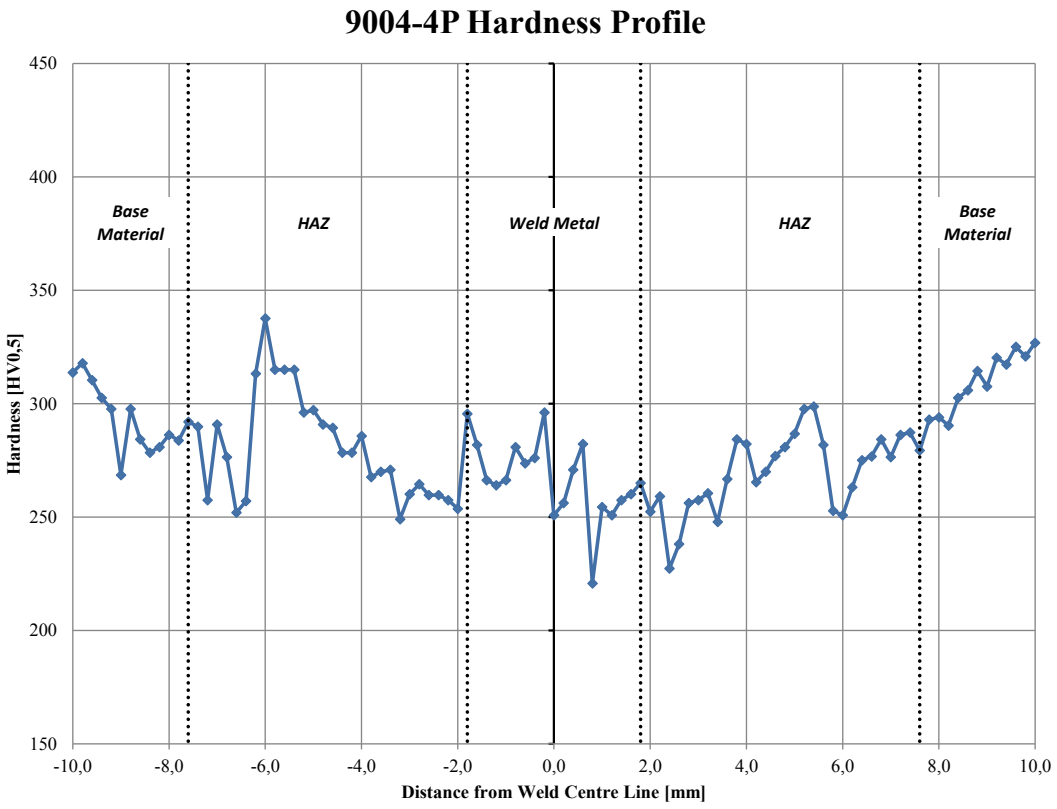

Figure 118. Microhardness profile of PAW welded sample 9004-4P.

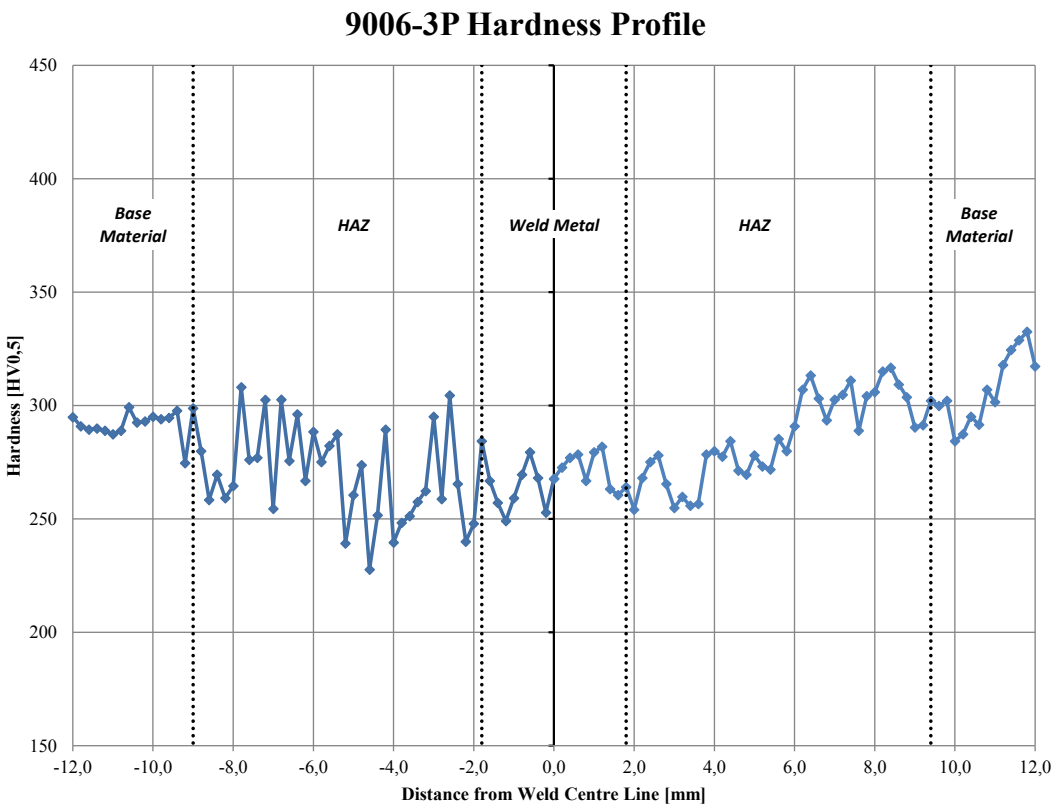

Figure 119. Microhardness profile of PAW welded sample 9006-3P.

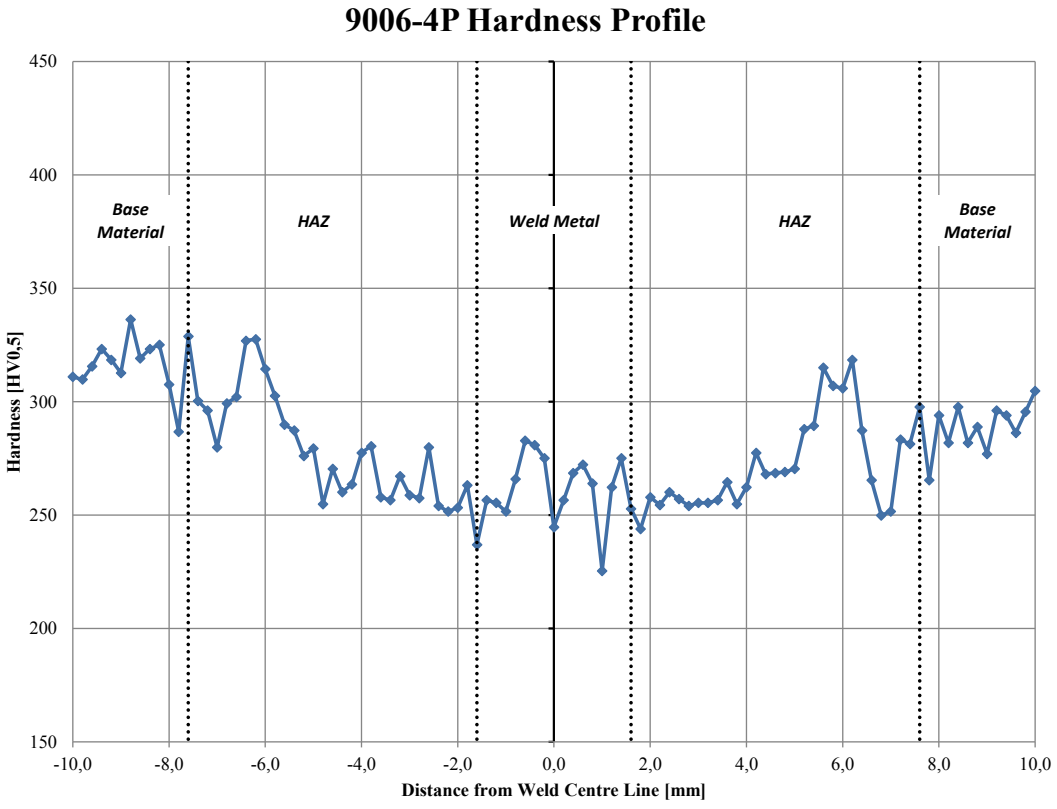

Figure 120. Microhardness profile of PAW welded sample 9006-4P.

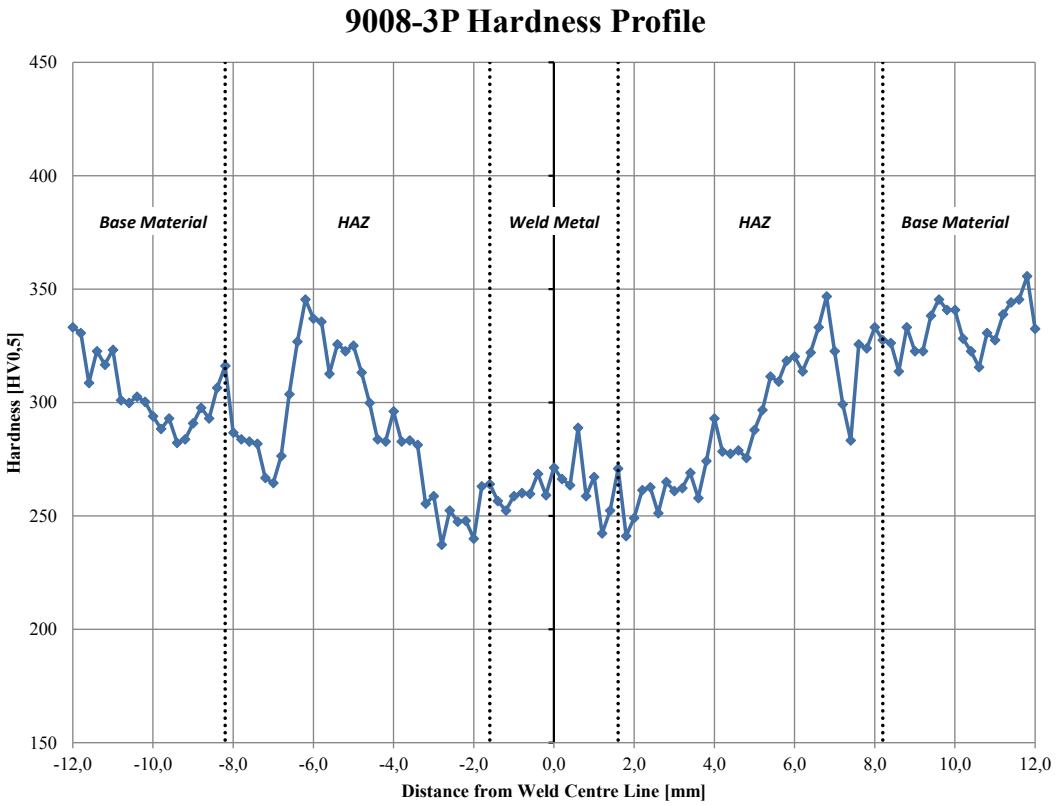

Figure 121. Microhardness profile of PAW welded sample 9008-3P.

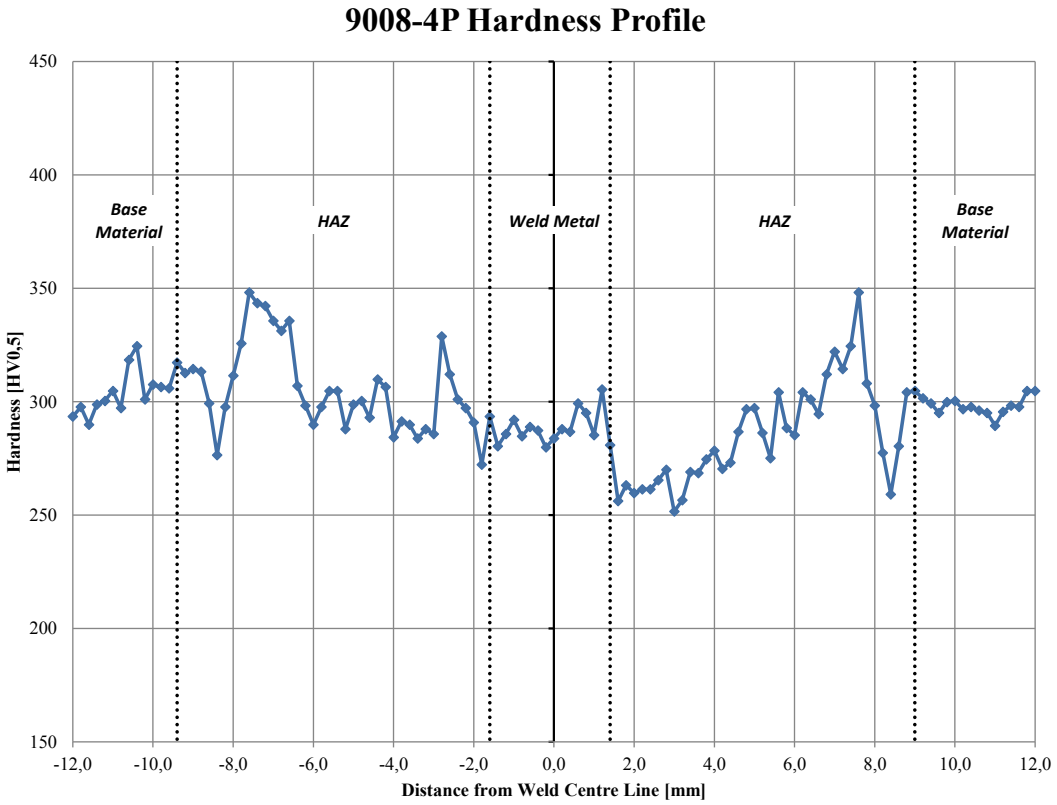

Figure 122. Microhardness profile of PAW welded sample 9008-4P.

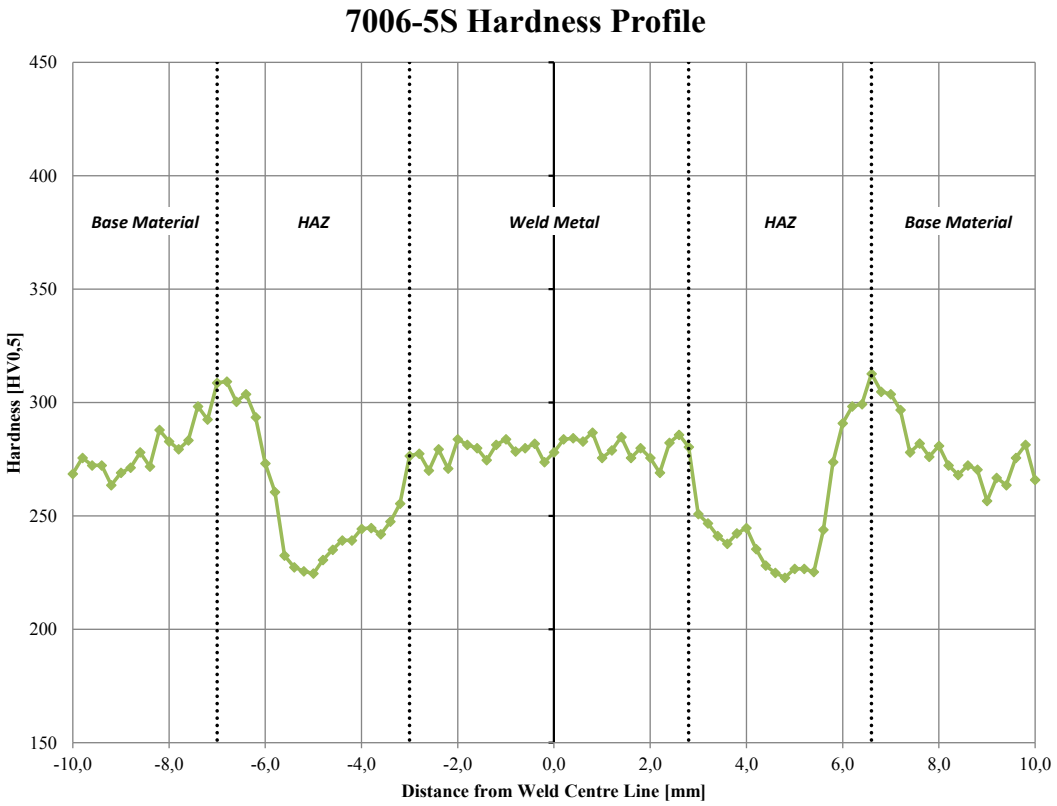

Figure 123. Microhardness profile of SAW welded sample 7006-5S.

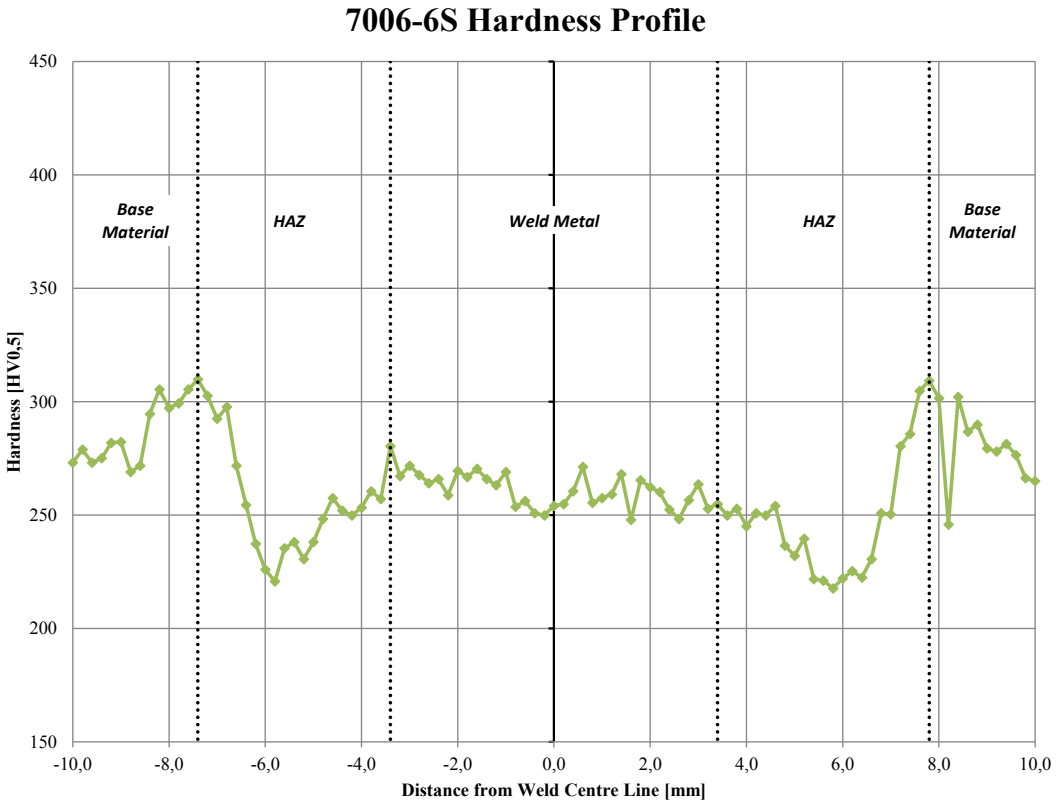

Figure 124. Microhardness profile of SAW welded sample 7006-6S.

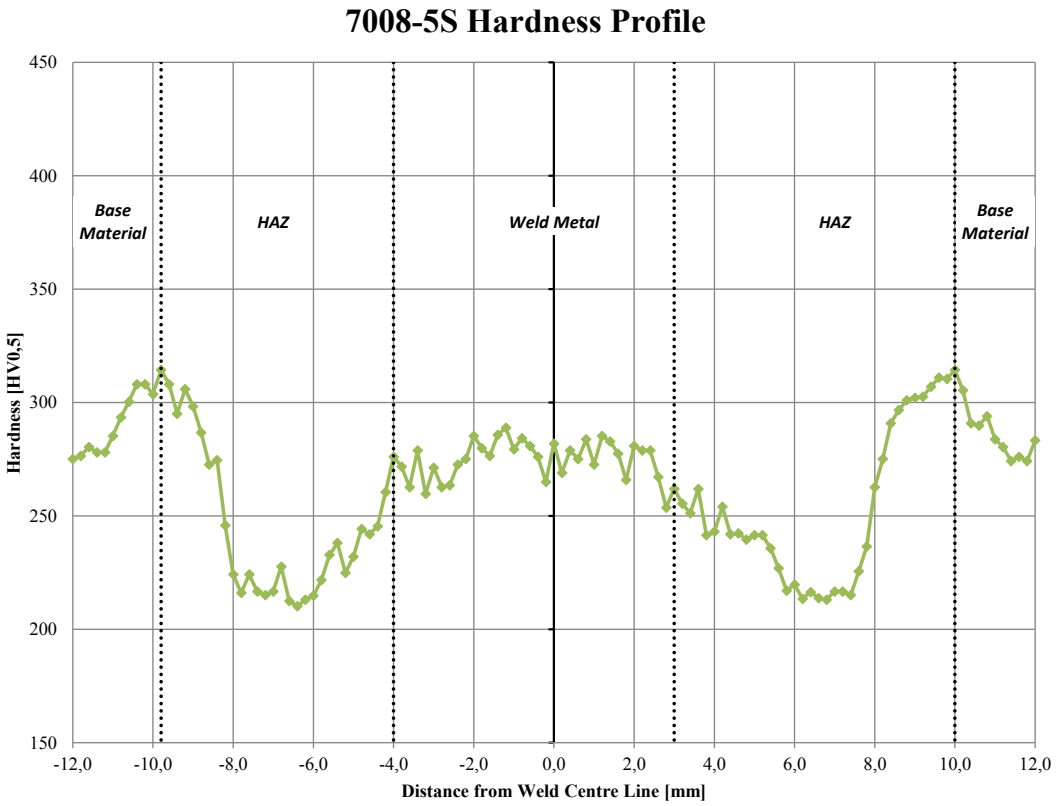

Figure 125. Microhardness profile of SAW welded sample 7008-5S.

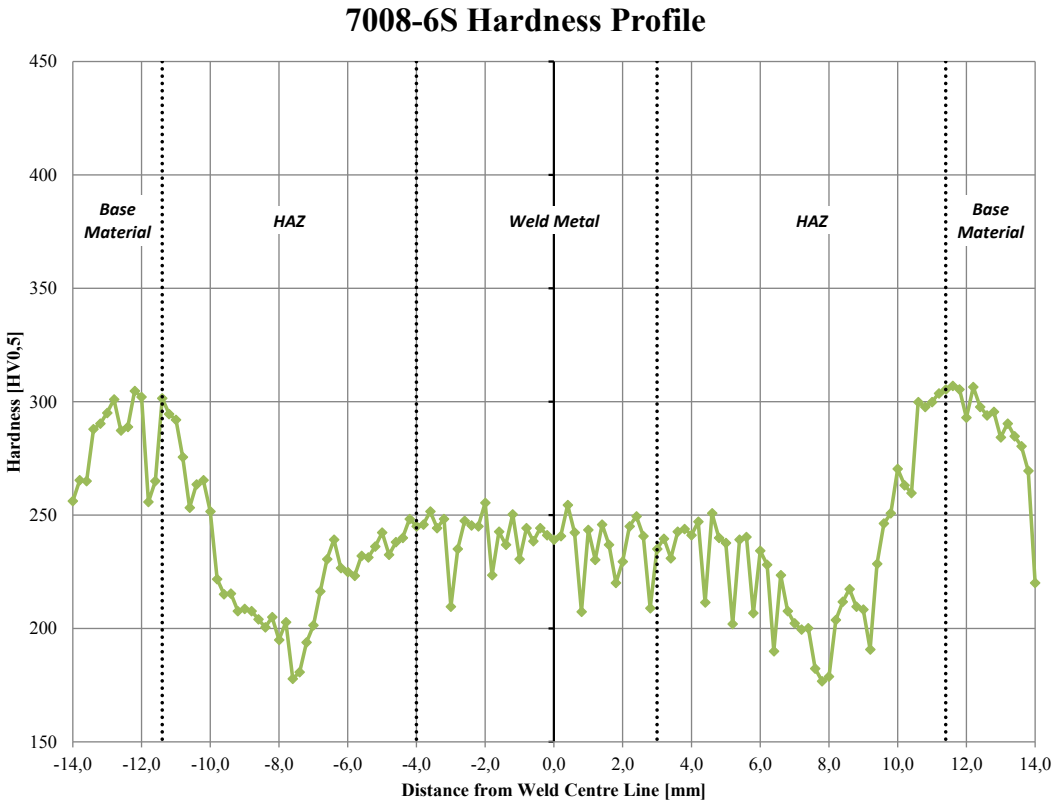

Figure 126. Microhardness profile of SAW welded sample 7008-6S.

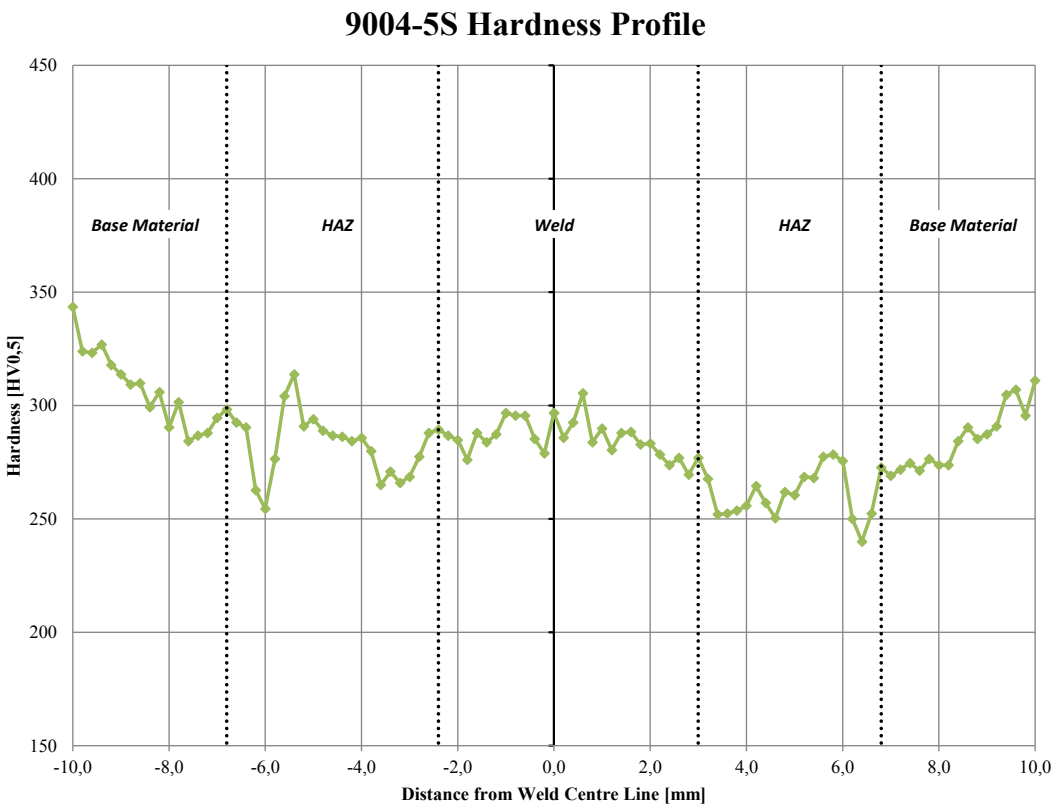

Figure 127. Microhardness profile of SAW welded sample 9004-5S.

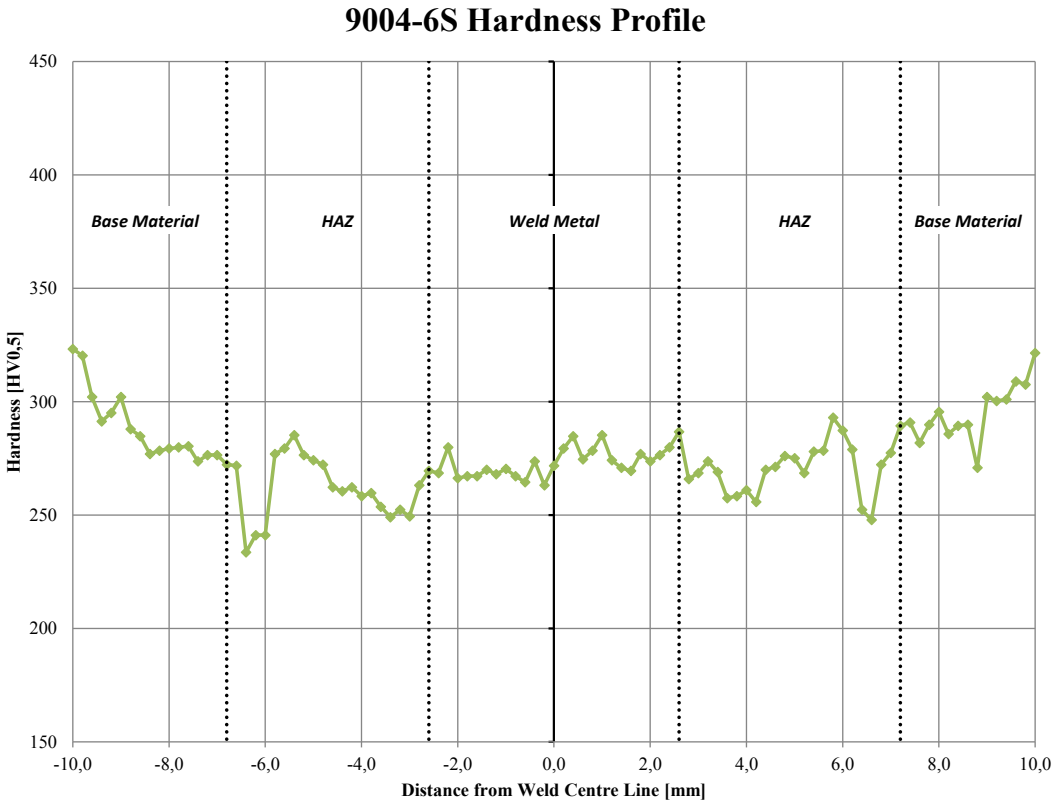

Figure 128. Microhardness profile of SAW welded sample 9004-6S.

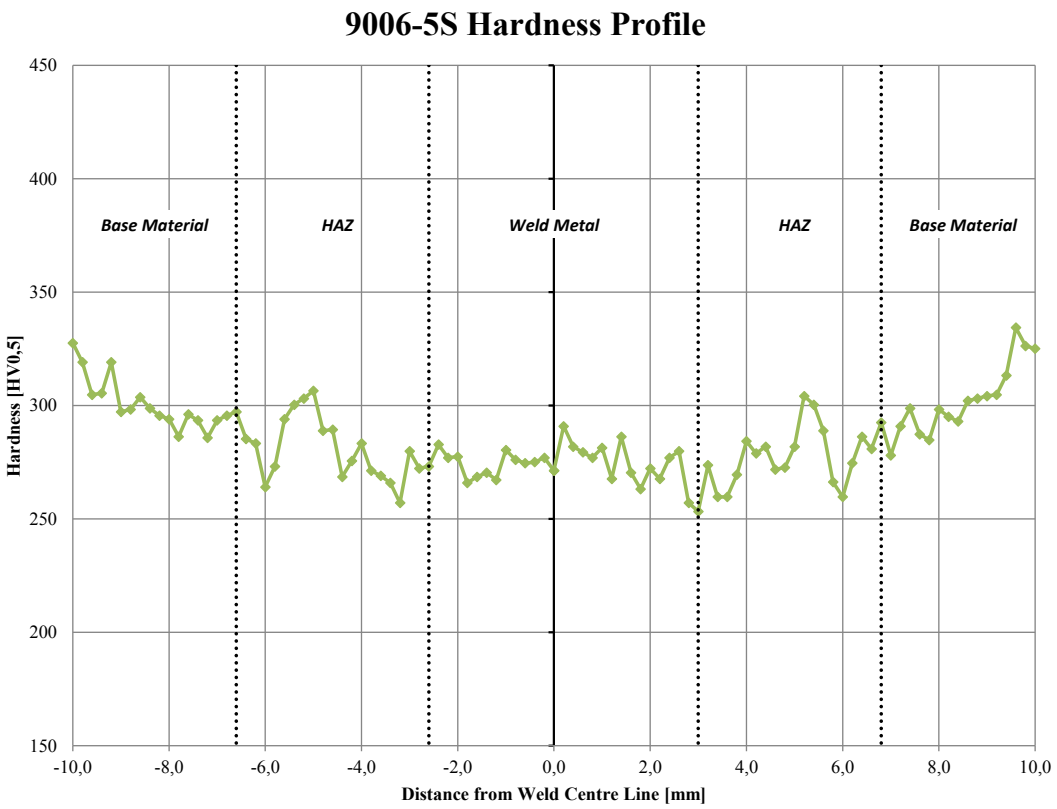

Figure 129. Microhardness profile of SAW welded sample 9006-5S.

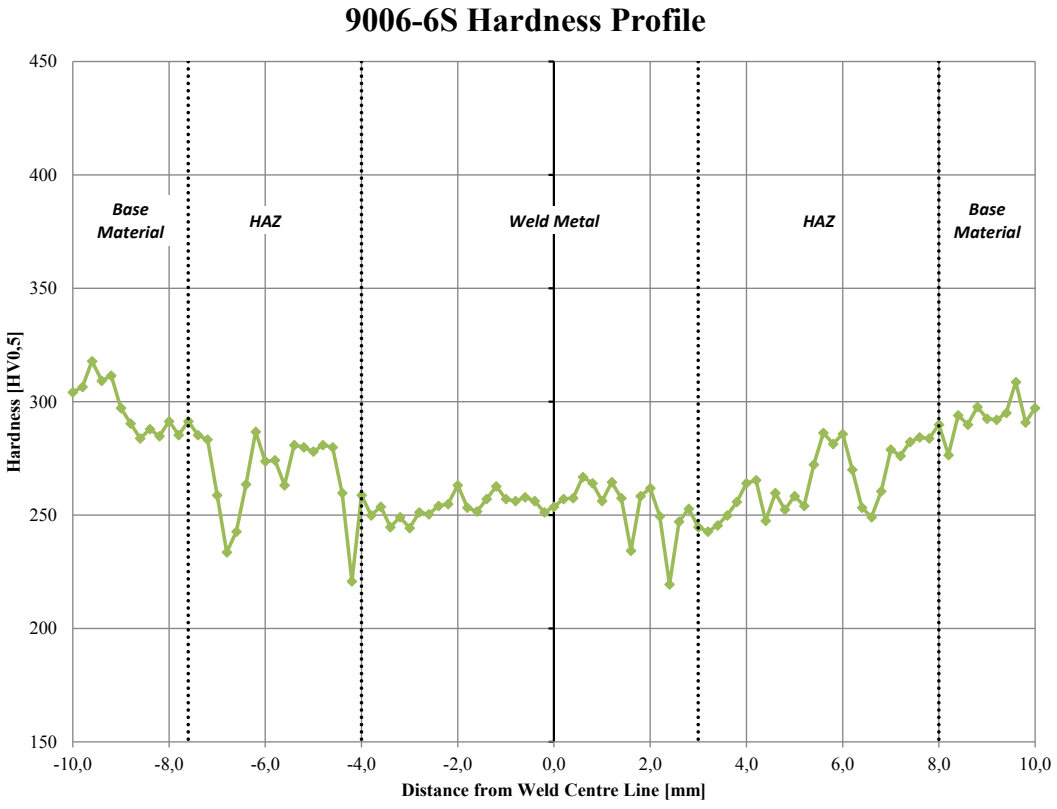

Figure 130. Microhardness profile of SAW welded sample 9006-6S.

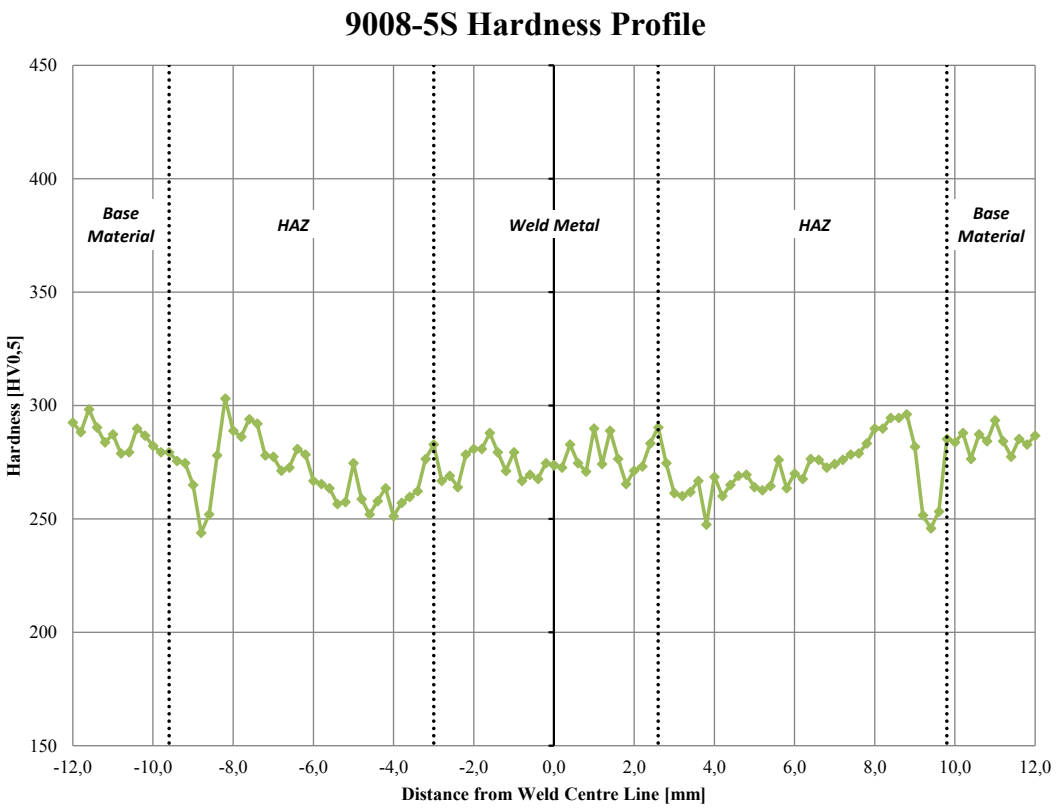

Figure 131. Microhardness profile of SAW welded sample 9008-5S.

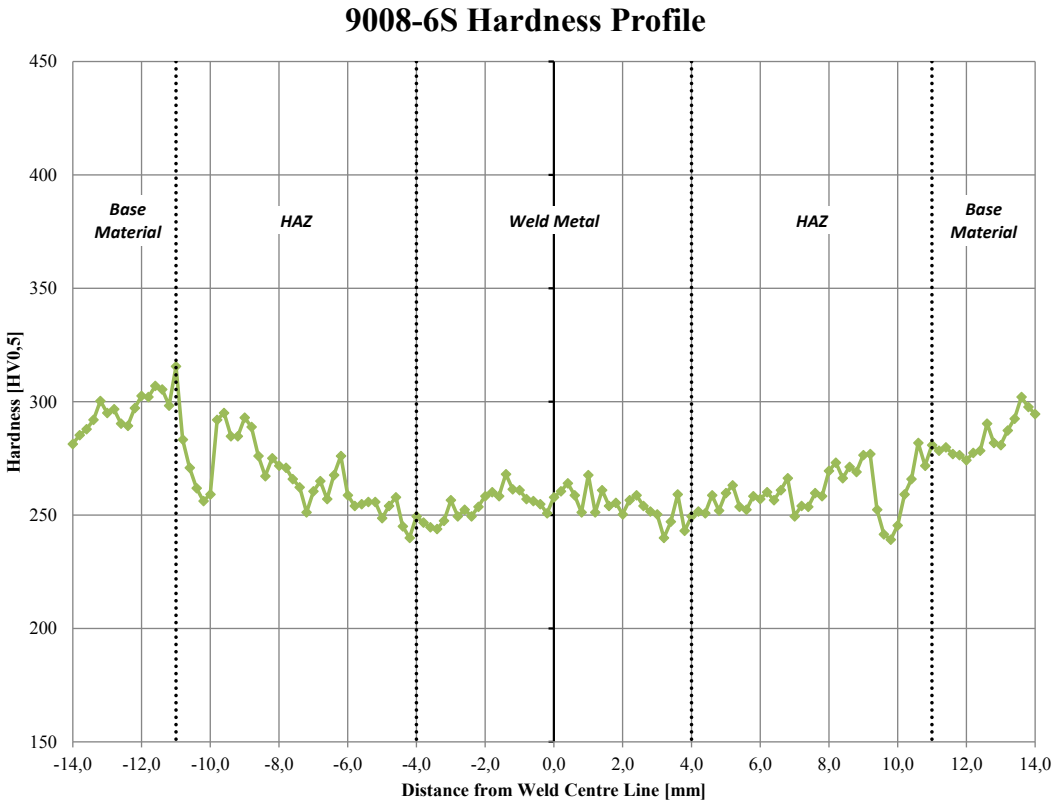

Figure 132. Microhardness profile of SAW welded sample 9008-6S.

$$\text{Heat Input}, Q = \frac{k * 60 * U * I}{1000 * v}$$

$$\text{Percentage Difference}, \delta = \frac{Q_{P\bar{X}} - Q_{PUI}}{Q_{PUI}} * 100$$

k = 0,8

$P_{\bar{x}}$ *= Average Welding Power [W]*

P_{UI} *= Calculated Welding Power [W]*

Test Case	I [A]	U [V]	v [mm/min]	$P_{\bar{x}}$ [W]	P_{UI} [W]	$Q_{P\bar{x}}$ [kJ/mm]	Q_{PUI} [kJ/mm]	δ [%]
7006-1M	338	29,1	900	10524,0	9835,8	0,56	0,52	7,0
7006-2M	336	31,0	900	11149,0	10416,0	0,59	0,56	7,0
7008-1M	355	25,3	700	9536,0	8981,5	0,65	0,62	6,2
7008-2M	348	31,8	700	11798,0	11066,4	0,81	0,76	6,6
9004-3M	328	27,2	950	9470,0	8921,6	0,48	0,45	6,1
9004-4M	333	27,2	950	9686,0	9057,6	0,49	0,46	6,9
9006-3M	319	26,3	900	8932,0	8389,7	0,48	0,45	6,5
9006-4M	347	28,3	900	10439,0	9820,1	0,56	0,52	6,3
9008-3M	360	24,9	700	9489,0	8964,0	0,65	0,61	5,9
9008-4M	358	28,0	700	10636,0	10024,0	0,73	0,69	6,1

Figure 133. The heat input calculation comparison of MAG welded samples.

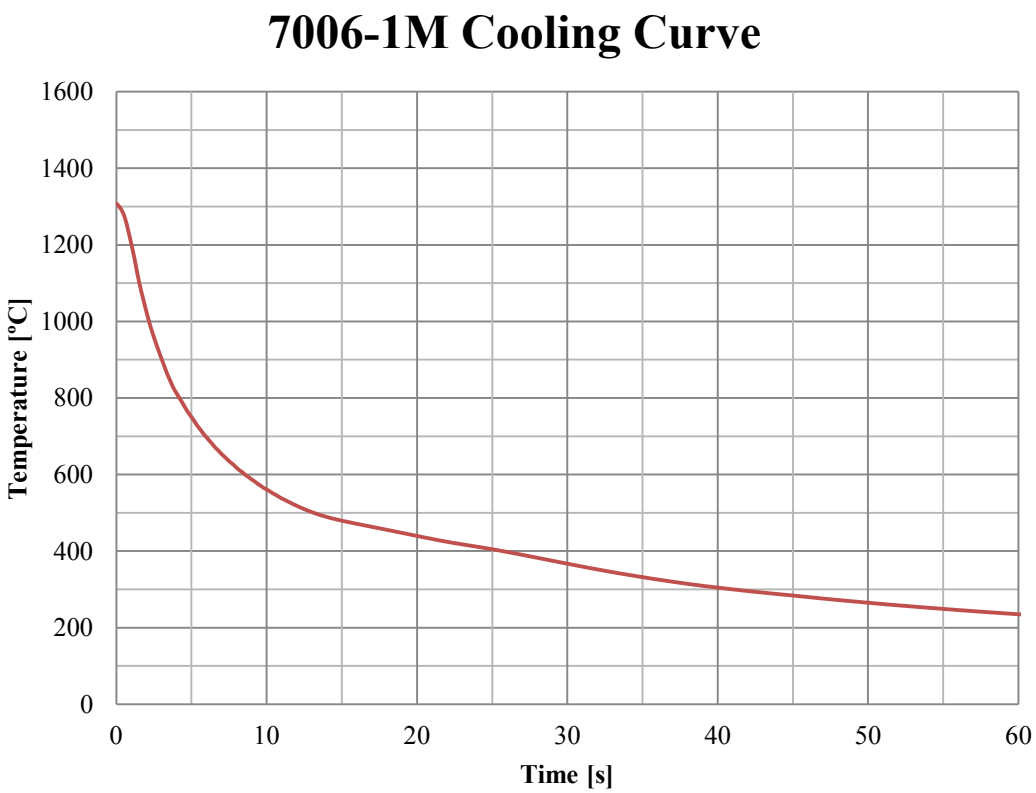

Figure 134. Cooling curve of MAG welded sample 7006-1M with $\Delta t_{8/5}$ of 9,2 s.

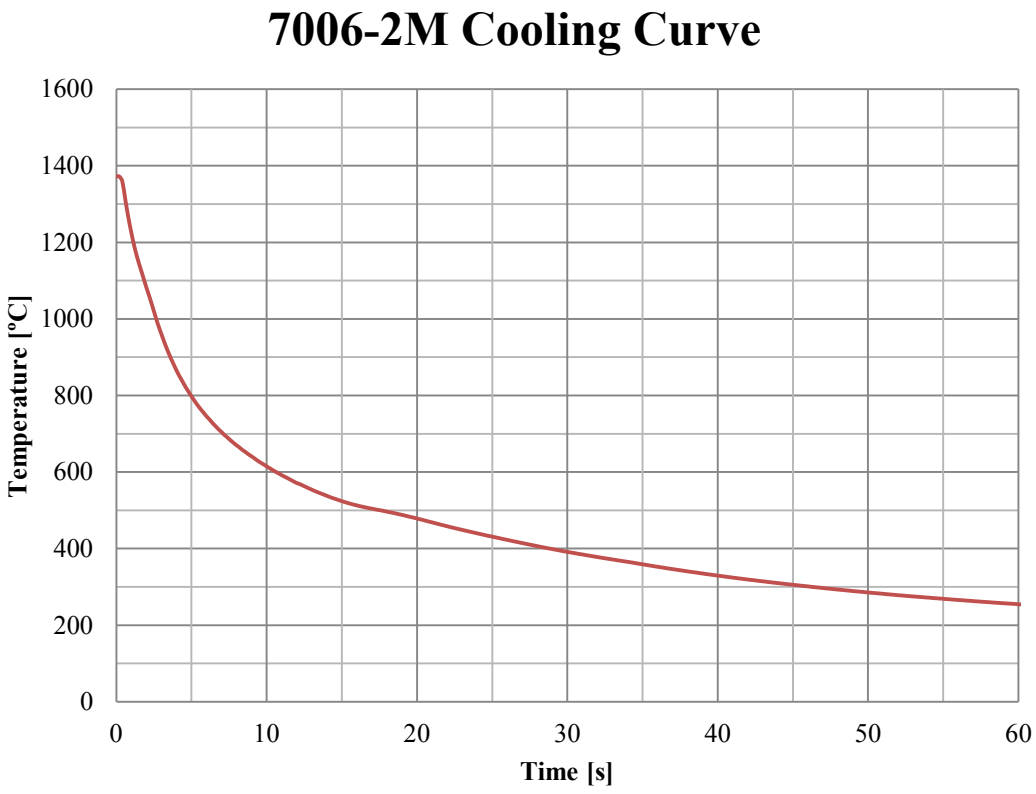

Figure 135. Cooling curve of MAG welded sample 7006-2M with $\Delta t_{8/5}$ of 13,5 s.

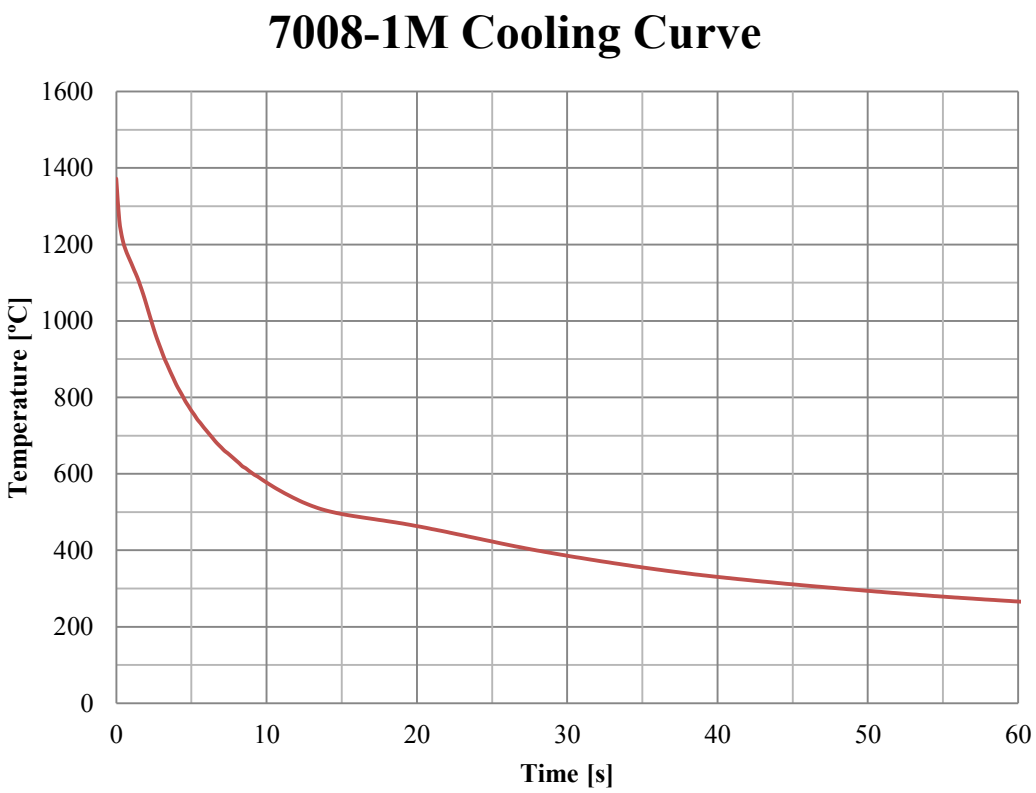

Figure 136. Cooling curve of MAG welded sample 7008-1M with $\Delta t_{8/5}$ of 11,5 s.

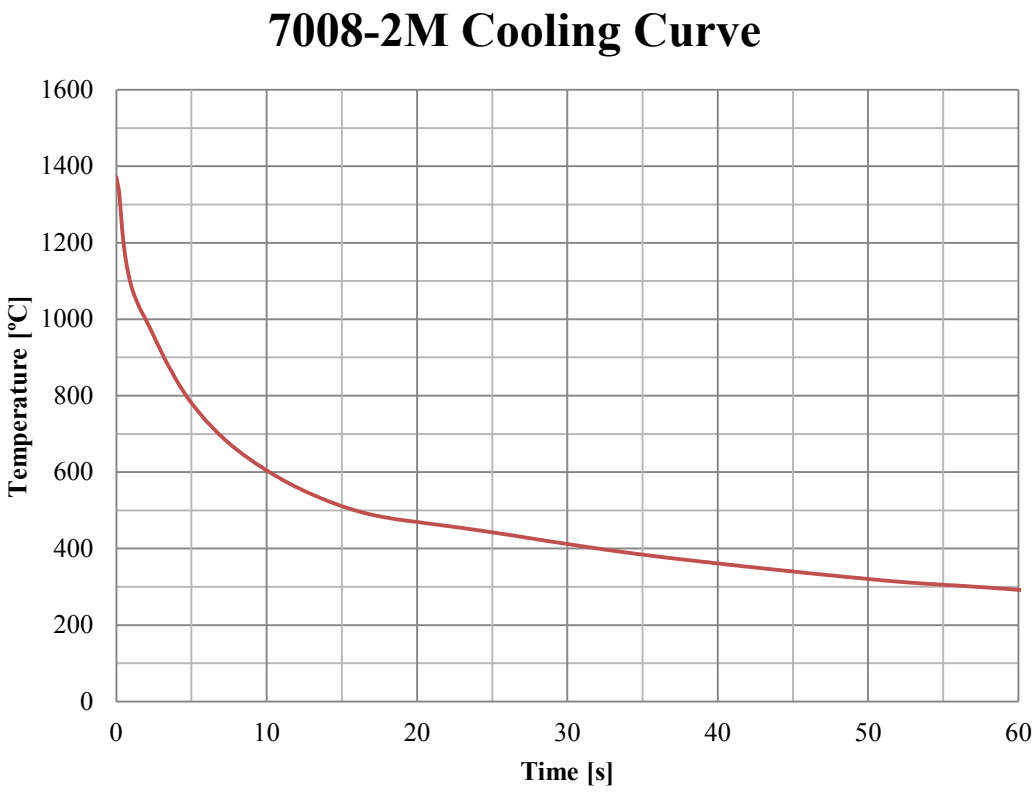

Figure 137. Cooling curve of MAG welded sample 7008-2M with $\Delta t_{8/5}$ of 13,1 s.

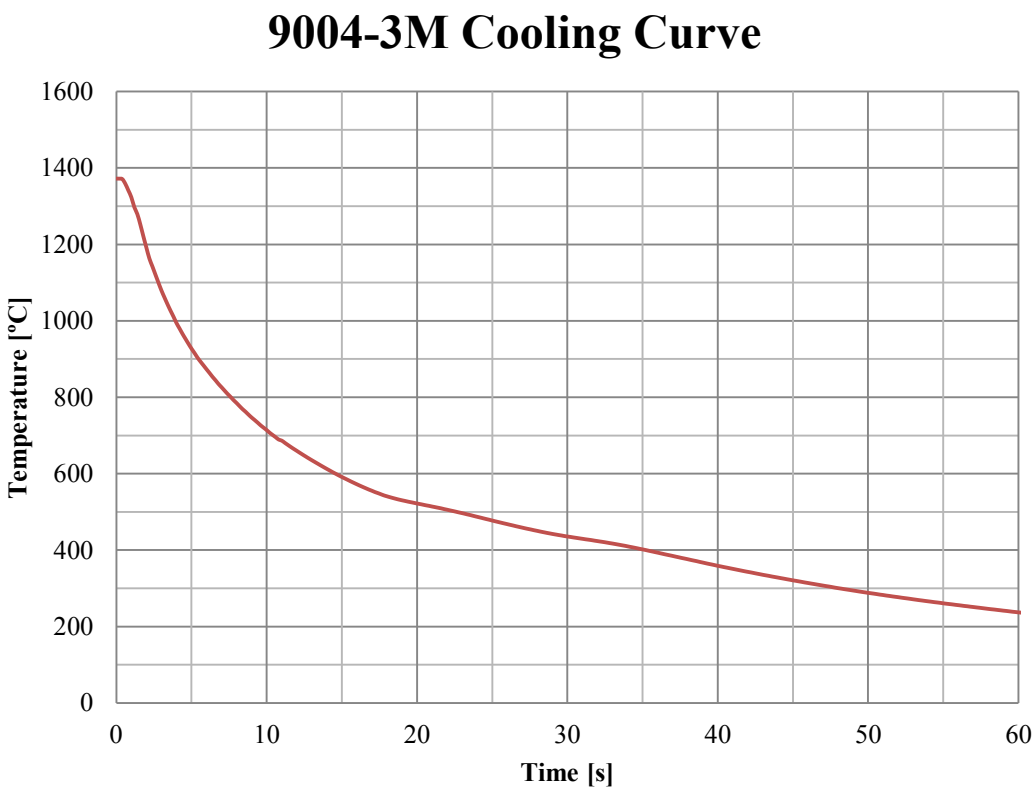

Figure 138. Cooling curve of MAG welded sample 9004-3M with $\Delta t_{8/5}$ of 15,6 s.

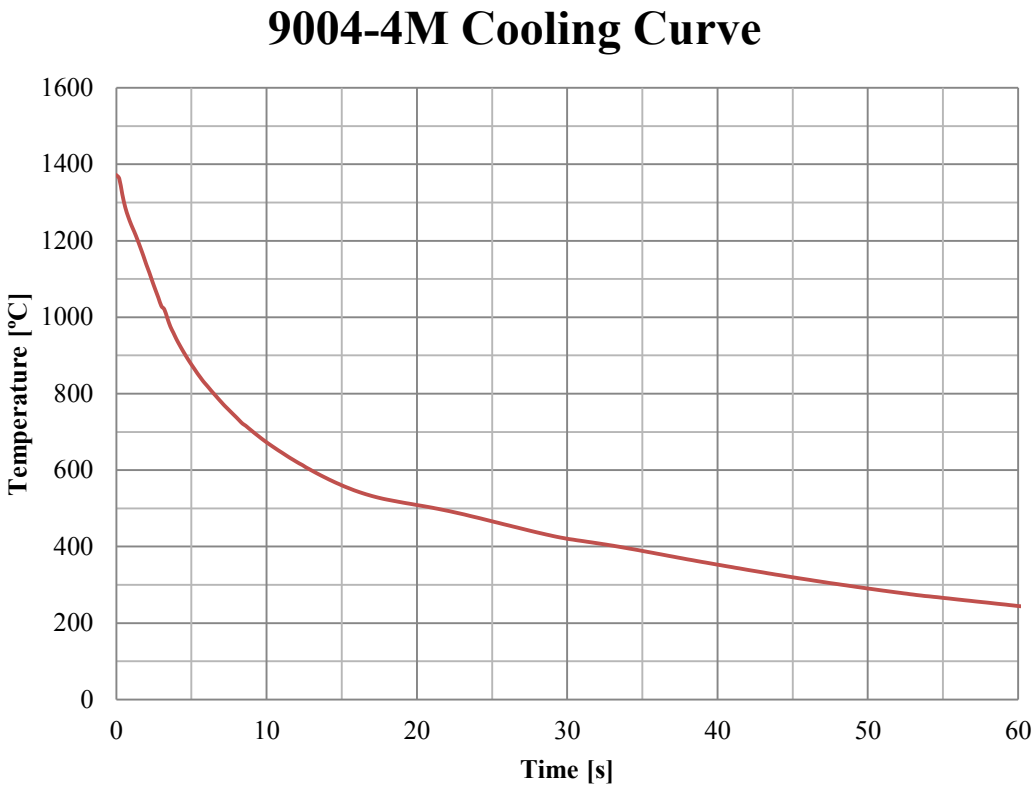

Figure 139. Cooling curve of MAG welded sample 9004-4M with $\Delta t_{8/5}$ of 15,9 s.

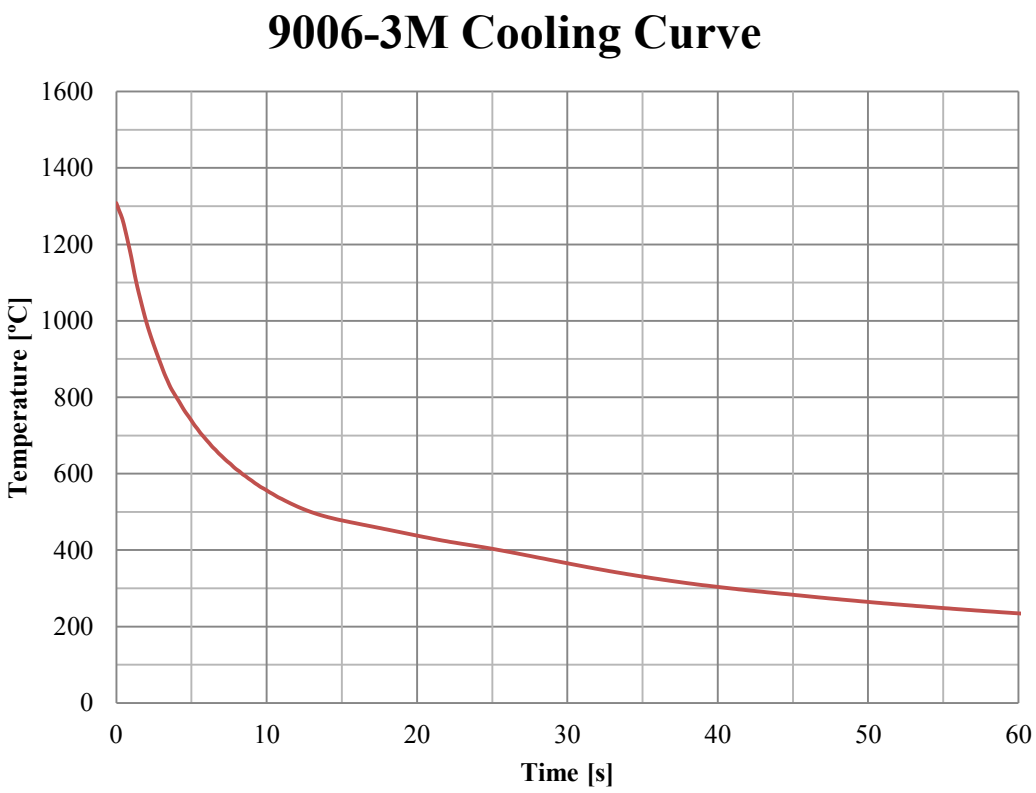

Figure 140. Cooling curve of MAG welded sample 9006-3M with $\Delta t_{8/5}$ of 9,0 s.

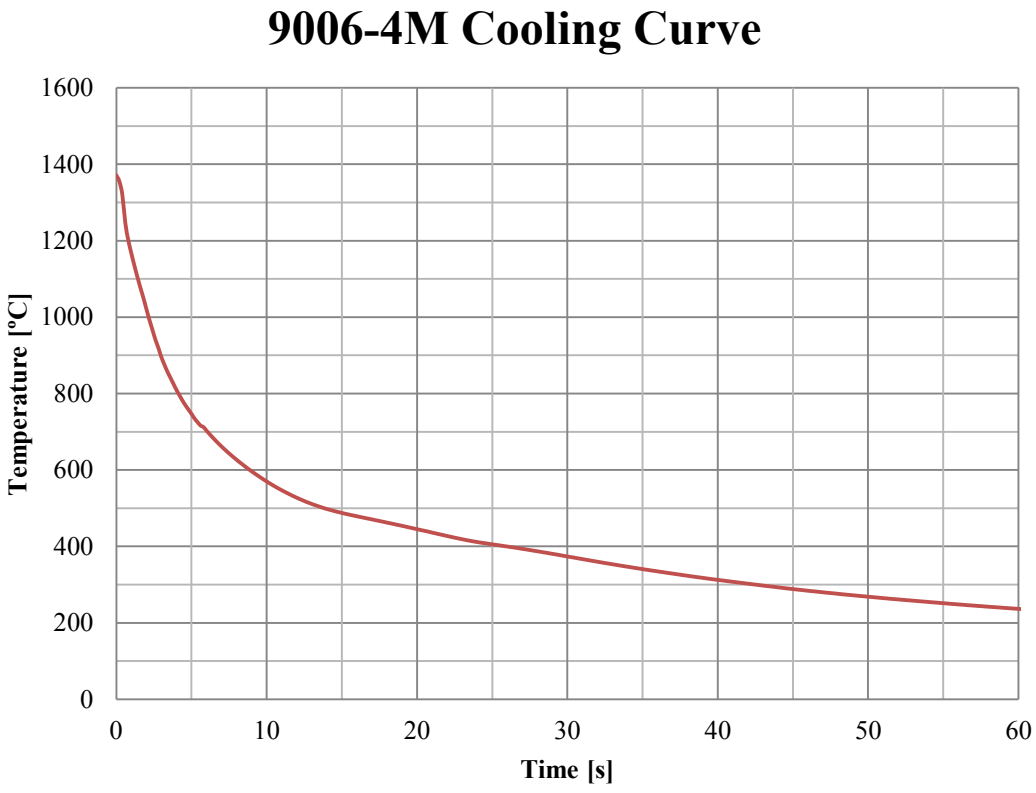

Figure 141. Cooling curve of MAG welded sample 9006-4M with $\Delta t_{8/5}$ of 9,6 s.

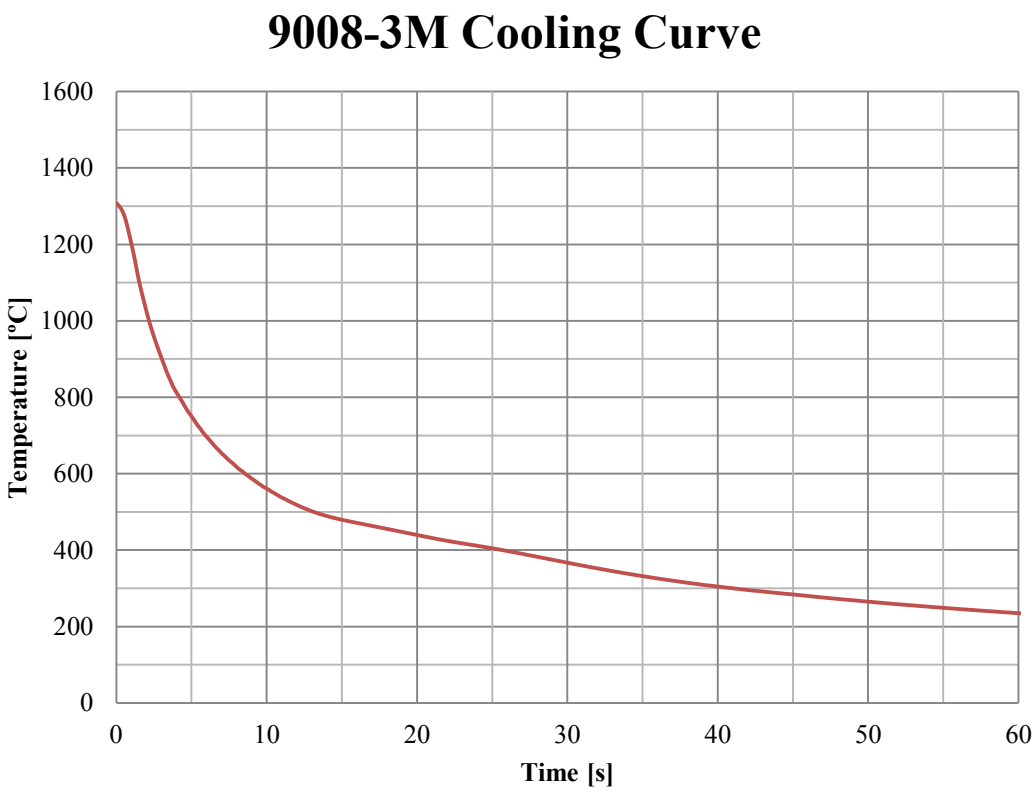

Figure 142. Cooling curve of MAG welded sample 9008-3M with $\Delta t_{8/5}$ of 9,1 s.

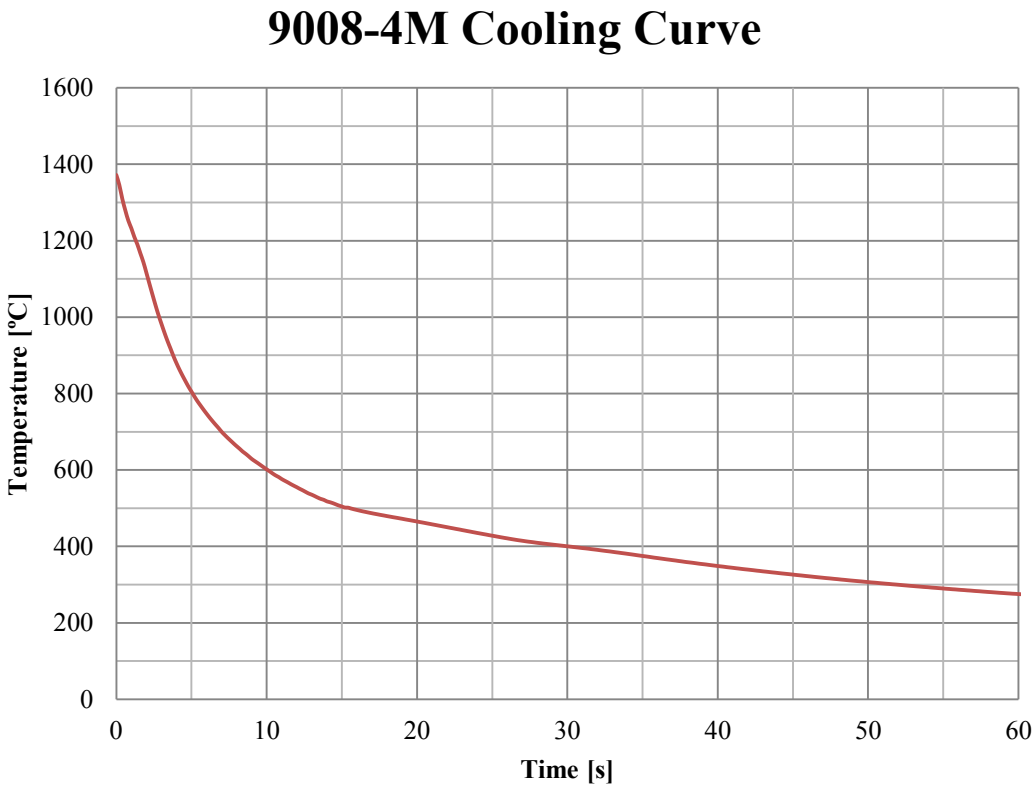

Figure 143. Cooling curve of MAG welded sample 9008-4M with $\Delta t_{8/5}$ of 11,3 s.

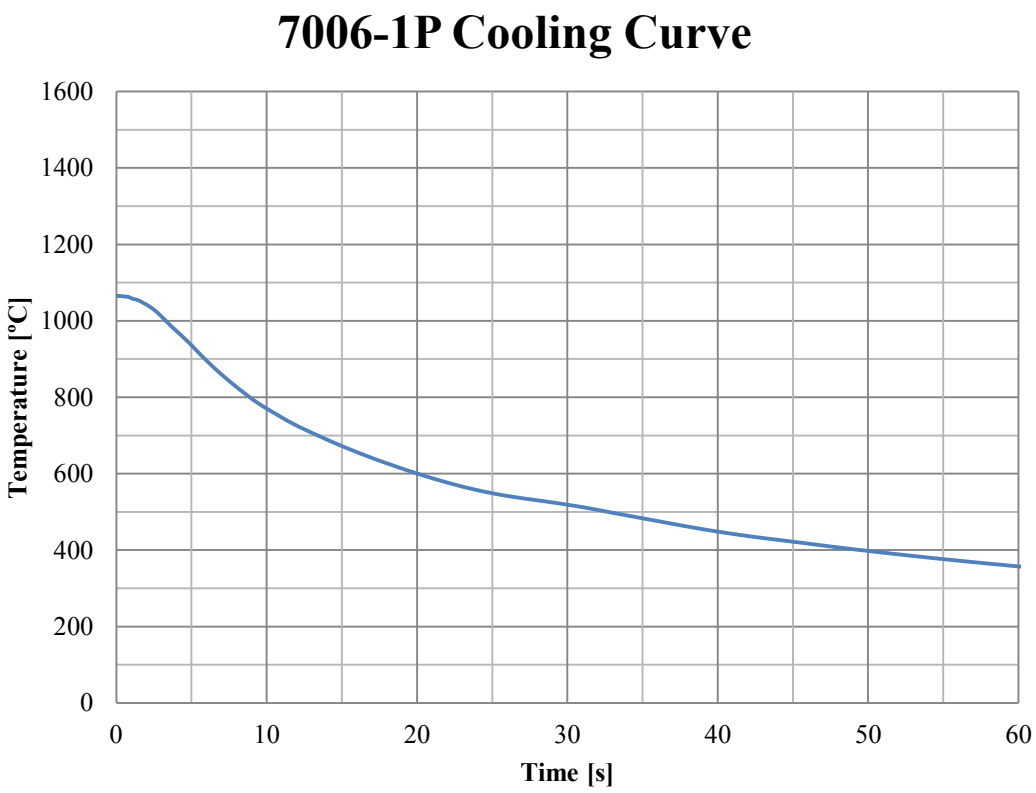

Figure 144. Cooling curve of PAW welded sample 7006-1P with $\Delta t_{8/5}$ of 23,6 s.

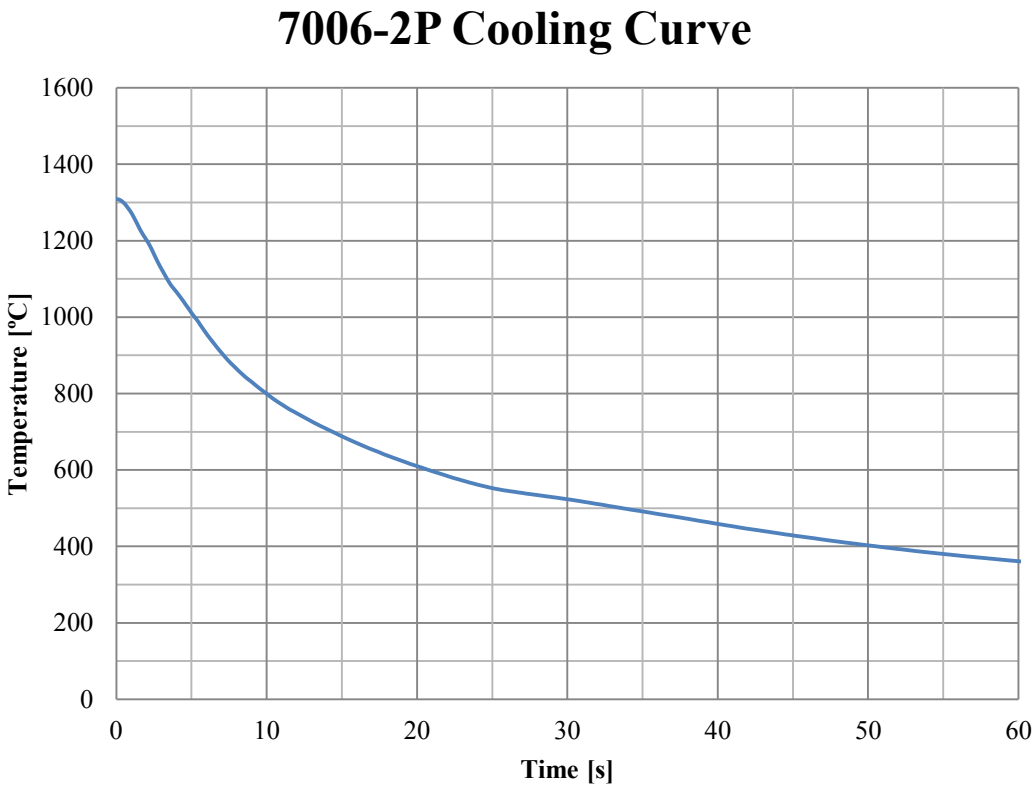

Figure 145. Cooling curve of PAW welded sample 7006-2P with $\Delta t_{8/5}$ of 24,8 s.

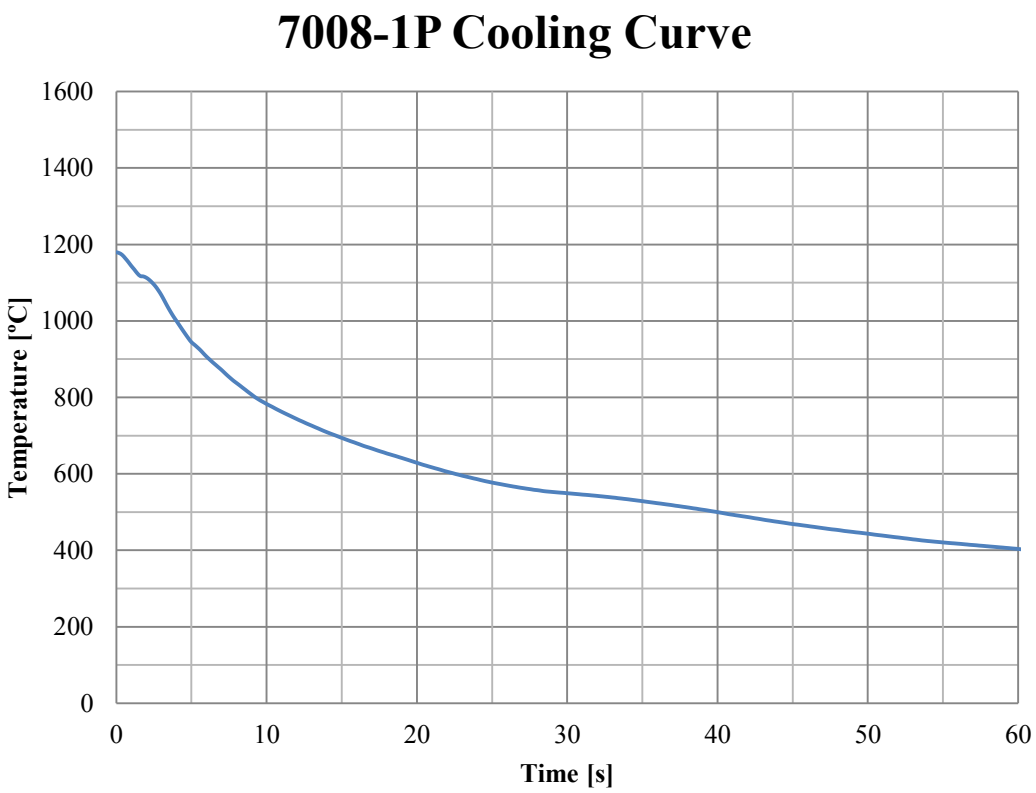

Figure 146. Cooling curve of PAW welded sample 7008-1P with $\Delta t_{8/5}$ of 30,6 s.

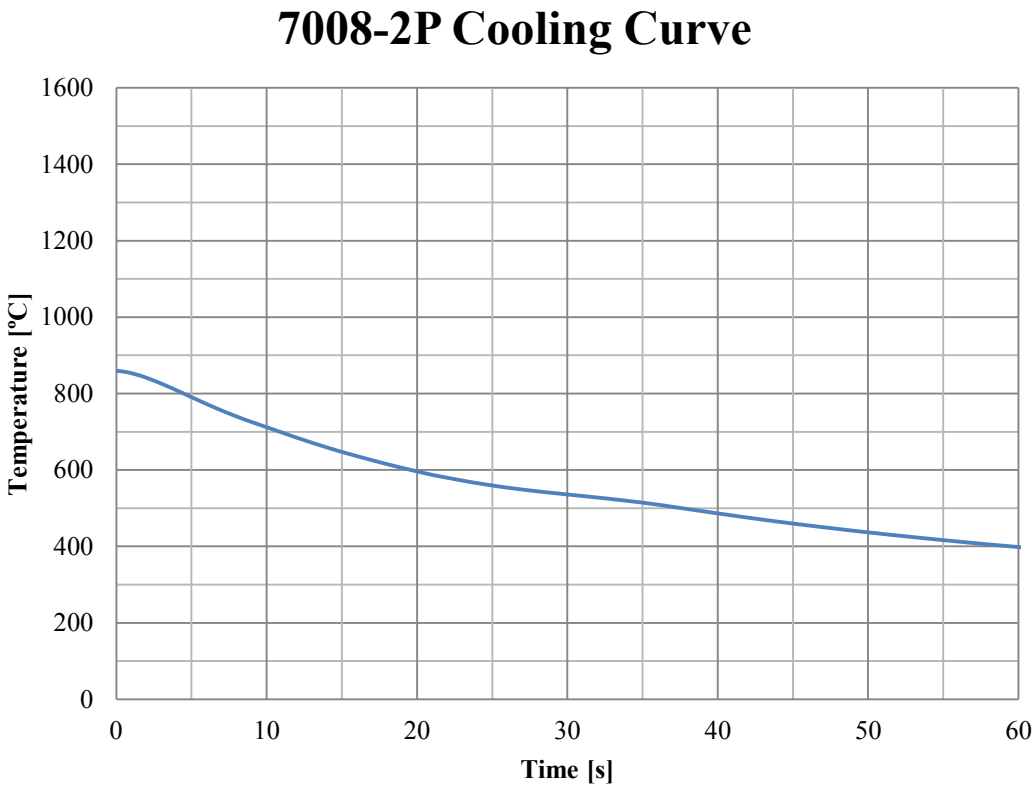

Figure 147. Cooling curve of PAW welded sample 7008-2P with $\Delta t_{8/5}$ of 33,2 s.

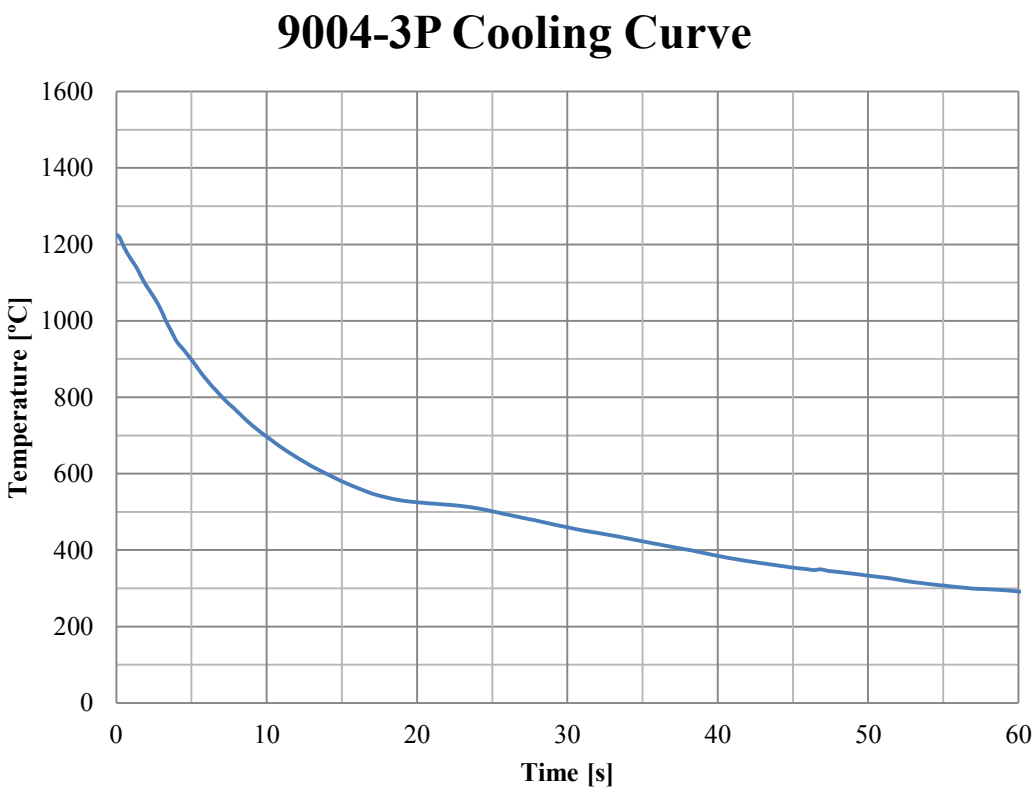

Figure 148. Cooling curve of PAW welded sample 9004-3P with Δt8/5 of 17,5 s.

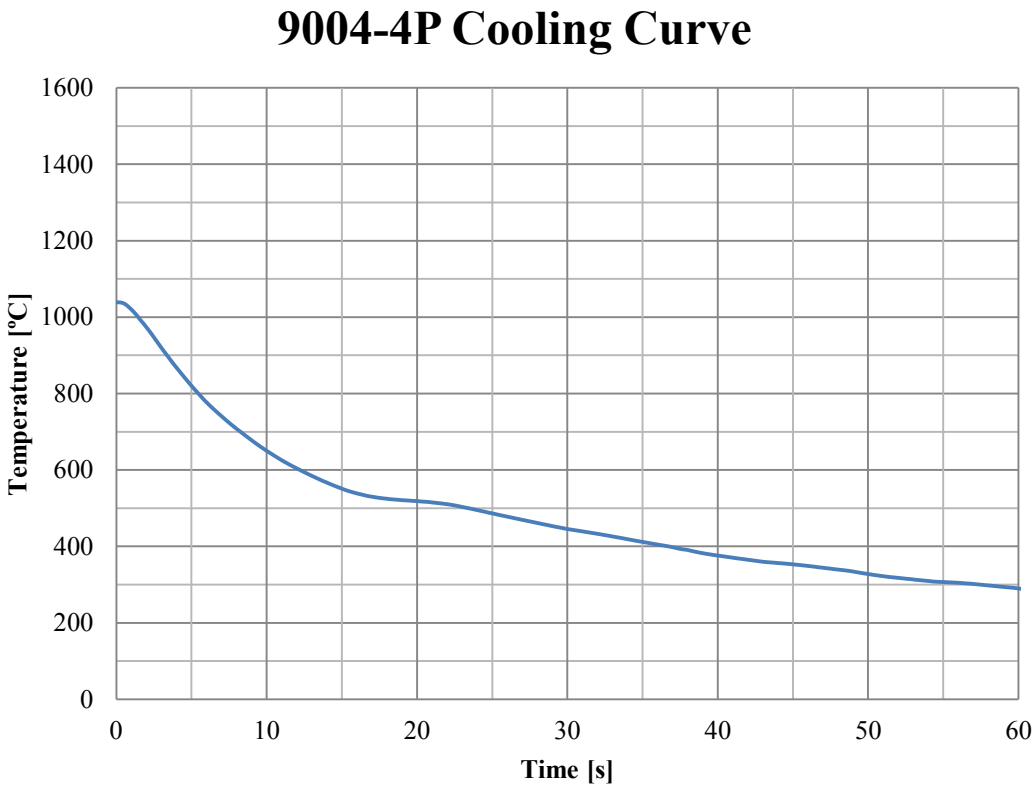

Figure 149. Cooling curve of PAW welded sample 9004-4P with $\Delta t_{8/5}$ of 18,0 s.

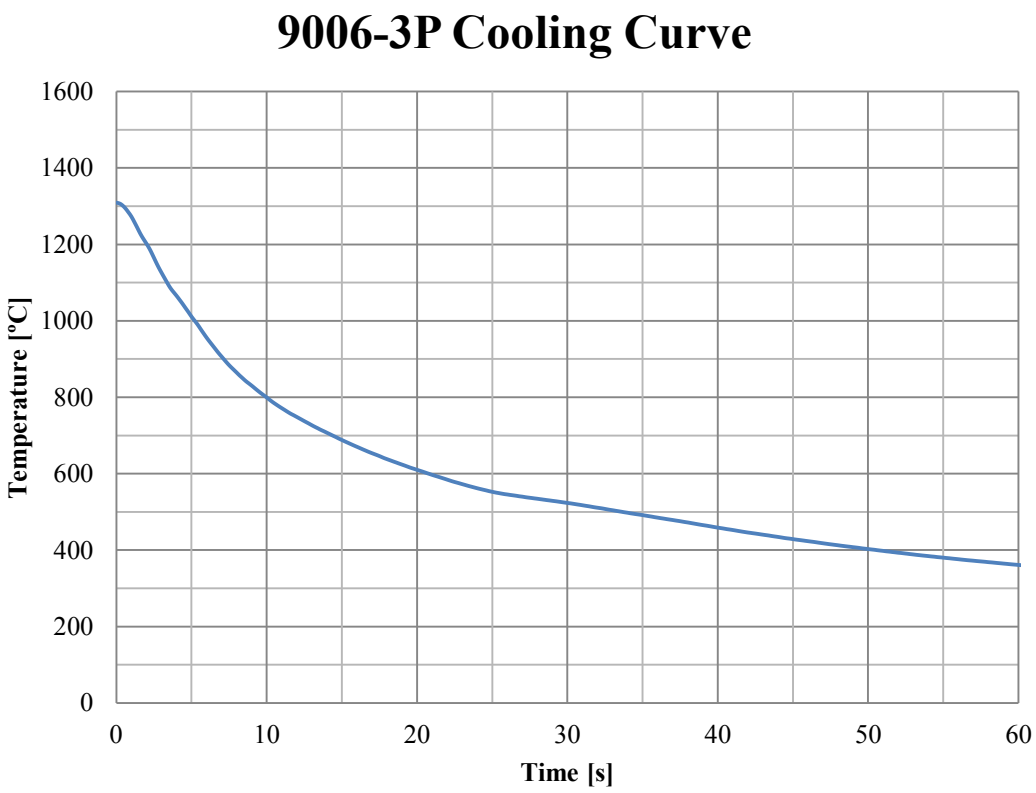

Figure 150. Cooling curve of PAW welded sample 9006-3P with $\Delta t_{8/5}$ of 24,8 s.

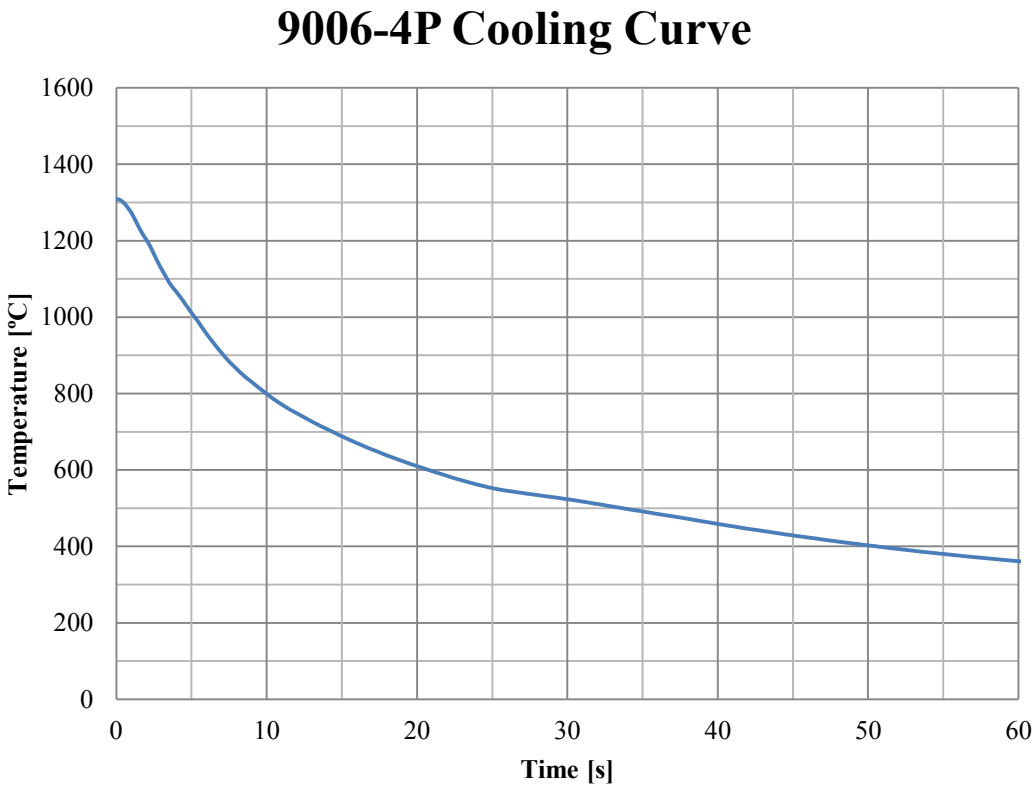

Figure 151. Cooling curve of PAW welded sample 9006-4P with $\Delta t_{8/5}$ of 24,0 s.

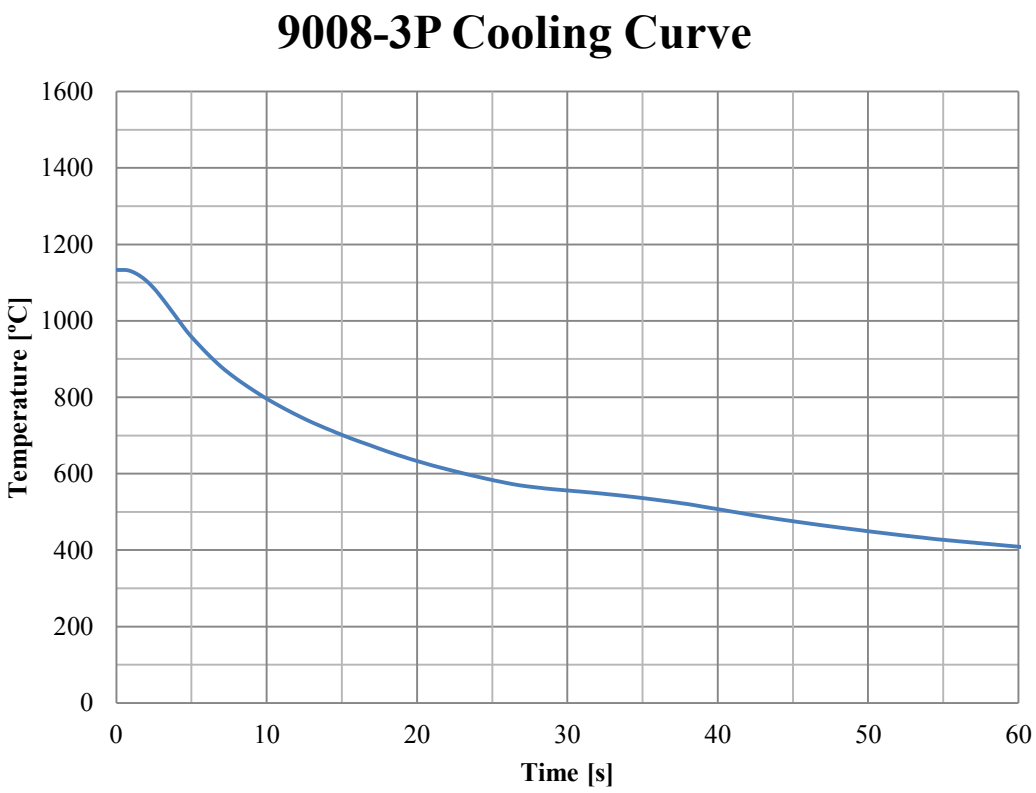

Figure 152. Cooling curve of PAW welded sample 9008-3P with $\Delta t_{8/5}$ of 31,8 s.

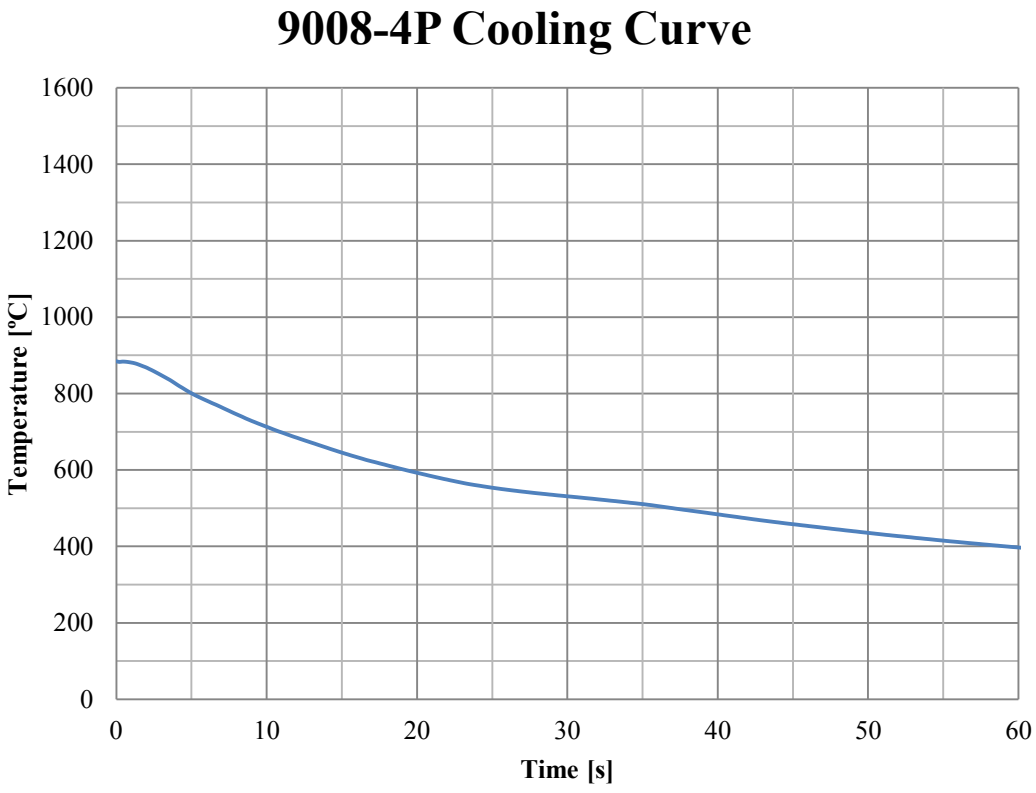

Figure 153. Cooling curve of PAW welded sample 9008-4P with $\Delta t_{8/5}$ of 33,2 s.

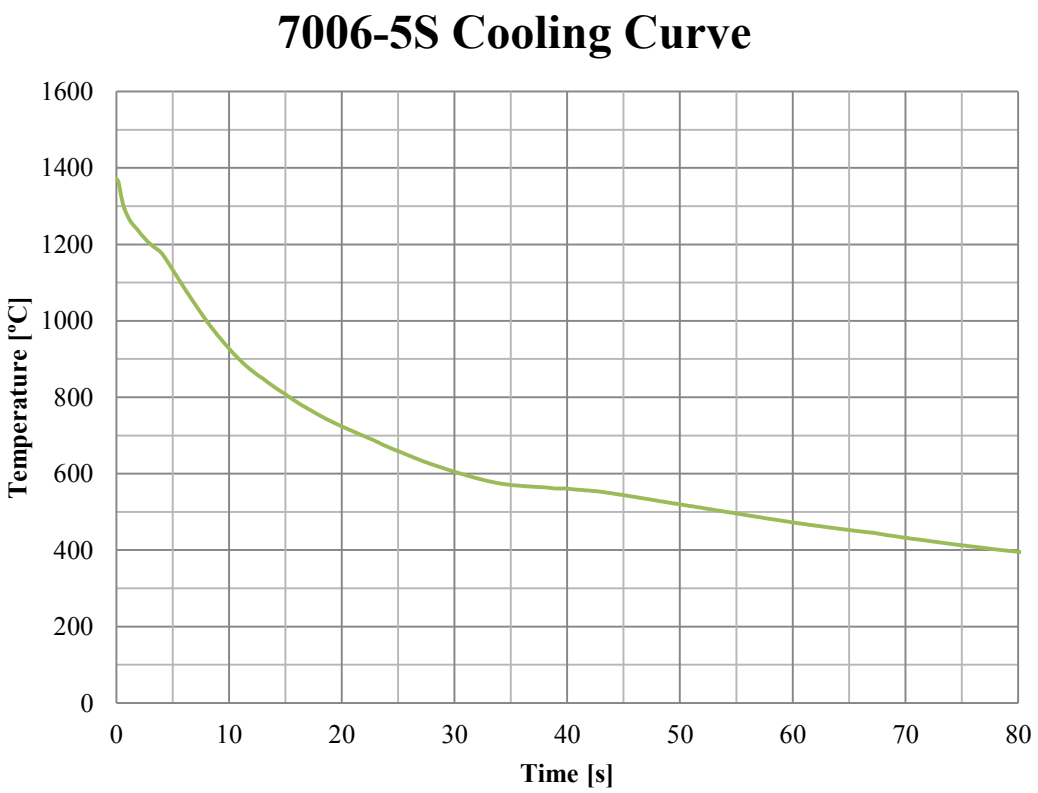

Figure 154. Cooling curve of SAW welded sample 7006-5S with $\Delta t_{8/5}$ of 38,8 s.

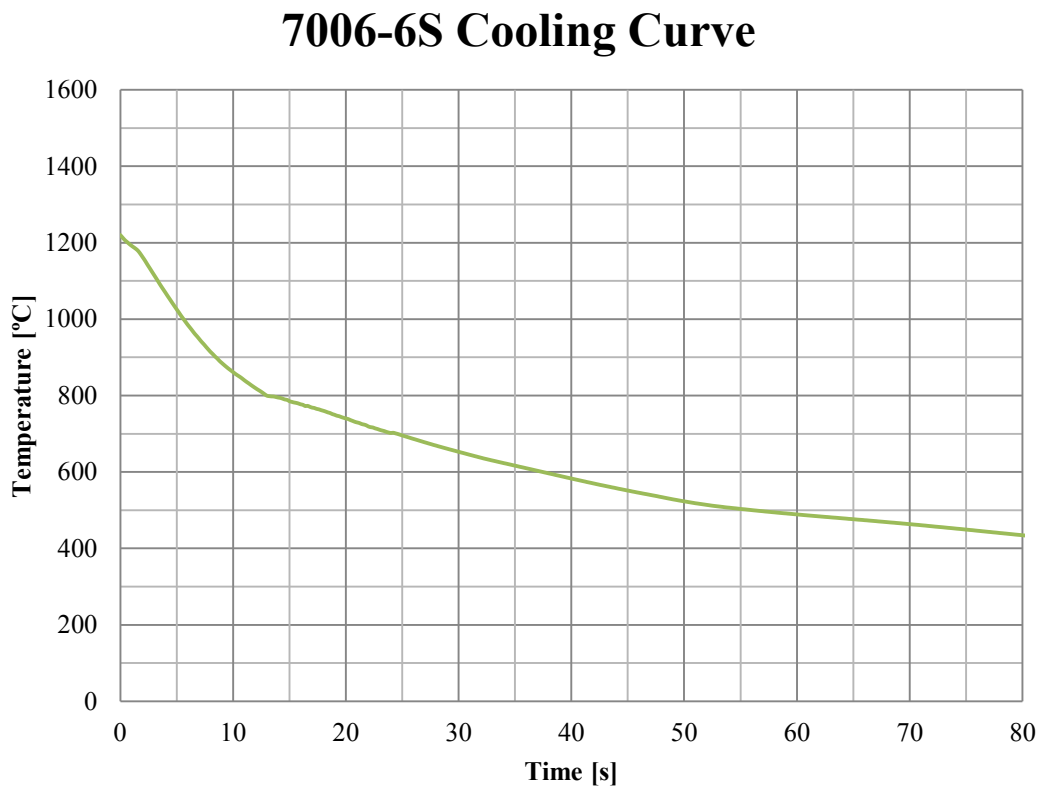

Figure 155. Cooling curve of SAW welded sample 7006-6S with $\Delta t_{8/5}$ of 43,6 s.

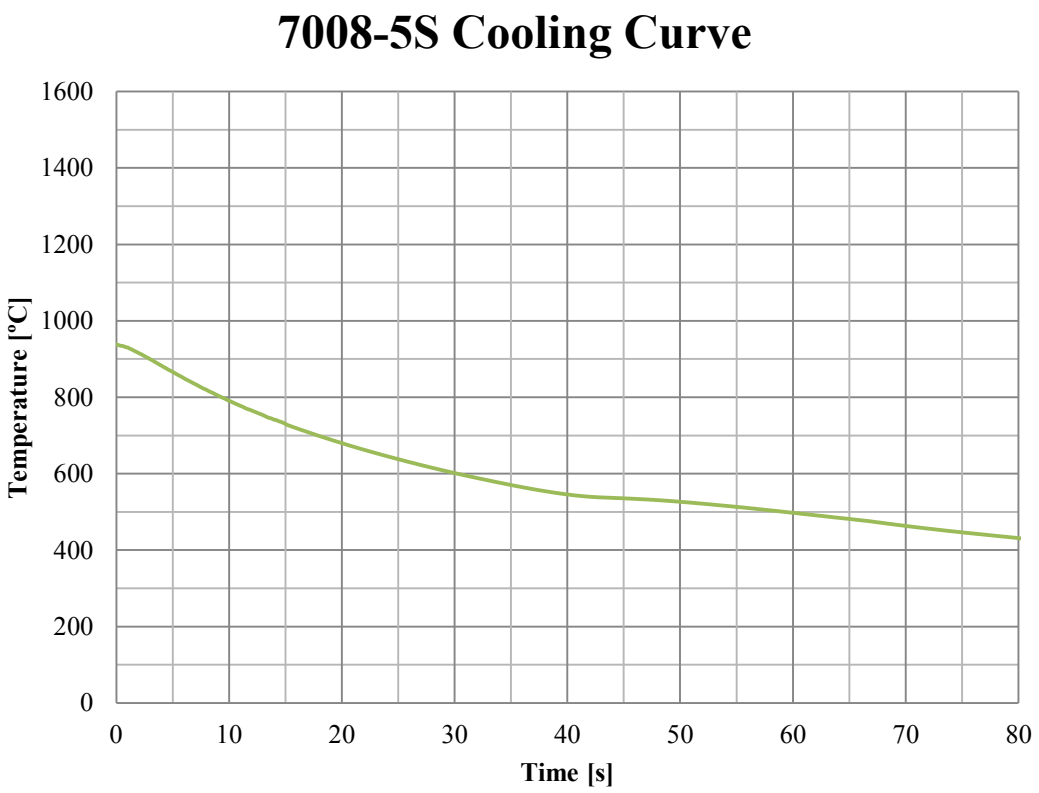

Figure 156. Cooling curve of SAW welded sample 7008-5S with $\Delta t_{8/5}$ of 49,7 s.

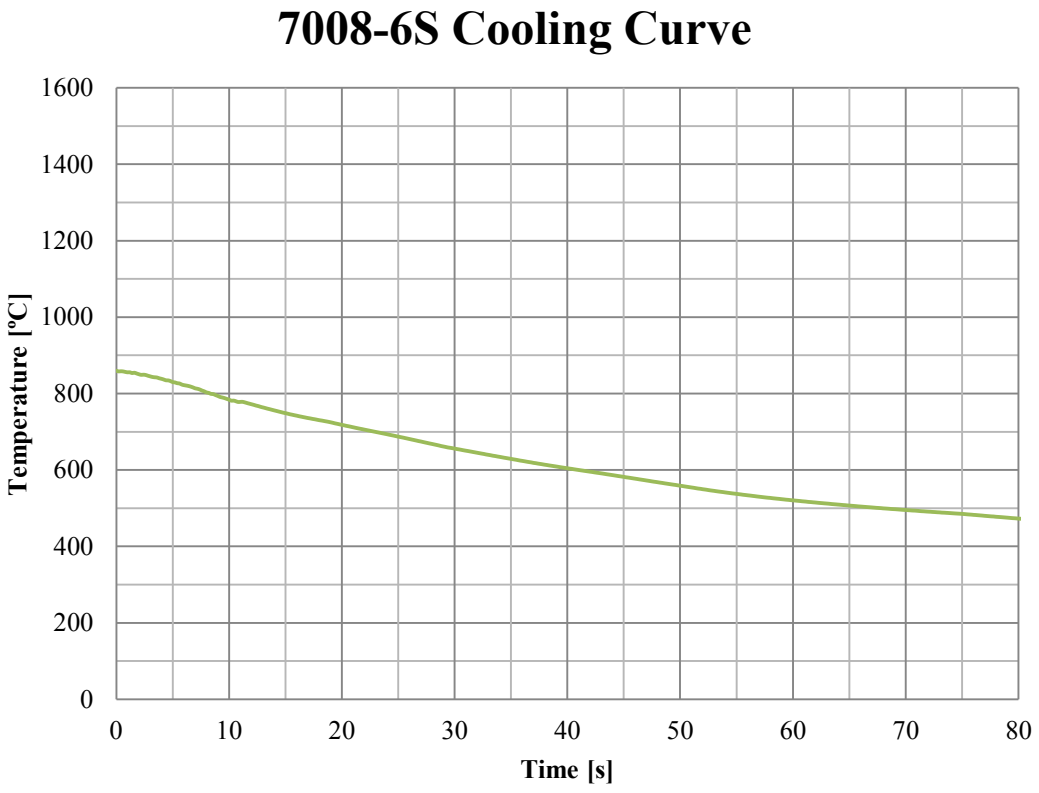

Figure 157. Cooling curve of SAW welded sample 7008-6S with $\Delta t_{8/5}$ of 62,0 s.

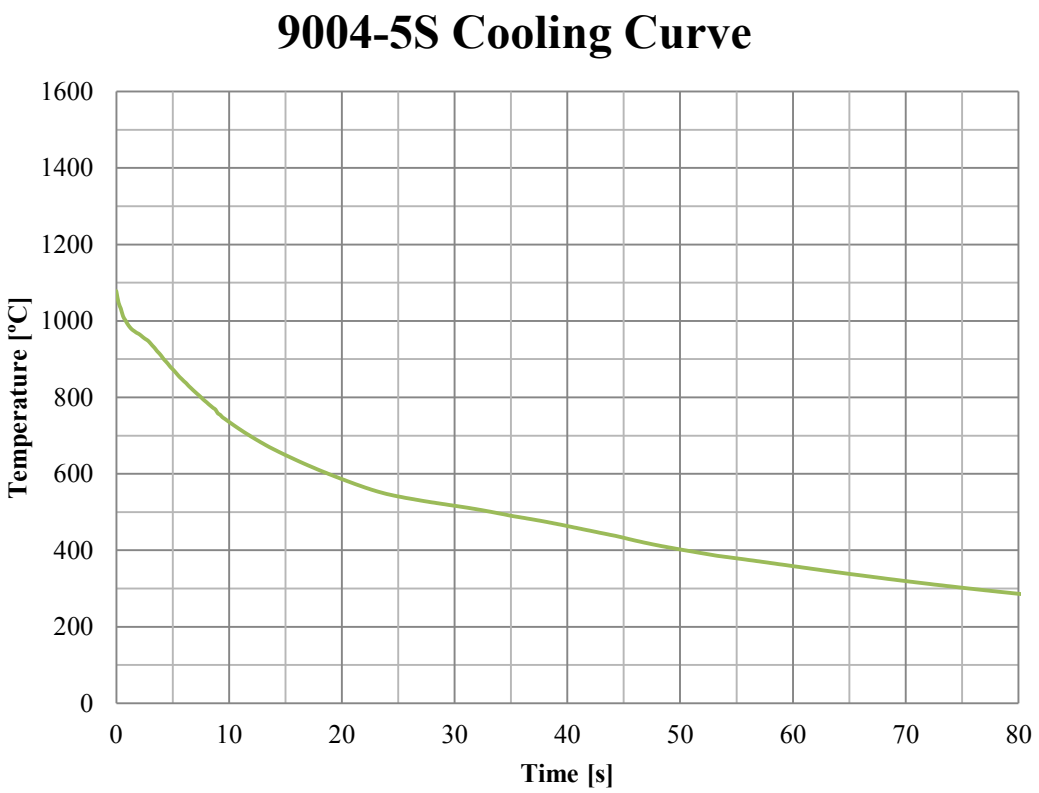

Figure 158. Cooling curve of SAW welded sample 9004-5S with $\Delta t_{8/5}$ of 25,7 s.

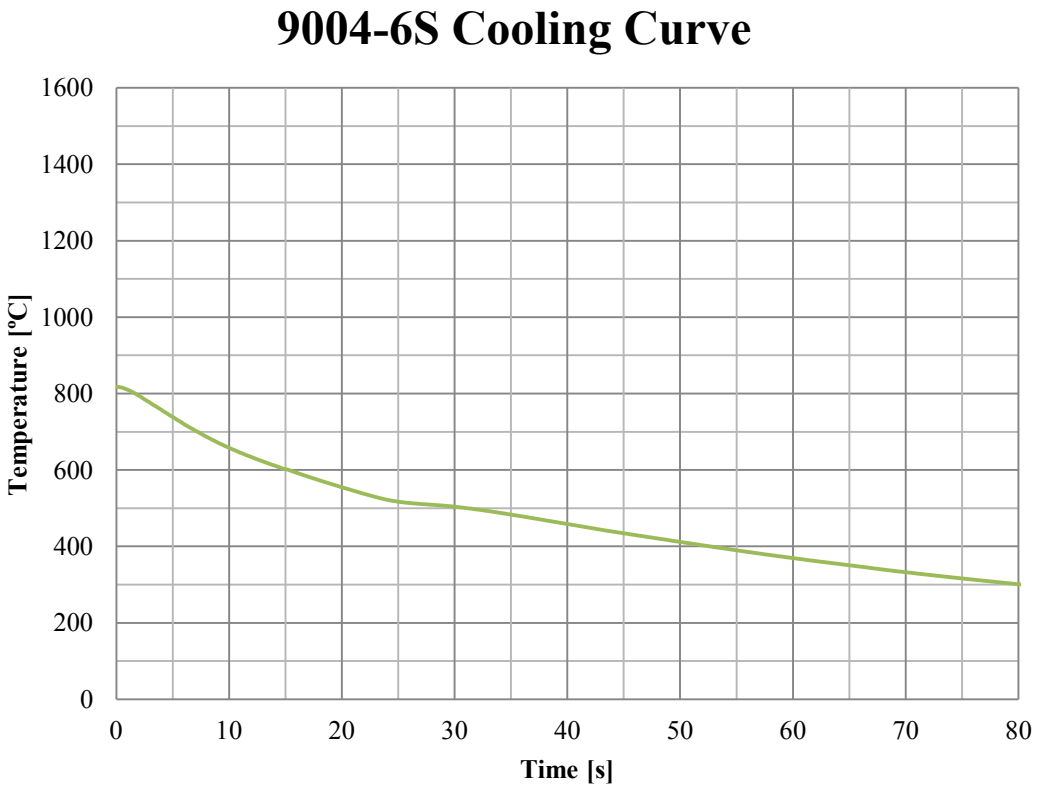

Figure 159. Cooling curve of SAW welded sample 9004-6S with $\Delta t_{8/5}$ of 29,4 s.

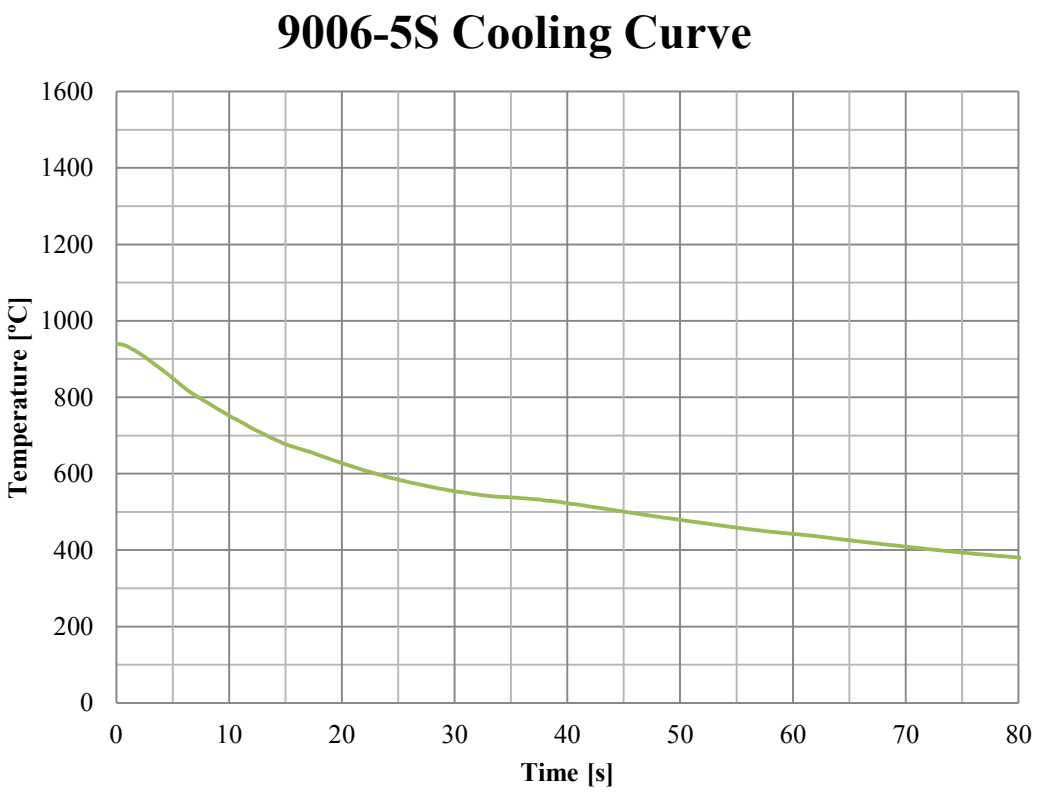

Figure 160. Cooling curve of SAW welded sample 9006-5S with $\Delta t_{8/5}$ of 39,0 s.

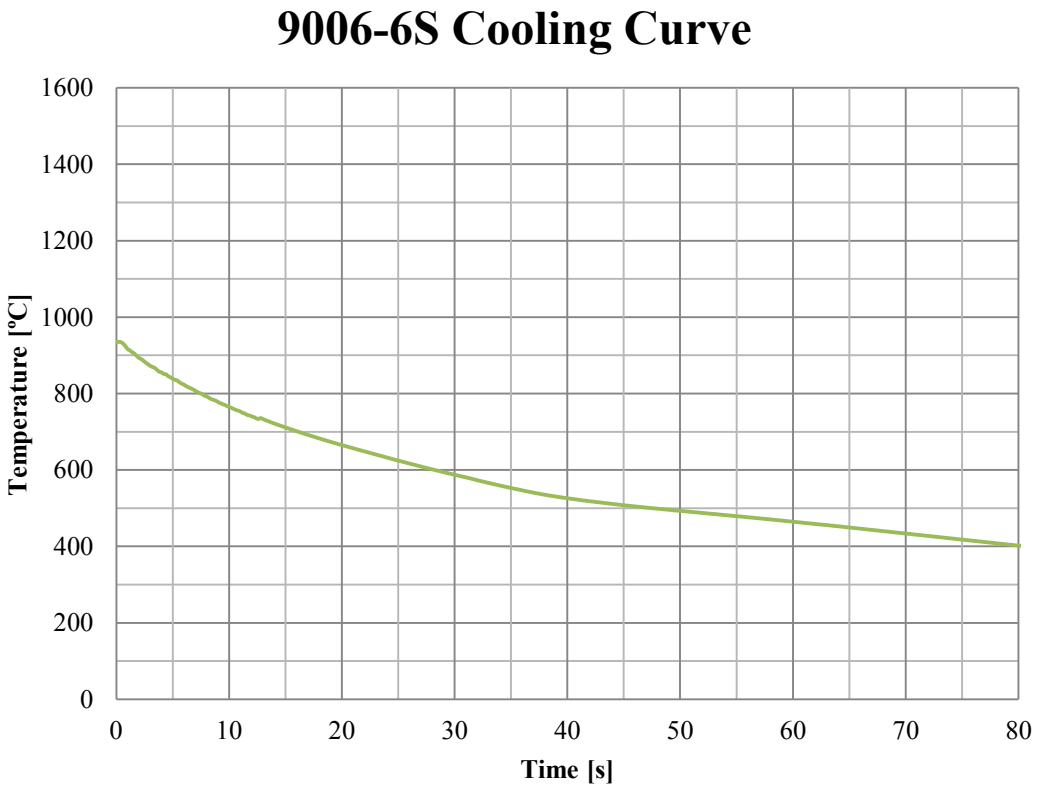

Figure 161. Cooling curve of SAW welded sample 9006-6S with $\Delta t_{8/5}$ of 42,2 s.

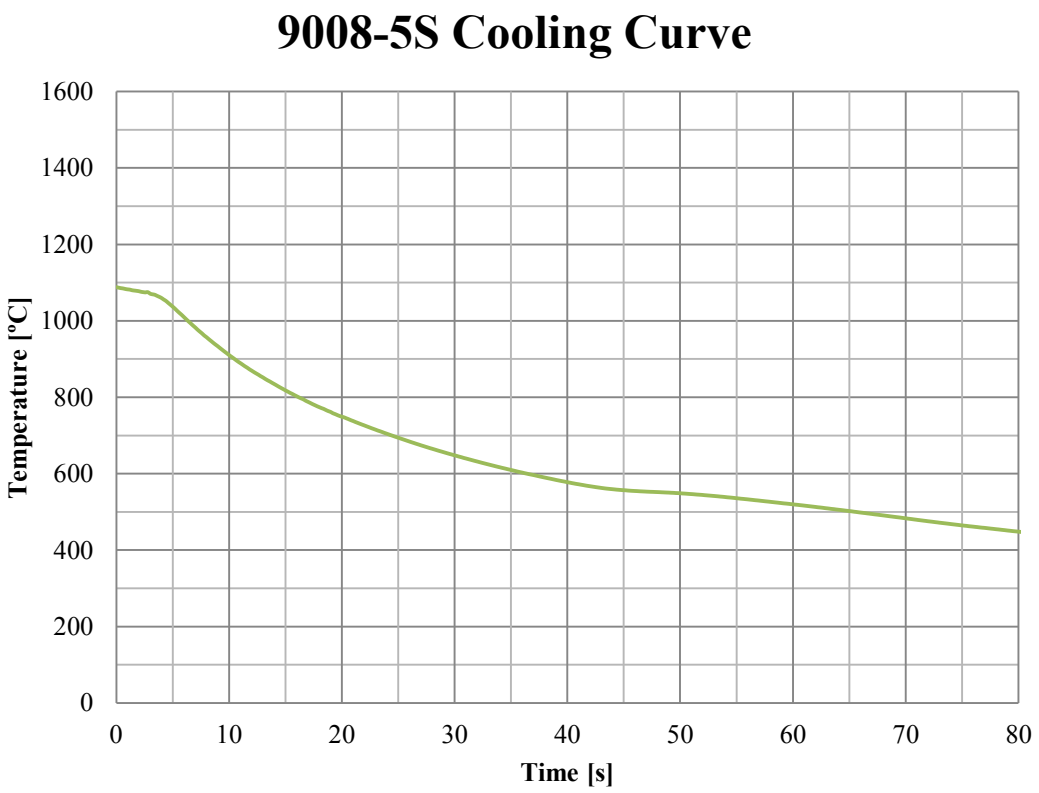

Figure 162. Cooling curve of SAW welded sample 9008-5S with $\Delta t_{8/5}$ of 49,4 s.

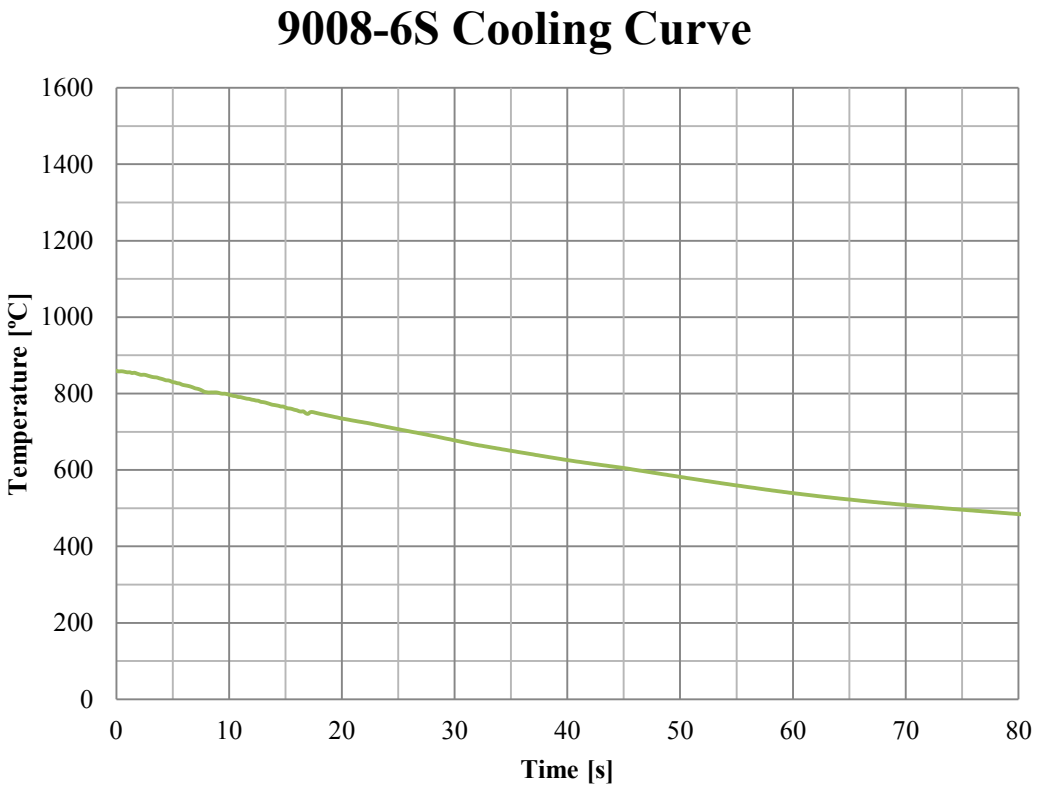

Figure 163. Cooling curve of SAW welded sample 9008-6S with $\Delta t_{8/5}$ of 62,9 s.

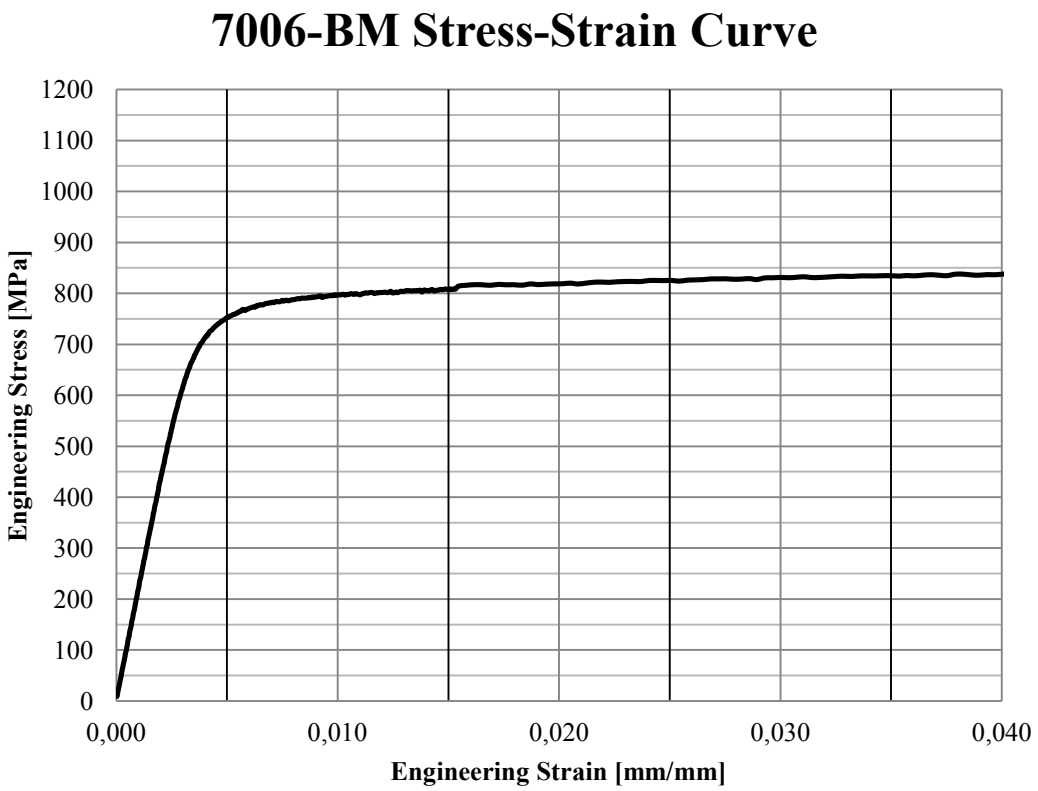

Figure 164. Stress-strain curve of 6 mm Optim 700 MC Plus steel plate.

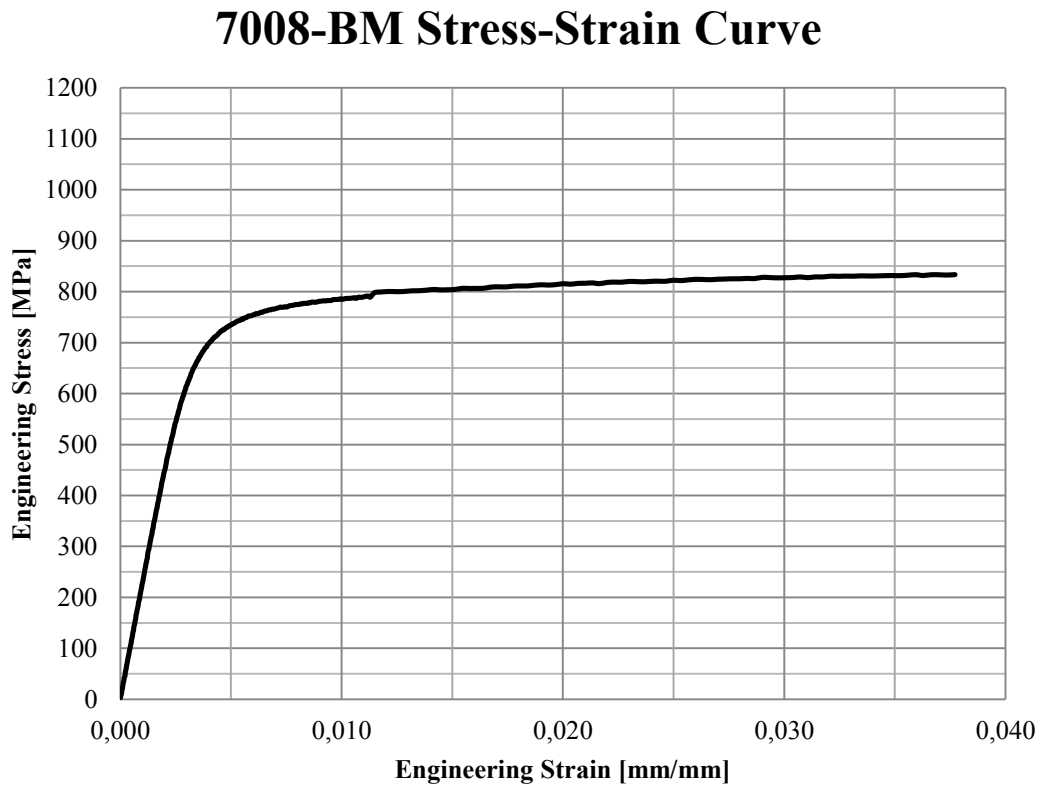

Figure 165. Stress-strain curve of 8 mm Optim 700 MC Plus steel plate.

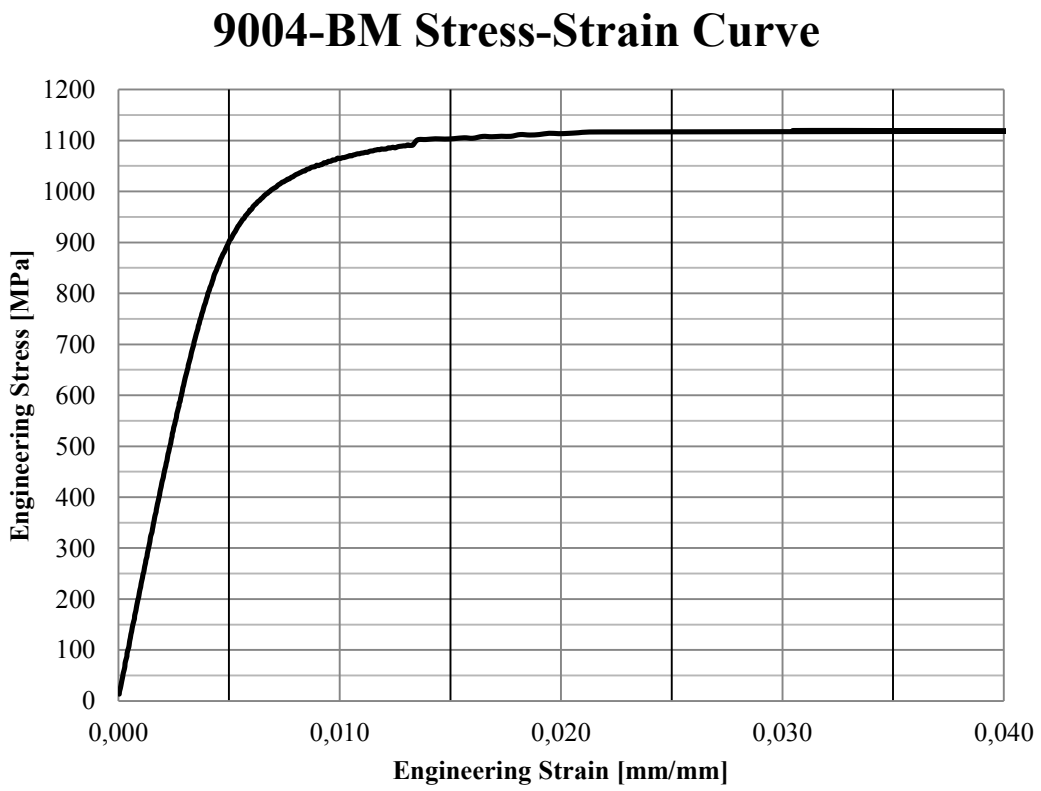

Figure 166. Stress-strain curve of 4 mm Optim 900 QC steel plate.

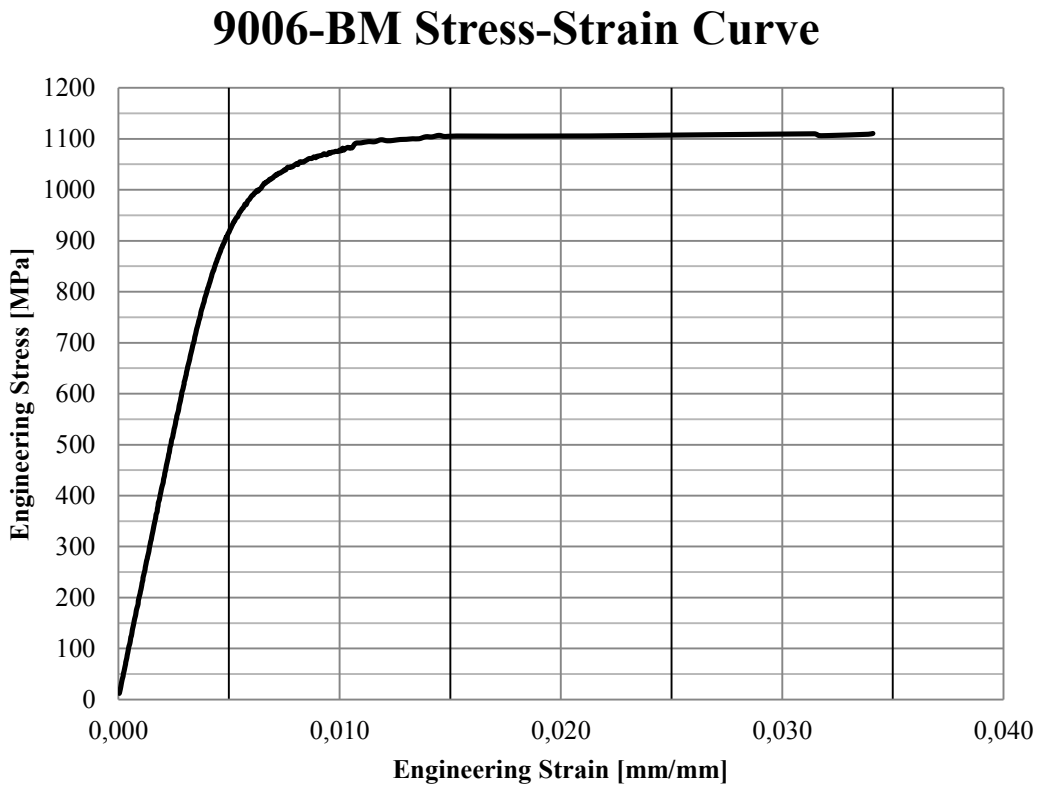

Figure 167. Stress-strain curve of 6 mm Optim 900 QC steel plate.

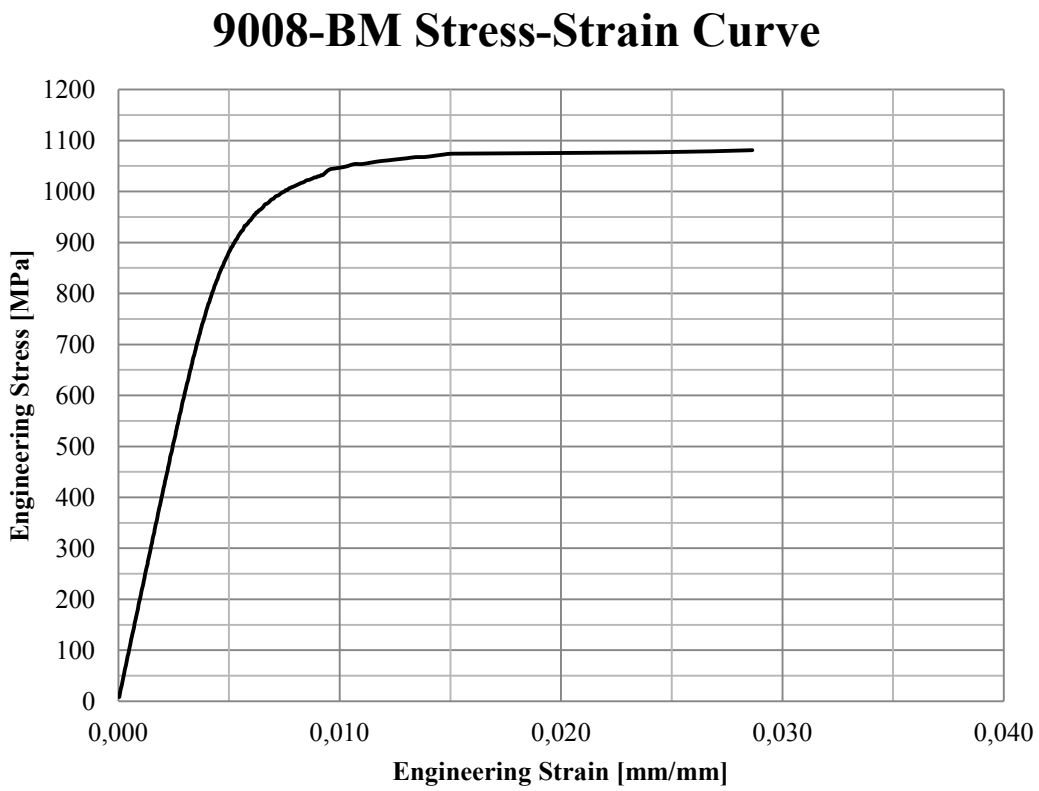

Figure 168. Stress-strain curve of 8 mm Optim 900 QC steel plate.

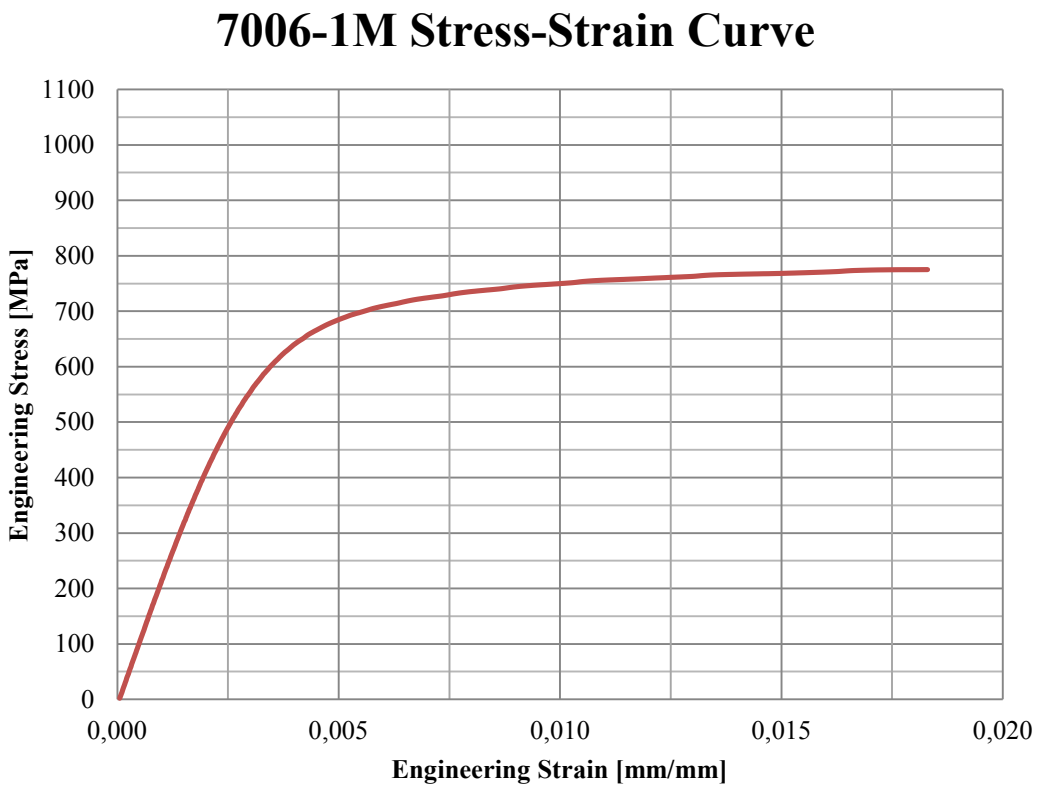

Figure 169. Stress-strain curve of MAG welded sample 7006-1M.

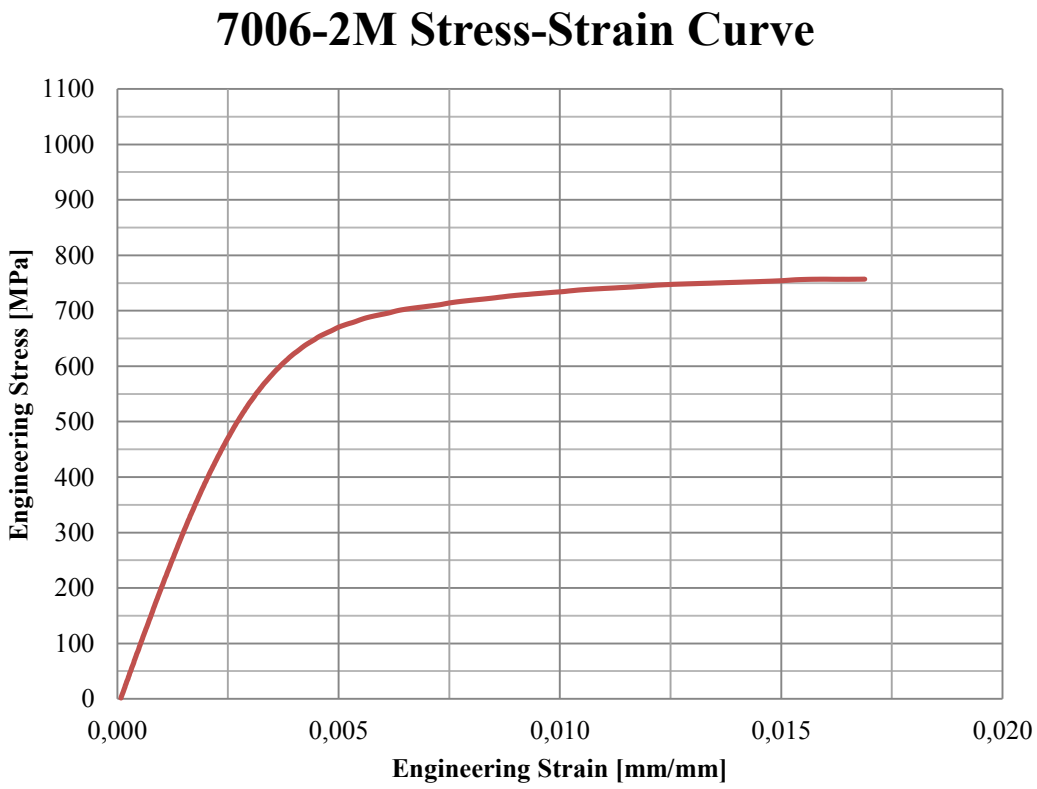

Figure 170. Stress-strain curve of MAG welded sample 7006-2M.

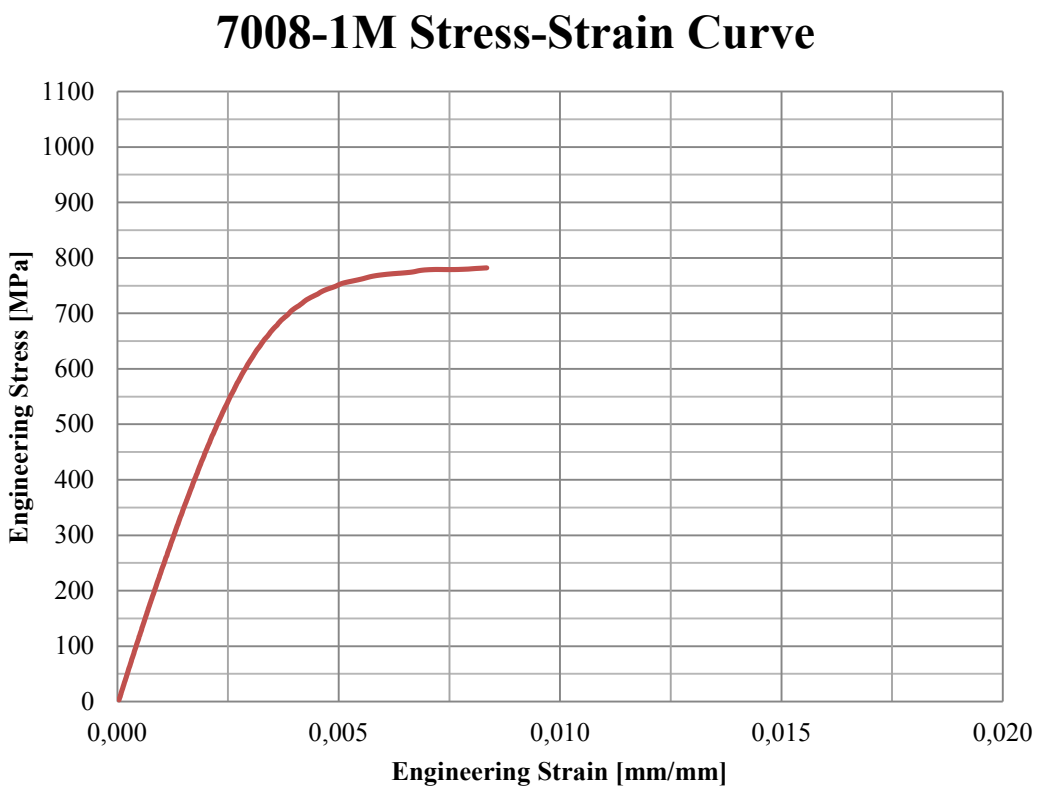

Figure 171. Stress-strain curve of MAG welded sample 7008-1M.

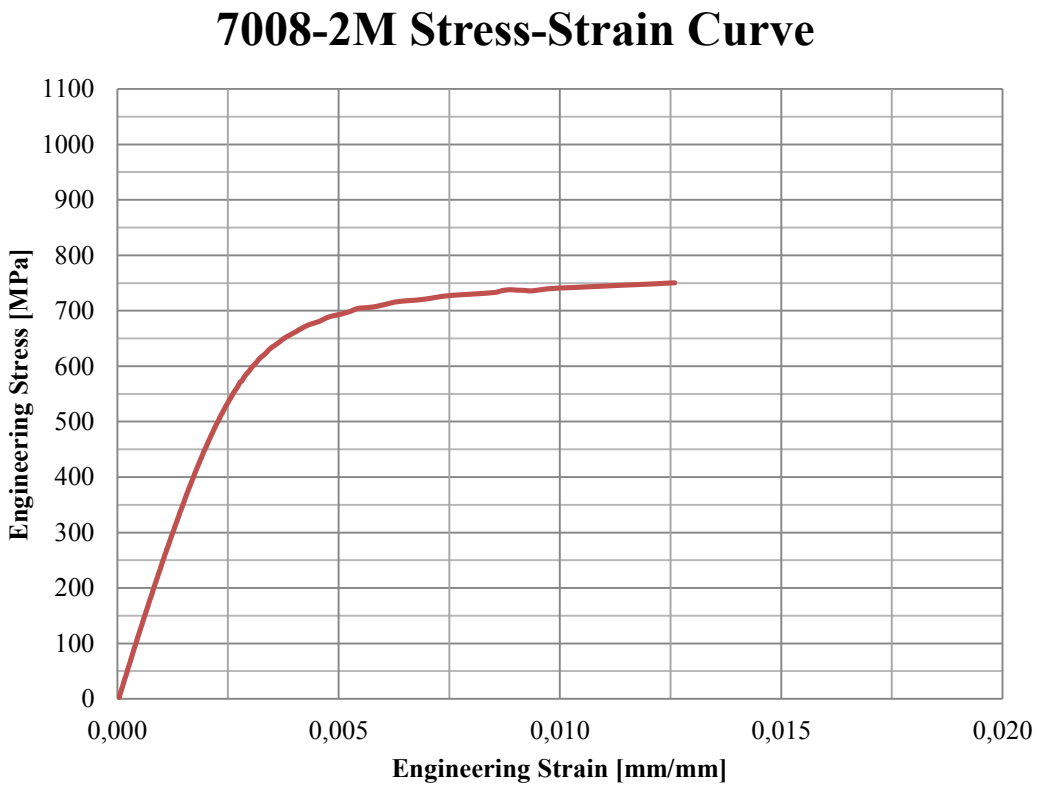

Figure 172. Stress-strain curve of MAG welded sample 7008-2M.

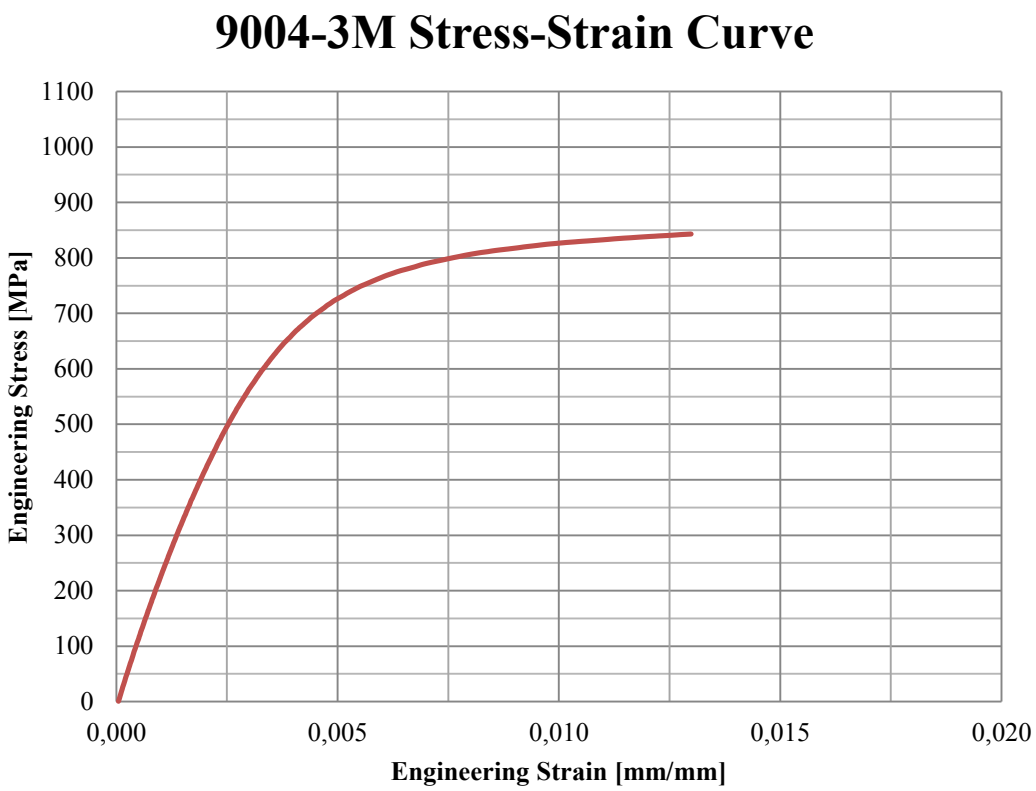

Figure 173. Stress-strain curve of MAG welded sample 9004-3M.

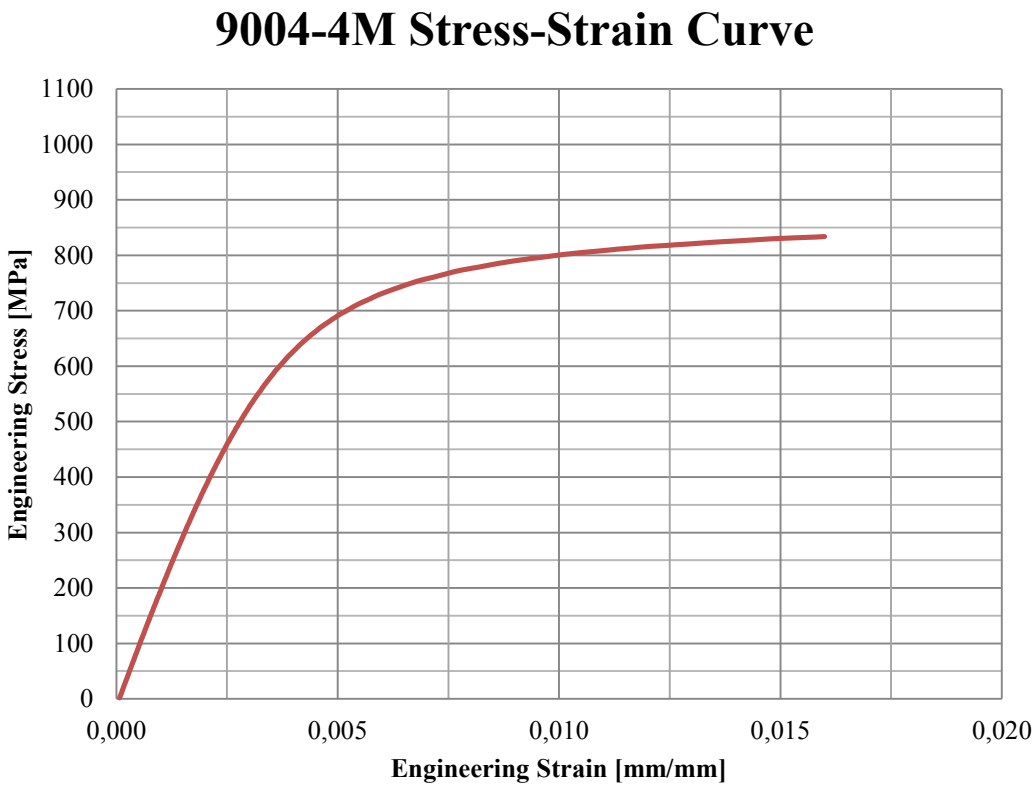

Figure 174. Stress-strain curve of MAG welded sample 9004-4M.

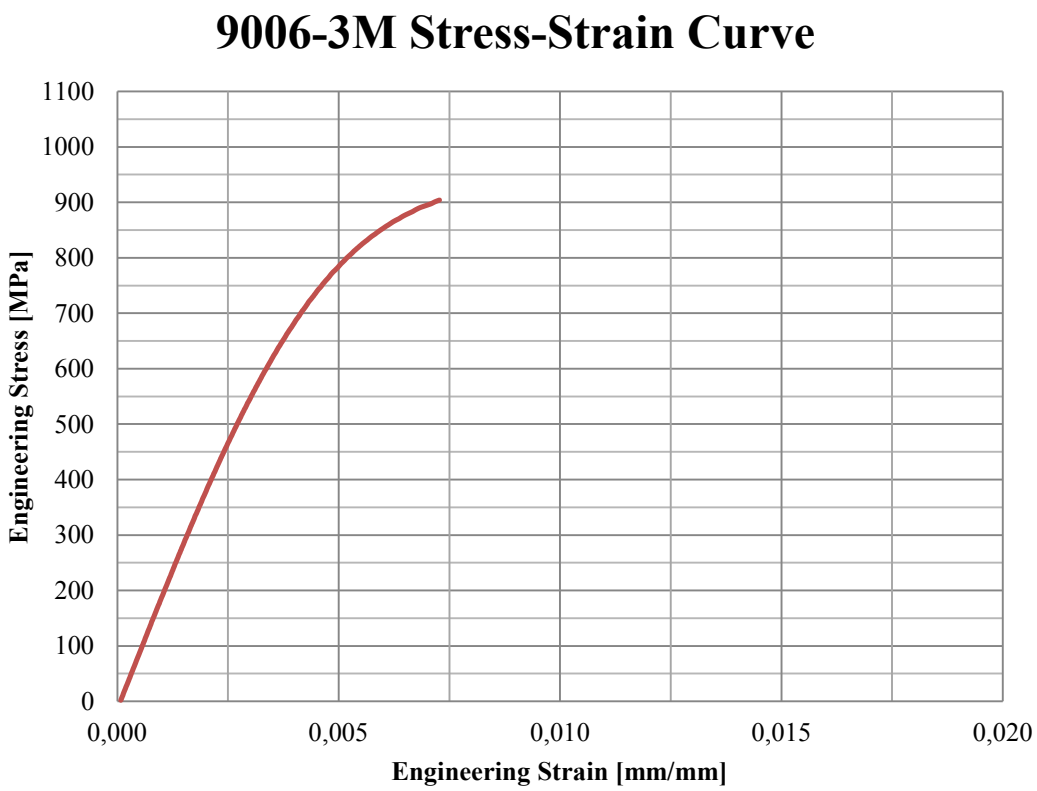

Figure 175. Stress-strain curve of MAG welded sample 9006-3M.

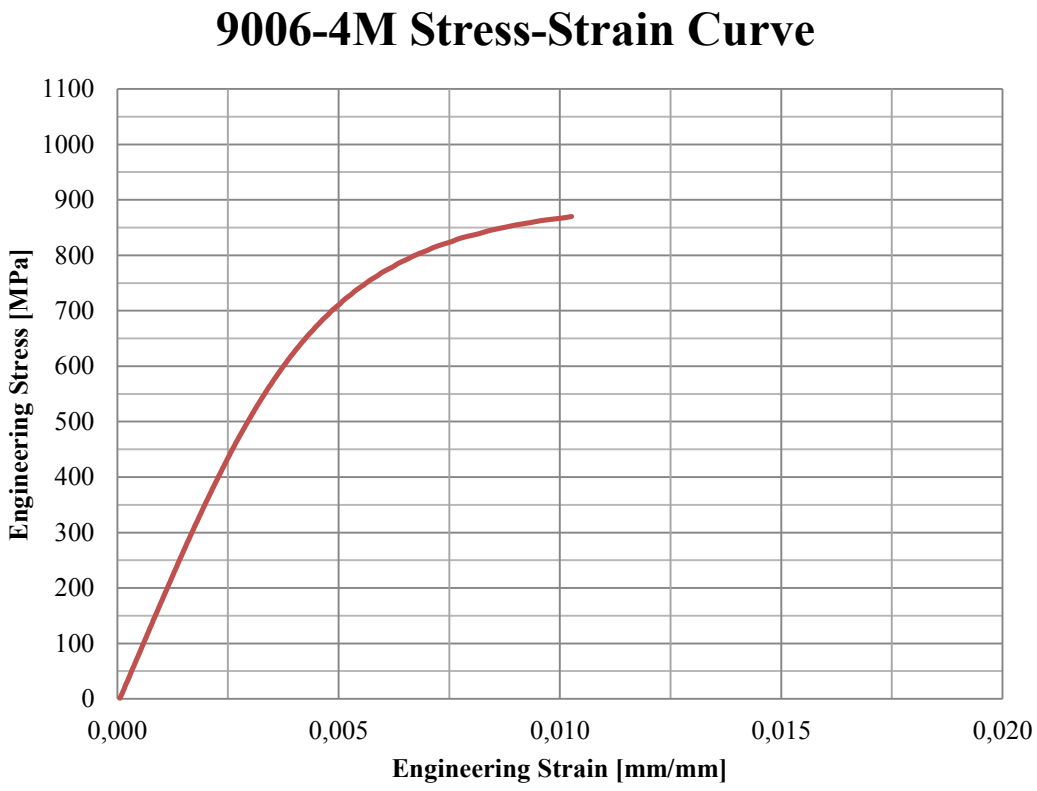

Figure 176. Stress-strain curve of MAG welded sample 9006-4M.

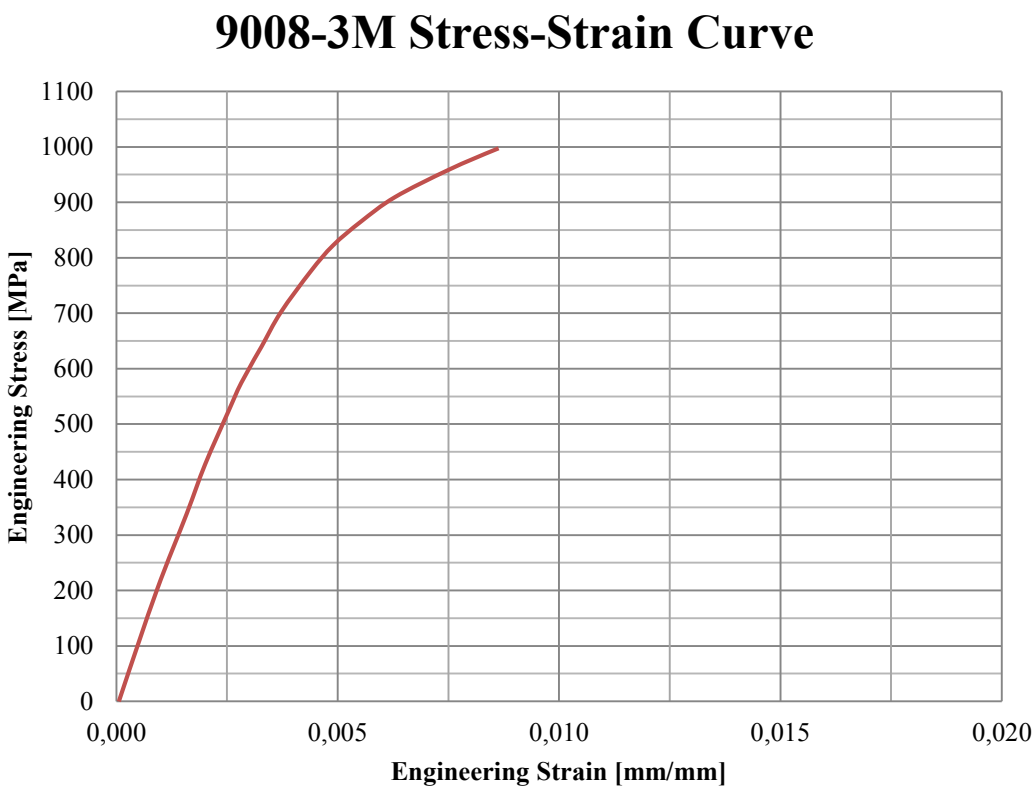

Figure 177. Stress-strain curve of MAG welded sample 9008-3M.

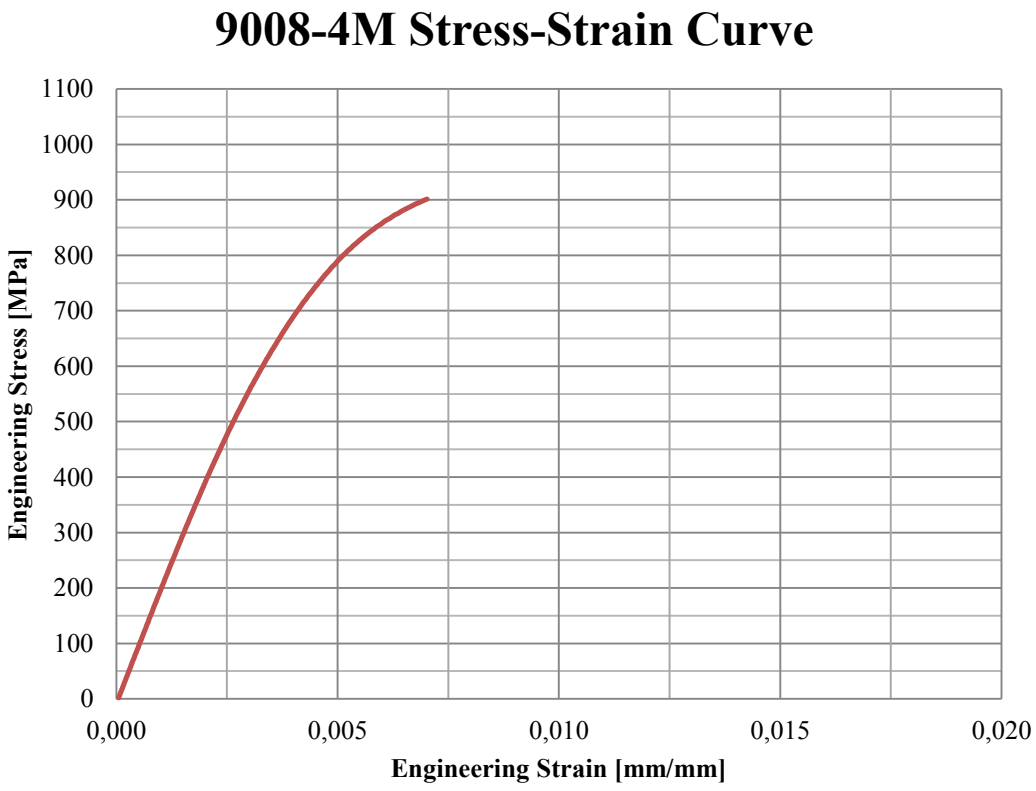

Figure 178. Stress-strain curve of MAG welded sample 9008-4M.

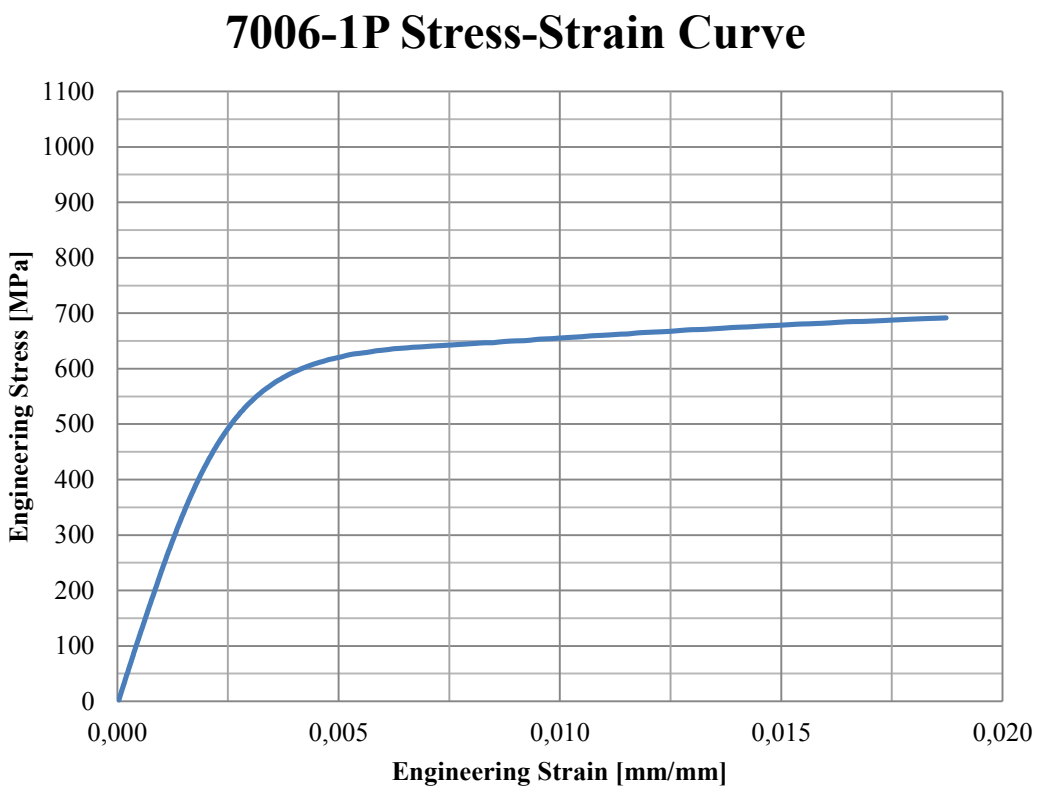

Figure 179. Stress-strain curve of PAW welded sample 7006-1P.

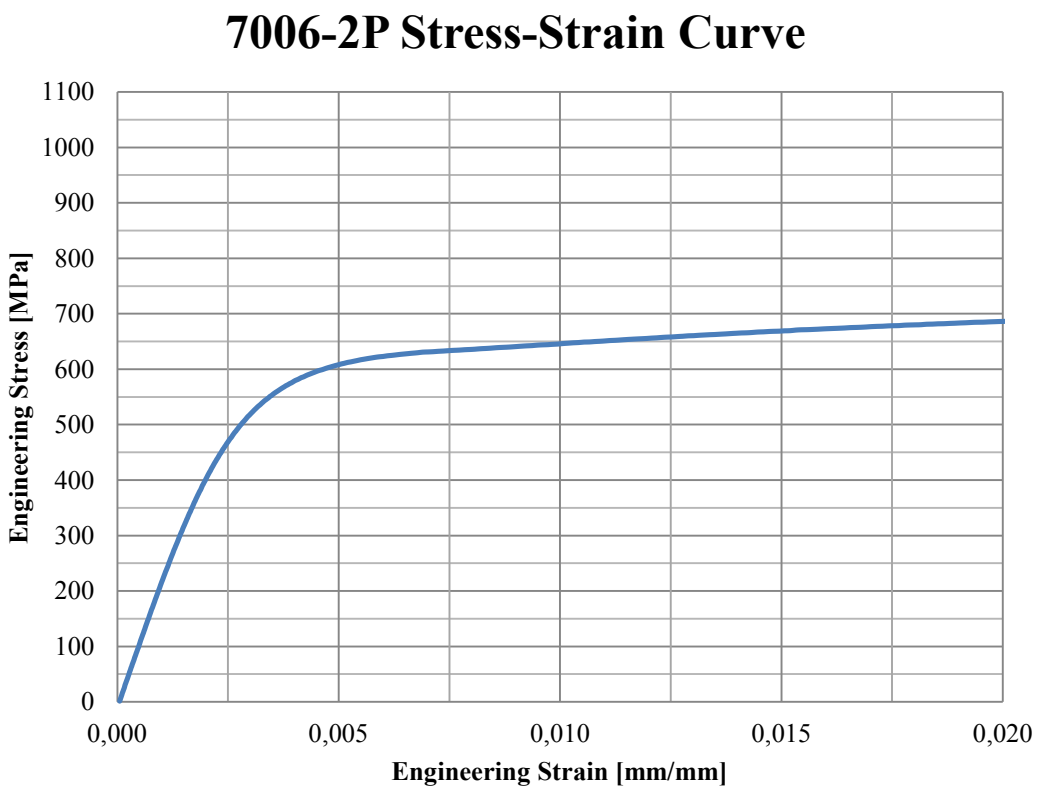

Figure 180. Stress-strain curve of PAW welded sample 7006-2P.

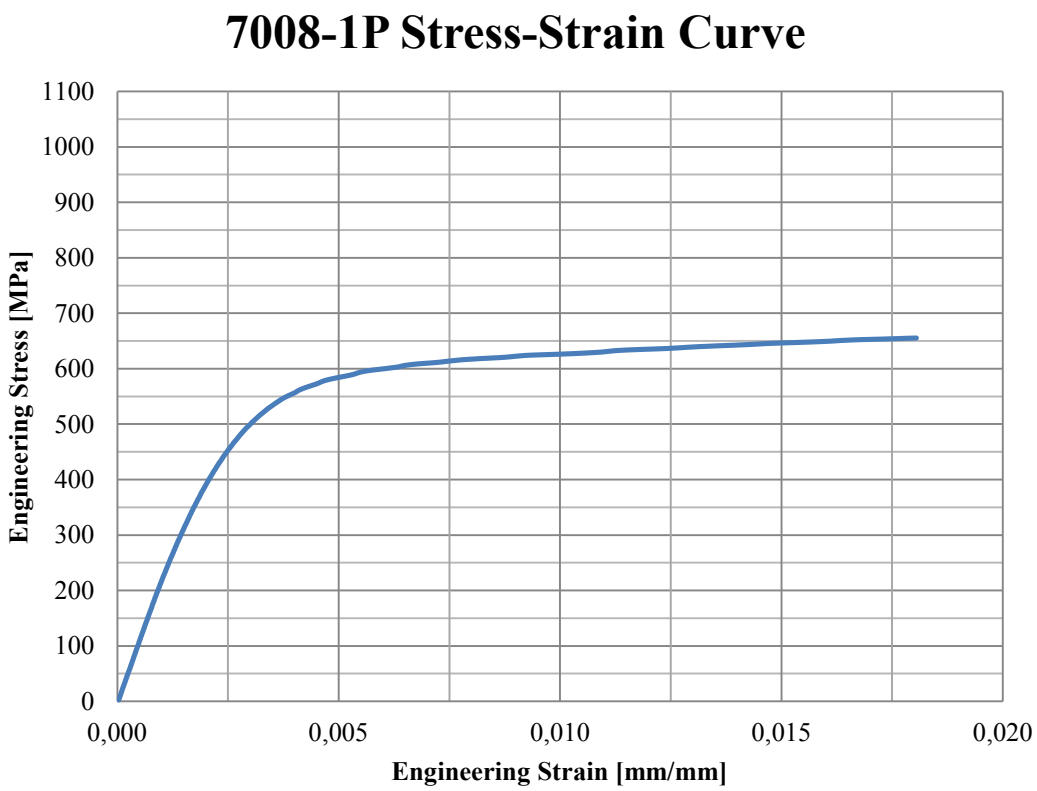

Figure 181. Stress-strain curve of PAW welded sample 7008-1P.

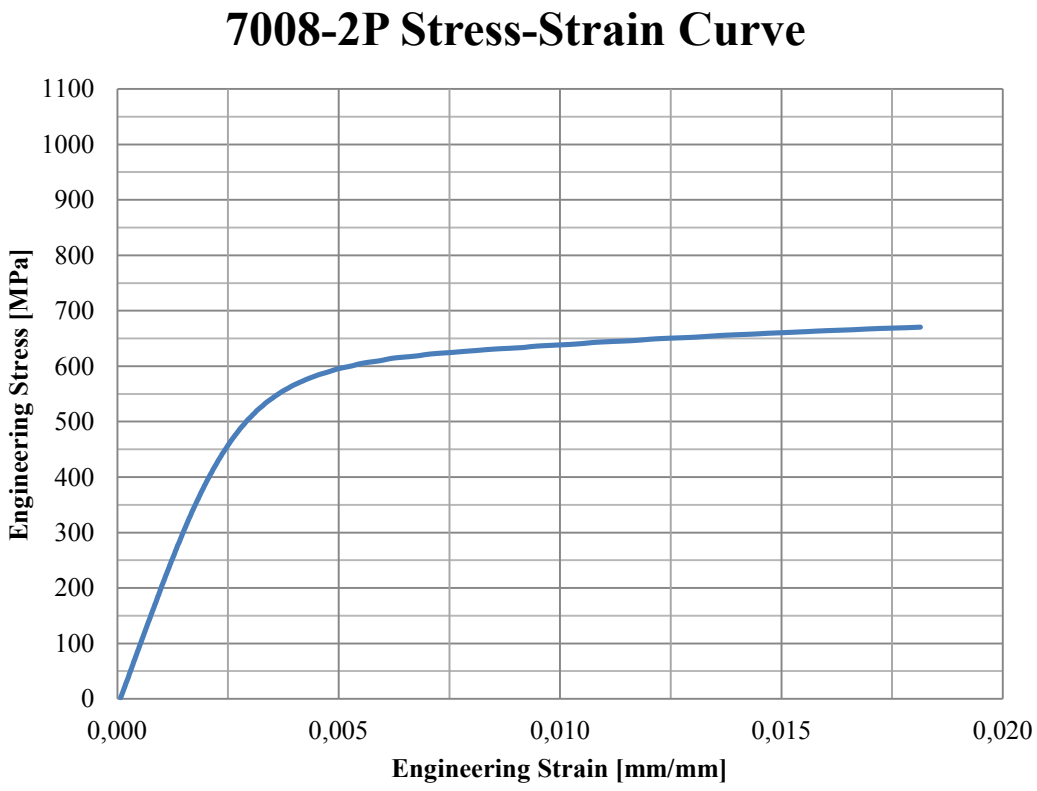

Figure 182. Stress-strain curve of PAW welded sample 7008-2P.

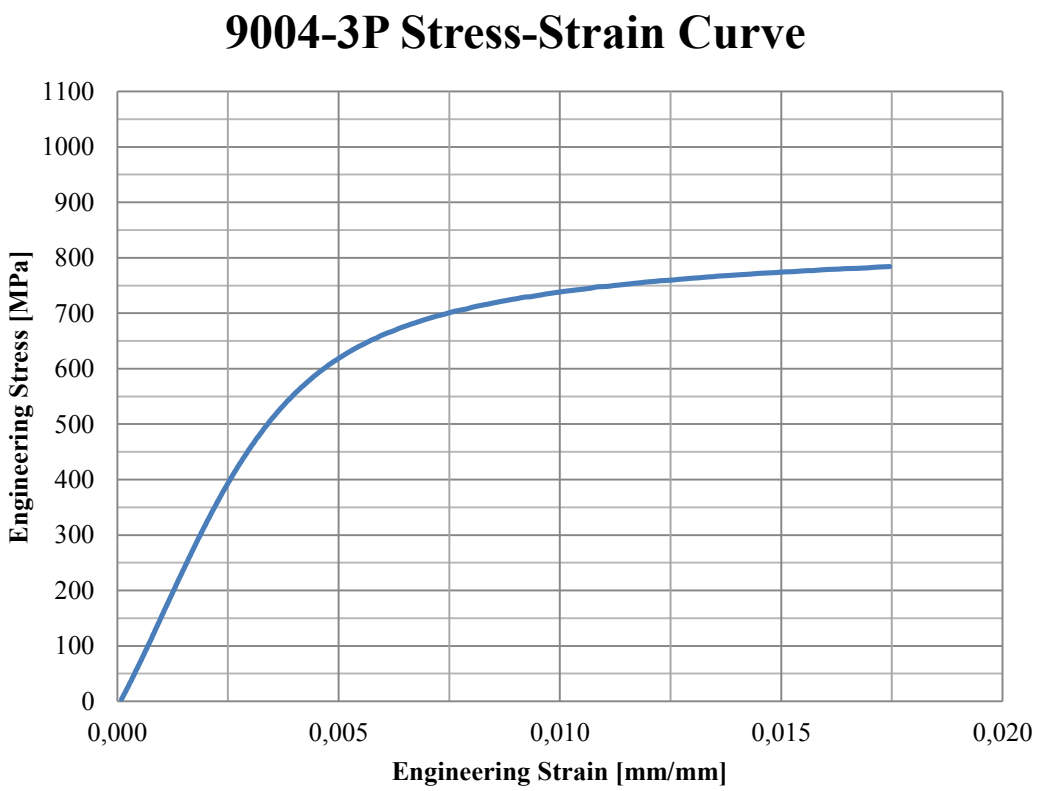

Figure 183. Stress-strain curve of PAW welded sample 9004-3P.

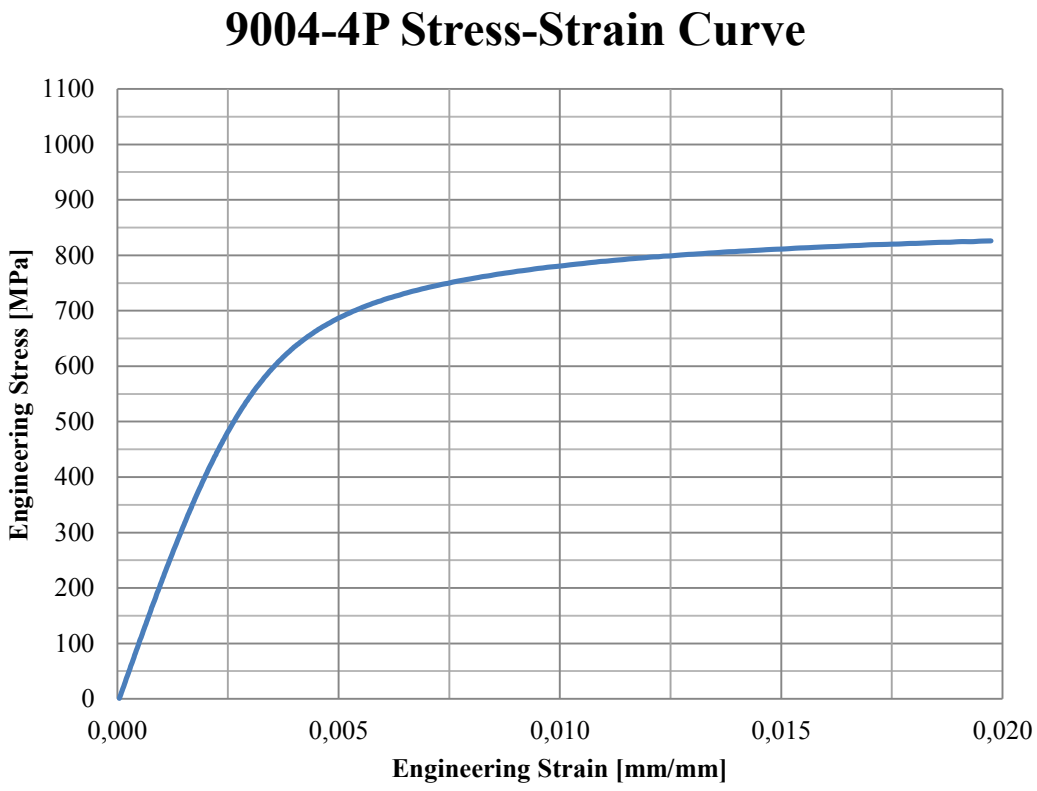

Figure 184. Stress-strain curve of PAW welded sample 9004-4P.

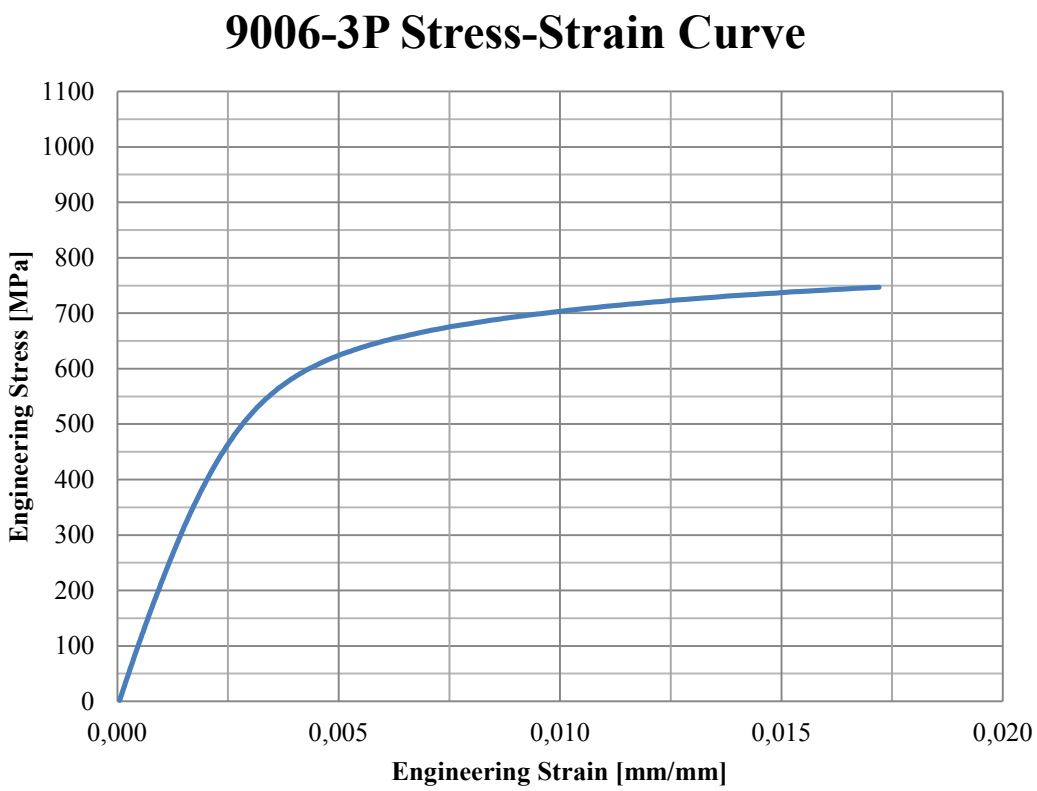

Figure 185. Stress-strain curve of PAW welded sample 9006-3P.

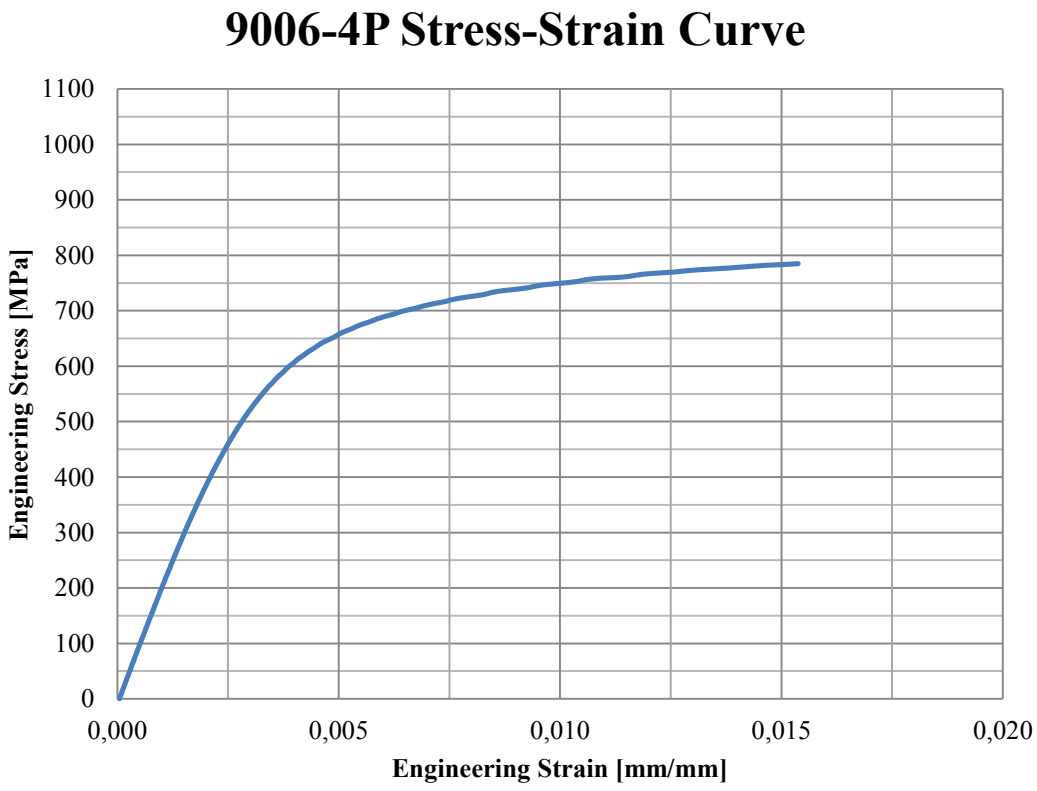

Figure 186. Stress-strain curve of PAW welded sample 9006-4P.

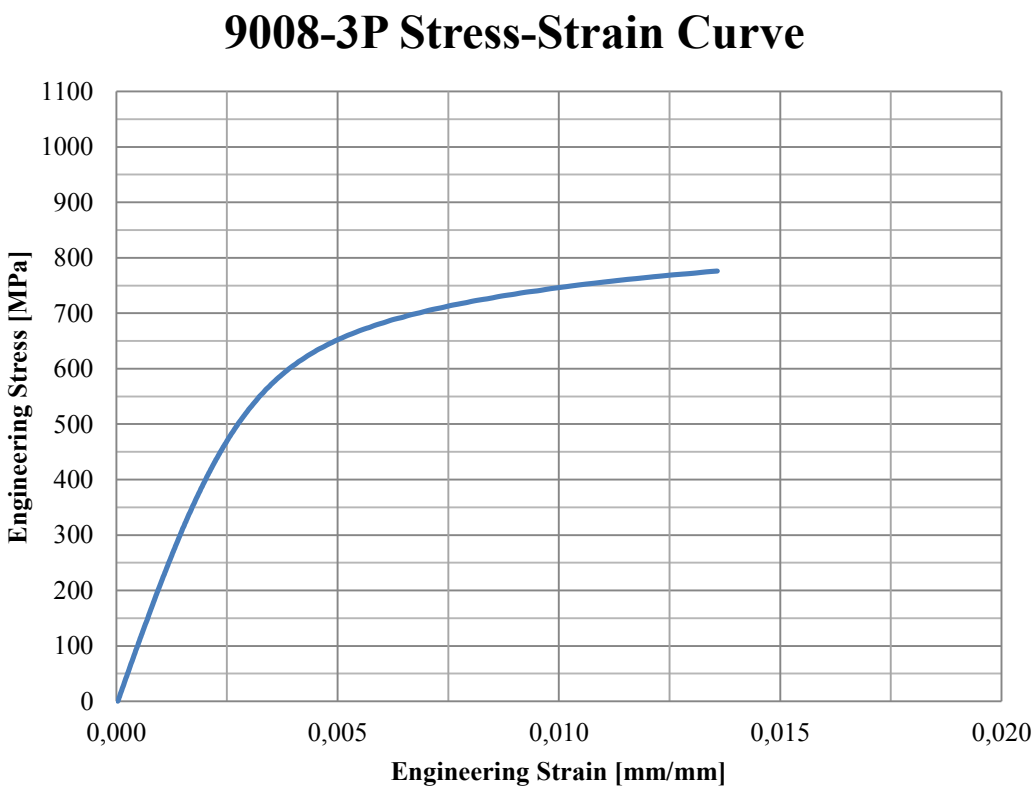

Figure 187. Stress-strain curve of PAW welded sample 9008-3P.

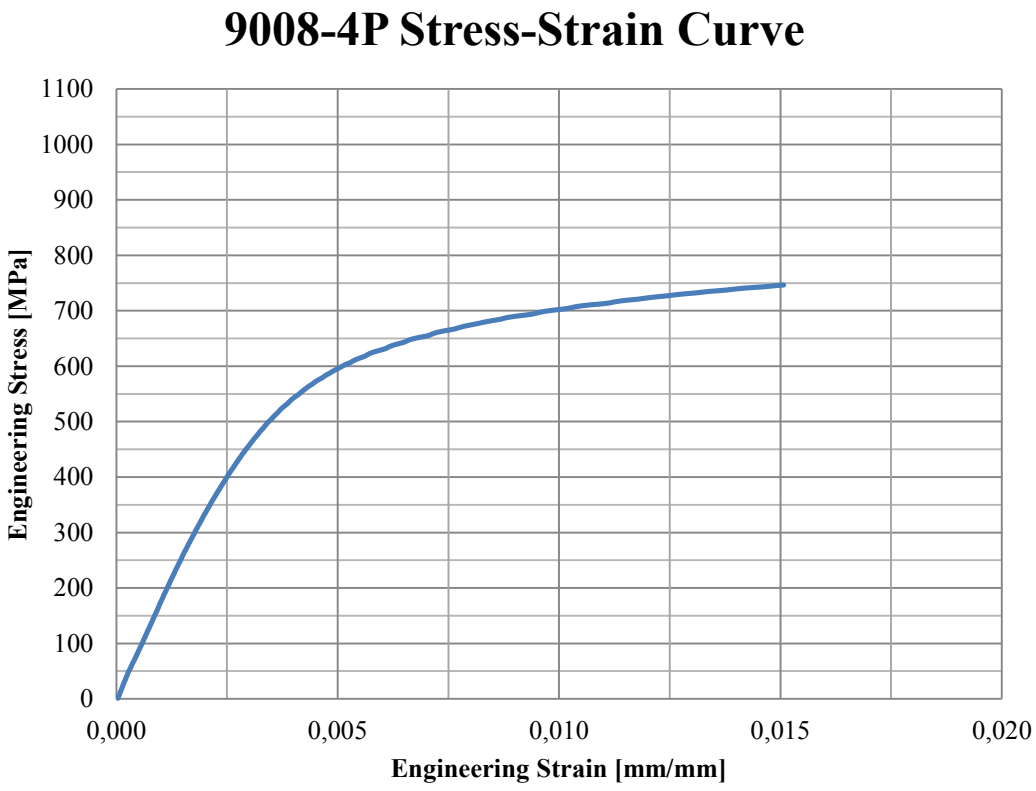

Figure 188. Stress-strain curve of PAW welded sample 9008-4P.

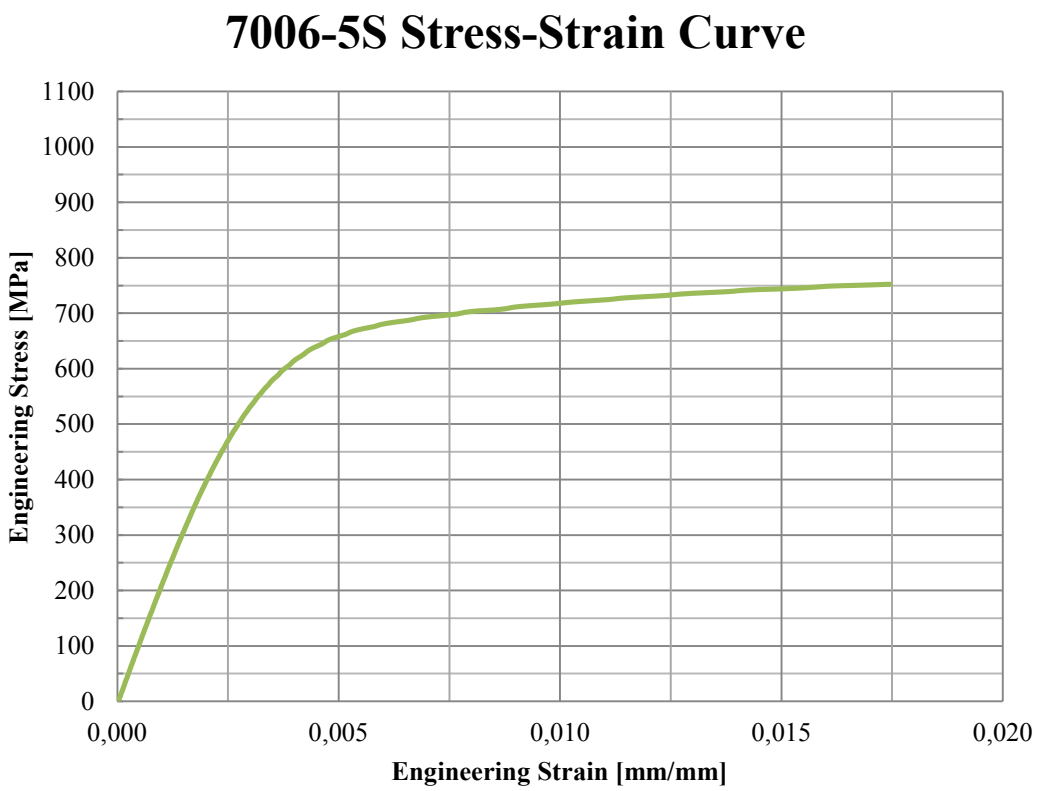

Figure 189. Stress-strain curve of SAW welded sample 7006-5S.

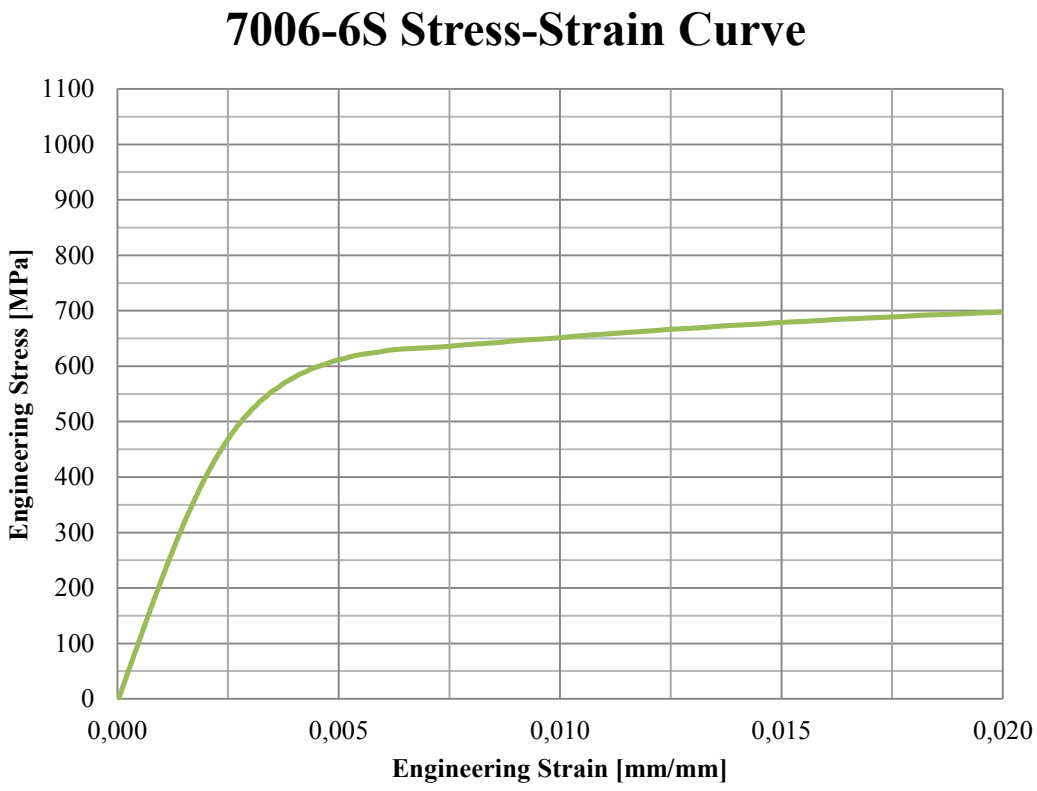

Figure 190. Stress-strain curve of SAW welded sample 7006-6S.

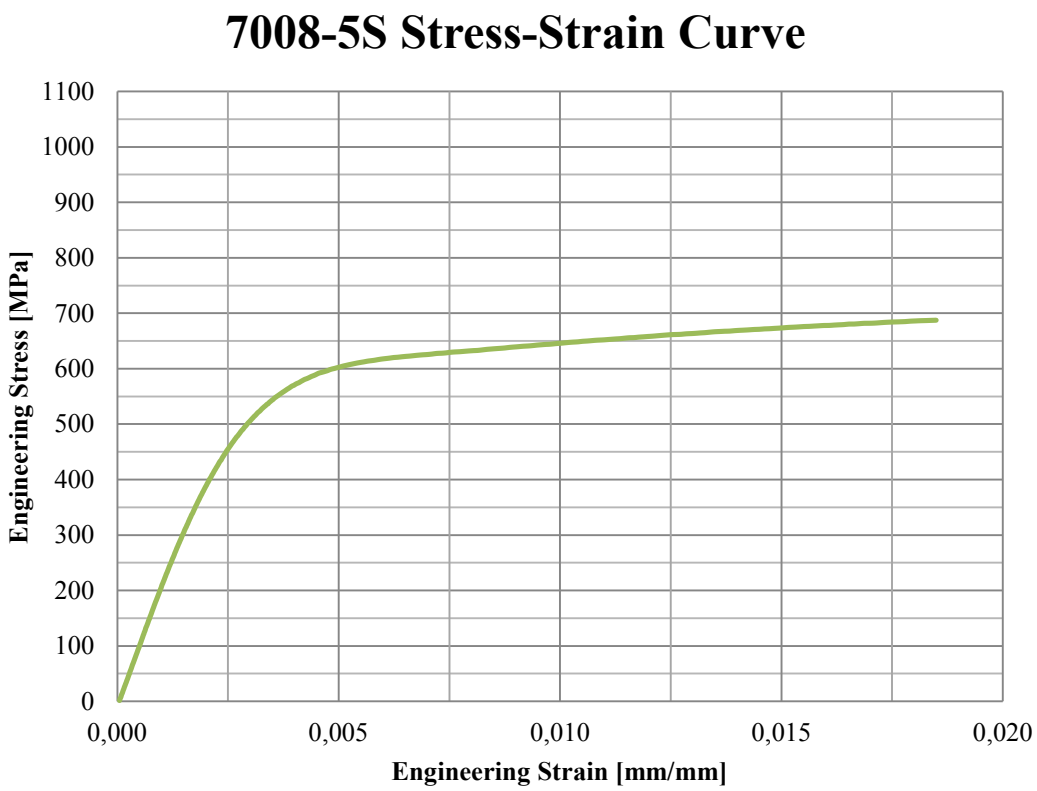

Figure 191. Stress-strain curve of SAW welded sample 7008-5S.

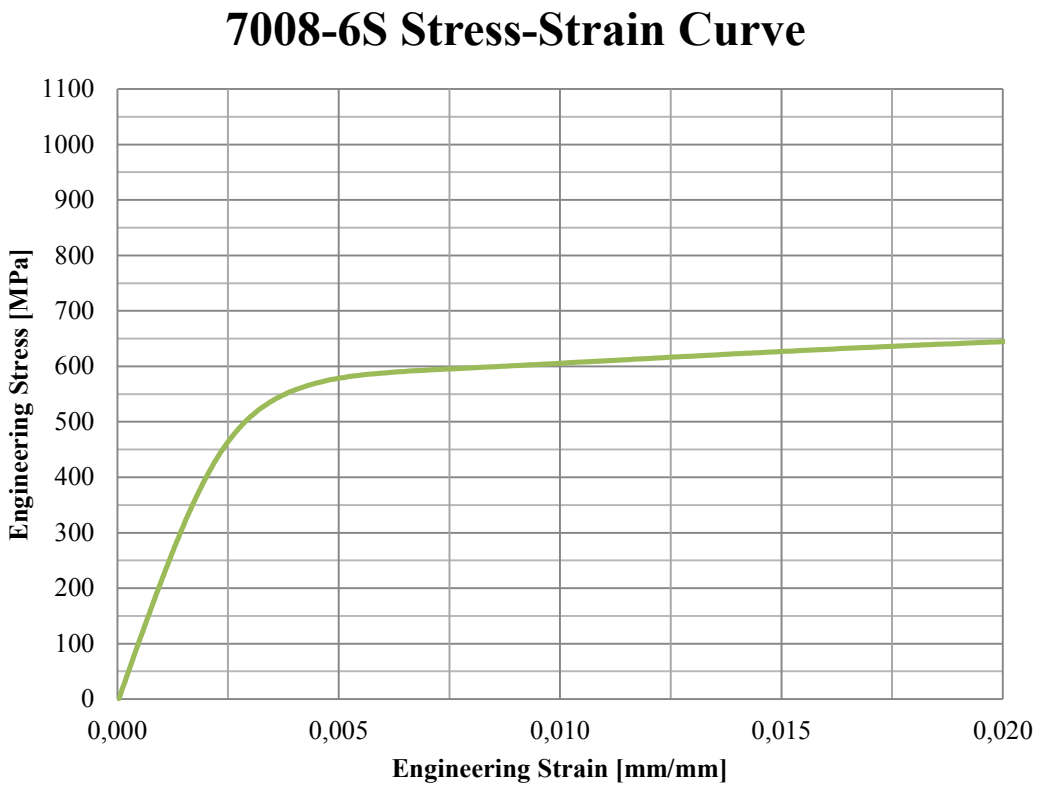

Figure 192. Stress-strain curve of SAW welded sample 7008-6S.

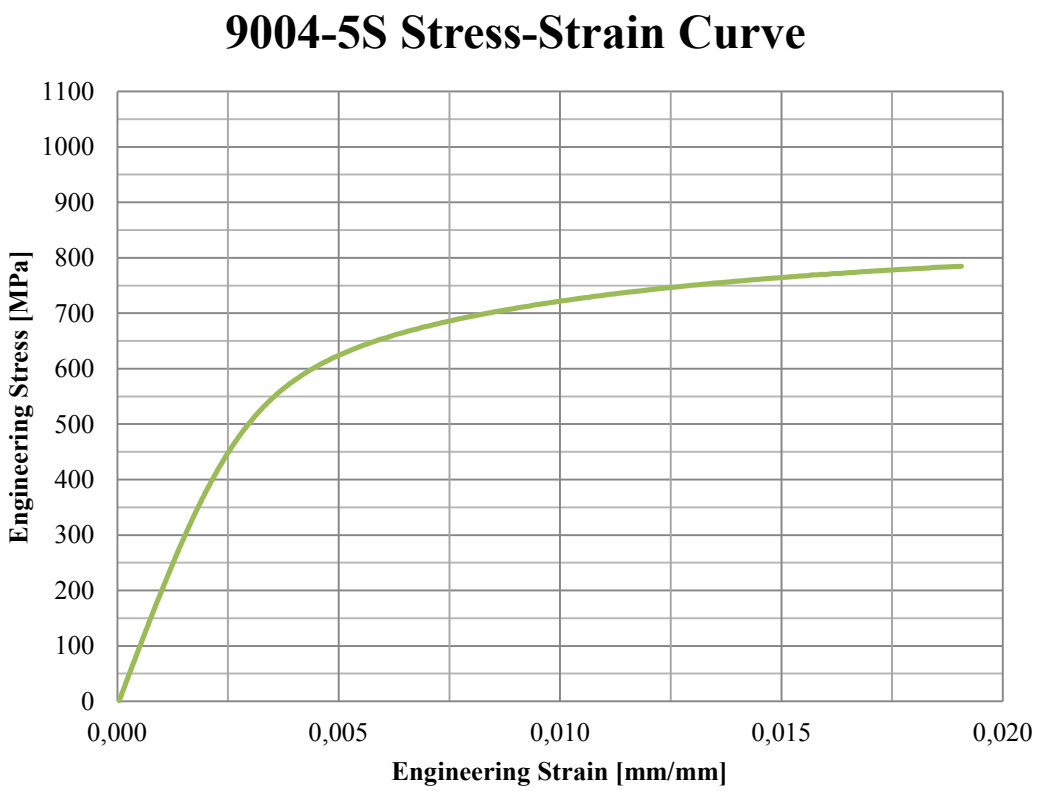

Figure 193. Stress-strain curve of SAW welded sample 9004-5S.

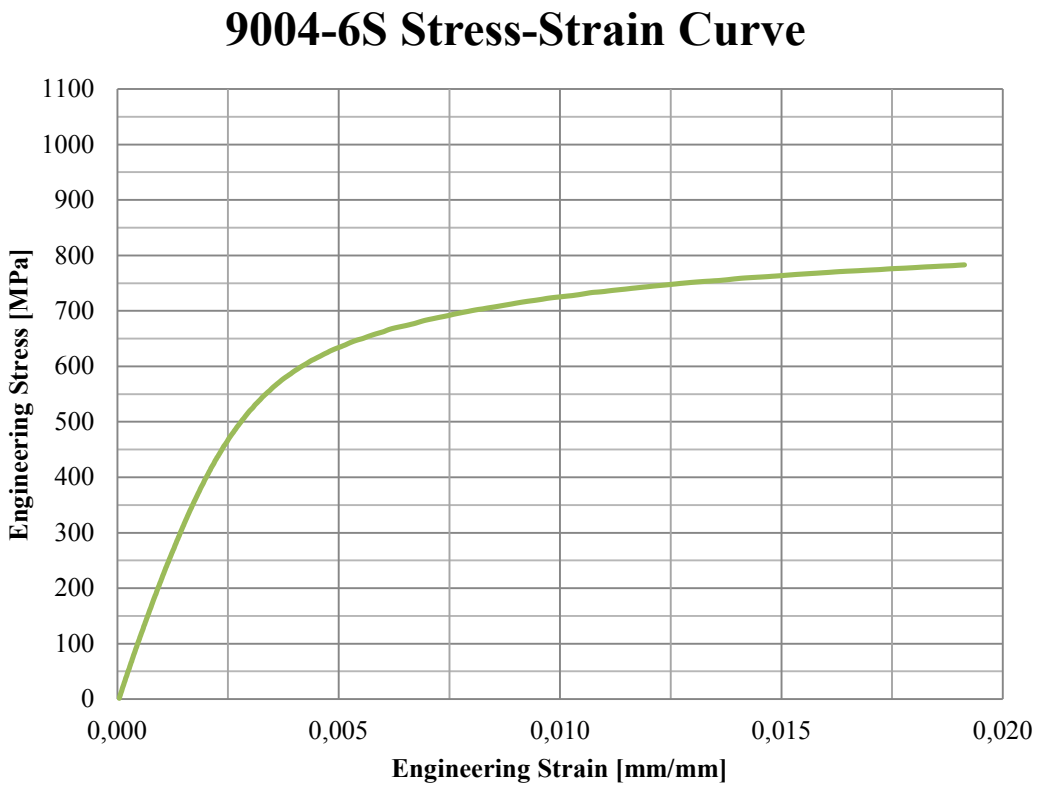

Figure 194. Stress-strain curve of SAW welded sample 9004-6S.

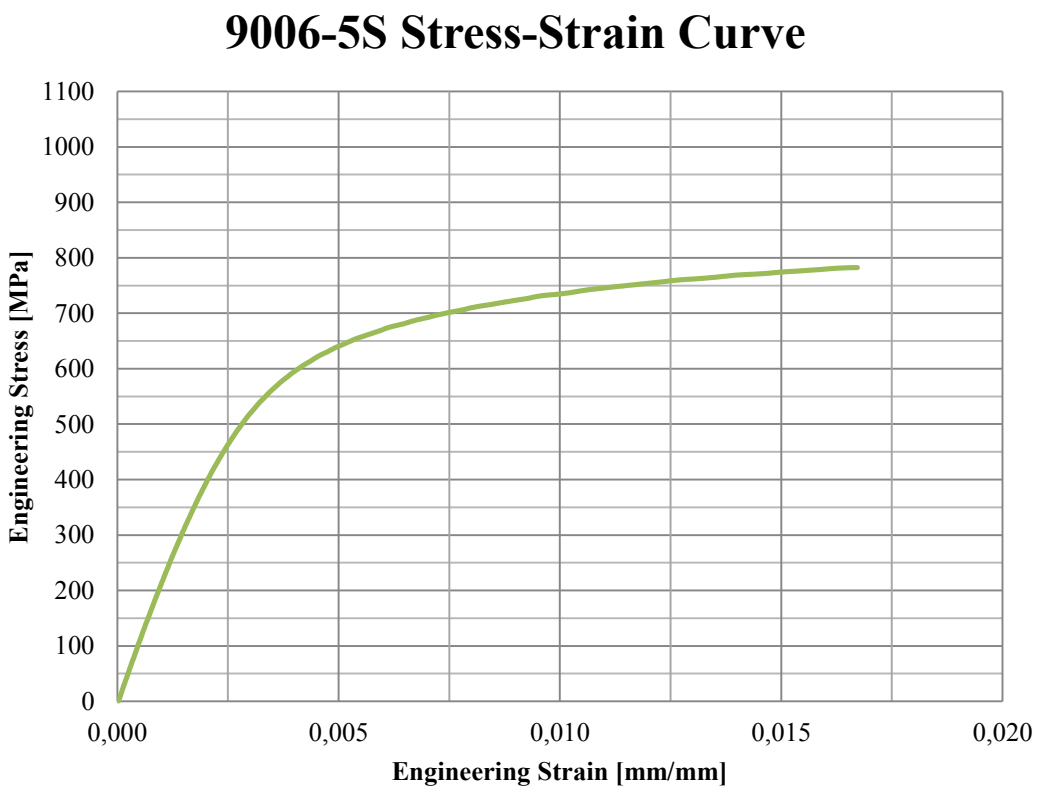

Figure 195. Stress-strain curve of SAW welded sample 9006-5S.

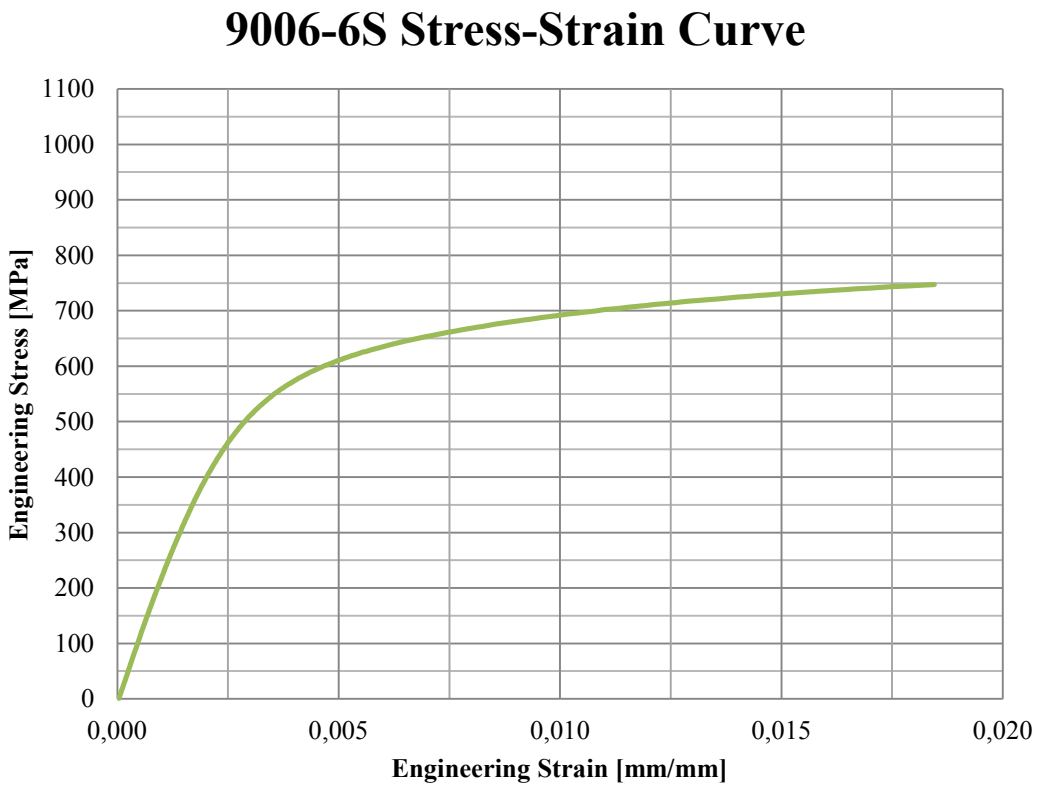

Figure 196. Stress-strain curve of SAW welded sample 9006-6S.

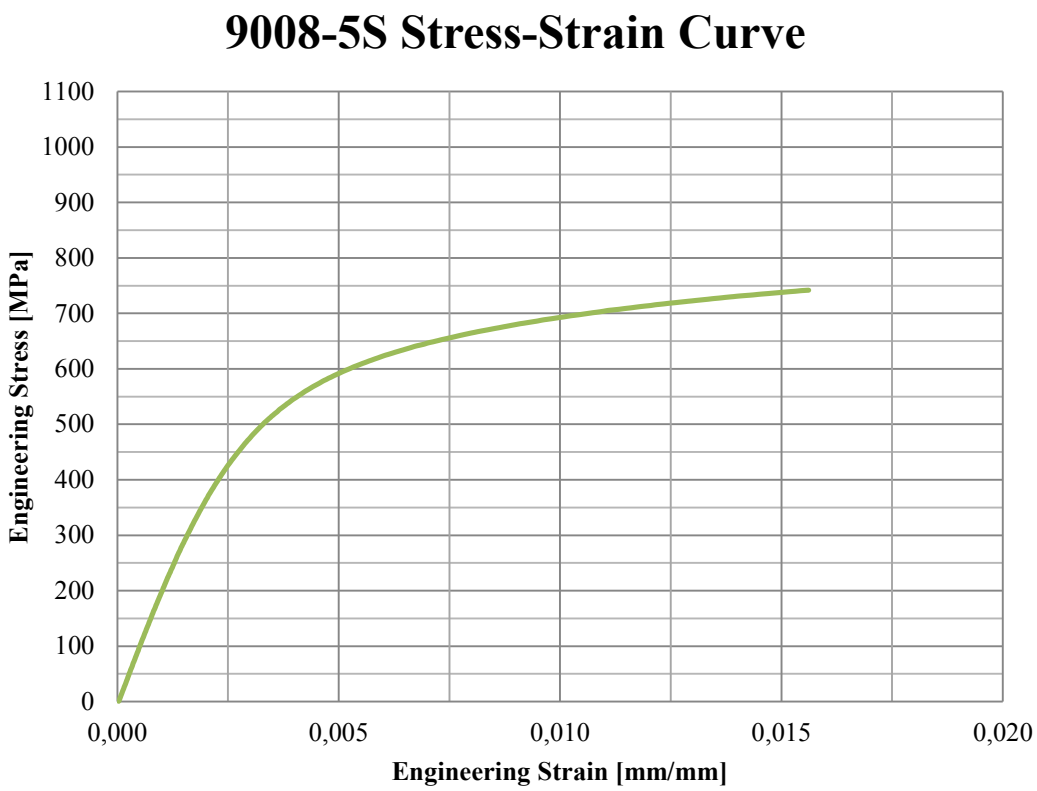

Figure 197. Stress-strain curve of SAW welded sample 9008-5S.

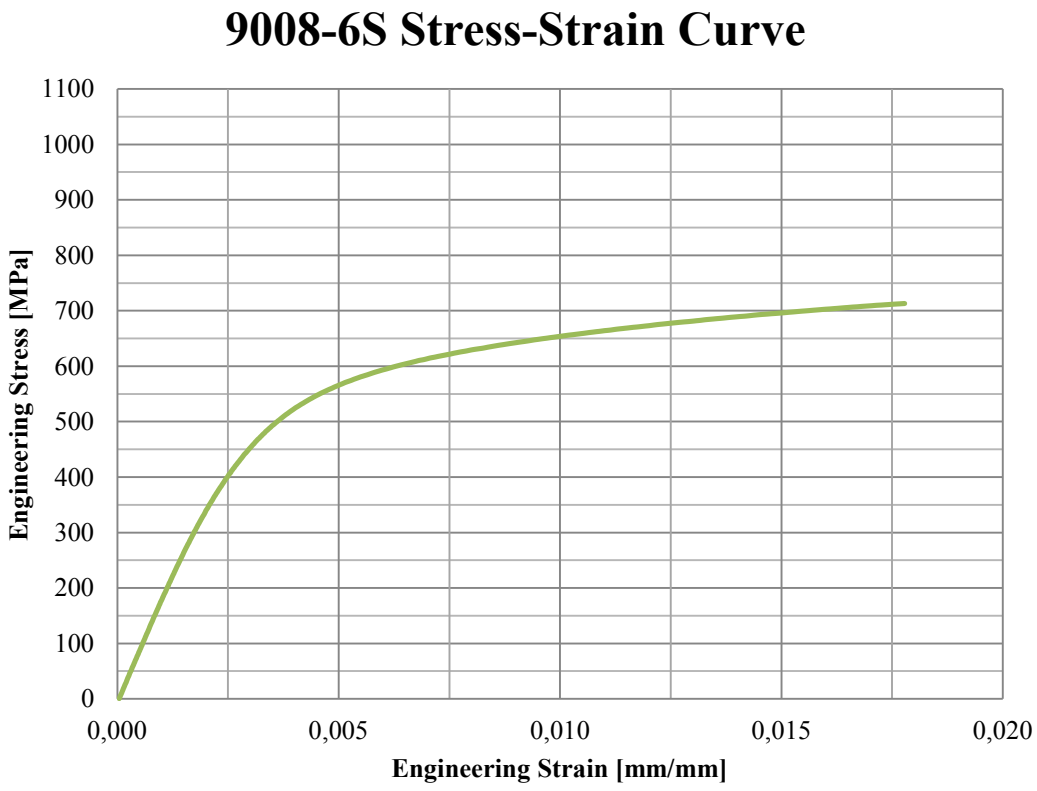

Figure 198. Stress-strain curve of SAW welded sample 9008-6S.

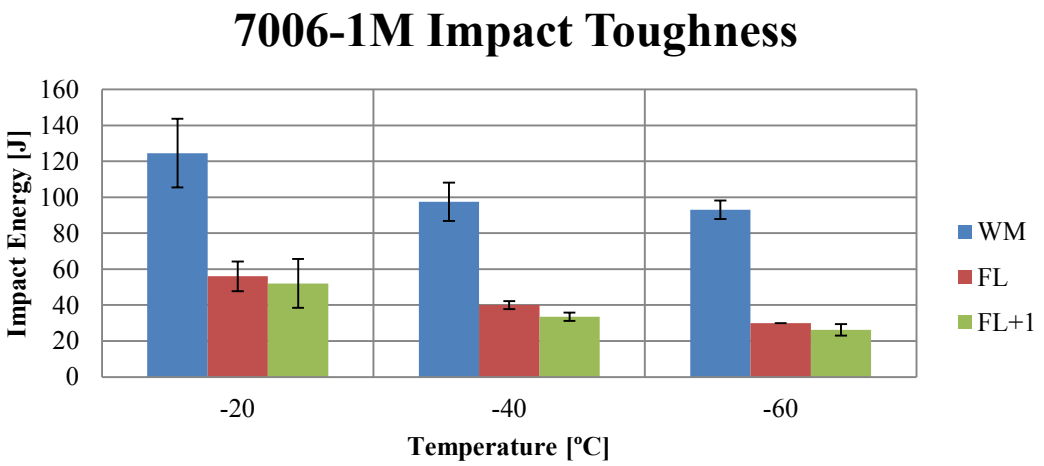

Figure 199. Impact energy of MAG welded sample 7006-1M.

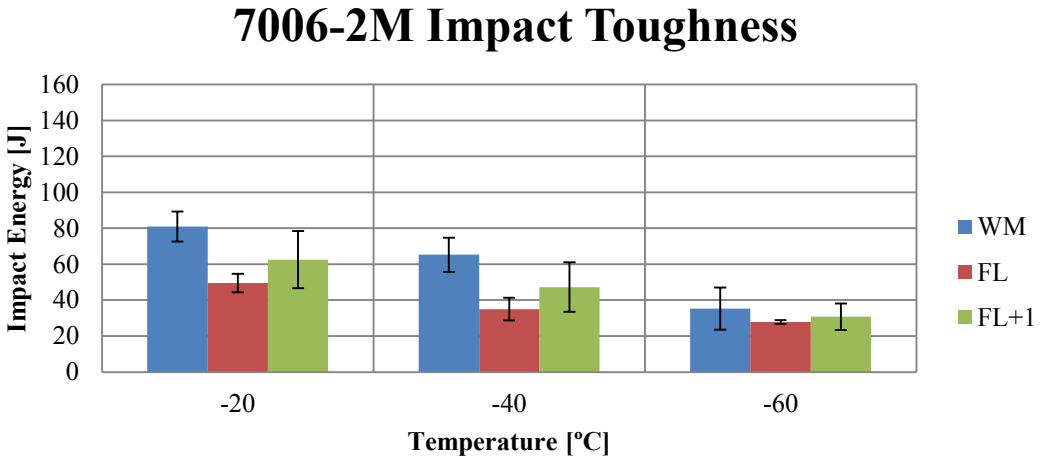

Figure 200. Impact energy of MAG welded sample 7006-2M.

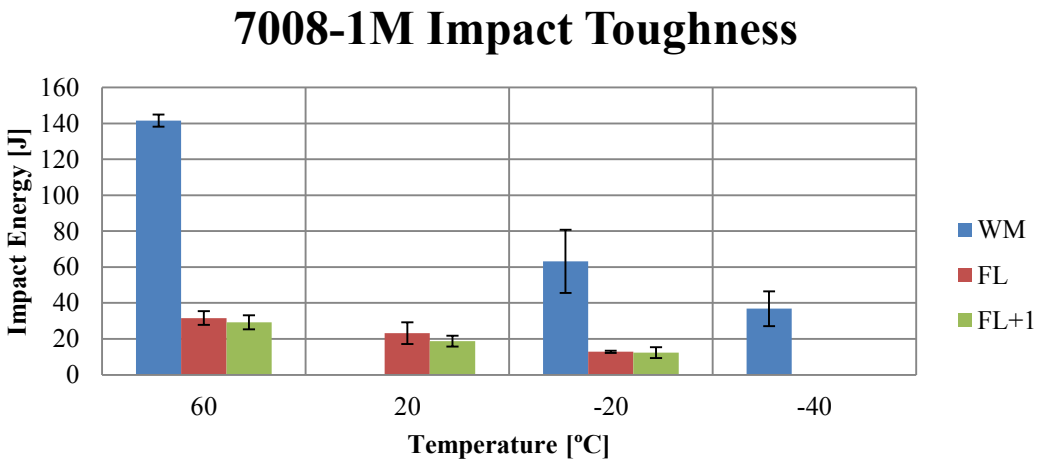

Figure 201. Impact energy of MAG welded sample 7008-1M.

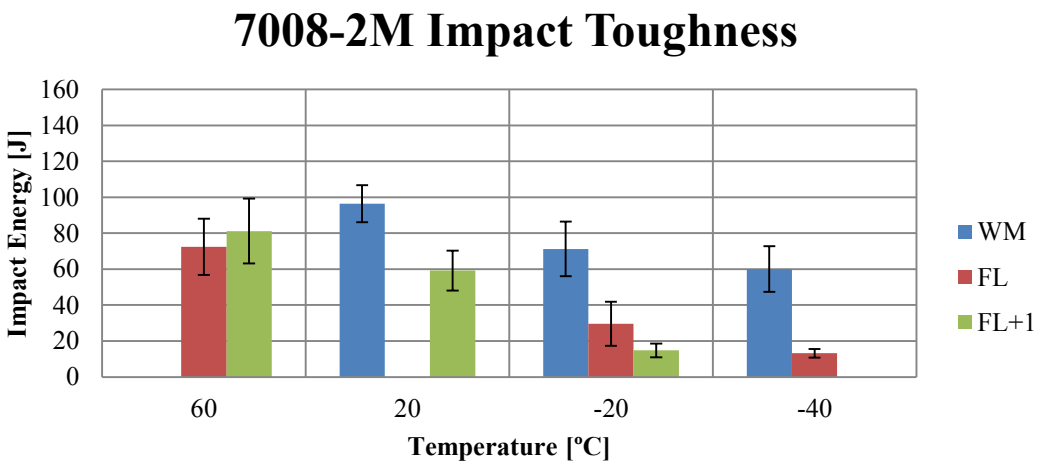

Figure 202. Impact energy of MAG welded sample 7008-2M.

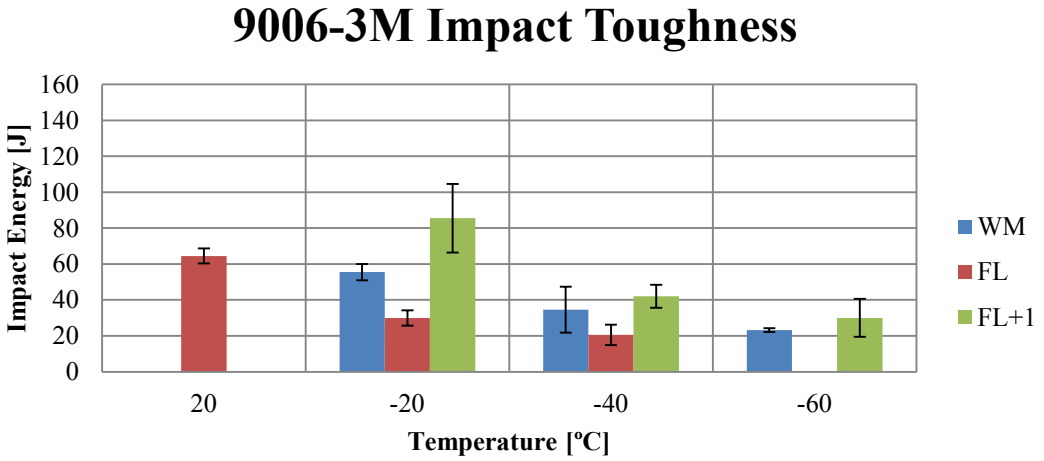

Figure 203. Impact energy of MAG welded sample 9006-3M.

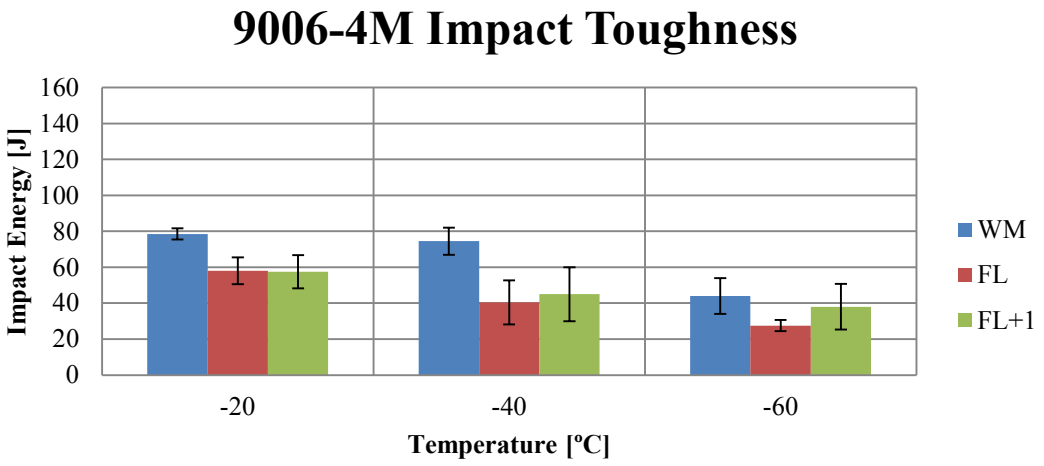

Figure 204. Impact energy of MAG welded sample 9006-4M.

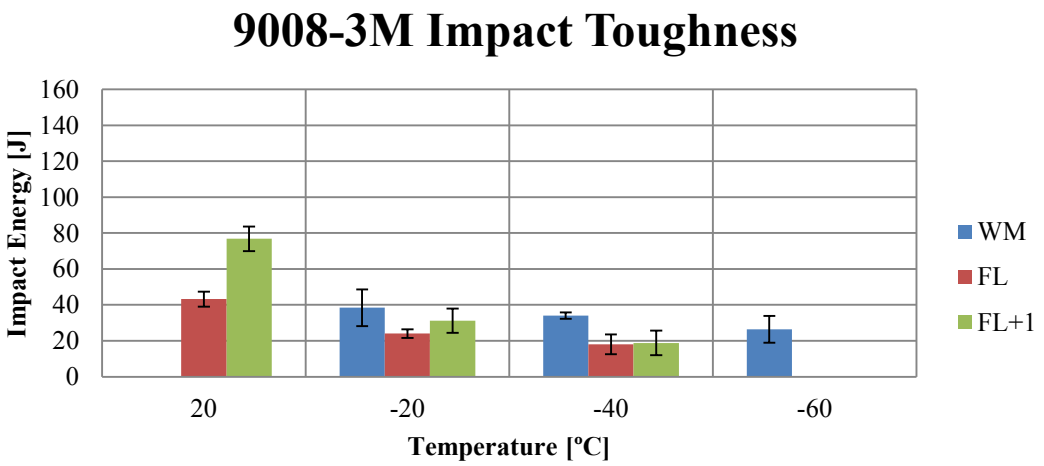

Figure 205. Impact energy of MAG welded sample 9008-3M.

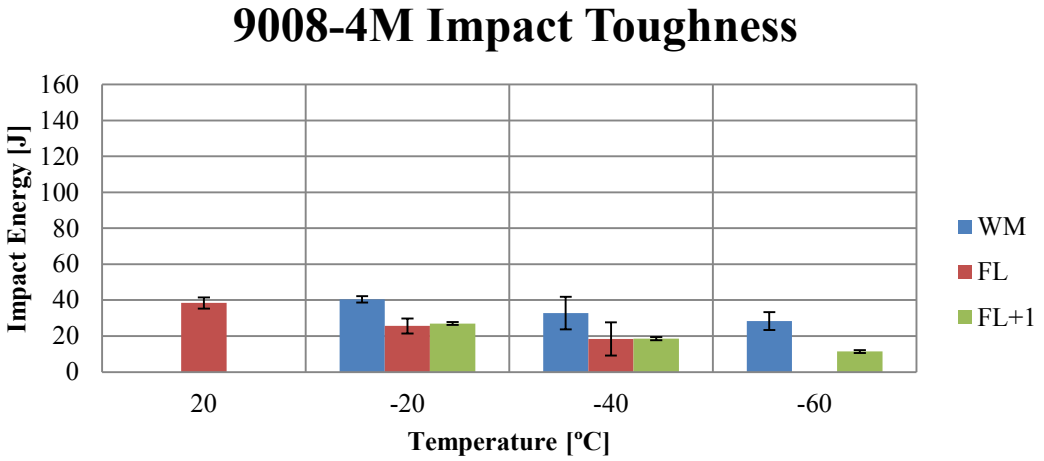

Figure 206. Impact energy of MAG welded sample 9008-4M.

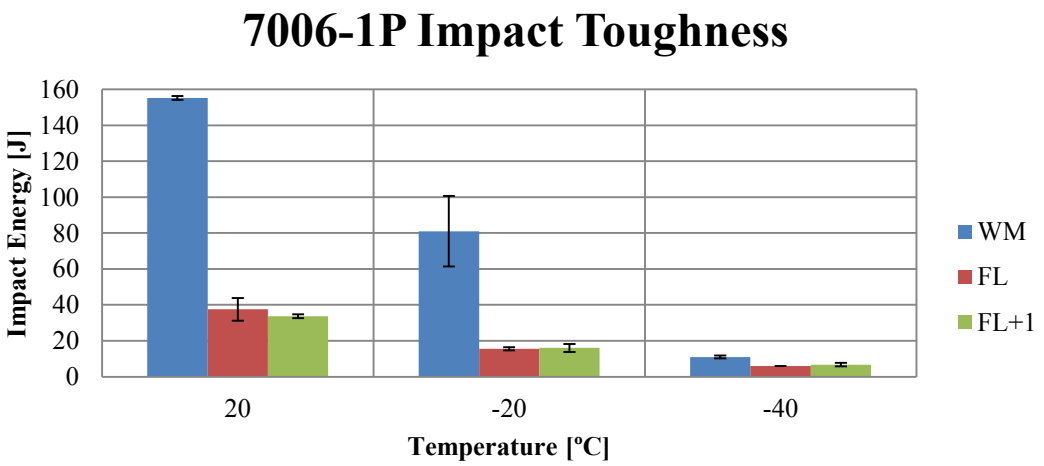

Figure 207. Impact energy of PAW welded sample 7006-1P.

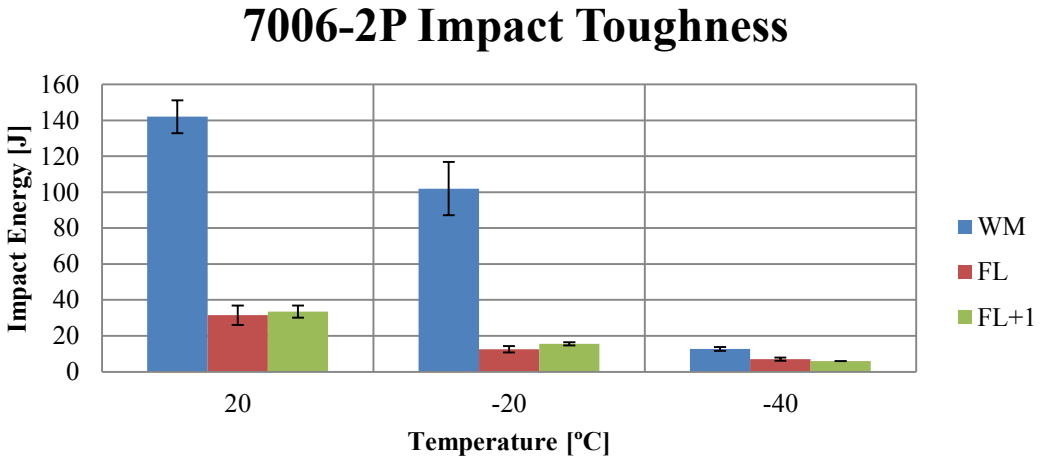

Figure 208. Impact energy of PAW welded sample 7006-2P.

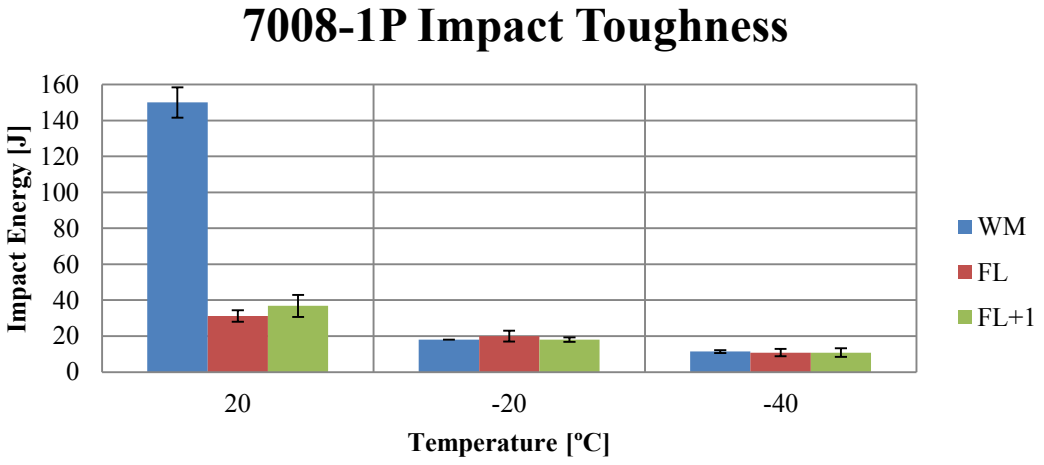

Figure 209. Impact energy of PAW welded sample 7008-1P.

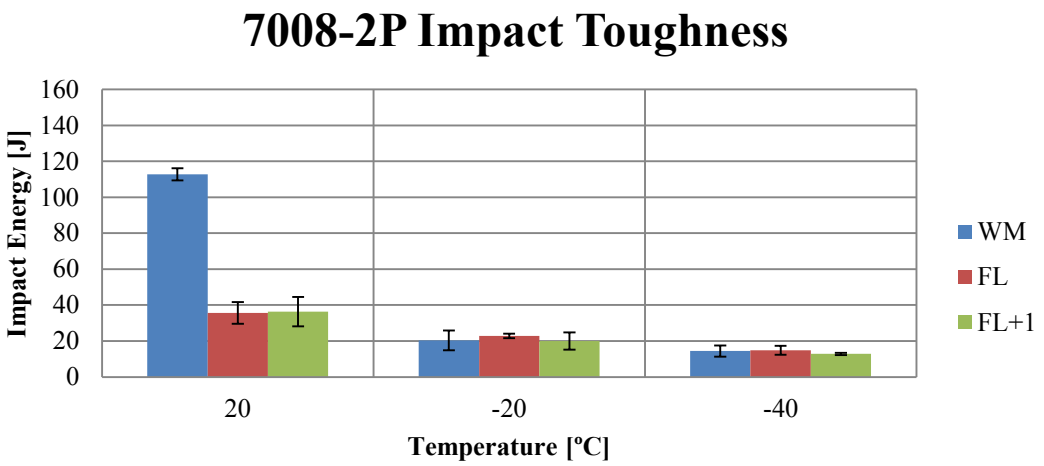

Figure 210. Impact energy of PAW welded sample 7008-2P.

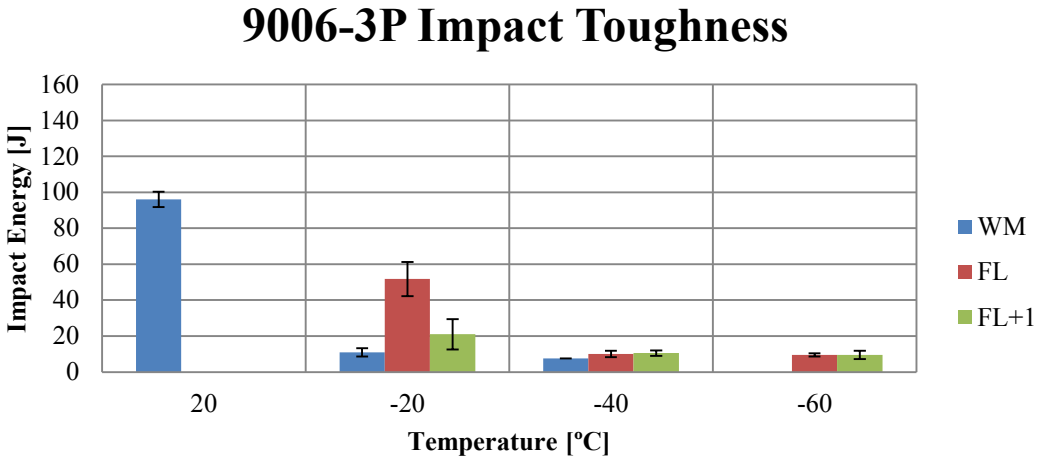

Figure 211. Impact energy of PAW welded sample 9006-3P.

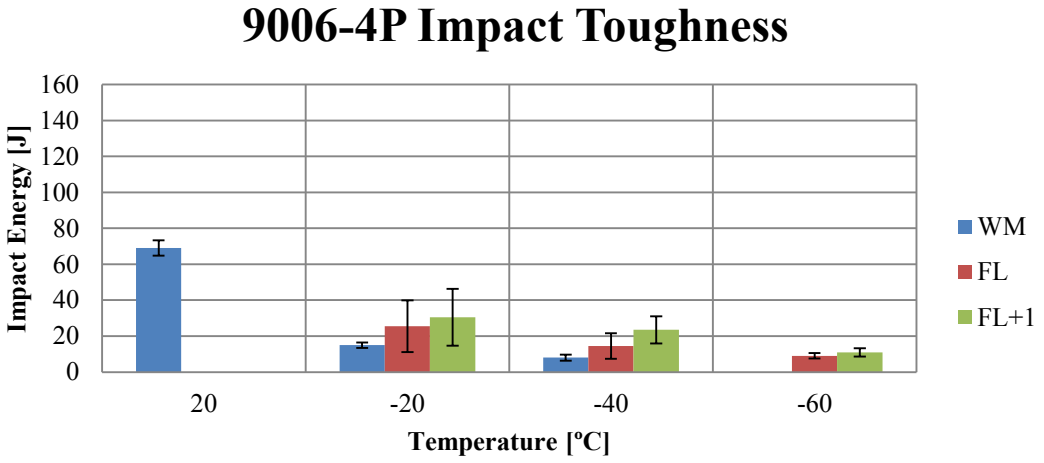

Figure 212. Impact energy of PAW welded sample 9006-4P.

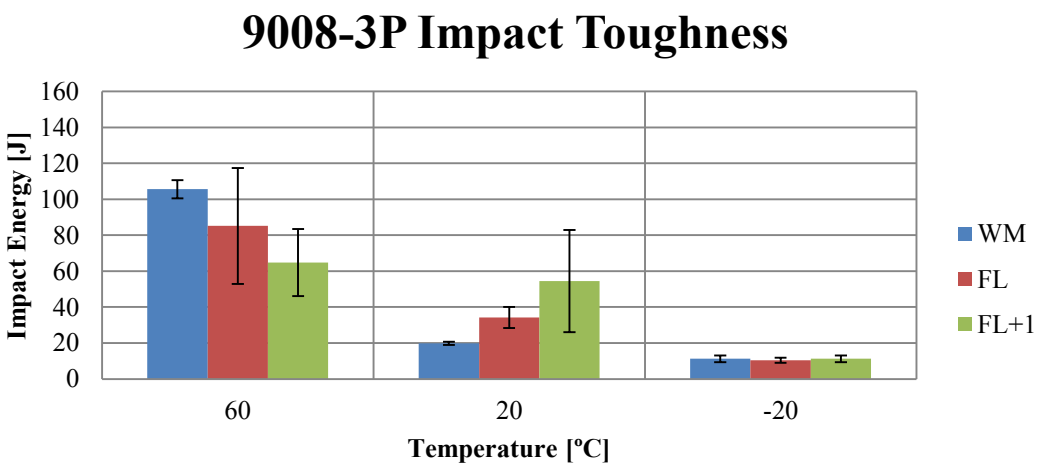

Figure 213. Impact energy of PAW welded sample 9008-3P.

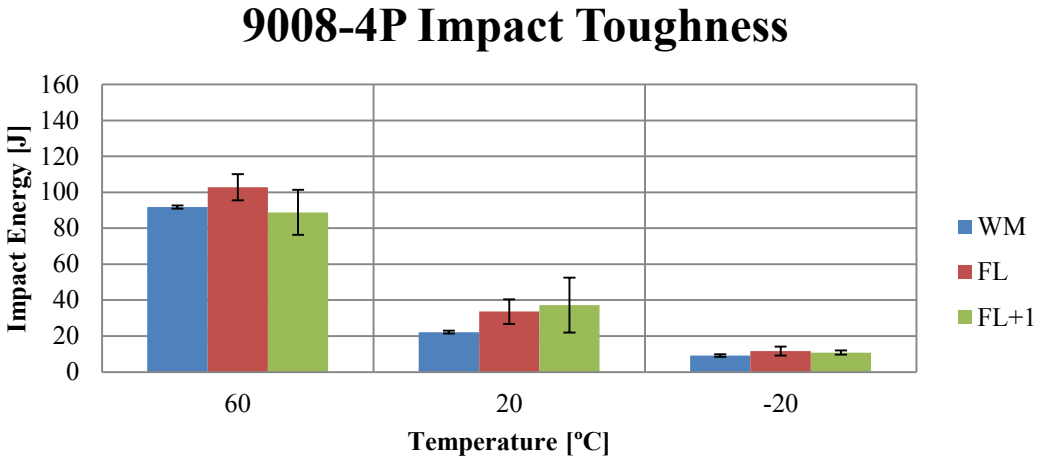

Figure 214. Impact energy of PAW welded sample 9008-4P.

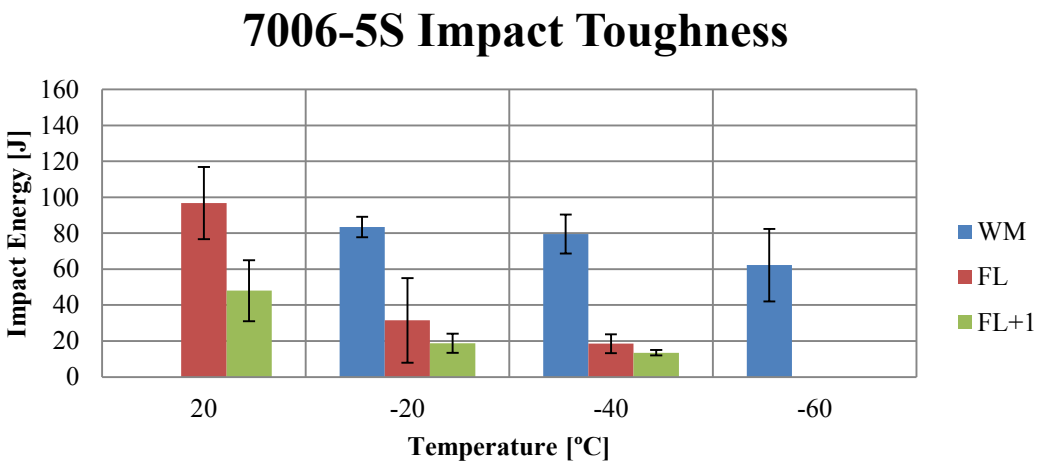

Figure 215. Impact energy of SAW welded sample 7006-5S.

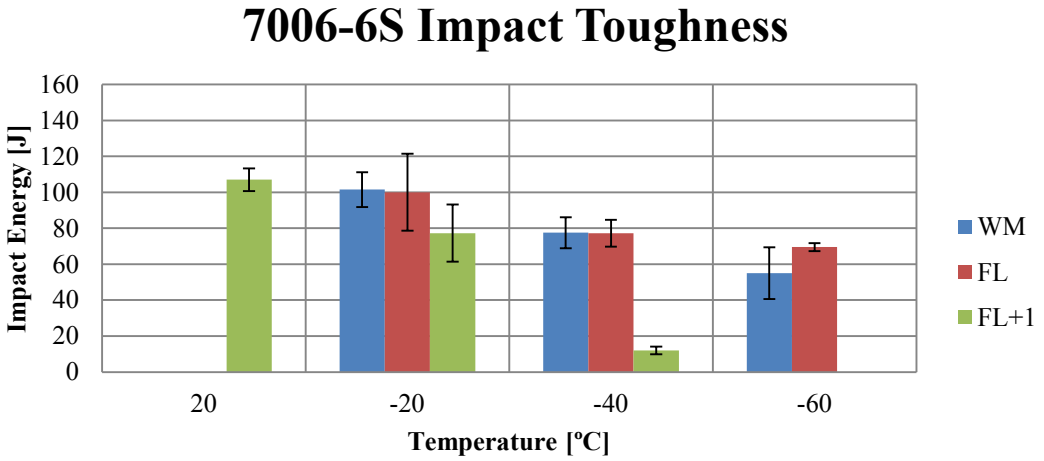

Figure 216. Impact energy of SAW welded sample 7006-6S.

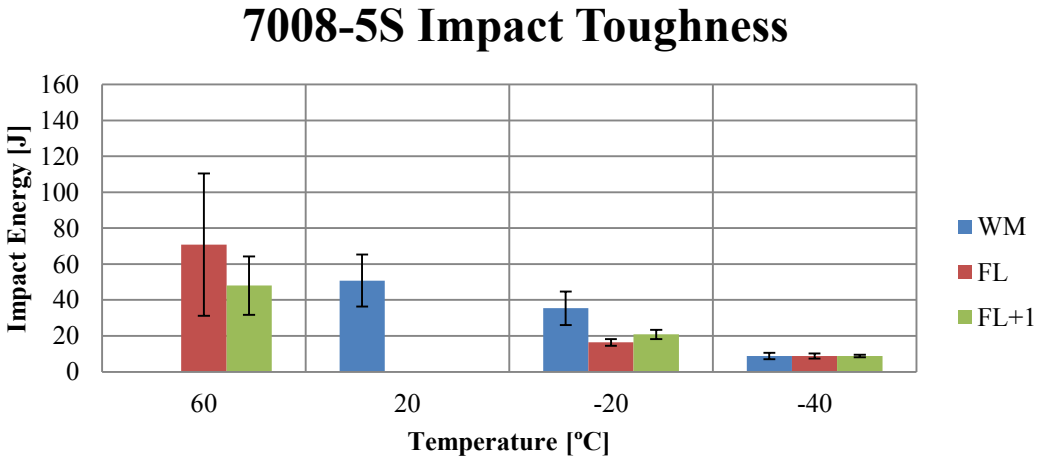

Figure 217. Impact energy of SAW welded sample 7008-5S.

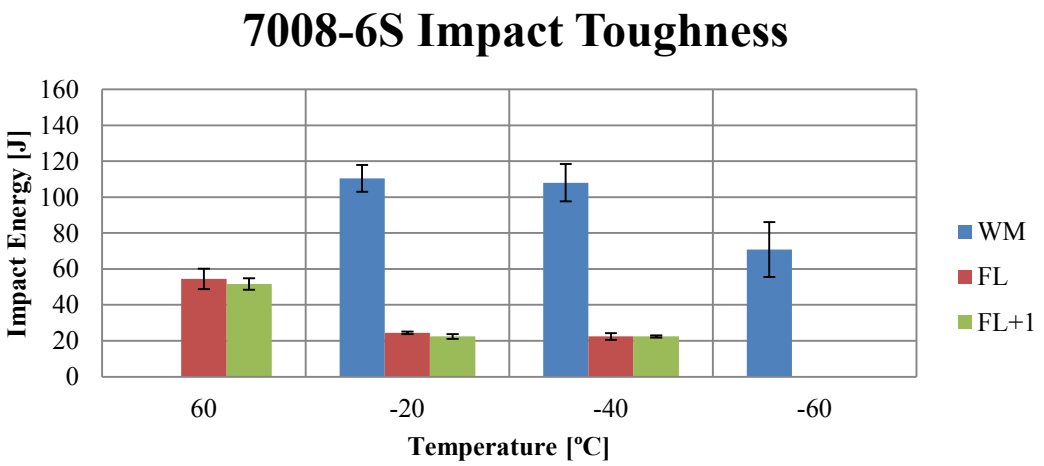

Figure 218. Impact energy of SAW welded sample 7008-6S.

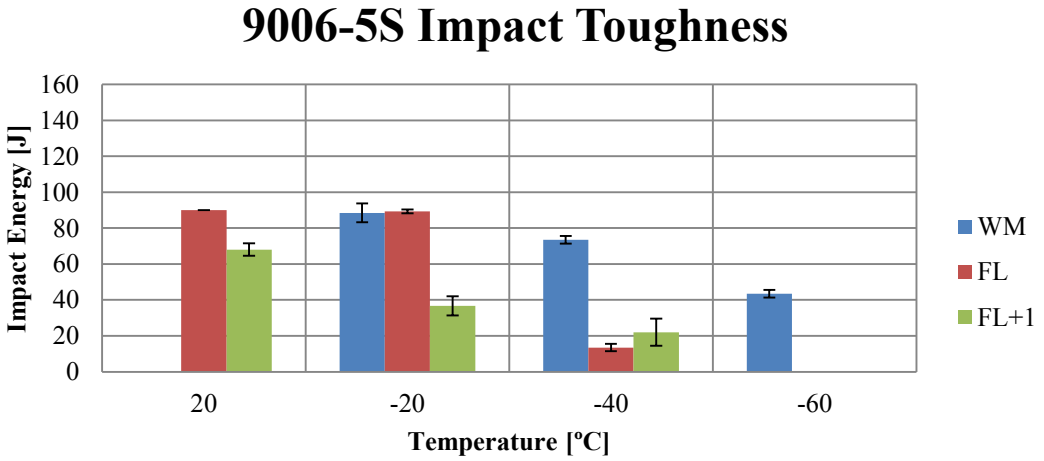

Figure 219. Impact energy of SAW welded sample 9006-5S.

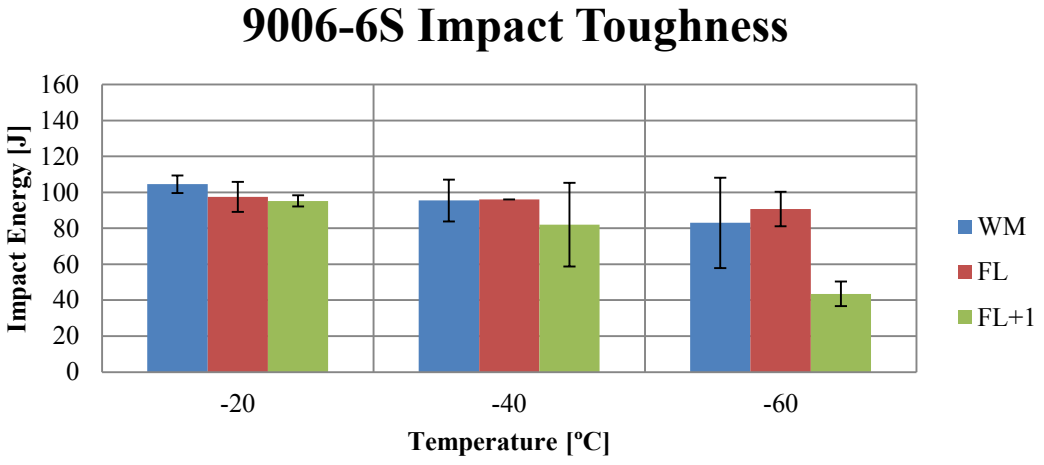

Figure 220. Impact energy of SAW welded sample 9006-6S.

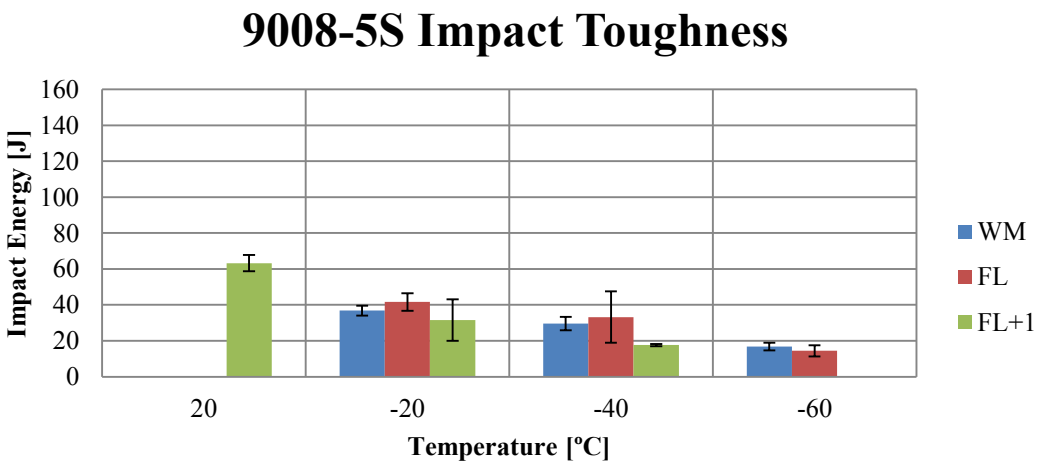

Figure 221. Impact energy of SAW welded sample 9008-5S.

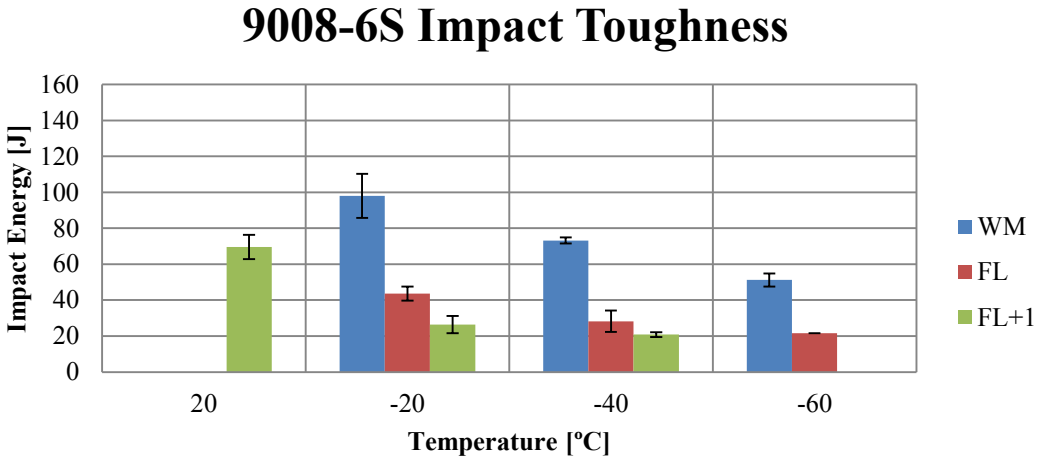

Figure 222. Impact energy of SAW welded sample 9008-6S.

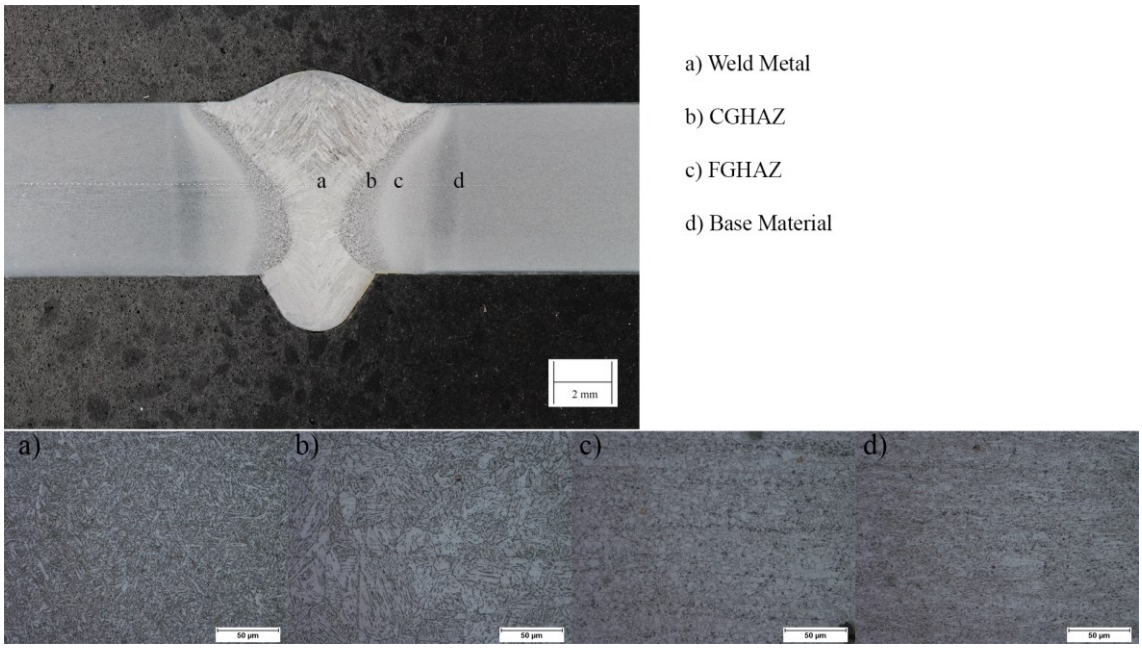

Figure 223. Sample 7006-1M.

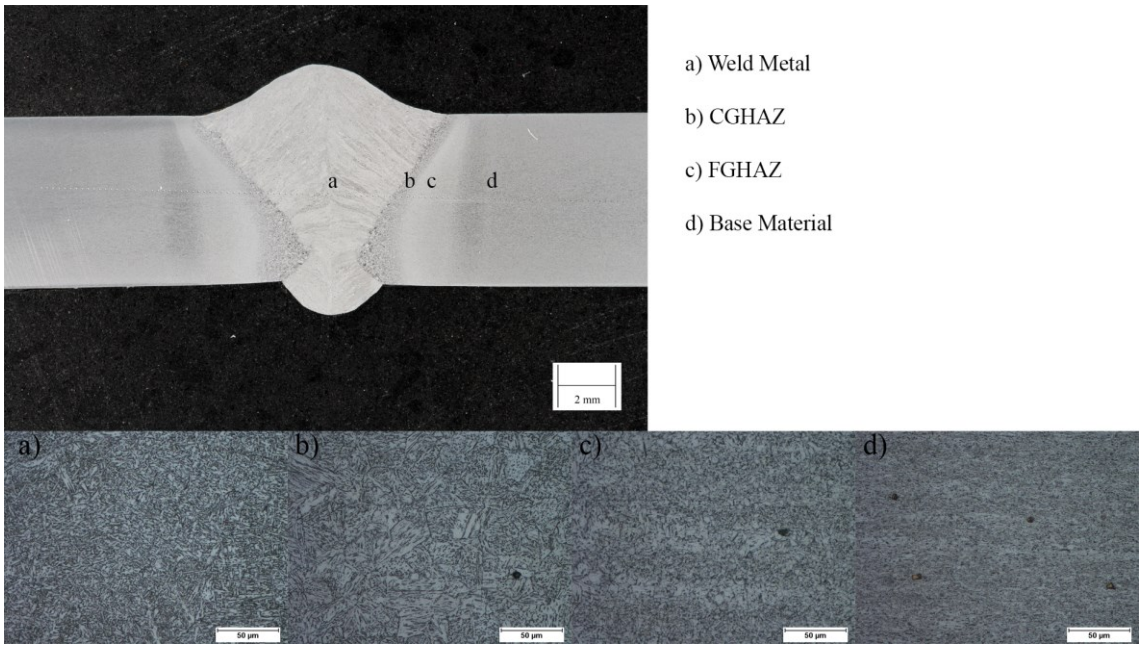

Figure 224. Sample 7006-2M.

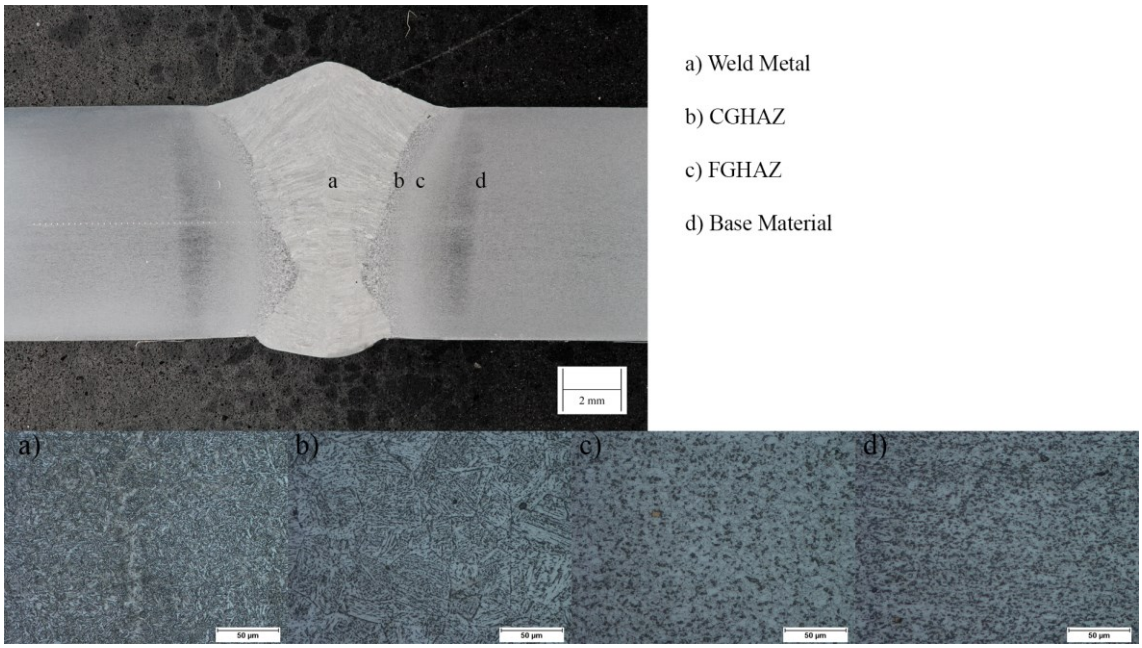

Figure 225. Sample 7008-1M.

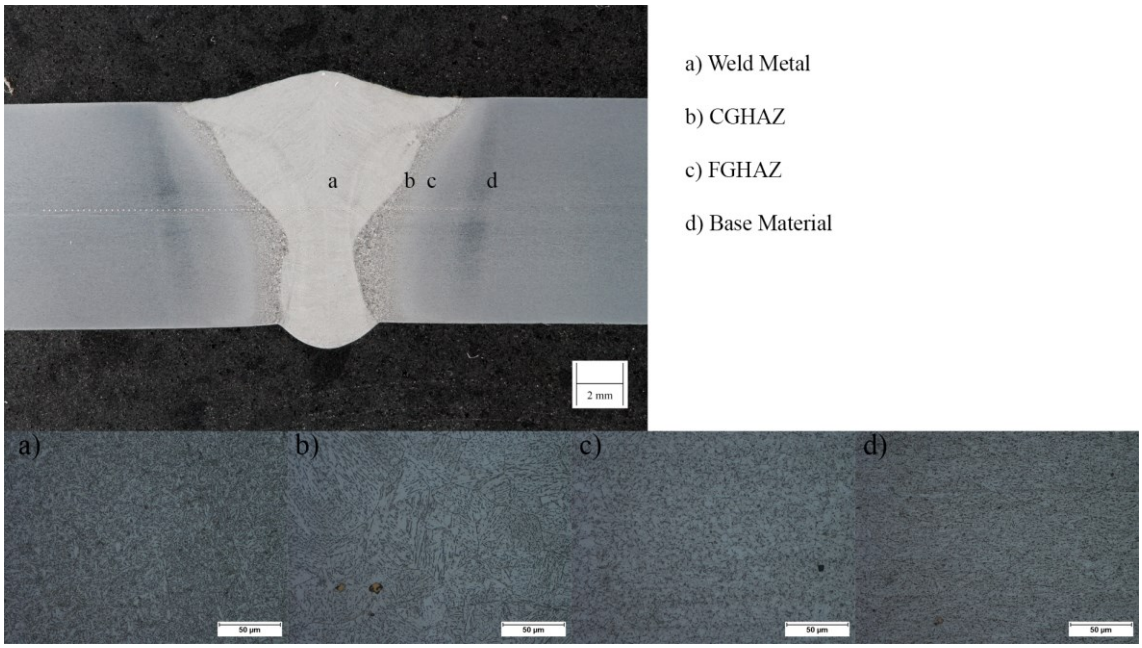

Figure 226. Sample 7008-2M.

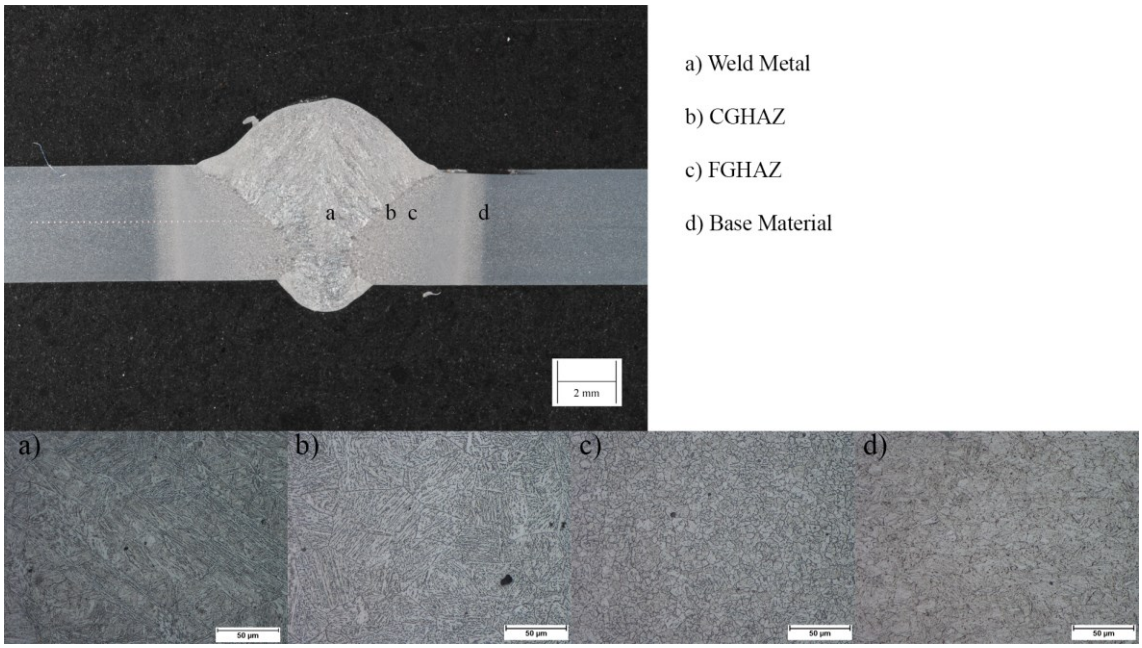

Figure 227. Sample 9004-3M.

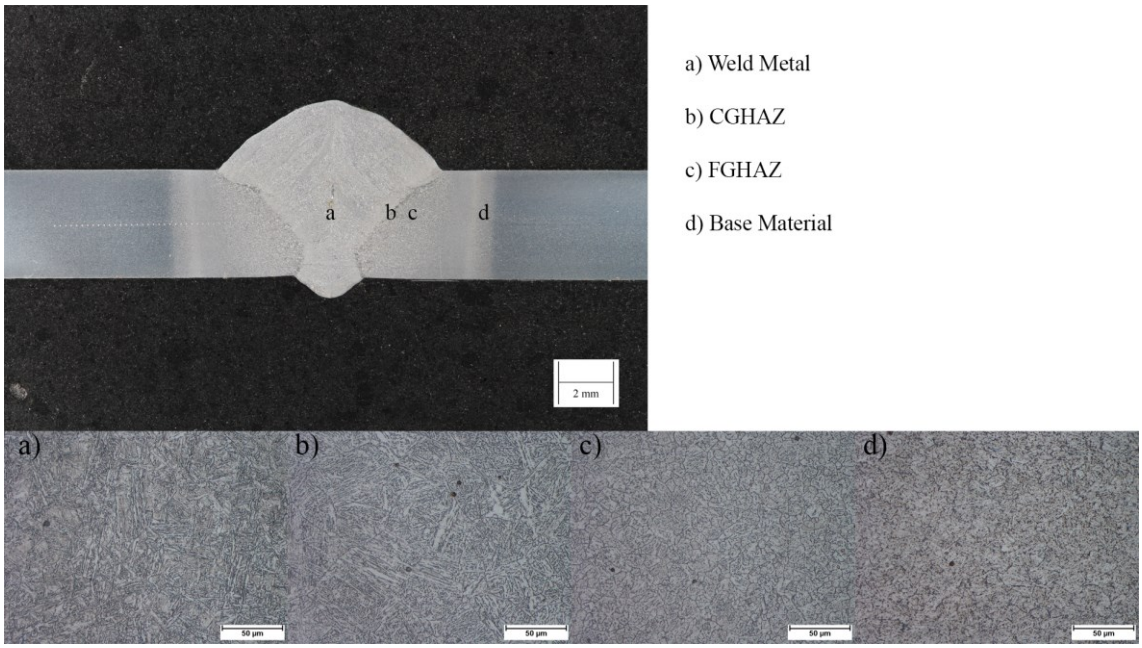

Figure 228. Sample 9004-4M.

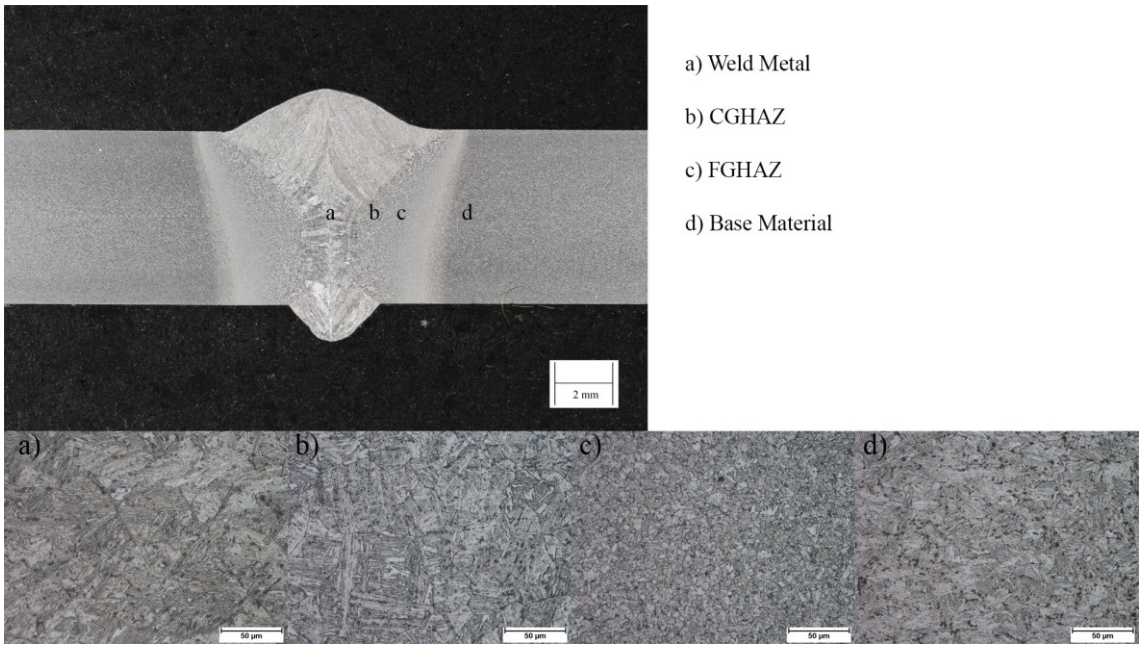

Figure 229. Sample 9006-3M.

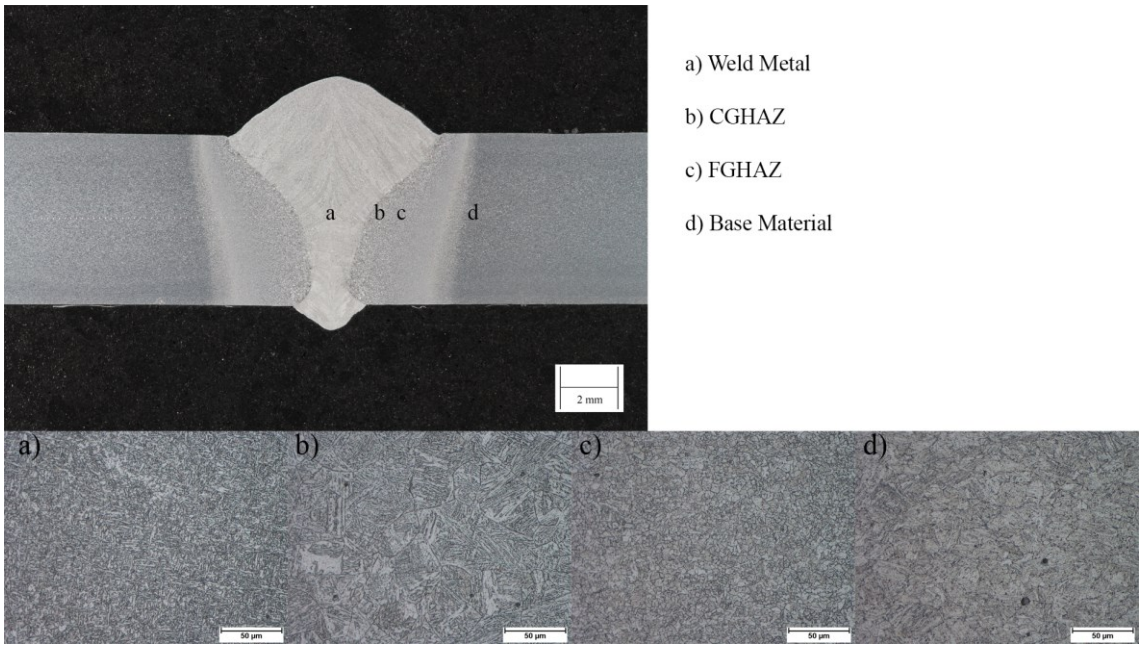

Figure 230. Sample 9006-4M.

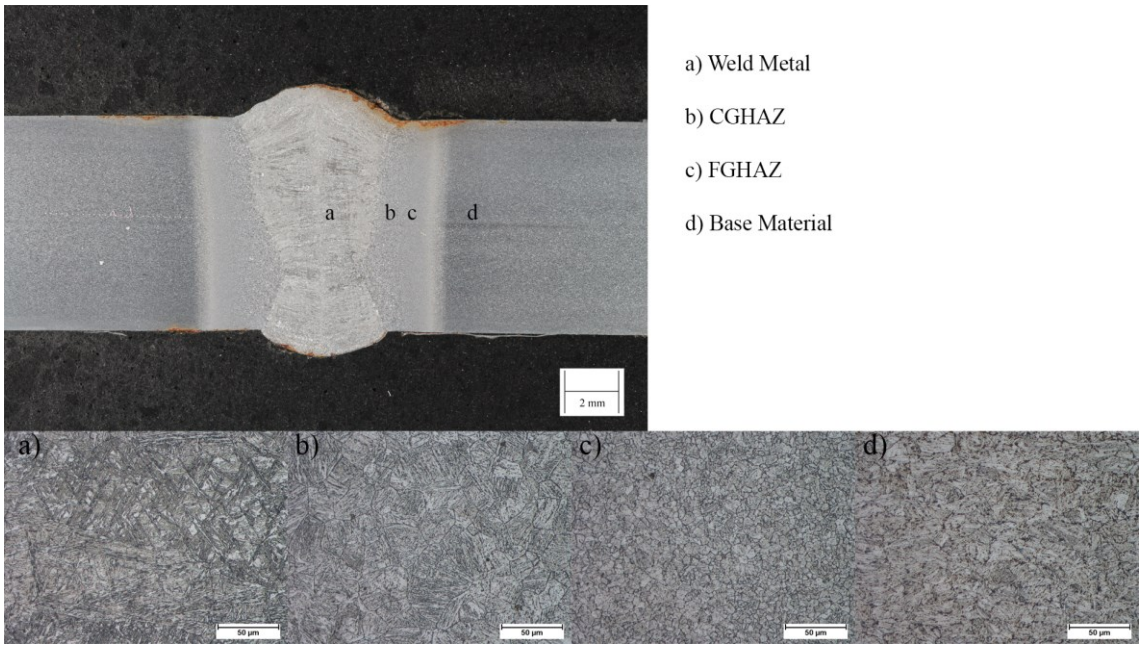

Figure 231. Sample 9008-3M.

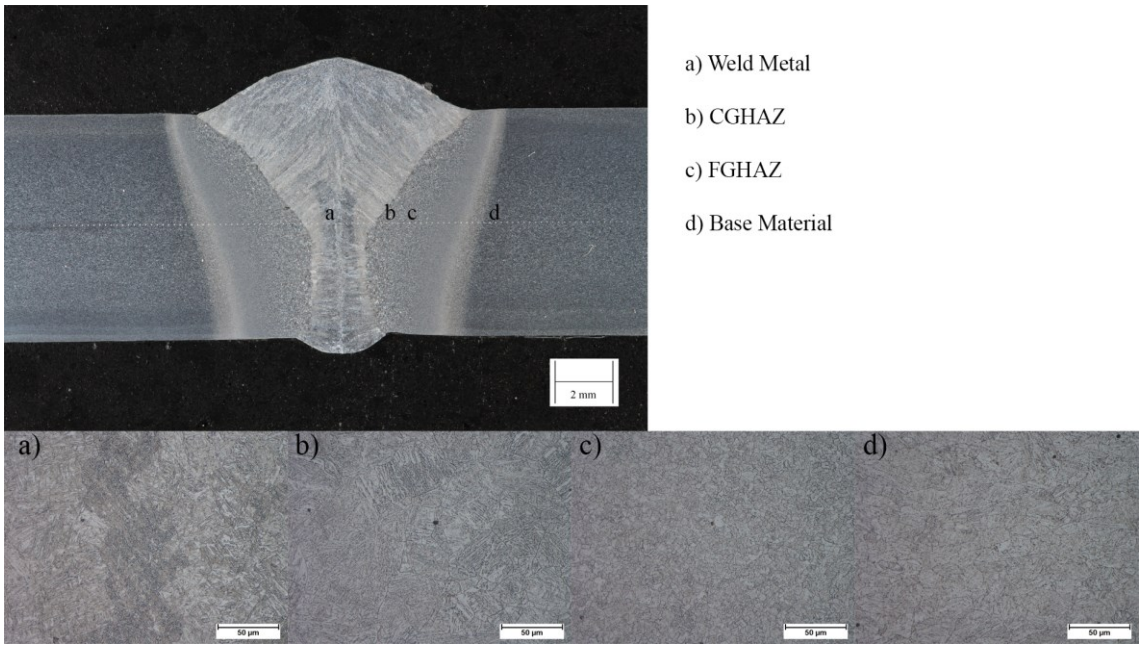

Figure 232. Sample 9008-4M.

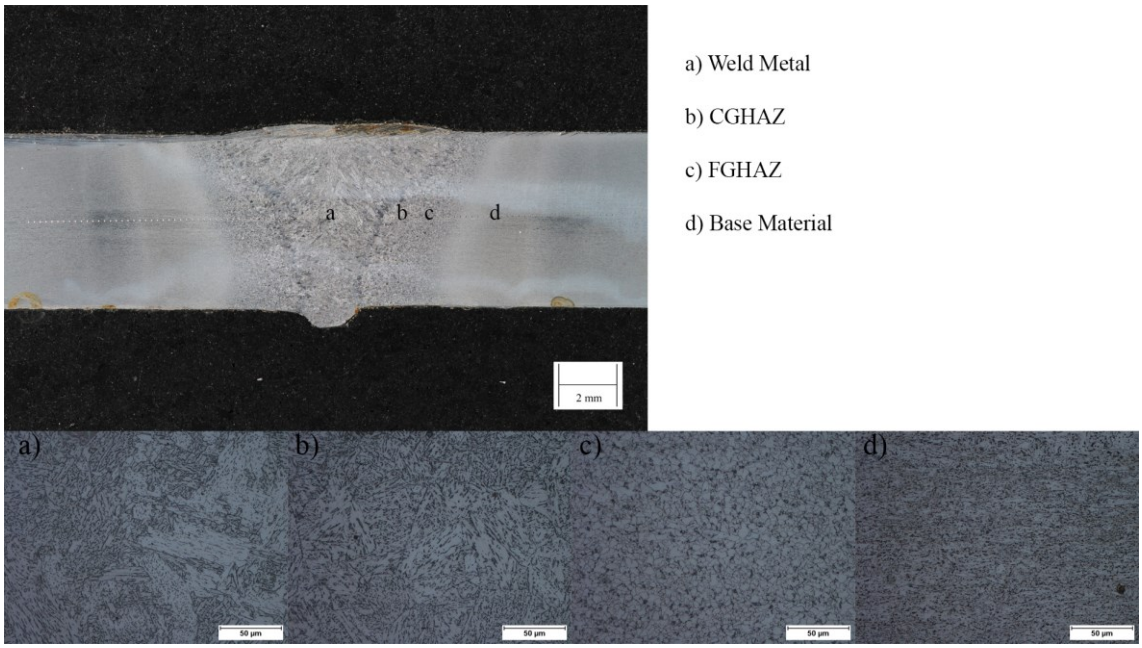

Figure 233. Sample 7006-1P.

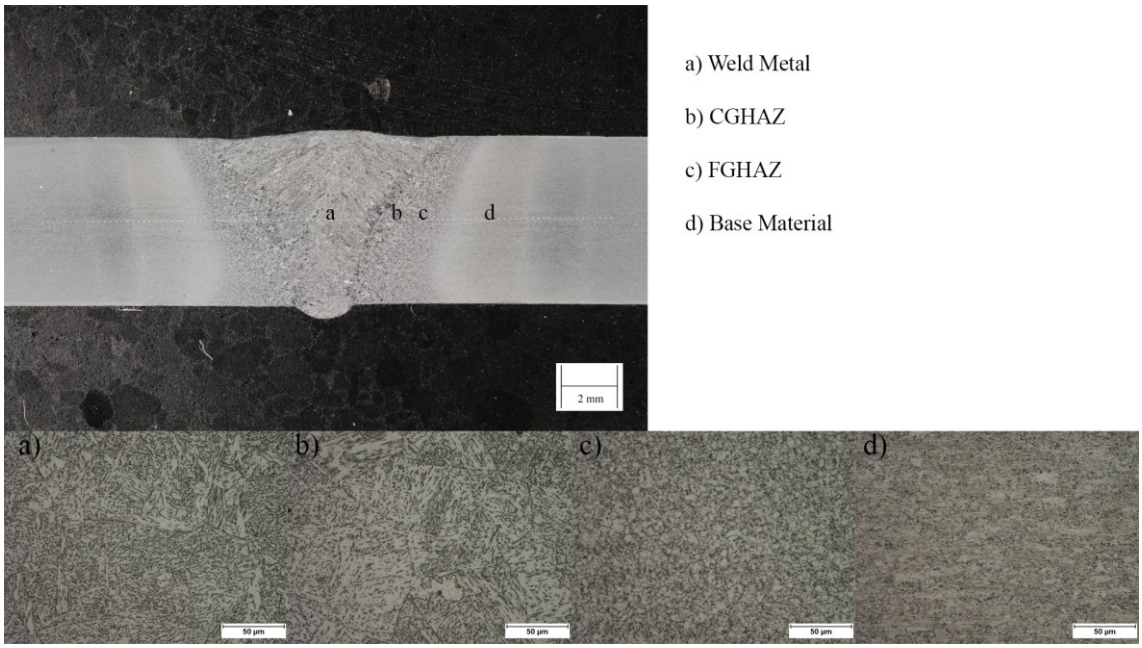

Figure 234. Sample 7006-2P.

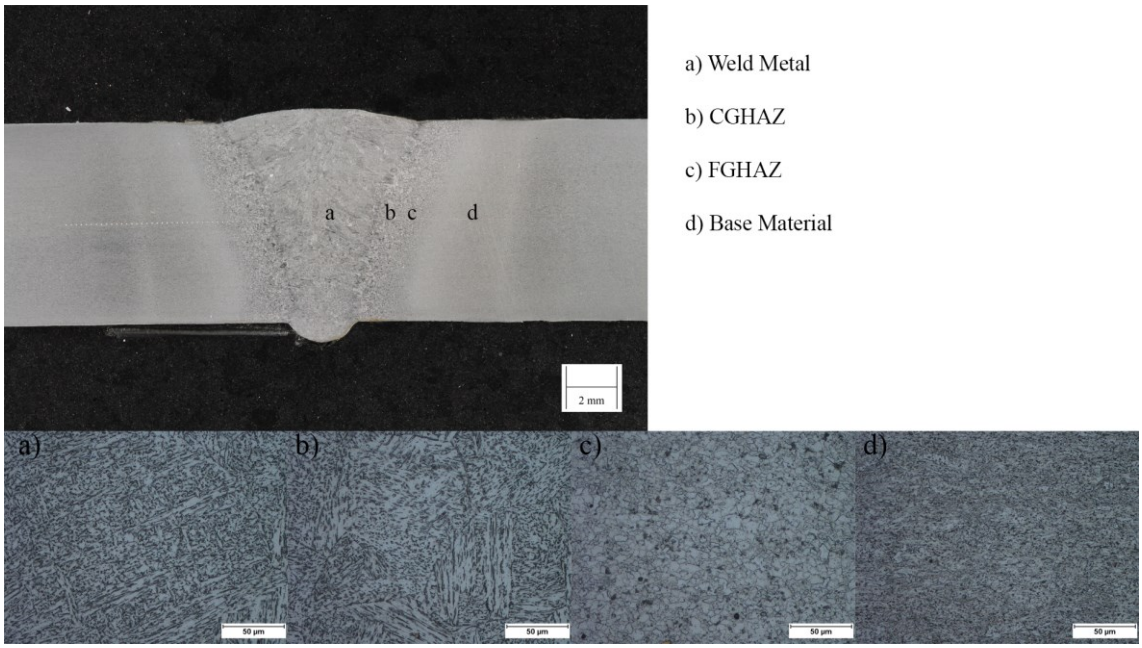

Figure 235. Sample 7008-1P.

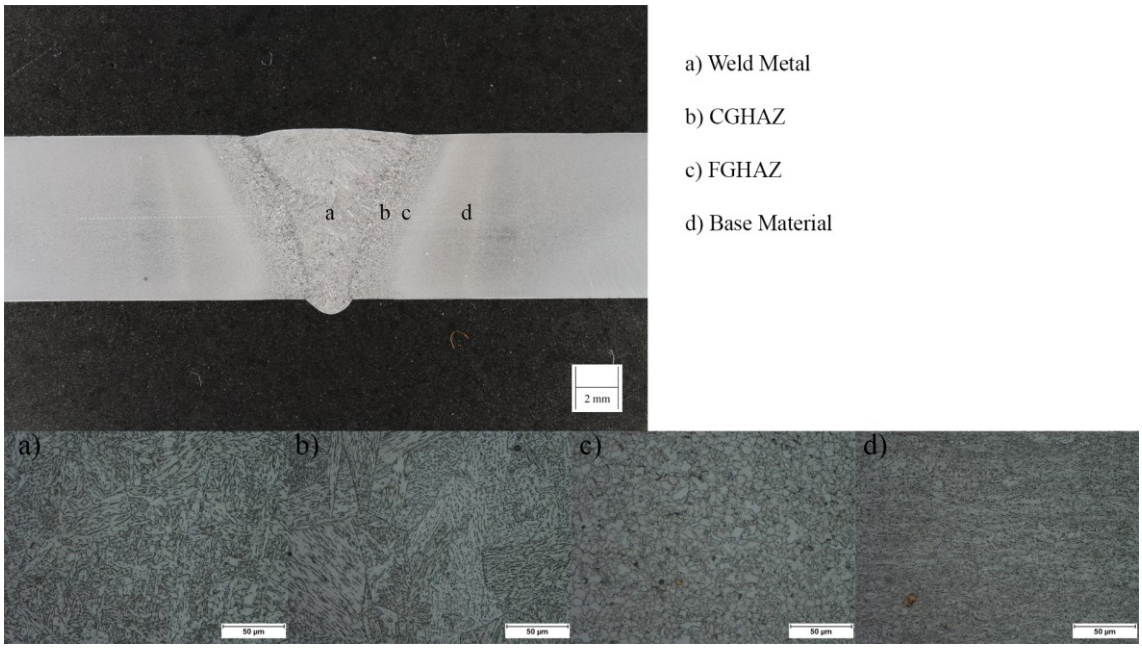

Figure 236. Sample 7008-2P.

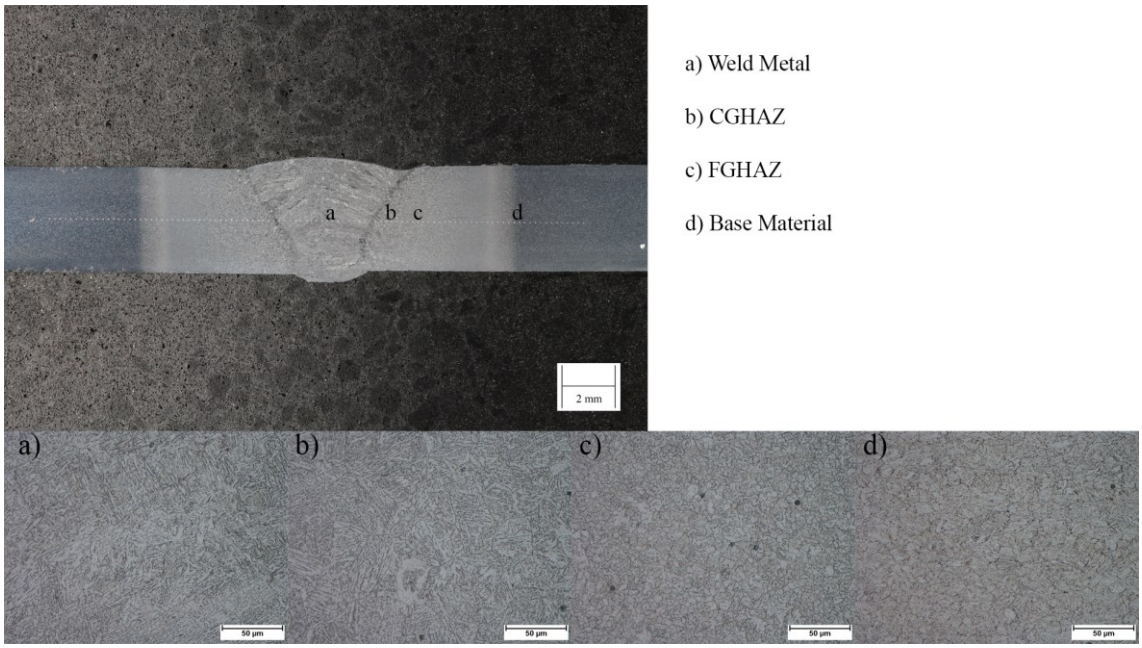

Figure 237. Sample 9004-3P.

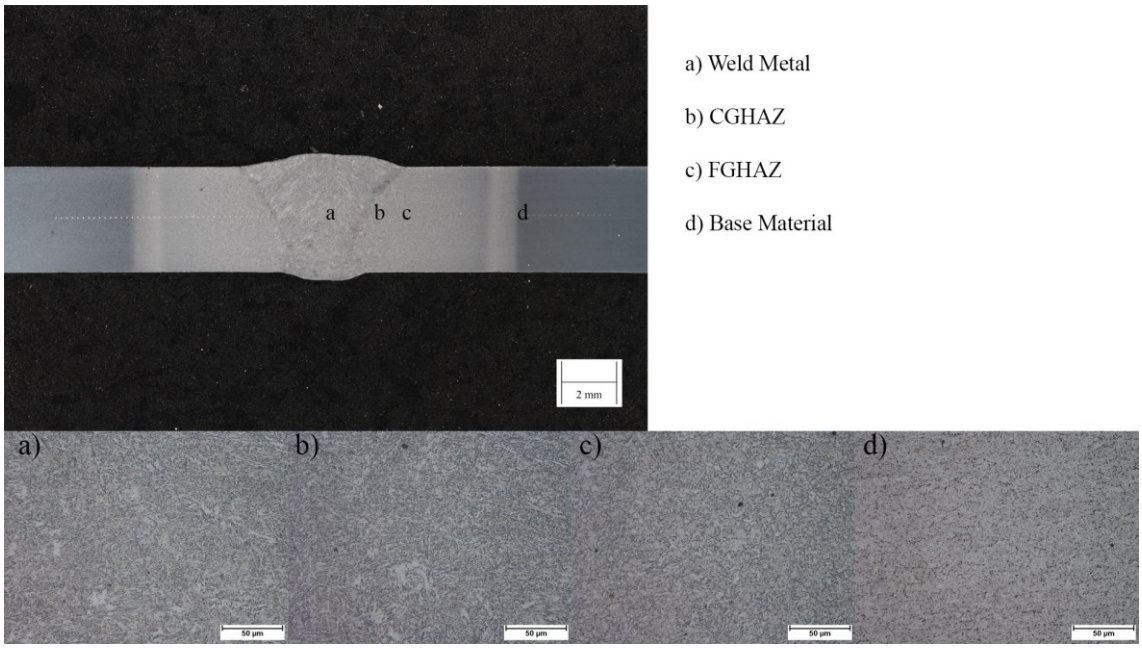

Figure 238. Sample 9004-4P.

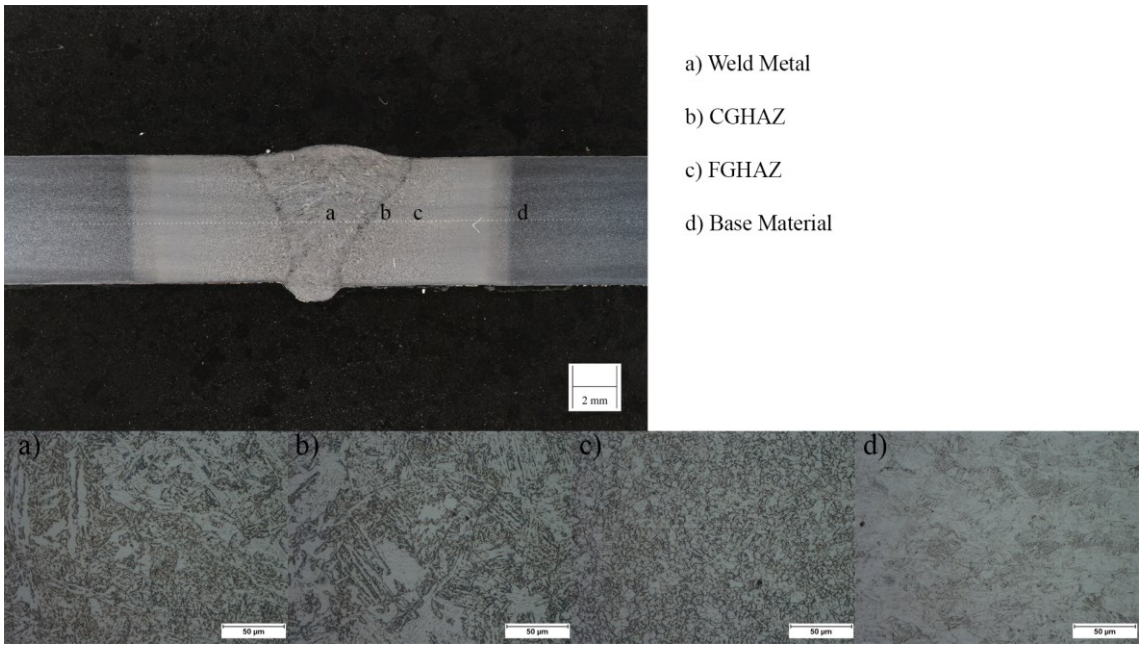

Figure 239. Sample 9006-3P.

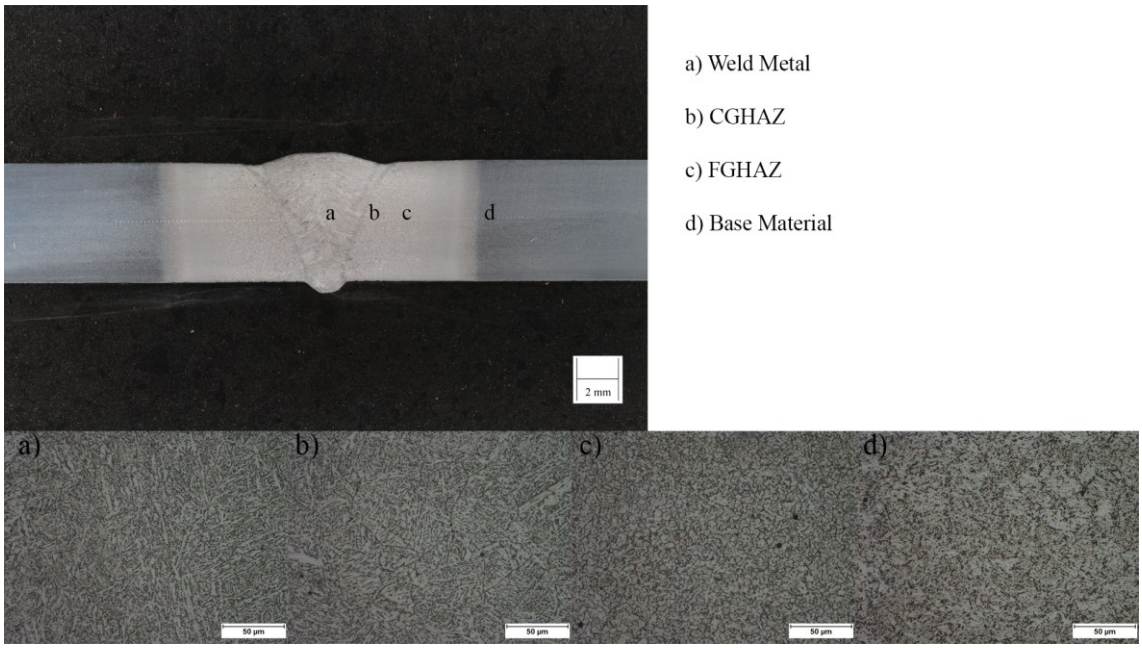

Figure 240. Sample 9006-4P.

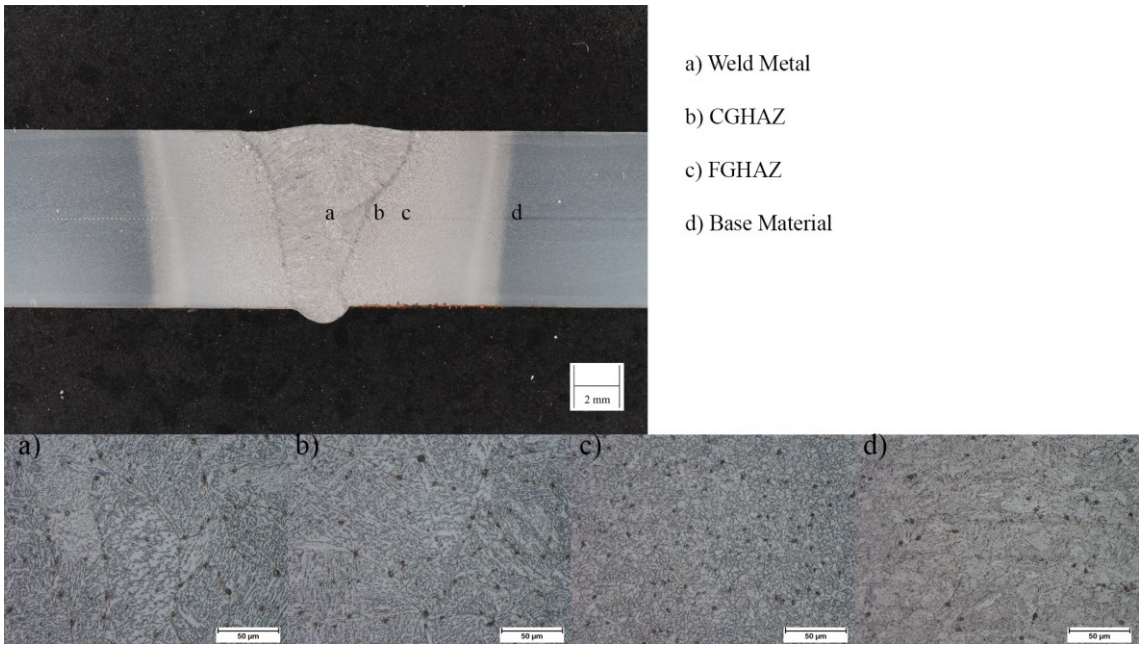

Figure 241. Sample 9008-3P.

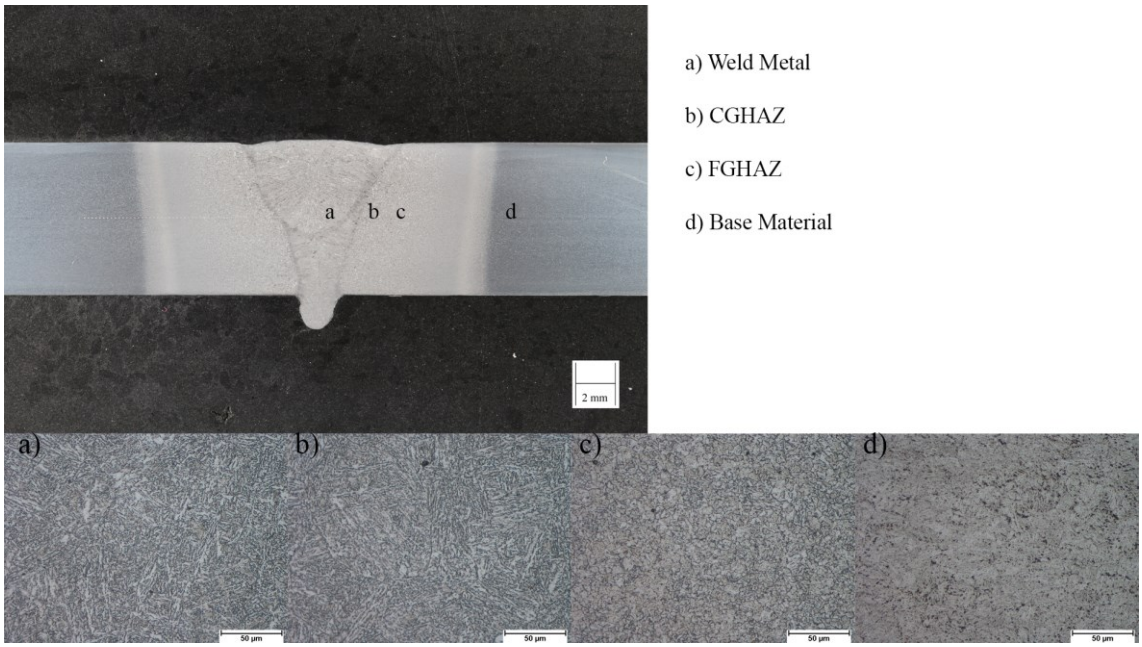

Figure 242. Sample 9008-4P.

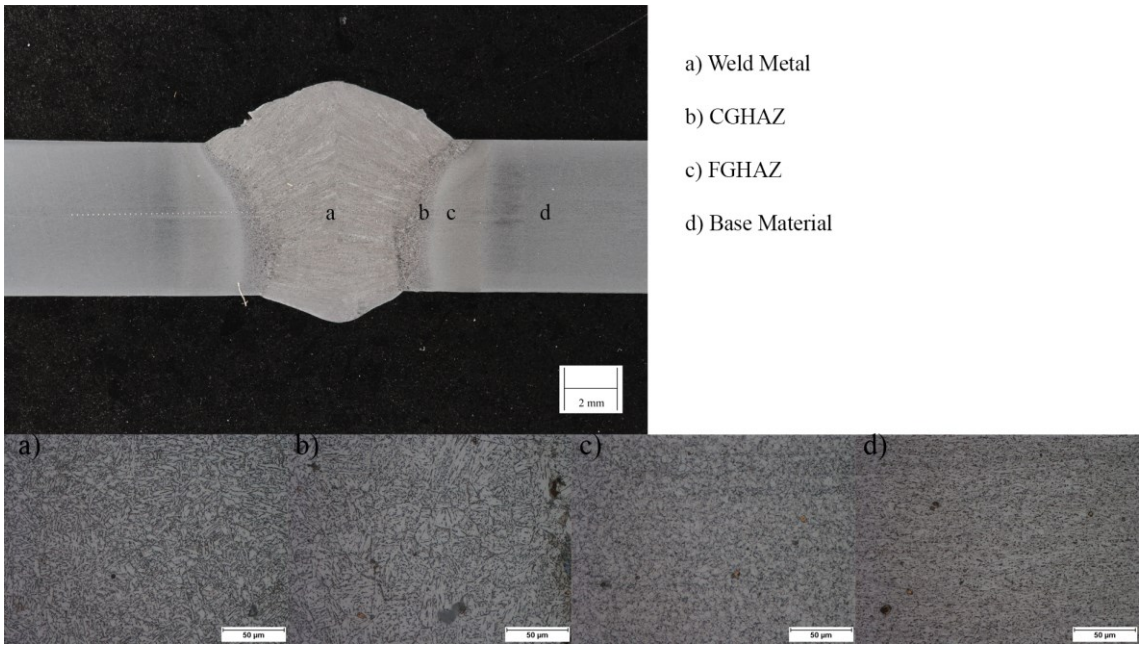

Figure 243. Sample 7006-5S.

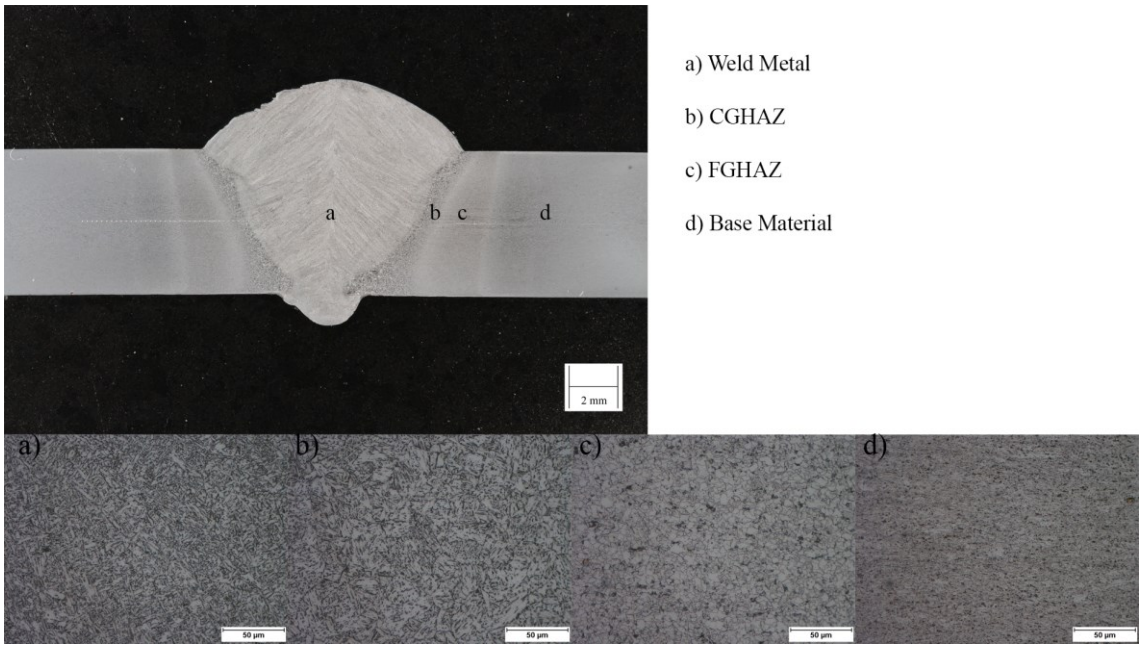

Figure 244. Sample 7006-6S.

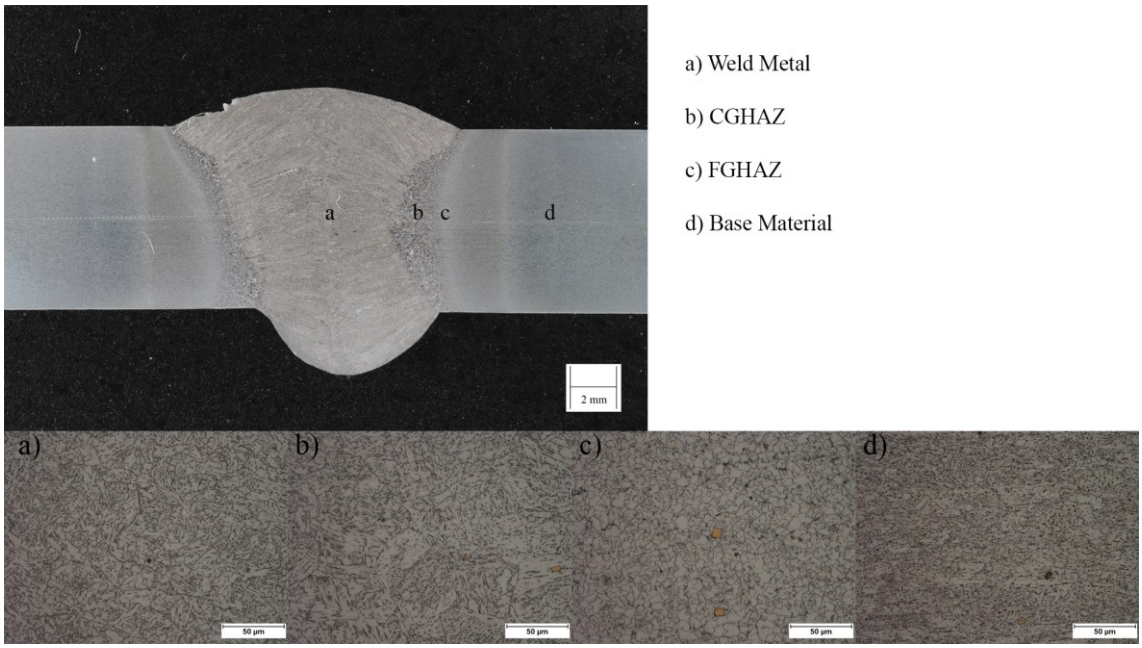

Figure 245. Sample 7008-5S.

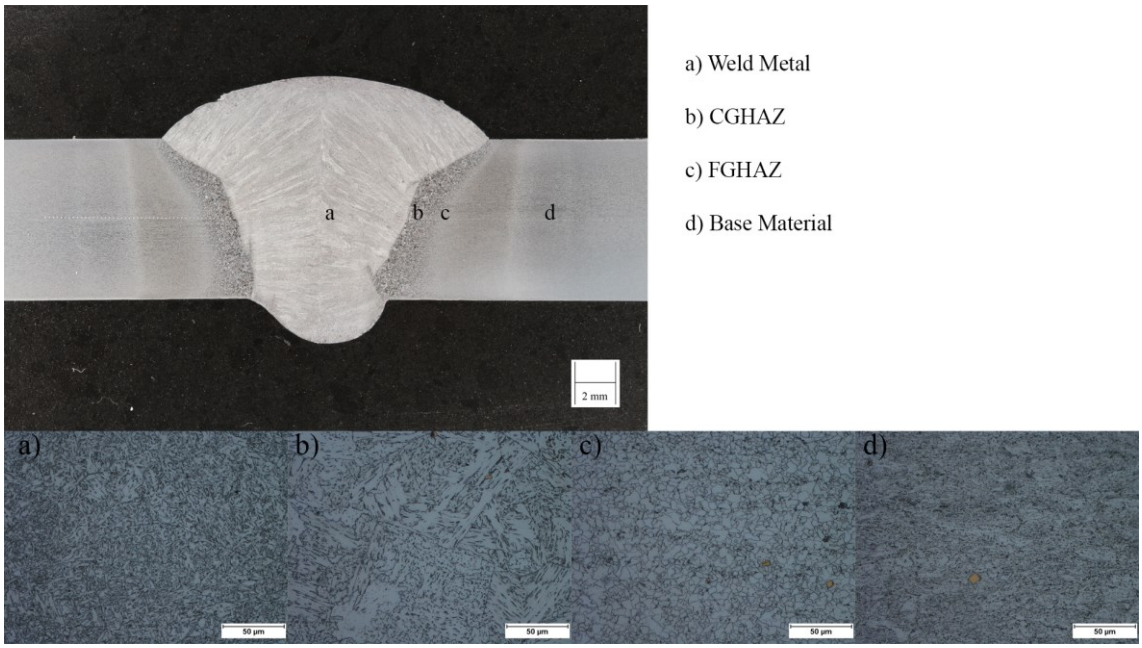

Figure 246. Sample 7008-6S.

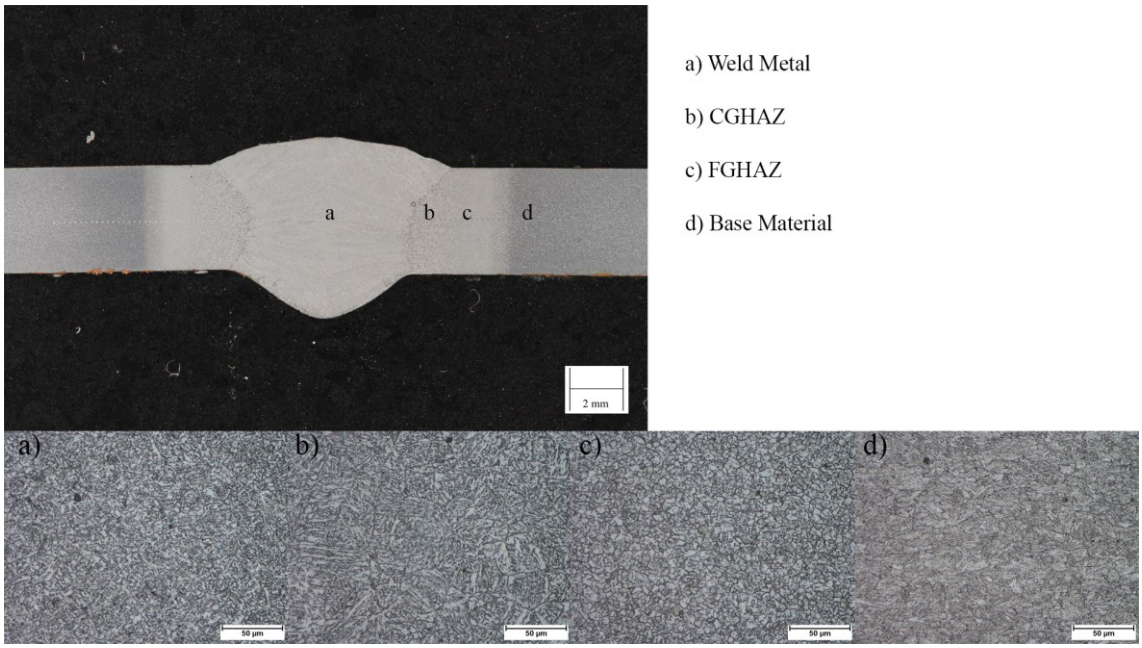

Figure 247. Sample 9004-5S.

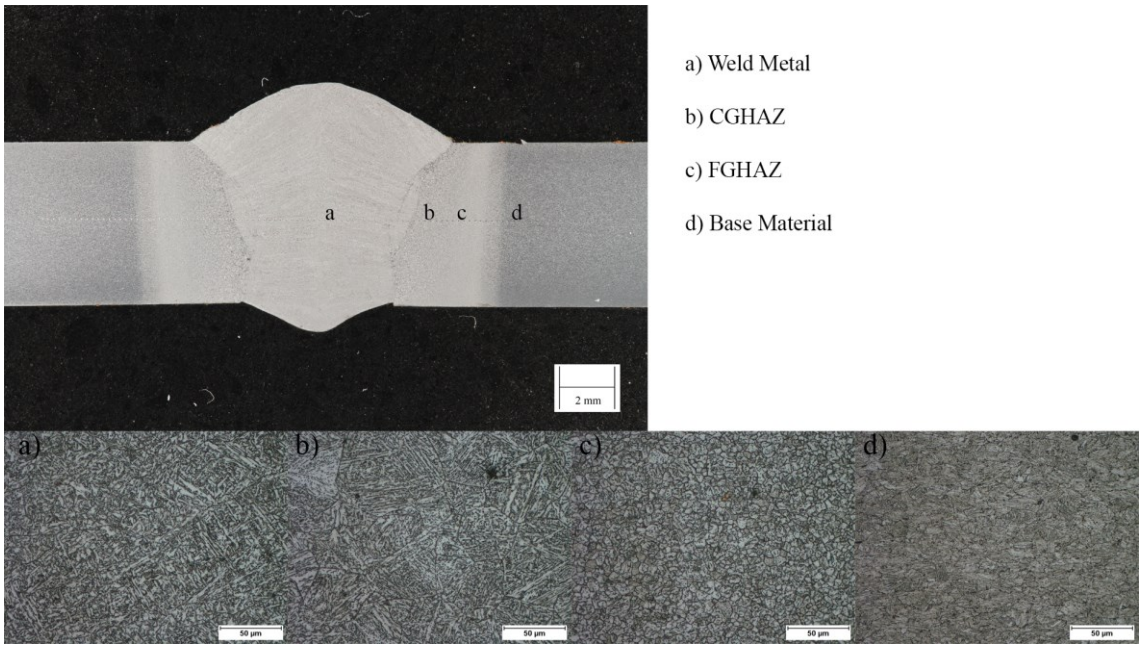

Figure 248. Sample 9006-5S.

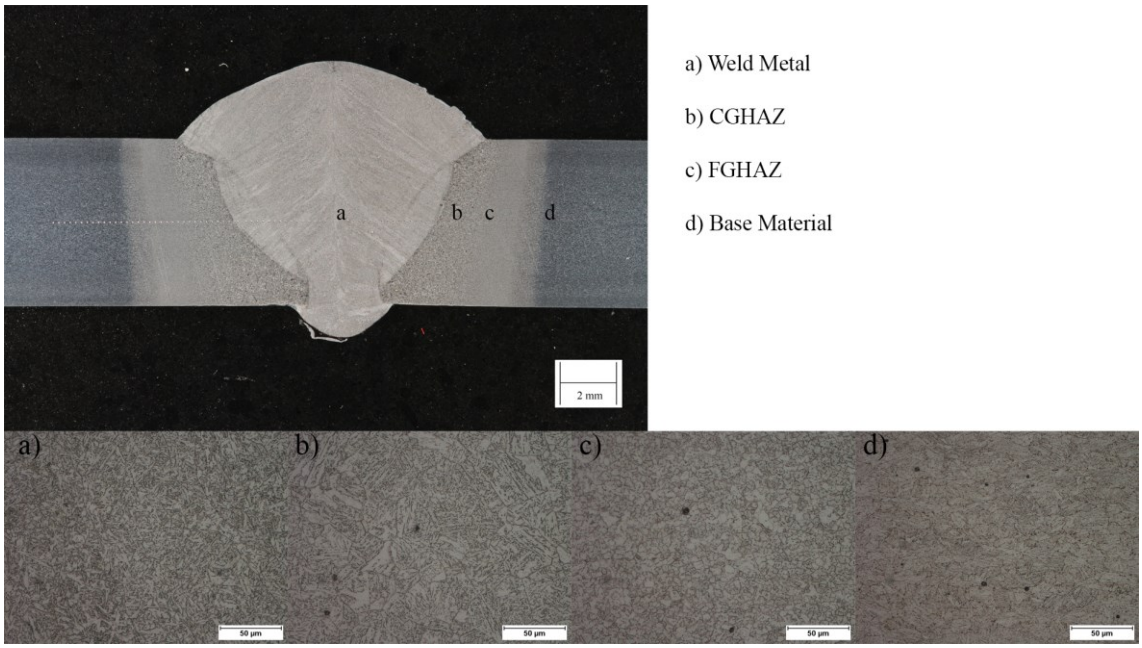

Figure 249. Sample 9006-6S.

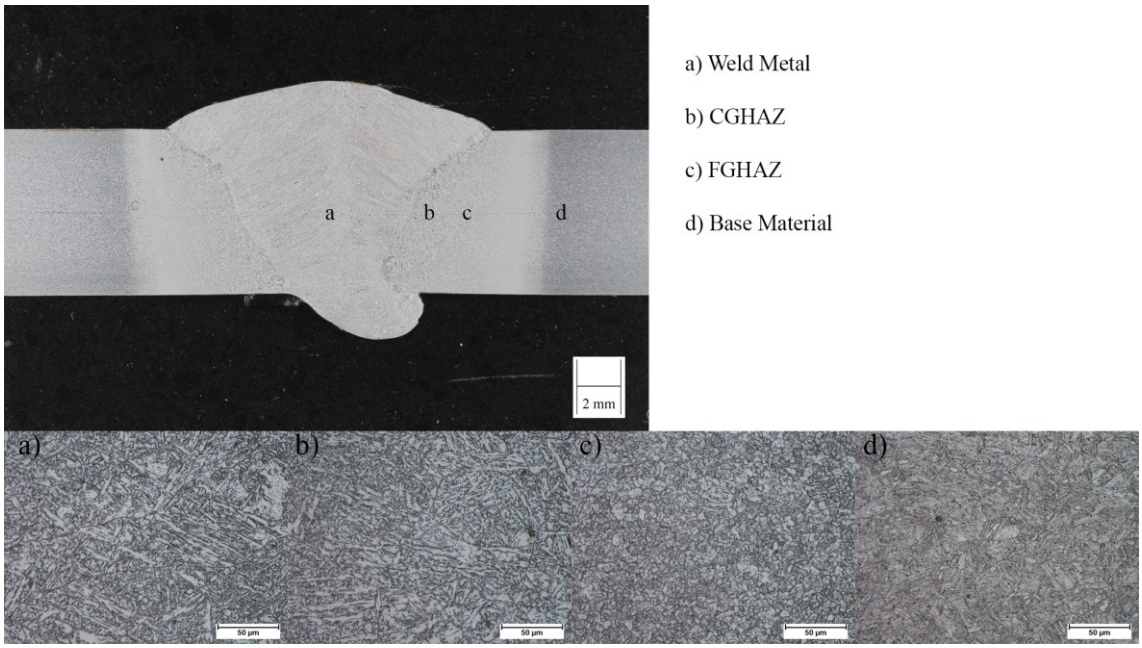

Figure 250. Sample 9008-5S.

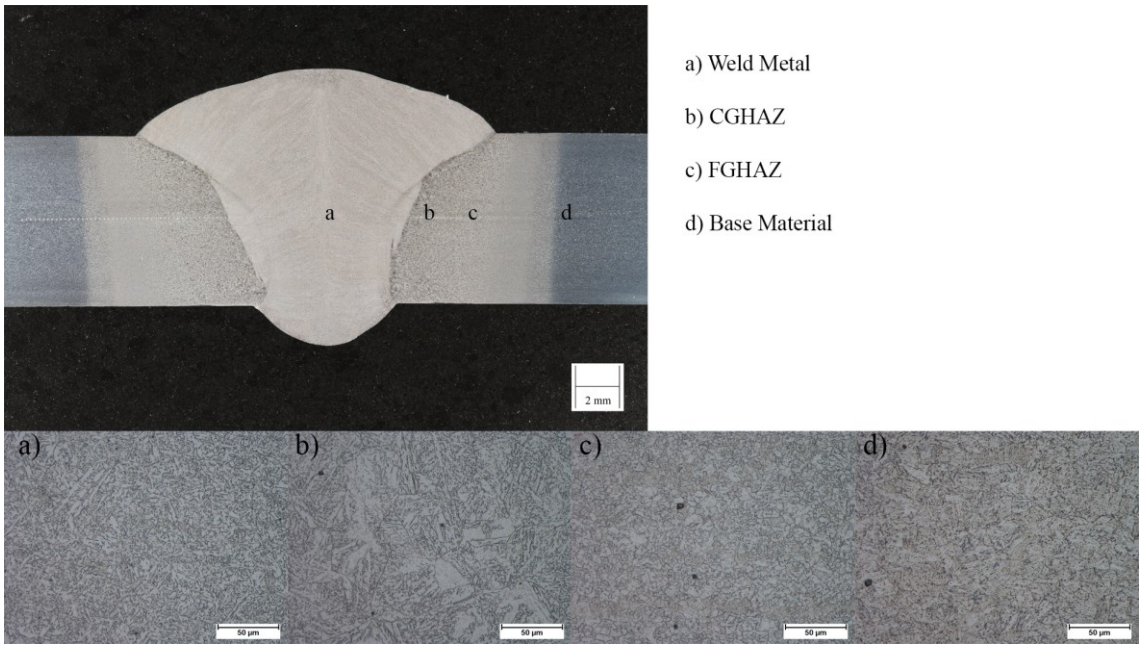

Figure 251. Sample 9008-6S.